TOPOLOGICAL PHASES, NON-EQUILIBRIUM DYNAMICS AND PARALLELS OF BLACK HOLE PHENOMENA IN CONDENSED MATTER

BY

SURAJ SHANKARANARAYANA HEGDE

DISSERTATION

Submitted in partial fulfillment of the requirements
for the degree of Doctor of Philosophy in Physics
in the Graduate College of the
University of Illinois at Urbana-Champaign, 2019

Urbana, Illinois

Doctoral Committee:

Professor Taylor Hughes, Chair
Associate Professor Smitha Vishveshwara, Director of Research
Professor Dale Van Harlingen
Assistant Professor Tom Faulkner

Abstract

This dissertation deals with two broad topics - Majorana modes in Kitaev chain and parallels of black hole phenomena in the quantum Hall effect. Majorana modes in topological superconductors are of fundamental importance as realizations of real solutions to the Dirac equation and for their anyonic exchange statistics. They are realised as zero energy edge modes in one-dimensional topological superconductors, modeled by the Kitaev chain Hamiltonian. Here an extensive study is made on the wavefunction features of these Majorana modes. It is shown that the Majorana wavefunction has two distinct features- a decaying envelope and underlying oscillations. The latter becomes important when one considers the coupling between the Majorana modes in a finite-sized chain. The coupled Majorana modes form a non-local Dirac fermionic state which determines the ground state fermion parity. The dependance of the fermion parity on the parameters of the system is purely determined by the oscillatory part of the Majorana wavefunctions. Using transfer matrix method, one can uncover a new boundary in the phase diagram, termed as 'circle of oscillations', across which the oscillations in the wavefunction and the ground-state fermionic parity cease to exist. This is closely related to the circle that appears in the context of transverse field XY spin chain, within which the spin-spin correlations have oscillations. For a finite sized system, the circle is further split into mutliple ellipses called 'parity sectors'. The parity oscillations have a scaling behaviour i.e oscillations for different superconducting gaps can be scaled to collapse to a single plot. Making use of results from random matrix theory for class D systems, one can also predict the robustness of certain features of fermion parity switches in the presence of disorder and comment on the critical properties of the MBS wavefunctions and level crossings near zero energy. These results could provide directions for making measurements on zero-bias conductance oscillations and the parameter range of operations for robust parity switches in realistic disordered system. On the front of non-equilibrium dynamics, the effect of Majorana modes on the dynamical evolution of the ground state under time variation of a Hamiltonian parameter is studied. The key result is the failure of the ground state to evolve into opposite parity sectors under the dynamical tuning of the system within the topological phase. This dramatic lack of adiabaticity is termed as parity blocking. A real-space time-dependent formalism is also developed using Pfaffian correlations, where simple momentum space methods

fail. This formalism can be used for calculating the non-equilibrium quantities, such as adiabatic fidelity and the residual energy in a system with open boundaries. The consideration of Majorana modes in non-equilibrium dynamics lead to deviation from Kibble-Zurek physics and non-analyticities in adiabatic fidelity even within the topological phase.

The second part of the thesis deals with uncovering structural parallels of black hole phenomena such as the Hawking-Unruh effect and quasinormal modes in quantum Hall systems. The Hawking-Unruh effect is the emergence of a thermal state when a vacuum of a quantum field theory on a given spacetime is restricted to a submanifold bounded by an event horizon. The thermal state manifests as Hawking radiation in the context of a black hole spacetime with an event horizon. The Unruh effect is a simpler example where a family of accelerating observers in Minkowski spacetime are confined by the lightcone structure and the Minkowski vacuum looks as a thermal state to them. The key element in understanding the Hawking-Unruh effect is the Rindler Hamiltonian or the boost. The boost acts as the generator of time translation for the quantum states in the Rindler wedge giving rise to thermality. In this thesis it is shown that due to an exact isomorphism between the Lorentz algebra in Minkowksi spacetime and the algebra of area preserving transformations in the lowest Landau level of quantum hall effect, an applied saddle potential acts as an equivalent to the Rindler Hamiltonian giving rise to a parallel of Hawking-Unurh effect. In the lowest Landau level, the saddle potential is reduced to the problem of scattering off an inverted harmonic oscillator(IHO) and the tunneling probability assumes the form of a thermal distribution. The IHO also has scattering resonances which are poles of the scattering matrix in the complex energy plane. The scattering resonances are states with time-decaying behavior and have purely incoming/outgoing probability current. These states are identified as quasinormal modes analogous to those occurring the scattering off an effective potential in black hole spacetimes. The quasinormal decay is an unexplored effect in quantum Hall systems and provides a new class of time-dependent probe of quantum Hall physics. The parallels between the relativistic symmetry generators and the potentials applied in the lowest Landau level also open up an avenue for studying Lorentz Kinematics and symplectic phase space dynamics in the lowest Landau level. These parallels open up new avenues of exploration in the quantum Hall effect.

To my guru C. V. Vishveshwara

Acknowledgments

I would like begin by remembering and paying respects to my *first teachers* with whom my life of thought and physics started. Those few formative years when I had the opportunity to work closely and learn under Prof. C. V. Vishveshwara were very important for my overall development. I am grateful for having been in his presence and thankful to him for initiating me into theoretical research, structural thinking, interest in literature and for strongly encouraging and guiding me to pursue an academic career in physics. The appreciation for the beauty of geometry and symmetry, which I developed under him, when learning about black holes and general relativity, remains with me to this day. I would also like to remember Prof. N. Kumar (Raman Research Institute, Bangalore) with whom I had the opportunity of interacting for a few months and started getting into condensed matter physics for the first time. His advice on approaching problems in physics is something that I will always remember. Though I had to endure through an engineering course for 4 years to get a formal degree in my undergrad, it is the informal REAP (Research education advancement program) at the J N Planetarium, Bangalore, that I call as my alma mater for physics. I am extremely thankful to the program and all the teachers there, from whom I learnt the fundamentals of physics and I would not have been doing physics if not for them. I would particularly like to thank H. R. Madhusudana for various inspiring conversations during REAP years and for later introducing me to C. V. Vishveshwara. Even though I've spent all these years in the US and come to end of completing my PhD, the remembrance of all these 'first teachers' always puts me into a 'beginner's mind' and continues to inspire me to pursue the fundamentals whenever I stray off .

I am extremely grateful to my advisor Smitha Vishveshwara for supporting and guiding me throughout my PhD. We started collaborating when I was working with her father C. V. Vishveshwara, during my undergrad in India, on optical analogs of light in black hole spacetimes. After I joined her group for grad school, we shifted more towards conventional condensed matter topics. But ultimately during the final years of grad school, we got back to black hole physics in the context of quantum Hall, which was the culmination of many things I had learnt since college. I am grateful to Smitha for giving an opportunity to work in her group. There was complete freedom and no pressure working with her. I am thankful to her for introducing

me to the topics of non-equilibrium dynamics, disorder and Josephson physics. I am grateful for her constant patience and enthusiasm for guidance and mentorship and showing keen interest in encouraging the students from the beginning to the end to pursue a good career. I would like thank the physics department and particularly Prof. Lance Cooper and Wendy Wimmer, for being a constant support for all the graduate students. I thank the members of my thesis committee Professors Taylor Hughes, Dale Van Harlingen and Tom Faulkner for their time and valuable feedback. I would like to thank my collaborators Diptiman Sen, Barry Bradlyn, Wade deGottardi and Dale van Harlingen. It is always fun to think through things sitting with Diptiman and see his fast thinking and calculating skills. I really enjoyed working with Barry on the black hole-quantum Hall project in my last year. I would like to thank my group mates Karmela Padavic and Varsha Subramanyan. It has been fun to think about quasiperiodicity and Hofstadter butterfly with Karmela and hope someday we will certainly find something amazing in this formidable problem. I had a great time discussing about physics, philosophy, Dostoevsky and things in general with Varsha. It was fun to take Prof. Chistopher Weaver's courses on philosophy of physics with her and have discussions after the classes. I would also like to thank Srivatsan Balakrishnan for various discussions on black hole physics, holography and Tomita-Takesaki theory. I want to thank the Institute for condensed matter theory(ICMT) for providing an great atmosphere for research and an amazing exposure to very diverse areas of physics, through weekly talks, seminars and workshops. I would like to the thank the various grants that have supported me throughout the grad school: National Science Foundation DMR-1745304 EAGER:BRAIDING, DMR 0644022-CAR and the U.S. Department of Energy, Division of Materials Sciences under Award No. DE-FG02-07ER46453.

"Live the full life of mind, exhilarated by new ideas, intoxicated by the romance of the unusual" says Ernst Hemingway. During my stay in Urbana, I have had the privilege of having wonderful companionship in the pursuit of exhilarating ideas and thinking. I have had amazing friends who have shared the zeal for 'theorizing' about anything and everything. Their presence helped me find a balance and facilitated my pursuit of physics. I would like to thank Yinghe Celeste Lu for being the theorizing buddy and sharing the same mind space of ideas. Those uninterrupted and long discussions with Celeste, Varsha and Manthos will remain memorable. I would like to thank Adnan Choudhary for sharing the zeal for allowing the unfold-ment of 'Being' and for all the practice sessions of the Alexander technique. I would like to thank Vatsal Dwivedi, Astha Sethi, Roshni Bano, Jelena for all the good times in Urbana and during travels, and particularly 'tiny Sethi' for being tiny throughout the grad school. I have been very lucky to have great teachers in my non-physics pursuits as well. I am thankful to Lois Steinberg and all the yoga teacher sat the Yoga institute of Champaign-Urbana. I would also like to thank my teachers Phillip Johnston, Sally and Yvonne in the

Alexander technique courses I took at the university. I could not have had a better start in those disciplines than learning from these teachers. Finally, I would like to thank my parents and family in India for having always supported me in all endeavors.

Table of Contents

List of Tables

List of Figures

List of Abbreviations

SPT	Symmetry protected topological phases.
MBS	Majorana bound states.
RMT	Random matrix theory.
SC-TI-SC	Superconductor-Topological Insulator-Superconductor.
COO	Circle of oscillations.
LY	Lyapunov exponent.
QCP	Quantum critical point.
LLL	Lowest Landau level.
IHO	Inverted harmonic oscillator.
$\mathfrak{sl}(2,\mathbb{R})$	Lie-algebra of special linear transformations in 2 dimensions(over real space).
$\mathfrak{sp}(2,\mathbb{R})$	Lie-algebra of symplectic transformations in 2 dimensions(over real space).
$\mathfrak{so}(2,1)$	Lie-algebra of Lorentz transformations in 2 dimensions.
$\mathfrak{su}(1,1)$	Lie-algebra of special unitary transformations.
QNM	Quasinormal modes.

Chapter 1

Introduction

In his famous 1972 article "More is different" [4], P. W. Anderson highlighted the importance of scales and complexity when dealing with conglomerates of large number of particles. It was an important critique of the fatal reductionist view of science that there exist a set of 'fundamental laws' of physics acting at a certain scale. These laws determine the dynamics of 'the fundamental constituents' and the knowledge of these fundamental laws would allow us to explain all the other phenomena in the world. Addressing this, Anderson pointed out that " The main fallacy in this kind of thinking is that the reductionist hypothesis does not by any means imply a "constructionist" one: The ability to reduce everything to simple fundamental laws does not imply the ability to start from these laws and reconstruct the universe...". Then he proceeds to show how the paradigm of 'broken symmetries' makes it clear the breakdown of constructionist converse of reductionism. The developments in condensed matter physics over the past few decades have shown the importance of studying every phenomena on the level of complexity of its own scale, be it nano-, micro-, meso- or cosmological. The description and understanding of the physics at each of these different scales comes with its own paradigm of formalism and their explanations need not be in terms of some kind of 'fundamental constituents'. If we take the theory of superconductivity, for example, while there is the BCS(Bardeen-Cooper-Schrieffer) theory at the level of electrons and cooper pairs as a mean field description, there is the Landau-Ginzburg theory capturing the physics at a different scale and covering different aspects in terms of an effective field. One could even go to the level of interacting electrons and through renormalisation group arguments show the emergence of the BCS pairing. At the same time, one could start by not worrying about how the superconductivity arises and explore its mesoscopic manifestations. The physics of superconducting Josephson junctions, for example, offers its own rich set of phenomena. Such mesoscopic manifestations are also much closer to experimental measurements. Thus, one comes to appreciate the rich domains of study over different scales. The challenge is always to understand the interpolations between the different scales.

One of the surprising things recurring over the past few decades in condensed matter physics is the occurrence of phenomena at 'condensed matter scales', that resemble in form and structure to exotic phenomena predicted originally in the context of high energy physics. This includes the Dirac equation in topologi-

cal phases followed by Majorana and Weyl fermionic description of certain aspects in those systems. Dirac monopoles, Skyrmions, axionic fields, holography are some more of such examples. These emerge as effective description at some scale of macroscopic, condensed matter materials. These condensed matter realisations are no longer seen as toy models of pure academic interest but are accessible to experiments and can be pushed to the limits of even having technological applications.

This thesis, presents the study of two such topics : Majorana modes and Black hole phenomena in condensed matter systems. Majorana modes have received immense attention due to their fundamental importance of being their own anti-particles and exhibiting non-Abelian exchange statistics [5, 6]. They have been experimentally realised in semi-conductor-superconductor heterostructures[7, 8] and are leading candidates in proposals to realise topological quantum computation[9]. This thesis presents a study of their wavefunction physics and non-equilibrium dynamics in a one-dimensional lattice model called the Kitaev chain, where Majorana modes are realised as edge states. The second part of the thesis demonstrates the emergence of sphenomena in the quantum Hall effect that are structurally parallel to those occurring in black holes. Black holes, a crowning consequence of general relativity, have been enigmatic since their original prediction. They are also among the simplest objects in the universe, characterized by just three parameters - mass, charge and angular momentum [10, 11]. These characteristic signatures of black holes manifest in gravitational waves [12], decay rates of quasinormal modes [13, 14] and Hawking radiation[15]. While black holes occur at astrophysical scales, at the mesoscopic scale we have the quantum Hall effect. In two dimensions, robust properties of electronic wavefunctions allow for a gapped phase having a precisely quantized Hall conductance[16, 17]. These quantum Hall systems host anyonic excitations, protected chiral edge states, and a universal thermal Hall conductance, and offer a promising route to topological quantum computing [18, 9]. Quantum systems in fact offer a multitude of ways to probe relativistic phenomena, from mimicking curved spacetimes [19] to investigating dynamic geometric backgrounds [20, 21, 22, 23, 24]. In this thesis, we show that signature features of black holes, and scattering in quantum Hall systems can be remarkably unified by a mapping to single particle physics in the presence of an inverted harmonic oscillator (IHO) potential. The IHO model exhibits potential scattering and temporally decaying modes, features that have made the model invaluable in a broad variety of contexts since the birth of quantum mechanics [25, 26, 27]. From its infancy, phenomena such as particle decay [28] and metastability [29] have been analyzed using the IHO. In developments across the decades, the IHO has played key roles in the context of chaos theory[30, 31, 32], decoherence [33, 34, 35] and quantum optics [36] . In modern high energy physics and cosmology, it has provided a basis for understanding 2D string theory, tachyon decay[37, 38, 39, 40] and even inflation in the early universe[41]. Thus, through its powerful simplicity, the IHO serves as an

archetype for phenomena in numerous realms, much like the more familiar simple harmonic oscillator. In this thesis, we shall focus more on the structural parallels of black hole phenomena occurring IHO realised in quantum Hall systems.

The organization of the thesis is as follows: Chapter 2 starts with an introduction to topological phases and Majorana modes in condensed matter systems. Then it presents work on effect of disorder and potential landscapes on the Majorana wavefunctions and the associated ground state fermion parity. This is based on the work published in Ref.[42] Chapter 3 presents the effect of Majorana modes on the non-equilibrium dynamics of topological superconductors based on work done in Ref.[43]. Chapter 4 deals with parallels of black hole phenomena in quantum Hall effect. First the basics of black hole physics and the quantum Hall effect are presented and then parallels to Hawking-Unruh effect and quasinormal modes are drawn based on symmetry arguments and physics of scattering off an inverted harmonic oscillator. Part of it is presented in Ref.[44] and parts of it are from my own individual study. Finally in chapter 5, a primer is presented on the inverted harmonic oscillator, a simple quantum mechanical model that shows many important and fundamental properties of scattering.

Chapter 2

Majorana wavefunction physics in topological superconductors

2.1 Topological phases

Characterization of a particular physical phenomenon based on minimal set of quantities and laws has been the project of most theories of physics. When we consider macroscopic conglomerates of atoms, molecules or electrons under specific physical conditions such as temperature, pressure and applied fields, despite the numerous and very significant differences in the details of how they occur in nature, we still see very specific classes or 'phases' of common behavior such as metals, insulators etc.These phases are characterized by minimal set of quantities such as conductivity, magnetisation etc. One can classify the different phases based on the symmetries of the system and whether the states of the system break those symmetries or not. Such phases are characterized by an 'order parameter' that has a finite expectation value in the lowest energy state or the ground state of the system. The order parameter can have a characteristic change as the system changes from one phase to the other and the transition occurs at a specific value of the parameter(such as temperature) called the 'critical point'.

Another paradigm for classifying different phases of matter is based on topological characteristics. Broadly speaking, topological characteristics are insensitive to the details and are only dependent on the connectivity of the manifold in question. Distinction in topological characteristics is based on certain numbers called 'topological invariants' which characterize the specific topology of the manifold. A very easy and rough (and famous)illustration of topological characterstics is that of a torus and a sphere. These two shapes are topological distinct as the torus has a hole and the sphere does not and the two shapes cannot be deformed into another smoothly. In the context of condensed matter, the topological invariants appear in experimentally measured quantities such as the conductance. For example, in the quantum Hall effect, the Hall conductance is quantized in terms of a topological invariant [45, 18]. The topology in this case is the topology associated with the electronic wavefunctions of a gapped system. The importance of these topological characterstics is that they are very robust aginst perturbations. For example, the robustness of quantization of Hall conductance allows one to determine the fine structure constant to an extremely high

precision. We shall make the notion of these topological invariants very precise and derive an example in the following sections. Here, we will be specifically focusing on a type of phases classified based on topology called the symmetry protected topological phases(SPTs). The properties of an SPT are [46] i) Presence of a gap in the bulk spectrum and ii) the boundary are gapless, must spontaneously break the symmetry in the system. A fundamental characteristic of SPTs is that the (d-1) dimensional boundary of a d-dimensional SPT cannot exist in isolation as a purely (d-1) dimensional object. The different classes of topological characterstics that could occur for non-interacting fermions are completely classified based on the SCT (Chiral, Charge conjugation and Time reversal) symmetry operations on the system. The topological phase and its characteristics are preserved as long as the symmetries corresponding to it are not broken. Thus, the name 'symmetry protected topological phases'. These are to be distinguished from phases with 'Intrinsic topological order' which need not have any symmetries, have fractonalisation of quasiparticles in the bulk and have long range entanglement properties [46].

To understand how this classification works consider a simple second quantised Hamiltonian of the form:

$$H = \sum_{A,B} \psi_A^\dagger \mathcal{H}_{AB} \psi_B \tag{2.1}$$

where the fermion creation and annihilation operators satisfying the commutation relations $\{\psi_A, \psi_B^\dagger\} = \delta_{A,B}$ and $\mathcal{H}_{A,B}$ is an $N \times N$ matrix (One can similarly obtain a matrix for a superconducting system in the space of $(\psi, \psi^\dagger)$, called the Nambu space). Since we are looking for topological features of the Hamiltonian, the features of the classification cannot change by adding perturbation terms that do not close the gap in the system. The properties must be robust if one breaks translational symmetry in the system by adding an on-site disorder term for exmaple. In general, one does not include such unitarily realised symmetries in the classification. The 'symmetries' we consider here are the ones anti-unitarily realised, such as the time-reversal symmetry, charge conjugation symmetry and sub-lattice symmetry [46]. The condition for time reversal symmetry of the Hamiltonian is given by:

$$\mathcal{T}: \quad U_T^\dagger \mathcal{H}^* U_T = +\mathcal{H} \tag{2.2}$$

The condition for charge conjugation/ particle-hole symmetry is given by

$$\mathcal{C}: \quad U_C^\dagger \mathcal{H}^* U_C = -\mathcal{H} \tag{2.3}$$

	sym. class	TRS	PHS	SLS
Wigner-Dyson	A	0	0	0
	AI	+1	0	0
	AII	-1	0	0
chiral	AIII	0	0	1
	BDI	+1	+1	1
	CII	-1	-1	1
BdG	D	0	+1	0
	C	0	-1	0
	DIII	-1	+1	1
	CI	+1	-1	1

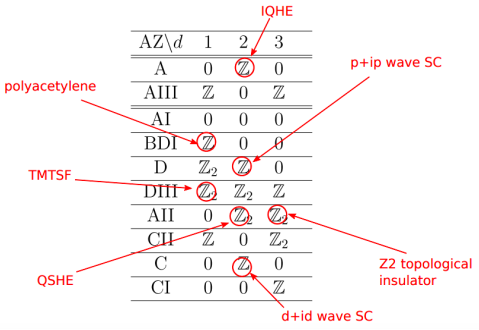

AZ\d	1	2	3
A	0	$\mathbb{Z}$	0
AIII	$\mathbb{Z}$	0	$\mathbb{Z}$
AI	0	0	0
BDI	$\mathbb{Z}$	0	0
D	$\mathbb{Z}_2$	$\mathbb{Z}$	0
DIII	$\mathbb{Z}_2$	$\mathbb{Z}_2$	$\mathbb{Z}$
AII	0	$\mathbb{Z}_2$	$\mathbb{Z}_2$
CII	$\mathbb{Z}$	0	$\mathbb{Z}_2$
C	0	$\mathbb{Z}$	0
CI	0	0	$\mathbb{Z}$

Figure 2.1: The periodic table for the different topological phases of non-interacting fermions. This is known as the 'Altland-Zirnbauer' classification. The columns TRS, PHS and SLS stand for time-reversal symmetry, particle-hole symmetry and sub-lattice symmetry respectively. Based on how these anti-unitarily realized symmetries act on the second quantized Hamiltonian, there are only ten different classes indicated by letters $A, AI, AII...$ The names 'Wigner-Dyson', 'Chiral' and 'BdG' correspond to different ensembles these Hamiltonian matrices belong to. On the right, is the table of topological invariants predicted for each of these classes in different dimensions . These invariants are indicators of the presence of edge modes in the corresponding topological phases.

. There is another operation

$$\mathcal{S} = \mathcal{T}.\mathcal{C} \tag{2.4}$$

This is a unitarily realised symmetry but does not commute with the Hamiltonian. From these, we will see that there are only 10 ways a system can respond to these symmetries. Let us first consider the time-reversal symmetry. The given Hamiltonian i) Is not time-reversal invariant which we will indicate as $T = 0$, ii)Is time reversal invariant and the operator $\mathcal{T}$ squares to one. Let us denote this by $T = 1$. iii) Is time reversal invariant but the operator $\mathcal{T}$ squares to -1. This is denoted as $T = -1$. This gives us 3 cases. One has similar 3 cases for the charge conjugation operator $\mathcal{C}$ with $C = 0, +1, -1$. That counts 3×3 cases. The behaviour of the Hamiltonian under $\mathcal{S}$ is uniquely fixed by the behaviour of $\mathcal{T}, \mathcal{C}$ in 8 out of 9 cases. When $T = 0, C = 0$, $S = 0, 1$ is possible. This yields $(3 \times 3 - 1) + 2 = 10$ cases. This gives an exhaustive classification of the phases as given in Fig.2.1. Once this classification is done one can obtain the topological invariants in a given dimension as shown in the Fig.2.1 [46]. The table also shows the different physical systems which belong to some of these classes. Thus, remarkably one obtains a 'periodic table' for the classification of different topological phases of non-interacting fermions purely based on the action of the symmetries and the dimension, without any other details. This proves to be an extremely strong method in predicting the topological features of a given system.

As mentioned, one of the characteristic features of these topological phases is the existence of a gapless boundary. Instead of a boundary one could also consider a topological defect such as a vortex. If the system has particle-hole symmetry, the gapless boundaries or vortices can harbor zero-energy modes and these zero-

energy modes have interesting properties. The value of the topological invariants indicates the presence of such zero modes. Let us consider a very specific system in which the time reversal symmetry is broken at the defect or the boundary but the particle-hole symmetry is preserved. This corresponds to a system of '*Class D*. From the table in Fig.2.1, the one-dimensional system with point like boundaries has an invariant Z_2, which allows zero-modes at the boundary as the topological invariant is non-zero. This is realised in a one-dimensional p-wave superconductor and the edge mode is a Majorana fermionic mode [47], which will be the object of our interest in the following chapters. One can also see from other examples in the table that invariant can be zero indicating the absence of boundary modes.

The Majorana fermions were first discovered theoretically as solutions to the Dirac equation. The Dirac equation in general plays an important role in the study of topological phases and it emerges in some cases as an effective description of the gapless modes at the boundaries of the the SPTs. In the next section we shall study the Dirac equation and consider a simple example in condensed matter model where it appears. As we shall see the edge modes in topological phases are obtained as solutions to the Dirac equation.

2.1.1 Dirac equation in lower dimensional condensed matter systems

Dirac in his 1930 paper [48] set out to find a relativistic formulation of quantum mechanics, which would would also include the spin angular momentum in its articulation. The starting point was the Schrödinger equation for describing the time-evolution of the quantum mechanical state:

$$H\Psi = i\frac{\partial}{\partial t}\Psi \tag{2.5}$$

This evolution is linear in time and Lorentz co-variance requires that the form of the Hamiltonian be linear in the momentum. Also, the energy-momentum relation should satisfy $E^2 = p^2 + m^2$, where p is the momentum, m is the mass and reminding that the convention of $c = 1$ is adopted.The Dirac equation is a manifestly Lorentz co-variant equation satisfying those condition and the Hamiltonian equation is written as

$$(\Gamma^\mu p_\mu - m)\Psi = (i\Gamma^\mu \partial_\mu - m)\Psi = 0 \tag{2.6}$$

where $p_\mu = (i\partial_t, \vec{p})$ ($p^\mu = (i\partial_t, -\vec{p})$). Γ^μ are the Dirac matrices and they obey the algebra (known as Clifford algebra)

$$\{\Gamma^\mu, \Gamma^\nu\} = \Gamma^\mu\Gamma^\nu + \Gamma^\nu\Gamma^\mu = 2\eta^{\mu\nu} \tag{2.7}$$

The $\eta^{\mu\nu}$ is the metric of the Minkowski space. The Dirac gamma matrices are of the form:

$$\Gamma^0 = \begin{pmatrix} I_2 & 0 \\ 0 & -I_2 \end{pmatrix} \quad \Gamma^k = \begin{pmatrix} 0 & \sigma^k \\ -\sigma^k & 0 \end{pmatrix} \quad k = 1, 2, 3 \tag{2.8}$$

Here σ^k are the Pauli matrices:

$$\sigma^1 = \begin{pmatrix} 0 & 1 \\ 1 & 0 \end{pmatrix} \quad \sigma^2 = \begin{pmatrix} 0 & -i \\ i & 0 \end{pmatrix} \quad \sigma^3 = \begin{pmatrix} 1 & 0 \\ 0 & -1 \end{pmatrix} \tag{2.9}$$

The Dirac gamma matrices are 4 dimensional matrices with complex numbers. As a result the solutions of the Dirac equation Ψ are 4-component complex fields, two of them with positive energy $\sqrt{p^2 + m^2}$ and the other two representing particles with negative energy $-\sqrt{p^2 + m^2}$. The latter are interpreted as 'anti-particles' of electrons a.k.a 'positrons' with positive charge. The double-multiplicity of the each of those solutions arise from the fact that the field represent spin-1/2 fermions.

Dirac equation in condensed matter: In the above discussion, the Dirac equation in $3 + 1$ dimensional Minkowski spacetime was considered. The form of the Dirac equation in lower dimensions becomes highly relevant in condensed matter systems especially in the context of topological phases [49, 50]. It appears as an effective Hamiltonian in the low energy limit of these systems. One can show this from some general considerations[51]. The many-body Hamiltonian of a electron system would be of the general form $\mathcal{H} = \mathcal{H}_0 + \mathcal{H}_{int}$, where $\mathcal{H}_0$ is the one-body kinetic energy part of the electrons and $\mathcal{H}_{int}$ is the many-body interaction part. For electrons moving in a periodic potential, one has the band spectrum $E_n(k)$ and wavefunctions $|\phi_{n,k}\rangle$,where n is the band index and k is the crystalline momentum. Consider two adjacent energy bands $E_{n+}(k)$ and $E_{n-}(k)$ whose difference is much smaller than their separation from the rest of the bands. The effective Hamiltonian for the two bands , without many-body effects, is then given by

$$\mathcal{H}_{eff} = \sum_k \psi_k^\dagger H(k) \psi(k) \quad H(k) = \begin{pmatrix} \langle u_k | \mathcal{H}_0 | u_k \rangle & \langle u_k | \mathcal{H}_0 | v_k \rangle \\ \langle v_k | \mathcal{H}_0 | u_k \rangle & \langle v_k | \mathcal{H}_0 | v_k \rangle \end{pmatrix} \tag{2.10}$$

This can be expanded in terms of the Pauli matrices as

$$H(k) = f(k) \mathbb{1}_2 + \sum_{j=1}^{3} \vec{g}(k) . \vec{\sigma} \tag{2.11}$$

The spectrum is then given by $E_\pm = f(k) \pm \sqrt{\sum_{j=1}^{3} g^2(k)}$. Suppose there exists a point k_0 in the Brillouin

zone where the two bands touch if for all j, $g_j(k_0) = 0$. Near these points the Hamiltonian can be linearised to the form of Dirac equation :

$$H(k) = E_{k_0} + \hbar\vec{v}_0.(\vec{k} - \vec{k}_0)\mathbb{1}_2 + \sum_{j=1}^{3} \hbar\vec{v}_j.(\vec{k} - \vec{k}_0)\sigma_j \tag{2.12}$$

This band-crossing can be achieved in two dimensions the presence of special symmetries in the system and by fine-tuning the parameters. The Pauli matrices could also generally correspond to other degrees of freedom such particle-hole or spin, as in the case of a topological superconductor.

In the presence of time-reversal and space-inversion symmetry, there is a double degeneracy of the energy bands corresponding to spin degeneracy. For every solution $\phi_k(r)$, there is a Kramer doublet $i\sigma_2\phi*(-r)$. The two nearby bands are now given by $u_{1k}(r)\left|\uparrow\right\rangle + u_{2k}(r)\left|\downarrow\right\rangle$, $-u^*_{1k}(r)\left|\downarrow\right\rangle + u^*_{2k}(-r)\left|\uparrow\right\rangle$ and $v_{1k}(r)\left|\uparrow\right\rangle + v_{2k}(r)\left|\downarrow\right\rangle$, $-v^*_{1k}(r)\left|\downarrow\right\rangle + v^*_{2k}(-r)\left|\uparrow\right\rangle$. The effective four-dimensional Hamiltonian is now given by

$$H(k) = f(k)\mathbb{1}_4 + \sum_{j=1}^{5} g_i(k)\Gamma_i \tag{2.13}$$

where the Gamma matrices are given by $\Gamma_1 = \tau_3 \otimes \mathbb{1}$, $\Gamma_2 = \tau_1 \otimes \mathbb{1}$, $\Gamma_3 = \tau_2 \otimes \sigma_3$ and $\Gamma_4 = \tau_2 \otimes \sigma_1$ and $\Gamma_5 = \tau_2 \otimes \sigma_2$. Here the τ Pauli matrices act in the (u, v) space and σ Pauli matrices act in the $(\uparrow, \downarrow)$ space. With additional symmetry constraints, the band crossing can happen in this case along one-dimensional curves in 3 dimensions and at points in 2 dimensions. Around such a band crossing the effective Hamiltonian can be linearised again to the form of Dirac equation. As noticed above, going from $3 + 1$- dimensions to lower dimensions, the $\gamma^\mu p_\mu$ term change to $\sigma^\mu p_\mu$ in the simplest case. This is related to change in the representation theory of the Lorentz group between the $3 + 1$ and $2 + 1$ dimensions.

A specific example where the above mentioned features of topological phases such as topological invariant, edge modes and the Dirac equation can be shown is a simple system called the Su-Schrieffer-Heeger(SSH) model. Its a one dimensional tight-binding model of a fermions on a lattice :

$$H = \sum_{i=1}^{N-1} (t + \delta t)c^\dagger_{Ai}c_{Bi} + (t - \delta t)c^\dagger_{Ai+1}c_{Bi} + \text{h.c} \tag{2.14}$$

where A,B are the two sublattice labels, δt is the dimerisation parameter. The dimerisation parameter is indicative of the coupling between neighboring sites that alternates along the chain and provides an energy scale, which manifests as a gap in the energy spectrum.

In the basis of sublattice degrees of freedom $\Psi = (c_A(k), c_B(k))^T$, the Fourier transformed Hamiltonian

is given by:

$$\mathcal{H} = \sum \Psi^{\dagger} H(k) \Psi(k) \quad H(k) = \vec{d}(k).\vec{\sigma} \tag{2.15}$$

Here,

$$d_x(k) = (t + \delta t) + (t - \delta t)\cos k, \quad d_y(k) = (t - \delta)\sin k, \quad d_z(k) = 0. \tag{2.16}$$

For small dimerisation parameter δt and focusing on the low energy states around $k \sim \pi + q$ and $q \to -i\partial_x$, the Dirac Hamiltonian is obtained:

$$H = -iv_F \sigma_1 \partial_1 + m(x)\sigma_2, \tag{2.17}$$

where $v_F = t$ and $m = 2\delta t$. Now if the spatial profile of m is that of a soliton (e.g a step function) $m(-\infty) > 0, m(-\infty) > 0$, there is a bound state at the domain wall of the two different dimerisation at zero energy. This zero-energy state is topologically protected and is related to the topological phase of the system. The wavefunction of this zero mode is given by :

$$\psi_0(x) = \exp\left(-\int_0^x m(x')dx' \right) \begin{pmatrix} 1 \\ 0 \end{pmatrix} \tag{2.18}$$

This is a fermionic Dirac mode and is the simplest example for the occurrence of edge modes in topological phases.

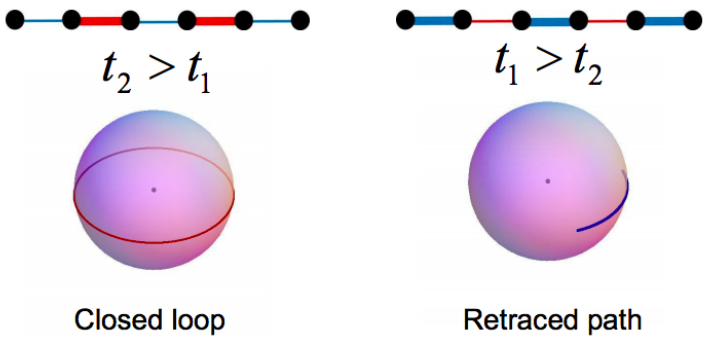

Figure 2.2: Two distinct phases of the Su-Schrieffer-Heeger model. For $t_1 > t_2$, the system is in a topological phase with an edge state as shown in the left. The vector $\vec{d}$ traces a full loop in the Brillouin zone leading to a topological invariant $\nu = 1$. For $t_1 < t_2$, one gets a trivial phase with no edge states and no winding in the Brillouin zone.

Topological invariant as a winding number– The term $\vec{d}(\vec{k})$ can be considered as a vector defined over the Brillouin zone. As the wavevector goes $k : 0 \to 2\pi$ it forms a loop in the Brillouin zone and $\vec{d}$ also forms a closed path in the d_x, d_y plane. For an insulating phase with a gap, the closed math avoids $\vec{d} = 0$ as the

Hamiltonian is not gapless. Since $d_z = 0$, the closed path forms a directed loop in the d_x, d_y plane as shown in Fig.(2.2) and can be associated with a 'winding number' . The winding number is then defined for a unit vector $\tilde{\vec{d}}$ as

$$\nu = \frac{1}{2\pi} \int \left(\tilde{\vec{d}} \times \frac{d}{dk} \tilde{\vec{d}} \right) dk \tag{2.19}$$

To calculate the topological invariant, introduce $h(k) = d_x(k) - id_y(k)$ and using $\ln(h) = \ln(|h|e^{iarg(h)})$, we get

$$\nu = \frac{1}{2\pi i} \int_{-\pi}^{\pi} dk \frac{d}{dk} \ln(h(k)) \tag{2.20}$$

Now one can obtain the topological invariants for different regimes of parameters $t_1 = t + \delta t, t_2 = t - \delta t$:

$$t_2 > t_1 : \nu = 1 \tag{2.21}$$

$$t_1 > t_2 : \nu = 0 \tag{2.22}$$

Now, we shall proceed to study a special form of solution to Dirac equation called the Majorana fermion and its avatar in the condensed matter setting called the Majorana bound state(MBS).

2.2 Majorana modes

2.2.1 General features

Majorana modes have become a topic of importance in condensed matter physics and high energy physics [6]. Their fundamental importance stems from their manifestation of a symmetry in the Dirac equation, which is the product of a beautiful confluence of Lorentz co-variance(special relativity) and quantum mechanics. Majorana fermions arise as 'real' solutions to the Dirac equation in that they are their own anti-particles. The emergence of Majorana quasiparticles in condensed matter physics is interesting in its own right and have additional fundamental significance that they have anyonic statistics in that setting. These Majorana modes occur in the topological phases of quantum matter as bounds states in vortices or at gapless boundaries.. Their properties as anyons allow their use in realising topological quantum computation. In this section, Majorana fermions are defined first in the simplest notion relevant for further discussions in the setting of condensed matter physics. Then, they are shown as solutions to the Dirac equation, as it appeared in the historical context.

Majorana fermions are defined as particles which are their own anti-particles. To understand what this means start with the notion of 'particle' that is represented by a creation operator $\hat{\psi}_a^\dagger$ acting on a 'vacuum'

state $|\Omega\rangle$. Here the sub-script 'a' represents any of the degrees of freedom such as momentum, spin or charge. Then the annihilation operator $\hat{\psi}_a$ represents an 'anti-particle' on the state $|\Omega\rangle$. One could think of $|\Omega\rangle$ as a many-body electron state, such as filled Fermi-sea and particle corresponds to the excitation over the Fermi-sea and the anti-particle corresponds to the 'hole' created by removing an electron from the Fermi-sea. These obey the canonical anti-commutation algebra corresponding to fermions. Now, consider the canonical transformation on these operators,

$$\hat{\psi}_a = \frac{\hat{\gamma}_{a1} + i\hat{\gamma}_{a2}}{2}; \quad \hat{\psi}_A^\dagger = \frac{\hat{\gamma}_{a1} - i\hat{\gamma}_{a2}}{2} \tag{2.23}$$

. The transformation preserves the algebra:

$$\{\hat{\gamma}_{a\alpha}, \hat{\gamma}_{b\beta}\} = \delta_{ab}\delta_{\alpha,\beta}; \quad \hat{\gamma}_{a\alpha}^\dagger = \hat{\gamma}_{a\alpha} \tag{2.24}$$

One can see from above that the operators $\hat{\gamma}_{a\alpha}$ obey the fermionic commutation relations and are identical to their own anti-particles. These are the Majorana fermions. In principle, the decomposition as shown above could be done in any condensed matter system with electrons, but the Majorana operators cannot be isolated as individual particles and are always part of the regular electrons. As will be seen in a later section, one can indeed obtain isolated Majorana modes as zero-energy, edge modes in topological superconductors.

2.2.2 Majorana's solution of Dirac's equation

Now, Majorana fermions are derived as solutions to the Dirac equation. In fact the notion of an 'anti-particle' is a natural outcome of Dirac's formulation. Majorana was seeking a theory which is symmetric with respect to the charge degree of freedom i.e a Dirac-like theory for neutral particles. Let us actually follow Majorana's formulation as presented in his original paper [52] as parts of it come close to resemble a tight binding Hamiltonian found in Kitaev's work. Majorana starts with the Lagrangian of a system with Hermitian(real) variables: q_is:

$$L = i\sum_{r,s}(A_{rs}q_r\dot{q}_s + B_{rs}q_rq_s) \tag{2.25}$$

Here A, B are real and $A_{rs} = A_{sr}$, $B_{rs} = -B_{sr}$ and $det|A| \neq 0$. Upon varying the Lagrangian and setting to zero, one obtains the Hamiltonian

$$H = -i\sum_{r,s} B_{rs}q_rq_s \tag{2.26}$$

assuming the anticommutation relations

$$q_r q_s + q_s q_r = \text{constant } \delta_{rs} \tag{2.27}$$

The equation of motion of such a Hamiltonian would give a Schrödinger like equation for real anti-commuting variables. Now Majorana, considers the Dirac equation and writes $\Psi = U + iV$, where U, V are real and chooses the following representation for the gamma matrices:

$$\tilde{\gamma}^0 = \begin{pmatrix} 0 & \sigma^2 \\ \sigma^2 & 0 \end{pmatrix} \quad \tilde{\gamma}^1 = \begin{pmatrix} i\sigma^3 & 0 \\ 0 & i\sigma^3 \end{pmatrix} \quad \tilde{\gamma}^2 = \begin{pmatrix} 0 & -\sigma^2 \\ \sigma^2 & 0 \end{pmatrix} \quad \tilde{\gamma}^3 = \begin{pmatrix} -i\sigma^1 & 0 \\ 0 & -i\sigma^1 \end{pmatrix} \tag{2.28}$$

Each of them individually follow Dirac's equation:

$$(i\tilde{\gamma}^\mu \partial_\mu - m)U = 0 \tag{2.29}$$

and an identical one for V. Now Majorana argues that such an equation can be derived from a quantization procedure outlined above for anti-commuting, real and continuous variables U, V. One starts with a Lagrangian quadratic in U or V similar to Eq. 2.25 and obtains the above real-Dirac equation. From this he concludes : *"It is remarkable, however, that the part of the formalism which refers to U (or V) can be considered, in itself, as the theoretical descriptions of some material system, in conformity with the general methods of quantum mechanics....constitute the simplest theoretical representation of neutral particles.'*. Thus Majorana showed the possibility of anti-commuting fields being their own anti-particles. These real fields are termed today as *" Majorana fermions"*.

2.2.3 Majorana zero modes in superconductors and anyonic statistics

Now we shall turn to the physical setting of superconductors which provide a platform for emergence of Majorana quasiparticles. The mere change in representation as shown in Eq. 2.23 is manifest physically in the superconductors where quasiparticles occur as coherent superposition of particles and holes. A typical BCS ('s-wave' order parameter) superconducting phase is formed by (i) Cooper-pairing of electrons of opposite spins and momenta and (ii)condensation of the Cooper pairs to a ground state. Now, exciting an electron from one of these pairs would leave a 'hole' in the condensate and leads to a 'Bogoliubov quasiparticle' which is superposition of the electron and a hole:

$$\gamma_k = u c_{k\uparrow} + v c^\dagger_{-k\downarrow}, \tag{2.30}$$

very much similar to the requirement in Eq. 2.23 except for the spin structure. However an equal superposition of particle and holes of same spin species would form a Majorana particle, which is its own antiparticle. Cooper pairing of electrons with same spins can occur if the 'Cooper pair wavefunction' or the corresponding order parameter has an odd parity part. This is satisfied in a p-wave or a $p_x + ip_y$ superconductor. Such system can be shown to host Majorana zero-modes .

To see this one starts with a mean-field description of a 'spin-less' superconductor in terms of the Bogoliubov-deGennes Hamiltonian written in the Nambu basis $(c_k, c^\dagger_{-k})$:

$$H = \sum_k \begin{pmatrix} c^\dagger_k & c_{-k} \end{pmatrix} H_{BdG}(k) \begin{pmatrix} c_k \\ c^\dagger_{-k} \end{pmatrix}, \tag{2.31}$$

where H_{BdG} is the Bogoliubov-deGennes Hamiltonian

$$H_{BdG}(k) = \begin{pmatrix} h_0(k) & \Delta(k) \\ \Delta^\dagger(k) & -h_0^T(k) \end{pmatrix} \tag{2.32}$$

Here Δ is the superconducting order parameter and h_0 is the kinetic part of the Hamiltonian. The Bogoliubov quasi-particles are of the form $\gamma_k = u_k c_k + v_k c^\dagger_{-k}$. The eigenvalue equations will be:

$$\begin{pmatrix} h_0 & \Delta \\ \Delta^\dagger & -h_0^T \end{pmatrix} \begin{pmatrix} u \\ v \end{pmatrix} = E \begin{pmatrix} u \\ v \end{pmatrix} \tag{2.33}$$

The Hamiltonian has an anti-unitary particle-hole symmetry $\mathcal{C}$

$$\mathcal{C} H_{BdG}(k) \mathcal{C}^{-1} = -H_{BdG}(k) \tag{2.34}$$

The symmetry transformation is of the form $\mathcal{C} = \tau_x K$, where τ_x is the Pauli matrix in the Nambu basis and K is the complex conjugation. The transformation acts on the energy eigenstates as $\mathcal{C}\Psi_E = \Psi_{-E}$ which implies for the Bogoliubov quasiparticles

$$\gamma^\dagger_E = \gamma_{-E} \tag{2.35}$$

At zero-energy this would satisfy the Majorana condition $\gamma^\dagger_0 = \gamma_0$ thus forming an isolated Majorana quasiparticle.

Non-Abelian braiding statistics: The Majorana zero modes are of importance not only for their fundamental Majorana nature but also due to their exchange statistics. In the case of exchanging two fermions

or bosons, the wavefunction describing the two particles gets an overall sign of ± 1: $\psi(r_1, r_2) \rightarrow e^{i\theta}\psi(r_2, r_1)$, where $\theta = 0, \pi$ for bosons and fermions respectively. In the case of anyons, the phase θ can take any value between 0 and π. The angle 'θ' is called the exchange angle of that anyon. As we shall see below, in the case of Majorana modes the angle can be matrix-value and the order of exchange matters , as result of which the MBS are called 'non-Abelian anyons'.

The simplest instance of non-Abelian exchange involves four MBSs, say denoted by γ_1, γ_2, γ_3, γ_4. As mentioned already, these Majorana modes in a condensed matter setting occur as isolated zero energy modes trapped in a vortex or at the edge of a topological superconductor. In principle, these isolated modes can be transported to braid their trajectories and study the exchange statistics. The details of how they are realized does not matter for this discussion as the exchange statistics is their inherent nature. ,As shown in Eq.2.23, a Dirac fermion can be split into two Majorana fermions. Given a pair of Majorana fermions, one can also define a Dirac state. Given four Majorana operators, we can construct 2 Dirac states. As a specific choice, consider $c_A = (\gamma_1 + i\gamma_2)/2$,$c_B = (\gamma_3 + i\gamma_4)/2$. The Dirac states c_i have an occupation number given by $N_i = c_i^\dagger c_i$, which is equal to 1 if occupied and 0 is empty. These Dirac operators act on the ground state that contains the Majorana modes: $c_i^\dagger |0\rangle = |1\rangle$. In the presence of four zero energy MBS, the ground state is then degenerate and has the following possibilities:

$$|N_A, N_B\rangle : |0,0\rangle, |1,1\rangle, |1,0\rangle, |0,1\rangle \tag{2.36}$$

where N_A, N_B denote the occupation of the electronic states. For N pairs of MBSs, the ground state is 2^N fold degenerate. N_i determines the fermion parity of the ground state, which will become our central aspect of study in later sections. The occupation of all the parity states decides the net fermionic parity of the ground of the system. Thus unlike conventional superconducting ground state, which is always a superposition of states having an even number of electrons in form of Cooper pairs, a topological superconductor can have states with net fermion parity either even or odd, depending on the occupation of the modes created by combining the Majoranas .

The simplest braiding operation is an exchange in the positions of the two MBSs. How does this exchange in the position space affect the space of ground states? It can be shown that [53] the exchange of two Majoranas γ_i,γ_j is represented in the ground state manifold as a unitary rotation in the space $\{|0,0\rangle, |1,1\rangle, |1,0\rangle, |0,1\rangle\}$ given by

$$U_{ij} = exp(\pm i\pi\gamma_i\gamma_j/4). \tag{2.37}$$

For example, if one starts with a state $|0,0\rangle$, then exchanging γ_2, γ_3 results in

$$U_{23}\,|0,0\rangle = (|0,0\rangle - i\,|1,1\rangle)/\sqrt{2} \tag{2.38}$$

In principle, one can track such rotations by measuring the fermion occupation i.e the fermion parity of the electronic states in the ground-state manifold. The order of consecutive exchanges matter as the unitary operations do not commute: $U_{12}U_{23} \neq U_{23}U_{12}$. Thus the name non-Abelian rotation. Now that we have studied the salient aspects of MBS, we shall commence a detailed study of the Kitaev's model Hamiltonian for realizing MBS in one dimension.

2.3 The Kitaev chain

The model and phase diagram–

In this section we will consider the simplest and paradigmatic model for topological supercoductor in one-dimension, the Kitaev chain. This was proposed by Kitaev in 2000 [47]. As seen in the section on the Dirac equation, Majorana's original paper already had a Hamiltonian of discrete, real 'Majorana' variables. The mathematical form of the Kitaev chain as a quadratic, fermionic Hamiltonian on a lattice appeared in the works of Lieb, Schulz and Mattis [54] and [55] . This was in the context of spin chain physics, where the spin variables are converted to fermionic operators through a non-local transformation. Kitaev's insight was in the identification of this Hamiltonian as a model for a topological p-wave superconductor and occurrence of an isolated Majorana zero modes at the edge in the topological phase of the model. Historically, this was set in the context of previous works which discovered Majorana modes as quasiparticles in fractional quantum Hall phases [56].Kitaev's further insight was the possible use of the MBS for topological quantum computation.

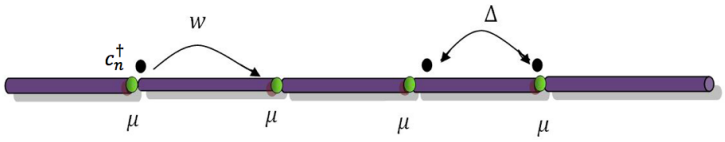

Figure 2.3: Kitaev chain - A lattice model of fermions in one-dimension, with hopping parameter w, Superconducting gap Δ and onsite chemical potential μ.

This lattice model consists of non-interacting spinless fermions on each site having nearest neighbor tunneling of strength w, nearest neighbor superconducting pairing of strength Δ, and an on-site chemical

potential μ_n (Fig. 2.3).Its associated Hamiltonian takes the form

$$H = \sum_{n=1}^{N-1} (-w c_{n+1}^{\dagger} c_n + \Delta c_{n+1}^{\dagger} c_n^{\dagger} + h.c) - \sum_{n=1}^{N} \mu_n (c_n^{\dagger} c_n - 1/2), \tag{2.39}$$

where $h.c.$ denotes Hermitian conjugate. Here, the $c_n^{\dagger}$ and c_n operators represent the creation and annihilation of electrons on site n, respectively. They obey the fermionic commutation relations $\{c_m, c_n\} = 0$ and $\{c_m, c_n^{\dagger}\} = \delta_{mn}$. In the thermodynamic limit (infinite wire) or for a closed chain, one can transform the Hamiltonian into Fourier space, and the single particle energy spectrum takes the form

$$E_k = \pm\sqrt{(2w\cos k + \mu)^2 + 4\Delta^2 \sin^2 k}. \tag{2.40}$$

The system exhibits multiples phases as shown in the Fig. **??**. The spectrum has a finite superconducting gap in all the phases except at the 'critical lines' $\mu/2w = 1$ and $\Delta = 0$(represented as dark lines in the figure). The gap vanishes as one crosses one of the 'critical lines' and reopens upon entering another phase. The study of isolated Majorana modes become transparent if the Hamiltonian is transformed to the Majorana basis. Let us introduce $2N$ Majorana fermion operators $\hat{a}_n$ and $\hat{b}_n$, namely, $\hat{a}_n = c_n + c_n^{\dagger}$ and $\hat{b}_n = i(c_n^{\dagger} - c_n)$. The Majorana operators satisfy the relations $\hat{a}_n^{\dagger} = \hat{a}_n$, $\hat{b}_n^{\dagger} = \hat{b}_n$ and $\{\hat{a}_n, \hat{a}_m\} = \{\hat{b}_n, \hat{b}_m\} = 2\delta_{mn}$. In terms of the Majorana operators, the Hamiltonian is given by

$$\begin{aligned} H_M &= -\frac{i}{2} \sum_{n=1}^{N-1} \left[(w - \Delta) \hat{a}_n \hat{b}_{n+1} - (w + \Delta) \hat{b}_n \hat{a}_{n+1} \right] \\ &\quad - \sum_{n=1}^{N} \frac{i\mu_n}{2} \hat{a}_n \hat{b}_n. \end{aligned} \tag{2.41}$$

Now let us look at the different phases of this model. The phases I and II are topologically non-trivial and, in the thermodynamic limit, have zero energy Majorana modes bound to the ends of the wire, whereas such modes are absent in the topologically trivial phases III and IV. These Majorana modes have finite support at the ends and decay rapidly into the bulk with a decay length proportional to the reciprocal of the bulk gap. One can understand the existence of the Majorana end modes by considering the extreme limit of $w = \Delta$ and $\mu = 0$. The Hamiltonian reduces to $H = iw \sum_n b_n a_{n+1}$. The Majorana operators a_1 and b_N are not paired with any other operators in the system and therefore do not appear in the Hamiltonian. These isolated modes correspond to the zero energy eigenvectors localized at the ends. The existence of these modes is robust even away from this extreme limit and they only disappear with the closing of the

bulk gap.

The ground state of the system in the topological phase is thus doubly degenerate and has two zero energy eigenvalues corresponding to the Majorana modes. These Majorana modes can be combined to form two complex Dirac fermion states, which can be either empty or occupied. Hence, each of the degenerate ground states has a specific fermion parity and the system can be characterized by a related Z_2-valued topological invariant.

Class D: The existence of the zero-energy modes is in fact a manifestation of the symmetry and the topology of the system. As described in one of the previous sections, the anti-unitary symmetries completely classify topological phases that can occur in gapped non-interacting fermionic systems and also provide the topological invariant in different dimensions. In the present case of a spin-less superconductor, there is the particle-hole symmetry as described above but no time-reversal symmetry. This identifies the system in class D and in one dimension, such a system is characterized by a $\mathcal{Z}_2$ topological invariant. One can calculate the invariant as a winding number from the Dirac form of the Hamiltonian in k-space [5]. This invariant also counts the number of zero modes in the topological defects such as vortices or the edges of the system.

Dirac equation and the edge mode: Finally let us see the emergence of the Dirac equation in the Kitaev Hamiltonian and show that the zero energy solution corresponds to the Majorana mode. By Fourier transforming the Hamiltonian in Eq. 2.39,

$$H_{BdG} = \frac{1}{2}\sum_{p} \Psi_k^\dagger \begin{pmatrix} -2w\cos k - \mu & 2i|\Delta|\sin k \\ -2i|\Delta|\sin k & 2w\cos k + \mu \end{pmatrix} \Psi_k \tag{2.42}$$

where $\Psi_k = (c_k c_{-k}^\dagger)^T$ is the Nambu-spinor. When this is expanded near $k \approx 0$ and $k \to i\partial_x$ one obtains

$$H_{BdG}(k) = |\Delta|(i\partial_x)\sigma_1 - \mu\sigma_3. \tag{2.43}$$

This is the Dirac Hamiltonian. To obtain the Majorana modes, consider the solitonic profile of the chemical potential- $\mu(x)$: $\mu(-\infty) < 0$ and $\mu(+\infty) > 0$. The zero energy solution of the BdG Hamiltonian is

$$\gamma_M = N\int dx \frac{e^{i\pi/4}}{\sqrt{2}} exp\Big(-\frac{1}{|\Delta|}\int_0^\infty \mu(x')dx'\Big)(c(x) - ic^\dagger(x)), \tag{2.44}$$

where N is the normalization. Thus we have seen that the Kitaev chain Hamiltonian is a simple lattice realization of a one-dimensional topological superconductor and harbors Majorana modes at the edges.

2.4 Mapping between the Kitaev chain and the transverse field XY-spin chain

As mentioned before, one of the first instances when the fermionic Kitaev chain Hamiltonian appeared was in the study of the one-dimensional quantum spin chain [54, 55]. The Hamiltonian for the XY-spin chain in the presence of a transverse field is given by

$$H = -\sum_{n=1}^{N-1}(J_x\sigma_{n+1}^x\sigma_n^x + J_y\sigma_{n+1}^y\sigma_n^y) - h\sum_{n=1}^{N}\sigma_n^z \tag{2.45}$$

where $\sigma_n^x, \sigma_n^y, \sigma_n^z$ are quantum spins located at the nth site in a one-dimensional lattice. The co-efficients J_x, J_y, J_z are the coupling between the neighboring spins. The spins obey the commutation relations $[\sigma^a, \sigma^b] = 2i\epsilon^{abc}\sigma^c$. The Jordan-Wigner transformation expresses these spins in terms of the fermions through a non-local transformation:

$$\sigma_n^z = 2c_n^\dagger c_n - 1, \tag{2.46}$$

$$\sigma_n^- = \frac{1}{2}(\sigma_n^x - i\sigma_n^y) = c_n \exp i\pi\sum_{j}^{n-1} c_j^\dagger c_j \tag{2.47}$$

$$\sigma_n^+ = \frac{1}{2}(\sigma_n^x + i\sigma_n^y) = c_n^\dagger \exp i\pi\sum_{j}^{n-1} c_j^\dagger c_j \tag{2.48}$$

where c_n obey the fermionic commutation $\{c_m, c_n^\dagger\} = \delta_{mn}, \{c_m, c_n\} = 0$. The spin chain Hamiltonian is then transformed to :

$$H = \sum_{n=1}^{N-1}[-(J_x + J_y)(c_n^\dagger c_n + 1 + \text{h.c}) + (J_x - J_y)(c_n^\dagger c_{n+1}^\dagger + \text{h.c})] \tag{2.49}$$

$$- (-1)_f^N[-(J_x + J_y)(c_N^\dagger c_1 + \text{h.c}) + (J_x - J_y)(c_1^\dagger c_N^\dagger + \text{h.c})] - \sum_{n=1}^{N}(2c_n^\dagger c_n - 1) \tag{2.50}$$

This is of the form 2.39 with identification $w = J_x + J_y$, $\Delta = J_x - J_y$ and $\mu = -2h$. The Majorana operators are rleated to the spins through the transformation $a_n = \prod_{j=1}^{n-1}\sigma_j^z\sigma_n^x$, $b_n = \prod_{j=1}^{n-1}\sigma_j^z\sigma_n^y$ for $2 \leq n \leq N$, $a_1 = \sigma_1^x$ and $b_1 = \sigma_1^y$. The phase diagram Fig. 2.4 also depicts the phases of the spin chain, where phases I and II are the ferromagnetic phases and phases III and IV are the paramagnetic phases [57]. This mapping between the two systems, even though non-local, helps in transferring insights between the two systems. This will be explicitly explored in the context of the Majorana wave function physics in the Kitaev chain.

2.5 Majorana wave function physics

Now that certain key features of Majorana modes, Kitaev chain and experimental realisations are reviewed we shall go to an indepth study of the various features of the Majorana wavefunction. The following sections are based on my original work presented in the paper [43].

2.5.1 Majorana transfer matrix and Lyapunov Exponent

The classification of topological phases, presented in the beginning of the chapter, characterized different phases through topological invariants and the invariants predict the existence of edge modes at the boundary to another topological phase or a vacuum. The formalism is also intricately connected to localisation physics of wavefunctions [46] for different ensembles of Hamiltonians. Specifically, the localization physics of the boundary modes are characterized by the topological phases. Here we shall explicitly study this aspect in the context of MBS in the Kitaev chains. Here we use the transfer matrix method to study the localization, delocalisation and oscillations of the Majorana wave functions.

The transfer matrix method is designed to study the manner in which wave functions propagate through the length of a system. It thus offers a natural means of probing localization aspects of Majorana end modes and the topological characteristics of the Kitaev chain. In [57, 58], the Majorana transfer matrix formalism has been employed for determining the topological invariants and charting the phase diagram of the Kitaev chain in the presence of different potential landscapes [57, 58] .

Here we briefly recapitulate this Majorana transfer matrix technique and the associated Lyapunov exponent description. Given the Majorana Hamiltonian of Eq.2.41, we first obtain the zero energy Heisenberg equation of motion $[\hat{a}_n, H_M] = 0$ for the Majorana operators $\hat{a}_n$. Using this, we obtain the equation for Majorana wave functions a_n as :

$$(w + \Delta)a_{n+1} + (w - \Delta)a_{n-1} + \mu a_n = 0. \tag{2.51}$$

(Note that the 'a' without a hat is the Majorana wave function and not the operator itself.) For $2 \leq n \leq N-1$, the modes at different sites are thus related by the transfer matrix:

$$\begin{aligned} \begin{pmatrix} a_{n+1} \\ a_n \end{pmatrix} &= A_n \begin{pmatrix} a_n \\ a_{n-1} \end{pmatrix}, \\ \text{where } A_n &= \begin{pmatrix} -\frac{\mu_n}{w+\Delta} & -\frac{w-\Delta}{w+\Delta} \\ 1 & 0 \end{pmatrix}. \end{aligned} \tag{2.52}$$

The transfer matrix for b_n modes have an identical structure except with a change in the sign in Δ. From this point on, $w = 1$ unless specified . We only consider Δ positive. Our results for the negative half of the phase diagram are the same except that the roles of a and b are switched. The full chain transfer matrix is given by an ordered product of all the transfer matrices from the first site to the last: $\mathcal{A} = \prod_n A_n$. The eigenvalues of the full transfer matrix, $\lambda_\pm$, determine features of the Majorana mode wavefunctions, such as oscillation and decay. The eigenvalues can be used to construct a topological invariant which determines whether or not the system is in the topological phase based on Majorana wavefunction normalizability [57]. Specifically, if the number of eigenvalues within the unit circle of a complex plane is even, then the system is in a topologically non-trivial phase.

A useful quantity to extract from transfer matrices is the Lyapunov exponent (LE), which in most cases relates to the inverse localization length of the corresponding wave function. For the purpose of analyzing a Majorana bound state at one end of the Kitaev chain, consider the Lyapunov exponent for a semi-infinite system having a boundary at one end, defined as

$$\gamma(\mu, \Delta) = \lim_{N\to\infty} \frac{1}{N} \ln[|\lambda|] \tag{2.53}$$

The largest of the two eigenvalues $\lambda_\pm$ is taken for the definition. In the topological phase the LE is always negative and a topological phase transition occurs when it crosses zero to become positive. This can be understood from the fact that the topological phase has the Majorana mode exponentially localised at the edge as was shown in Eq. 2.44 for the continuous case .Thus starting from one edge the Majorana wavefunction decays into the bulk. This is captured with a negative LE of the transfer matrix. On crossing the critical point the Majorana mode delocalises and the LE goes to zero. Thus the loci of points of zero LE give the phase boundary [57]. Here, the LE is considered not only as a probe of this topological phase transition but also to investigate detailed features of the Majorana wave function.

Mapping to a nnon-superconducting system– In obtaining the LE for a generic potential landscape, the Majorana transfer matrix could be mapped to that of the transfer matrix of a normal system without a superconducting gap. The map proves powerful in that knowledge of normal state wavefunction properties immediately leads to those of the topological superconducting chain. This map is achieved through the following similarity transformation on the transfer matrix in Eq.[2.52] [58], defined for $0 < \Delta < 1$:

$$A_n = \sqrt{l_\Delta} S \tilde{A}_n S^{-1} \tag{2.54}$$

where $S = diag(l_\Delta^{1/4}, 1/l_\Delta^{1/4})$ and $l_\Delta = \frac{1-\Delta}{1+\Delta}$. The matrix $\tilde{A}_n$ is the transfer matrix for a normal tight-binding

model in the absence of a superconducting gap (Note that $w = 1$ compared to Eq.2.52). Its on-site chemical potential terms are rescaled by the transformation $\mu_n \to \mu_n/\sqrt{1-\Delta^2}$. Explicitly, the full chain transfer matrix is given by

$$\mathcal{A}(\mu_n, \Delta) = \left(\frac{1-\Delta}{1+\Delta}\right)^{N/2} S\tilde{\mathcal{A}}(\mu_n/\sqrt{1-\Delta^2}, \Delta = 0)S^{-1} \tag{2.55}$$

This map allows the Lyapunov exponent to be written as a sum of two components, $\gamma(\mu, \Delta) = \gamma_S + \gamma_N$, one that depends purely on the superconducting gap $\gamma_S(\Delta)$ and the other corresponding to the underlying normal tight-binding model $\gamma_N(\mu/\sqrt{1-\Delta^2})$. Such a splitting of the Lyapunov exponent was already hinted in Ref. [59] and the mapping to the normal system in the context of scattering matrices in Ref.[60]

In the following sections, the Majorana transfer matrix, the Lyapunov exponent and the mapping to a normal system will be used to study the oscillations in Majorana wave functions and associated fermion parity switches in both uniform and disordered chains.

2.5.2 Majorana wave functions and oscillations

The generic transfer matrix given in Eq. 2.52 directly provides information on the Majorana end mode decay profile and oscillatory behavior. Given this matrix for a single slice of the chain, the full-chain transfer matrix is given by $\mathcal{A} = \prod_n A_n$. The eigenvalue equation for the transfer matrix is given by

$$\lambda^2 + \mathrm{Tr}(\mathcal{A})\lambda + \det(\mathcal{A}) = 0 \tag{2.56}$$

Given that $\det(A_n) = (\frac{1-\Delta}{1+\Delta})$, $\det(\mathcal{A}) = \prod_n^N \det(A_n) = (\frac{1-\Delta}{1+\Delta})^N$. Thus, the two eigenvalues of the full transfer matrix take the form

$$\lambda_\pm = \frac{\mathrm{Tr}\mathcal{A}}{2} \pm \sqrt{\left(\frac{\mathrm{Tr}\mathcal{A}}{2}\right)^2 - \left(\frac{1-\Delta}{1+\Delta}\right)^N} = e^{\pm i\beta}\left(\frac{1-\Delta}{1+\Delta}\right)^{N/2}. \tag{2.57}$$

Here, the phase β can only be real or imaginary depending on the value of $\mathrm{Tr}\mathcal{A}$ given its structure,

$$\beta = \tan^{-1}\left(\frac{\sqrt{(\frac{1-\Delta}{1+\Delta})^N - (\frac{\mathrm{Tr}\mathcal{A}}{2})^2}}{\frac{\mathrm{Tr}(\mathcal{A})}{2}}\right). \tag{2.58}$$

This phase β, which is a function of μ,Δ and N plays an important role in determining the nature of the Majorana wave function.

One can see that if β is real, the eigenvalues are complex and the wave functions have an oscillatory component in addition to the exponentially decaying envelope $(\frac{1-\Delta}{1+\Delta})^{N/2}$. When β becomes purely imaginary,

then the eigenvalues are purely real, corresponding to over damped wave functions. The specific conditions for the phase β to change from real to imaginary depends on the specific potential landscape. In general, the phase β alone tracks the response to different potential landscapes, while the scaling factor $(\frac{1-\Delta}{1+\Delta})^{N/2}$ is responsible for the localization of the Majorana mode irrespective of the potential μ_n.

Now, using the similarity transformation Eq.2.55, it can be seen that this phase factor is completely determined by a simple underlying tight-binding problem that lacks a superconducting gap. The transformed transfer matrix for a single μ_n can be easily seen to be a simple tight-binding model as follows:

$$\tilde{A}_n \quad = \quad \begin{pmatrix} -\frac{\mu_n}{\sqrt{1-\Delta^2}} & -1 \\ 1 & 0 \end{pmatrix}. \tag{2.59}$$

The Heisenberg equation for the wave function $\tilde{a}_n$ corresponding to the above transfer matrix equation is explicitly of the normal tight-binding form:

$$(\tilde{a}_{n+1} + \tilde{a}_{n-1}) + \frac{\mu_n}{\sqrt{1-\Delta^2}}\tilde{a}_n = 0. \tag{2.60}$$

Since the similarity transformation S is purely a function of Δ and does not depend on the individual μ_n, the full chain transfer matrices respect the relationship

$$\prod_n A_n = (\sqrt{l_\Delta})^N S(\prod_n \tilde{A}_n(\mu_n/\sqrt{1-\Delta^2}))S^{-1} \tag{2.61}$$

Since the similarity transformation preserves the trace, the full chain transfer matrix traces are related as

$$\mathrm{Tr}(\mathcal{A}) = (\sqrt{l_\Delta})^N \mathrm{Tr}(\tilde{\mathcal{A}}) \tag{2.62}$$

where $\tilde{\mathcal{A}}$ is the full chain transfer matrix for the underlying normal tight-binding model. Using this identity in the expression for β in Eq.2.58, one obtains

$$\beta = \tan^{-1}\left(\frac{\sqrt{1-(\frac{\mathrm{Tr}\tilde{\mathcal{A}}}{2})^2}}{\frac{\mathrm{Tr}(\tilde{\mathcal{A}})}{2}}\right) \tag{2.63}$$

Thus the phase factor β of the Majorana transfer matrix is solely determined by an underlying normal tight-binding model without a superconducting gap, but with a scaled on-site chemical potential $\mu_n/\sqrt{1-\Delta^2}$. Therefore, oscillations of the Majorana wave function and the behavior in a specific potential landscape are completely determined by properties of the underlying normal state chain.

It is precisely these oscillations in Majorana zero modes which determine the degeneracy-splitting of the ground state in a finite sized Kitaev chain and associated fermion parity switches. Further they also have direct bearing on the oscillations in the spin-spin correlation functions of transverse field XY spin chain, to which there is an exact mapping from the Kitaev chain. The fact that these oscillations can be obtained from a simple tight-binding model easily enables one to extend the study to disorder, periodic and quasi-periodic potential landscapes.

Further, the division of Majorana wave function into the two features of oscillations and decay manifests as an additivity in the Lyapunov exponent (LE). Invoking the definition of the LE in Eq. 2.53, $\gamma(\mu, \Delta) = \lim_{N\to\infty} \ln[|\lambda|]/N$ and referring back to the expression for the eigenvalues in Eq. 2.57, consider the two cases of purely real and purely imaginary β:

(i) When β is real, $|\lambda_{\pm}| = (\frac{1-\Delta}{1+\Delta})^{N/2}$. Therefore, the LE is only given by $\gamma_S = -\frac{1}{2}\ln(\frac{1+\Delta}{1-\Delta})$. γ_S is termed as the 'superconducting' component of the LE. In this case the LE is always negative assuming a finite, positive superconducting gap. This implies that the system is in the topological phase. Moreover, β gives rise to an oscillatory piece in the Majorana wave function.

For a small superconducting gap, on expanding in terms of small Δ, it can be seen that $\gamma_S \sim -\Delta$. In the continuum limit, the wave function of the Majorana mode has an exponentially decaying envelope $e^{-x/\xi}$, where $\xi \sim 1/\Delta$ is the superconducting coherence length, which characterizes the localization of the Majorana mode deep in the topological phase. Thus the superconducting component of the LE corresponds to the localization of the Majorana mode at the edge, protected by the superconducting gap. These localization features are immune to any perturbations that do not close the gap.

(ii) When β is purely imaginary, the phase factor $e^{i\beta}$ is real. As a result, the LE contains two terms. Since $|\lambda_{\pm}| = e^{\mp|\beta|}(\frac{1-\Delta}{1+\Delta})^{N/2}$, the LE is given by (considering only the largest eigenvalue):

$$\begin{aligned} \gamma &= \lim_{N\to\infty} \frac{1}{N}\ln|\exp(i\beta(\mu, \Delta, N))| - \frac{1}{2}\ln(\frac{1+\Delta}{1-\Delta}) \\ &= \lim_{N\to\infty} \frac{1}{N}\beta(\mu, \Delta, N) - \frac{1}{2}\ln(\frac{1+\Delta}{1-\Delta}) \qquad (2.64) \\ &= \gamma_N + \gamma_S \qquad (2.65) \end{aligned}$$

The LE is thus a sum of two components $\gamma_N + \gamma_S$, where γ_N is the 'normal component' and γ_S is the 'superconducting component' discussed in case i) above and in Ref.[58]. The 'normal component' takes the form $\gamma_N = \lim_{N\to\infty} \frac{1}{N}\ln|\exp(i\beta(\mu, \Delta, N))|$; it corresponds to the LE of a one-dimensional normal tight-binding model having a general potential landscape represented by a scaled on-site chemical potential [59]. To be specific, the tight-binding problem considered now contains onsite terms μ_n, which are scaled by a

factor involving Δ , thus giving a LE of the form $\gamma_N(\mu_n/\sqrt{1-\Delta^2}, 0, N)$ [58]. For a given Δ and number of lattices sites, N, in the Kitaev chain, we thus need only solve the underlying normal tight-binding problem. While the 'superconducting' component is always present in the LE in the presence of a gap, the 'normal component' depends on the specific potential landscape under consideration. In the context of disorder, this enables one to use known results from the vast literature of Anderson localization to readily comment on the features of Majorana modes in Kitaev chain.

2.5.3 New feature in the phase diagram: Circle of oscillations

In the case of a homogeneous wire in which the the on-site chemical potential takes on the same value on each site, we can exactly analyze features of the previous sub-section concerning Majorana wave function decay and oscillations. As discussed below, the exact wave function can be obtained by solving the difference equation Eq.2.51 by using the Z-transform method, which is an equivalent of Laplace transform for functions of discrete variables. For the homogeneous case, the equation of motion is a second order difference equation having constant co-efficients :

$$(1+\Delta)a_{n+1} + (1-\Delta)a_{n-1} + \mu a_n = 0. \tag{2.66}$$

The solution to the above equation proceeds by introducing a power series

$$A(z) = \sum_{n=0}^{\infty} z^{-n} a_n \equiv \mathcal{Z}[a_n], \tag{2.67}$$

where z is a complex variable. The function $A(z) = \mathcal{Z}[a_n]$ is called the Z-transform of a_n. Taking the Z-transform of the above difference equation and using properties such as : $\mathcal{Z}\{a_{n-1}\} = z^{-1}A(z)$, $\mathcal{Z}\{a_{n+1}\} = zA(z) - za_0$,($a_0$ is a constant determined by boundary conditions) one can obtain a closed form expression for the Z-transform $A(z)$, given by:

$$A(z) = \frac{a_0 z^2}{z^2 + \frac{\mu}{1-\Delta} z + \frac{1+\Delta}{1-\Delta}} \tag{2.68}$$

This Z-transform has a unique inverse, which is the exact solution to the difference equation. Thus the obtained wave function is of the form

$$a_n = a_0 C^n \left[\cos(\beta n) + \frac{1}{\tan\beta} \sin(\beta n) \right]. \tag{2.69}$$

Here, the constant $C = (\frac{1-\Delta}{1+\Delta})^{1/2}$ explicitly reflects the superconducting component and $\beta = \arctan \frac{\sqrt{4-4\Delta^2-\mu^2}}{\mu}$ the phase in Eq.2.58. Thus, as shown in the phase diagram of Fig. 2.5, the phase β takes on real values only within the circular regime $\mu^2 < 4(1-\Delta^2)$. We call this regime the circle of oscillations (COO); the reality condition on the phase β renders the Majorana wavefunctions oscillatory. Outside this regime, the oscillating terms of Eq.2.69 become hyperbolic and the modes, instead of oscillating, become overdamped[43, 61].

This circle of oscillations (COO) has also long been identified in the context of the transverse-field XY spin chain, to which the Kitaev chain can be exactly mapped using the Jordan-Wigner transformation. This circle, termed as the disorder circle, separates the regime of oscillations in spin-spin correlation functions from the regime of no oscillations[62]. Exactly on the circular locus, the ground state becomes separable and can be expressed as a direct product state [63, 64]. As a result, certain entanglement measures, such as the global geometric entanglement, vanish on this locus [65]. Another measure, the 'entanglement range', diverges and reflects a change in the pattern of entanglement across this circle [66]. There are similar oscillations in the entanglement spectrum within the circle [67]. These aspects in spin chains might have some bearing on the features of Majorana modes. In fact, some aspects of Majorana physics can be used to obtain results in spin chains very easily, which otherwise involve cumbersome calculations, as already pointed out in Ref.[57].

An understanding of the nature of the wave functions oscillations can be obtained using the underlying tight-binding problem resulting from the similarity transformation of Eq.2.55. For the homogeneous case, the equation of motion for the underlying normal model takes the form

$$(\tilde{a}_{n+1} + \tilde{a}_{n-1}) + \frac{\mu}{\sqrt{1-\Delta^2}}\tilde{a}_n = 0 \tag{2.70}$$

Here $\tilde{a}_n$ is the wave function describing the Majorana mode under the envelope coming form the gap Δ . Solutions to this equation have the plane-wave form $\tilde{a}_n = D_n e^{\pm ikn}$. Simplifying the equation, we get $2w\cos k + \frac{\mu}{\sqrt{1-\Delta^2}} = 0$. This relationship imposes the condition that the modes oscillate/propagate only in the region

$$\frac{\mu}{\sqrt{1-\Delta^2}} < 2 \tag{2.71}$$

If the above condition is not satisfied, the solutions lie outside the band of propagating modes and are purely decaying. Now recasting the above condition, we obtain the relationship : $\mu^2/4 + \Delta^2 = 1$, which is precisely the equation for the circle of oscillations(COO). Thus, mapping the original Majorana problem to an underlying tight-binding problem, we obtain a picture of the mechanism responsible for oscillations in Majorana modes and how these oscillations immediately vanish outside the circle.

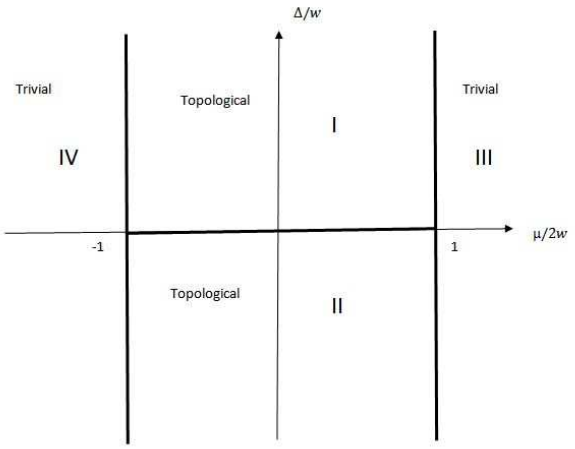

Figure 2.4: The phase diagram of the one-dimensional Kitaev Hamiltonian for the Majorana wire. Phases I and II are topologically non-trivial and have Majorana end modes, whereas phases III and IV are topologically trivial. The thick lines $\mu = \pm 2w$ and $\Delta = 0$ are the quantum critical lines where the bulk gap vanishes.

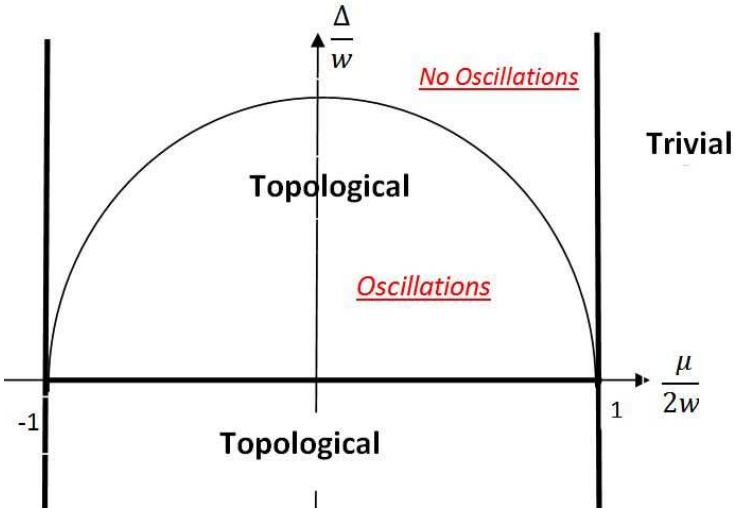

(a)

Figure 2.5: The topological phase diagram for the uniform Kitaev chain as a function of superconducting gap Δ/w and chemical potential $\mu/2w$. The focus here is the circle of oscillations (COO) $[\mu^2/4w^2 + \Delta^2/w^2 = 1]$ within each topological phase marking the boundary across which the nature of Majorana wave functions changes. Within the circle, the wave function has oscillations under the decaying envelope whereas they are absent outside the circle.

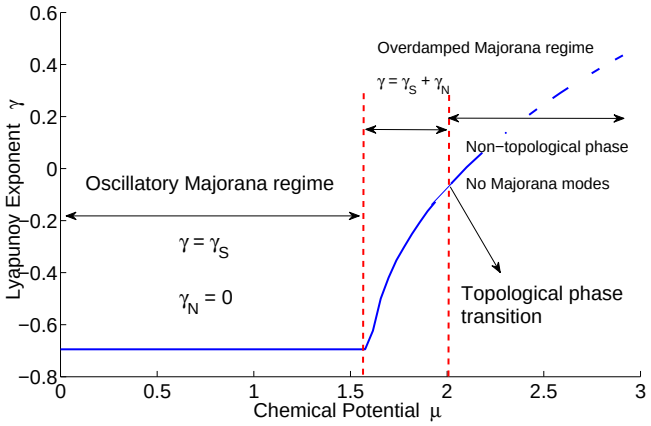

Figure 2.6: The homogeneous Kitaev chain Lyapunov exponent(LE), γ as a function of chemical potential for fixed superconducting gap ($\Delta = 0.6$). The LE is a sum of a normal and a superconducting component $\gamma = \gamma_N + \gamma_S$. It is a constant within the circle of oscillations as $\gamma_N = 0$ and γ_S is constant for fixed Δ. On crossing the circle, γ_N becomes a non-zero increasing function of μ and ultimately cancels γ_S, resulting in a zero LE, at the topological phase transition at $\mu = 2$.

This change in the nature of Majorana oscillations is also tracked by the two components of the Lyapunov exponent. As discussed in the previous subsection, when β is real i.e everywhere within COO , $\gamma_N = \ln(1) = 0$ and the localization of the Majorana mode is only due to the superconducting component $\gamma = \gamma_S = \frac{1}{2}\ln(\frac{1-\Delta}{1+\Delta})$. If Δ is kept constant, then the LE and thus the localization length are also constant, independent of the chemical potential μ as shown in Fig.2.6. Hence, in this region, the Majorana wave function shows an oscillation having an associated wave vector k_β and a decay length ξ_S given by

$$\begin{aligned} k_\beta &= \beta = \arctan \frac{\sqrt{4 - 4\Delta^2 - \mu^2}}{\mu}, \\ \xi_S &= 1/\gamma_S = 2/\ln(\frac{1-\Delta}{1+\Delta}), \end{aligned} \tag{2.72}$$

respectively. Outside the circle, as discussed earlier, the oscillations disappear and β becomes imaginary. Consequently, γ_N becomes a non-zero positive number and provides a second localization length. The Majorana wave function thus decays over a length scale given by

$$(\gamma_S + \gamma_N)^{-1} = \xi. \tag{2.73}$$

This expression remains valid within the topological phase; upon encountering the phase boundary between the topological and non-topological phase, the decay length diverges.

Topological phase transition. — The fate of the Majorana wave function upon encountering the phase

boundary can be studied, for instance, by fixing Δ and increasing μ, as shown in the diagram of Fig.2.6. If we start deep within topological phase, γ_N starts off as zero within the circle, becomes non-zero outside and increases until it becomes equal to γ_S. This happens exactly at the topological phase transition $\mu = 2$, thus resulting in a vanishing of the total LE, indicating complete delocalization of the Majorana mode.

Since γ_S is always non-zero, such delocalization in a generic potential landscape is possible only through its cancellation with γ_N. Thus the condition for a topological phase transition in general *for any potential landscape* obeys: $|\gamma_S| = |\gamma_N|$.

This concludes the section on properties of Lyapunov exponent and Majorana wave functions in a general potential landscape. We shall apply the results here to disordered Kitaev chain in a later section. Now we turn to discussion of ground state Fermion parity in finite sized systems where the Majorana modes at the two ends couple to each other.

2.6 Ground state fermion parity in Kitaev chain

2.6.1 Fermion parity switches and mid-gap states in finite-size wires

In the thermodynamic limit, the Kitaev chain in the topological phase has a doubly degenerate ground state. The two zero energy Majorana end modes corresponding to the degeneracy can be combined to form a non-local Dirac fermionic state. This non-local electronic state can either be occupied or unoccupied and this in turn determines the fermion parity of the entire many body ground state. Thus the double degeneracy also corresponds to degeneracy in fermion parity.

For finite-sized systems, the degeneracy undergoes an exponentially small splitting J due to the overlap of the Majorana wavefunctions. The associated parity states form an energy pair $\pm J$ closest to zero energy. Now the fermion parity of the ground state is determined by the fermion parity of the lowest of these two states. Explicitly, for two Majorana end modes depicted by $\Gamma_{R,L}$, the effective tunnel-coupled Hamiltonian is given by [47]

$$H_{eff} = iJ\Gamma_R\Gamma_L/2 = J(\tilde{n} - 1/2). \tag{2.74}$$

Here $\tilde{n} = \tilde{C}^\dagger\tilde{C}$ and $\tilde{C} = (\Gamma_L - \Gamma_R)/2$ is the non-local Dirac fermionic mode obtained from the linear combination of Majorana end modes. The occupation $\tilde{n} = 0, 1$ determines the ground-state parity of the system. In earlier sections, we discussed the regime in which the Majorana wavefunctions is endowed with an oscillatory component. Consequently, the tunneling amplitude of the two end Majorana modes too becomes an oscillatory function of the parameters of the system, crossing zero at specific points in parameter space.

Thus varying the parameters can lead to level crossings of these states and corresponding fermion parity switches. As explored in several recent works, these parity switches leave definitive signatures in various macroscopic phenomena such as the fractional Josephson effect, non-equilibrium quench dynamics and charge fluctuations in these systems[68, 69, 43, 70, 71, 72, 73, 74, 75]. Given the possibility of using Majorana modes as a tool for topological quantum computation, the Z_2 fermion parity has also drawn interest as a possible way of implementation of topological qubits [76, 77, 78]. There have also been proposals for detecting parity effects of the Majorana zero modes in Josephson junctions using microwave spectroscopy [79, 80].

An interesting feature of the uniform Kitaev chain is that the number of parity crossings as a function of parameters increases linearly with the system size [43]. As a result, while the splitting between parity states varies exponentially, the ground state parity shows frequent parity switches in realistic systems and can have important effects. Here, we study these switches in depth for uniform as well as disordered systems.

The tunnel coupling between the Majorana modes at the ends is a good approximation for the splitting of the degenerate states and explaining the parity crossings. Below, we use the transfer matrix technique outlined in the previous sections to go beyond the approximation and obtain the precise points where the level crossings occur.

2.6.2 Pfaffian measure of fermion parity

The method of calculating the ground state fermion parity that we use in this work was formulated in Ref. [47] by A. Kitaev and is as follows. Consider the Majorana Hamiltonian of Eq. (2.41) and the transformation B that reduces the Hamiltonian to the canonical form, i.e., $D = B^T H_M B$. Here D is an anti-symmetric matrix having non-zero matrix elements only along the first off-diagonal entries. It can be shown that the ground state parity of the system is related to the unitary properties of B. Specifically, the parity of the system is given by

$$\mathrm{P(H)=sgn[det(B)]}. \tag{2.75}$$

As a simple illustration of this expression for parity, its application to a two-site system is as follows. The Hamiltonian of Eq. 2.41 in the Majorana basis $[a_1, b_1, a_2, b_2]$ for a two-site system is given by

$$\begin{pmatrix} 0 & -i\mu/2 & 0 & i(-1+\Delta)/2 \\ i\mu/2 & 0 & i(1+\Delta)/2 & 0 \\ 0 & -i(1+\Delta)/2 & 0 & -i\mu/2 \\ -i(-1+\Delta)/2 & 0 & i\mu/2 & 0 \end{pmatrix}$$

In general, the Pfaffian of a matrix A is defined as $(Pf(A))^2 = det(A)$. The pfaffian of a 4×4 matrix is given by

$$Pf \begin{pmatrix} 0 & a & b & c \\ -a & 0 & d & e \\ -b & -d & 0 & f \\ -c & -e & -f & 0 \end{pmatrix} = af - be + dc \tag{2.76}$$

Therefore, Pfaffian for the above Hamiltonian is

$$Pf(H) = -\frac{\mu^2}{4} + \frac{1-\Delta^2}{4} \tag{2.77}$$

Thus, the Pfaffian changes its sign at $\frac{\mu^2}{4} = \frac{1-\Delta^2}{4}$. This is for the specific case of $N = 2$ and this result can be verified by explicitly diagonalizing the Hamiltonian and obtaining the matrix B. The general condition for the points where the Pfaffian changes sign for a Hamiltonian of N sites is given in the next subsection.

2.6.3 Majorana transfer matrix and parity crossings

Here we describe how the Majorana transfer matrix can be used to track the occurrence of zero energy crossings. In Sec.2.5.1 we presented the form of the Majorana transfer matrix corresponding to zero energy solutions confined to the ends of a wire. For finite sized systems, due to the hybridization of these two modes, in general, a zero energy solution does not exist and the corresponding transfer matrices couple the degrees of freedom associated with the two modes. For each transfer matrix to correspond to a strict zero energy solution, it must satisfy certain conditions imposed through the boundary conditions for Majoranas to be end bound states. These boundary conditions are as follows.

In previous sections, we showed that the set of individual transfer matrices $\tilde{A_n}$ in Eq. 2.59 corresponds to that of the normal tight-binding problem, which carried all necessary information on the corresponding zero energy Majorana wave function in the presence of a finite superconducting gap Δ. As the most general finite size situation applicable for any potential landscape, consider the transfer matrix relating the wave function at the first site to the wave function at the last site -

$$\begin{pmatrix} \tilde{a}_{N+1} \\ \tilde{a}_N \end{pmatrix} = \begin{pmatrix} \tilde{\mathcal{A}}_{11} & \tilde{\mathcal{A}}_{12} \\ \tilde{\mathcal{A}}_{21} & \tilde{\mathcal{A}}_{22} \end{pmatrix} \begin{pmatrix} \tilde{a}_1 \\ \tilde{a}_0 \end{pmatrix}, \tag{2.78}$$

The full-chain transfer matrix is given by $\tilde{\mathcal{A}} = \prod_n \tilde{A}_n$. For the corresponding decoupled Majorana mode to exist, we demand that its wavefunction naturally be confined to the length of the wire. To impose this

boundary condition, we may introduce two fictitious sites at 0 and $N+1$[81]. As the condition for the existence of the mode, we then have

$$\tilde{a}_{N+1} = \tilde{a}_0 = 0 \tag{2.79}$$

The transfer matrix gives the equations

$$\tilde{a}_{N+1} = \tilde{\mathcal{A}}_{11}\tilde{a}_1 + \tilde{\mathcal{A}}_{12}\tilde{a}_0. \tag{2.80}$$

The boundary conditions now gives a strict condition on the elements of the transfer matrix, namely

$$\tilde{\mathcal{A}}_{11} = 0. \tag{2.81}$$

Thus for *any finite-sized chain*, the general condition for the existence of a zero energy solution is $\tilde{\mathcal{A}}_{11} = 0$.

For the case of a homogeneous chain, below we can explicitly illustrate how this condition is satisfied.

2.6.4 Parity sectors in the Kitaev chain phase diagram

The degeneracy splitting, level crossing and fermion parity switches can be tracked exactly in the case of a uniform chain. The points at which the split-levels cross, thus restoring degeneracy even at finite size, form ellipses within the COO of the phase diagram (Fig.2.7). As we will show below, the elliptical boundaries can be derived by enforcing this degeneracy condition on the transfer matrix of Eq.2.52 to yield

$$\Delta^2 + \frac{\mu^2 sec^2(\pi p/(N+1))}{4} = 1, \tag{2.82}$$

where $p = 1, 2...N/2$ for even N and $p = 1, 2...(N-1)/2$ for odd N. These ellipses divide the circle into different parity sectors. Consistent with Fig. 2.7, for fixed Δ, parity crossings occur at chemical potential values satisfying

$$\mu_{switch} = 2\sqrt{1-\Delta^2}\cos\left(\frac{\pi p}{N+1}\right). \tag{2.83}$$

Larger values of p correspond to lower values of chemical potential. As each crossing is accompanied by a fermion parity switch, the adjacent areas across the elliptic boundaries are sectors of opposite parity. Thus for any given system size N, there are a number of parity sectors within the COO in the phase diagram.

Even vs Odd number of sites. — It is important to note the difference in the features of the parity sectors for even and odd number of sites. For even number of sites, there is a symmetry in the parity sectors across the line $\mu = 0$, whereas it is anti-symmetric for odd number of sites. This feature has a significant effect on

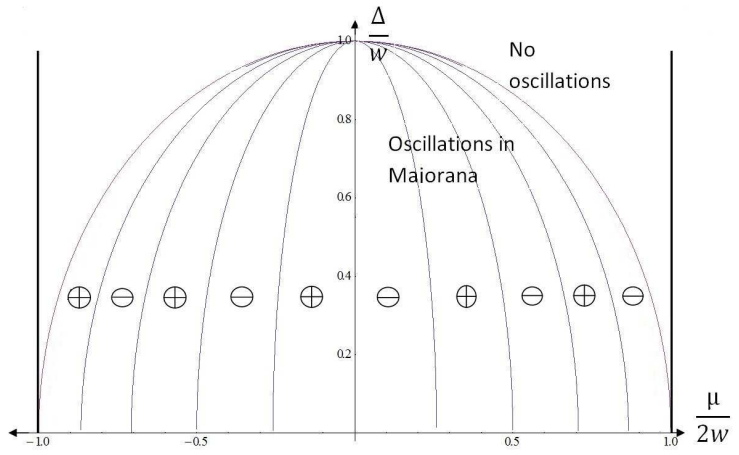

(a)

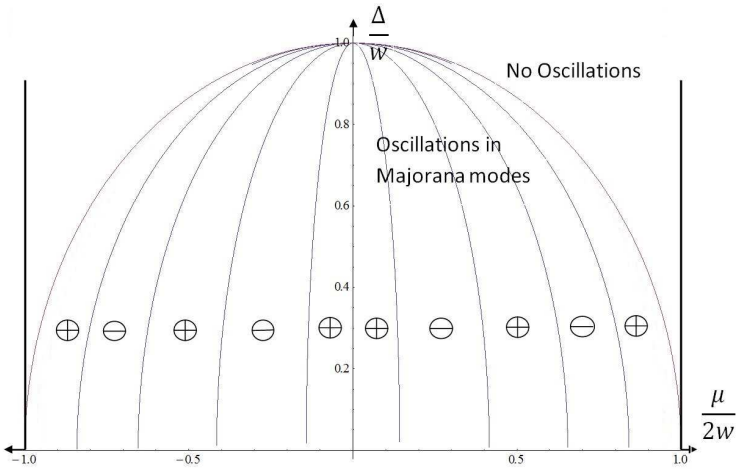

(b)

Figure 2.7: Ground state parity for a uniform *finite length* Kitaev chain within the topological phase in the phase diagram of Fig.2.5. Within the circle bounding the region where Majorana bound state wave function exhibit oscillations, alternating parity sectors are demarcated by ellipses. The parity of the sectors are indicated by $\pm$, for even and odd parities respectively. These parity sectors depend on the length of the chain. For chains of odd length (N=11)(fig.(a)) the sectors are anti-symmetric across $\mu = 0$ and are symmetric for chains of even length (N=10)(fig.(b)). Outside the circle, the Majorana modes are over damped with no oscillations.

parity switches in the disordered case, as discussed later on.

Majorana transfer matrix and parity switches. — Here we show the manner in which the Majorana transfer matrix offers an effective means of tracking the fermion parity switches. Consider the version of the individual transfer matrix of Eq.2.59 that is applicable to the homogeneous case. The chemical potential μ is the same on each site and the associated transfer matrix takes the form

$$\tilde{A}_n = \begin{pmatrix} -\frac{\mu}{\sqrt{1-\Delta^2}} & -1 \\ 1 & 0 \end{pmatrix} \tag{2.84}$$

Its eigenvalues are given by $\lambda_\pm = e^{\pm i\alpha}$ where $\alpha = \tan^{-1}\left(\frac{\sqrt{4(1-\Delta^2)-\mu^2}}{\mu}\right)$. Using Eq. 2.82 and as elaborated in Ref. [43], we have the condition on α for the zero-energy crossings

$$\alpha = \frac{\pi p}{N+1} \tag{2.85}$$

$p = 1, 2...N/2$ for even N and $p = 1, 2...(N-1)/2$ for N odd. The full-chain transfer matrix can be calculated exactly using Chebyshev's identity for uni-modular matrices [82] to yield

$$\begin{pmatrix} -\frac{\mu}{\sqrt{1-\Delta^2}} & -1 \\ 1 & 0 \end{pmatrix}^N = \begin{pmatrix} -\frac{\mu}{\sqrt{1-\Delta^2}}U_{N-1} - U_{N-2} & U_{N-1} \\ U_{N-1} & -U_{N-2} \end{pmatrix} \tag{2.86}$$

where $U_N = \sin(\alpha(N+1))/\sin\alpha$. Now the condition for the existence of an edge state reads

$$[\tilde{A}^N]_{11} = -\frac{\mu_n}{\sqrt{1-\Delta^2}}U_{N-1} - U_{N-2} = U_N = 0 \tag{2.87}$$

Here we have used the identity $2\cos\alpha U_{N-1} - U_{N-2} = U_N$. Therefore the condition for zero-energy crossings becomes

$$\sin(\alpha(N+1))/\sin\alpha = 0 \tag{2.88}$$

which is in fact satisfied precisely when $\alpha = p\pi/(N+1)$.

From the above, we find that at each level crossing, $[\tilde{A}^N]_{11}$ tends to $0^\pm$ depending on p being an even/odd value. Figure 2.8 shows the numerical results for parity switches and the sign of $[\tilde{A}^N]_{11}$ identically track each other, confirming our arguments.

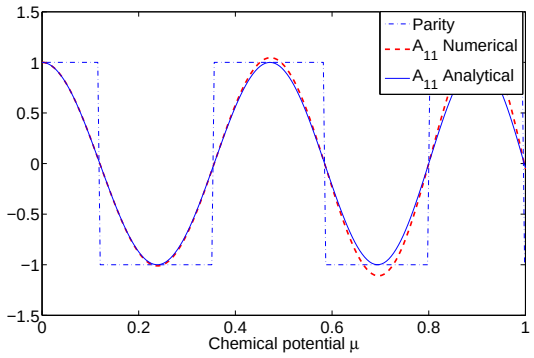

(a)

Figure 2.8: Plots which show the comparison between the fermion parity in a uniform Kitaev chain, calculated using Eq.2.75, and the matrix element $\tilde{\mathcal{A}}_{11}$ of the zero-energy Majorana transfer matrix whose vanishing value reflects the existence of a zero-energy state. The matrix element is calculated both analytically using Eq.2.86 and numerically for a uniform chain. One can see that the parity switches coincide exactly with the matrix element going to zero. Here $N = 21, \Delta = 0.6$

2.6.5 Scaling in parity switches for different superconducting gaps

Parity switches as a function of the chemical potential in the homogeneous chain exhibit an interesting scaling behavior. These parity switches are found only within the COO of the topological phase in which the Majorana wave functions are oscillatory. Within this regime, if we consider the parity switches for the chains with same length but different values superconducting gaps, the variation of the chemical potential in each case can be scaled to collapse all switches to a single curve. One can understand the collapse as follows: start with a system having a zero superconducting gap and obtain the switches in parity as function of μ. Using this, one can reproduce the parity switches at any value of finite gap Δ by scaling μ by a Δ-dependent factor, which as seen in Eq.2.60, is $\sqrt{1-\Delta^2}$.

Fig.[2.9] shows the collapse of the scaled parity oscillations at different superconducting gaps for the homogeneous case. The collapse of all the plots appropriate for different values of the superconducting gap Δ_i is expressed as

$$P(H[\mu, \Delta = 0, L]) = P(H[\mu\sqrt{1-\Delta_i^2}, \Delta_i, L]) \tag{2.89}$$

This scaling within the COO of the topological phase can be understood from the previous arguments on the origin of the oscillations from an underlying tight-binding model in the absence of a gap. The oscillations of Majorana wave functions are given by the solutions of the equation Eq. 2.70, which is the Heisenberg equation of motion for the normal system having the scaled chemical potential. For $\Delta = 0$, the scaling factor

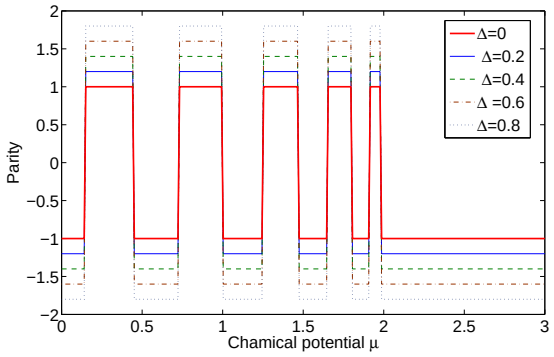

(a)

Figure 2.9: Fermion parity switches are concurrent in wires of differing superconducting gap Δ as a function of the scaled chemical potential $\mu' = \mu\sqrt{1-\Delta^2}$. This is shown here for the uniform Kitaev chain of length $N = 20$, where parity is calculated using Eq.[2.75]. The thick red plot is for $\Delta = 0$. The other plots (scaled away from unity for proper visibility) are for finite superconducting gaps.

$\sqrt{1-\Delta^2}$ is 1 and the wave function oscillations are functions of only μ. For finite gap Δ, the wave function oscillations are functions of a scaled down chemical potential $\mu/\sqrt{1-\Delta^2}$. Therefore, the resulting parity oscillations for the gapless case can be visualized to be 'stretched out' along the axis of μ, when compared to the case of finite gap. To map the parity oscillations in the gapped case to the gapless case,we need to scale up μ to $\mu\sqrt{1-\Delta^2}$ in the gapped Hamiltonian, such that it cancels the scaling factor of μ in the underlying gapless, normal tight-binding model. This is shown in Eq.[2.89].

In fact, this scaling can be obtained as function of length of the chain too. Such a 'universal scaling' has been reported in the context of entanglement spectrum of the transverse field XY spin chain [64]. As we have seen this spin chain has an exact mapping to the Kitaev chain. From the correspondence between the spin chain entanglement spectrum and edge spectrum in topological superconductors[83],it is natural that there be a mapping between the entanglement oscillations in the spin chain and parity oscillations in the Kitaev chain.

We now turn to the consideration of disordered landscape in the Kitaev chain and its effect on the wave functions and parity switches.

2.7 Effect of Disorder in Kitaev chain

Disordered Kitaev chains have formed the topic of active research for over a decade for several reasons[59, 84, 85, 86, 87, 60, 88, 89, 90, 91, 92, 93, 94, 95, 96, 97, 98, 99, 100, 101, 74, 102]. Belonging to the symmetry classes D and BDI (depending on whether they respect time reversal symmetry breaking or not), these systems exhibit behavior that starkly deviates from that of their normal counterparts. One of

the highlighting features is the presence of a delocalization-localization transition as a function of disorder strength[59, 84, 85, 103]. This transition also corresponds to the transition between the topological phase and non-topological phase, as shown in Ref.[58]. In contrast to Anderson localization physics of normal systems in one-dimension, the critical point in fact forms a mobility edge separating two localized phases. The mobility edge itself possesses a zero energy multifractal state that extends through the bulk of the entire system and offers a route for the Majorana end modes in the topological phase to permeate and disappear into the bulk upon entering the non-topological phase[59, 85].

2.7.1 Wave functions in the disordered Kitaev chain

Here, building upon known salient features of disordered Kitaev wires, we focus on finite sized systems and the behavior of the zero-energy degeneracy splitting, associated Majorana wave function physics, and parity switches. We now consider the situation in which the on-site chemical potential, μ_n, in the Kitaev chain described by the Hamiltonian in Eq. 2.41 exhibits spatial variations. As with normal Anderson localized systems, these variations would reflect a disordered potential landscape. Therefore, the values μ_n satisfy a typical random distribution, for instance, a Lorentzian, Gaussian or box distribution of an energy scale width W. We use the 'box disorder' for numerical studies, where the values of the chemical potential μ_n is taken from a uniform distribution of width W. Such a distribution with zero mean is given by

$$\mu_n = \left[-\frac{W}{2}, \frac{W}{2} \right] \tag{2.90}$$

Additional localization due to disorder.— The addition of Lyapunov exponents in Eq.2.65 allows us to immediately deduce the effect of disorder in μ_n on the nature of the Majorana wave function. The disordered Majorana wave function decays over a length scale given by

$$\xi_{dis} = (\gamma_S + \gamma_N)^{-1}. \tag{2.91}$$

The part γ_S is not affected directly due to the variation of μ and is equal to $-\frac{1}{2}\ln(\frac{1+\Delta}{1-\Delta})$. As long as there is a finite superconducting gap, there is always a corresponding localization scale for the Majorana mode. As for the contribution from γ_N, this stems from the underlying normal tight-binding model having a scaled on-site disorder potential $\mu_n/\sqrt{1-\Delta^2}$, in other words, a scaled Anderson model in one-dimension. In contrast to the uniform chain, the phase factor β in Eq. 2.57 is always imaginary and thus there never exists a region in the phase diagram where $\gamma_N = 0$. This observation is consistent with the absence of translational invariance and associated band oscillations and hinges on the well known statement that all states in the Anderson

model are localized in dimensions less than two [104]. The behavior of γ_N is thus dictated by the localization scale of the disordered wave function at zero energy (with respect to the Fermi energy) in the Anderson localization problem and can be studied by invoking the exhaustive literature on the Anderson problem.

As a simple example, consider the case of 'Lorentzian disorder' of strength W in which the values of μ_n are taken from a probability distribution of the form $P(\mu; W) = \frac{1}{\pi}\frac{W}{\mu^2+W^2}$. The value of the Lyapunov exponent for such a distribution, assuming the scaled chemical potential configuration appropriate for the Kitaev chain, is given by the form originally derived by Thouless [105]:

$$\gamma_N\left(\frac{W}{\sqrt{1-\Delta^2}}, 0\right) = \ln\left(\frac{W}{2\sqrt{1-\Delta^2}} + \sqrt{1+\frac{W^2}{4(1-\Delta^2)}}\right) \tag{2.92}$$

Thus, the normal component of the Lyapunov exponent is a non-zero function of the disorder strength characterized by W and increases as the disorder strength is increased as well as when the superconducting gap becomes comparable to the nearest neighbor hopping. The function $\gamma_N(W)$ for other disorder distributions can be similarly extracted from the existing literature.

Oscillations.— While band oscillations are washed out, the wave function of the underlying Anderson problem can still have short range oscillations under the decaying envelope, but these are qualitatively different from the band oscillations in the uniform case. Local variations of the Majorana wave functions, a_n, are governed by Heisenberg equations of motion, Eq.2.60.

As emphasized throughout, this equation exactly corresponds to the Heisenberg equation of motion for the Anderson problem. Solutions of the corresponding wavefunction have been avidly studied in past literature. The localized wavefunction typically exhibits random oscillations on the scale of the lattice spacing. They are heavily dependent on the disorder configuration and have large sample-to-sample fluctuations. They are known to have correlations on the scale of the mean free path and obey statistics independent of the decaying envelope [106, 107].

Thus, disorder qualitatively changes the nature of Majorana wave function in that it i) imposes an extra localization scale in addition to the localization due to the superconducting gap and ii) changes the nature of underlying oscillations Fig.2.10.

This as we shall see has consequences on the finite-size splitting of ground state degeneracy and fermion-parity switches.

Critical properties of Majorana wave function. — Turning to the critical point separating the topological and non-topological phases, as discussed in previous sections, at this point, the Majorana decay length

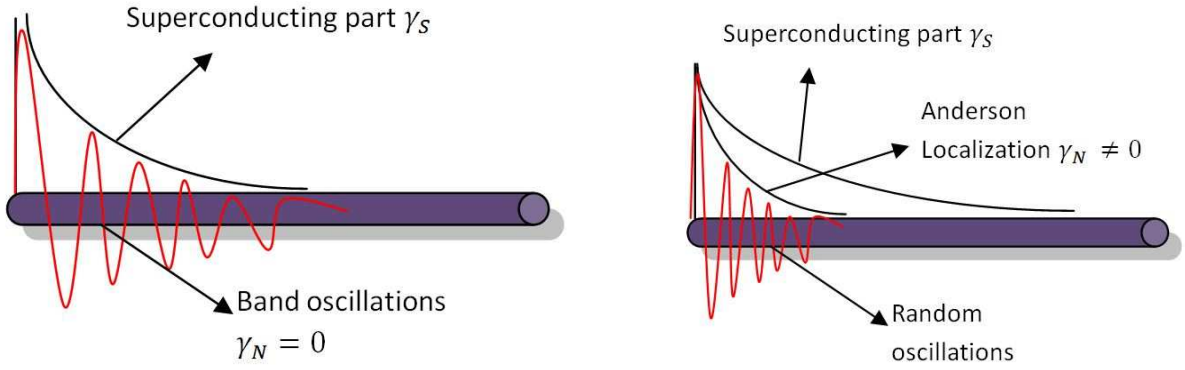

(a) (b)

Figure 2.10: A schematic of the Majorana wave function in (a) the uniform case within the oscillatory regime and (b) the disorder case. (a) Within the parameter regime containing the circle of oscillations (see text), in addition to a decaying envelope having an associated Lyapunov exponent γ_s, stemming purely from the superconducting order, band oscillations are present. (b) For the disordered case, band oscillations are replaced by random oscillations and a second decaying scale associated with a Lyapunov exponent γ_N, both stemming from the underlying Anderson localization setup of a non-superconducting normal wire having the same disorder configuration.

diverges. Equivalently, the Lyapunov exponent vanishes and thus, from Eq. 2.91, we have the relationship

$$\gamma_S + \gamma_N = 0. \tag{2.93}$$

For the specific case of Lorentzian disorder discussed above, this condition enables us to identify the critical point to be $W_c = 2\Delta$[[102]]. At this point, in going between the topological and non-topological states, the Majorana end modes completely extend into the bulk, in contrast to typical Anderson localization physics, and then vanish upon crossing the critical point.

Several insights on critical behavior in disordered Kitaev chains can be extracted by studying properties of the extensively studied spin-1/2 random transverse field Ising chain [108]. It has been shown in a previous section that the Kitaev chain can be exactly mapped to a close relative, the transverse field XY spin chain [54]. This XY model has two kinds of critical lines, an Ising type (ferro- to paramagnetic) and an anisotropic type (change in direction of magnetization). This transition from the ferro- to the paramagnetic phase corresponds to the the topological phase transition in the Kitaev chain of spinless fermions and is thus of interest in this context. The disordered Kitaev chain corresponds to the XY spin chain in the random transverse field and, in a particular limit ($\Delta = 1$), to the random field Ising model(RFIM), the critical properties of which are well known [108, 109, 110]. The ferro- to paramagnetic transition in this case belongs to the universality class of infinite disorder fixed point. One of the key features of the phase

transition in RFIM[109, 108] is the existence of two characteristic divergent length scales having different values of critical exponent ν, where, as a function of distance to criticality, Δ, each length scale diverges as $\xi \sim \Delta^{-\nu}$. One length scale, ξ_{mean}, characterizes the decay of average Green's function $C_{av}(r) \sim e^{-r/\xi_{av}}$, and diverges as $\nu_{av} = 2$. The second, the typical localization length,ξ_{typ}, reflects the most probable correlation length. It can be extracted from the single particle density-of-states and diverges with an exponent $\nu_{typ} = 1$.

As pointed out in Ref. [86], the Lyapunov exponent of the transfer matrix at zero energy corresponding to the random matrix ensemble of Class D corresponds to the 'typical' value of the correlation length. We expect the Lyapunov exponent of the Majorana transfer matrix to reflect the same properties and the correlation length, which in this case is the decay length of the Majorana, to have a critical exponent of $\nu = 1$. In other words, the Lyapunov exponent corresponding to the Majorana transfer matrix vanishes near the topological phase transition to the trivial phase linearly as a function of distance to criticality. Further studies on the critical exponent of the 'mean' correlation length in the context of physics of Majorana modes are in order.

Topological phase transition: Relating to result by Brouwer et al. — In addition to the observations made above, one can relate to the results obtained in Ref. [90] on the disorder driven topological phase transition. In this work, a condition is derived for the critical disorder strength for transition into non-topological phase as : $2l = \xi$, where l is the mean free path in the disorder configuration and ξ is the superconducting coherence length. This can be seen from our condition of cancellation of the components of LE at the transition : $|\gamma_S| = |\gamma_N|$. We have already identified $\gamma_S \sim 1/\xi \sim \Delta$. In order to relate to the result of [90], let us recall that γ_N is the inverse localization length of the underlying Anderson problem. As known from previous literature Ref.[111], the localization length is equal to the twice the mean free path: $\gamma_N = 1/(2l)$. Thus our condition translates to : $1/\xi = 1/(2l)$, which is precisely result of Ref. [90], obtained through calculations involving Langevin dynamics.

So far we have considered only semi-infinite wires to study the Majorana wave functions. In the next sections we consider finite sized wires to study fermion parity effects in the presence of disorder

2.7.2 Fermion parity switches and low-energy states in finite-sized disordered wires

Evolution of the density-of-states (d.o.s.). — A striking feature of the disordered Kitaev chain is the presence of a large gapless regime around the phase transition. As a function of disorder strength, low disorder smears the d.o.s near the gap edges, filling in some previously forbidden states. Increasing the disorder results in a proliferation of low energy localized bulk states, followed by a divergent d.o.s about zero energy. This

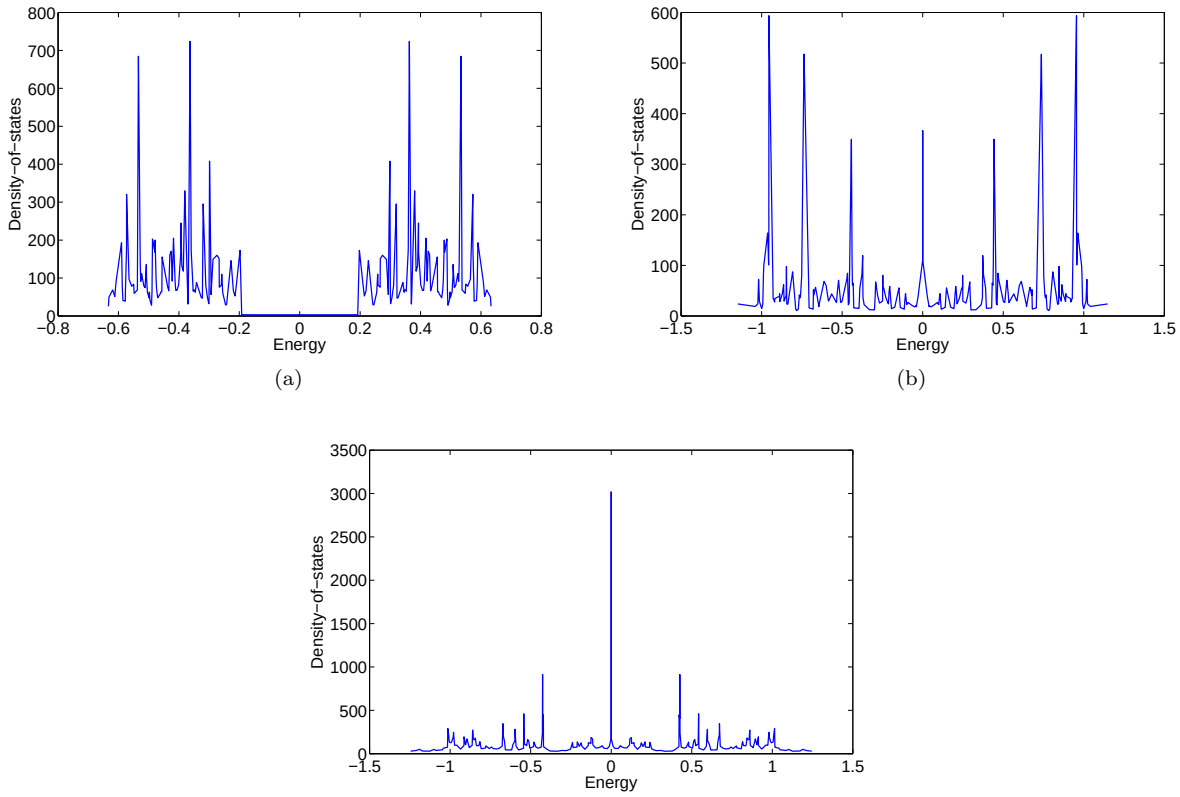

Figure 2.11: Density-of-states plots for a disordered Kitaev chain ($\Delta = 0.6$) as a function of distance from the Fermi energy for a single disorder configuration of box disorder 2.90. (a) For weak disorder ($W < 8$), there is a well-defined superconducting gap in the density-of-states. (b) As the disorder strength is increased, the gap is filled due to the proliferation of low-energy bulk states.(c) At a critical disorder strength, there is 'singularity' in the density-of-states. The behavior beyond the critical point resembles that of (b).

gapless region around the disorder critical point is called the Griffiths phase. Further increase in disorder results in a divergent d.o.s that respects universal dependence on energy ϵ of the form $\epsilon^{-1}|\epsilon|^{-3}$ at the critical point, corresponding to the Dyson singularity[59, 86]. Still further, the system enters the non-topological gapless phase. Several investigations on the distribution of these mid-gap states have explored scaling of density-of-states in Griffiths phases, transport properties and topological phase transitions in the context of disordered Majorana wires. [59, 87, 60, 88, 89, 90, 91, 92, 93, 94, 95, 96, 97, 98, 99, 100, 101, 74, 102]. Here, as a simple illustration, in Fig. 2.11, we show the evolution of the d.o.s for a single sample as a function of increasing disorder strength using exact numerical diagonalization. While detailed features cannot be resolved through our methods, the evolution clearly demonstrates the trends described above.

Behavior of low-energy mid-gap states and Majorana physics. — Reflecting the behavior of the d.o.s, at very low disorder, the only low energy states correspond to the Majorana end modes. In finite sized

wires, these states hybridize and exhibit a zero-energy splitting. Upon increasing disorder, while low-energy bulk states proliferate into the gap, the lowest energy states in the topological phase still correspond to robust Majorana modes (typically hybridized). Extensive applications of random matrix theory (RMT) for class D in previous work [[98, 74] and references therein] show that the spacing between energy levels of the disordered Kitaev chain (class D) respect the probability distribution of energy levels given by [112]]

$$P(E)dE = \prod_{i<j} |E_i^2 - E_j^2|^\beta \prod_k |E_k|^\alpha e^{-E_k^2/v^2} dE_k \qquad (2.94)$$
$$\text{Class D}: \quad \alpha = 0 \quad \beta = 2$$

Here v is the variance of the distribution. The exponent β, which measures level correlations between energy states that are not particle-hole symmetric, is non-zero. Thus, for any two such energy states, level repulsion ensures that the probability of the two energy levels crossing goes to zero, avoiding any crossings. For two states with energies $\pm E$, however, since $\alpha = 0$, the level crossing is allowed.

In Fig.2.12, we show the evolution of the behavior of the lowest three particle-hole symmetric energy pairs as a function of disorder. As described above, for low disorder, only two energy levels corresponding to Majorana modes can be seen close to zero energy. As the disorder strength is increased, other levels converge towards zero energy in close succession. Disorder causes fluctuations in the energy level spacing. For a significant portion of the topological phase, the scale of energy level splitting is very different for the Majorana modes compared to the next higher energy levels. As in the uniform case, the splitting of the Majorana modes as a function of system size is expected to be exponentially small while that of the other states is expected to be algebraic [90]. It can be seen that beyond the critical disorder strength for the topological phase to exist, the lowest energy modes now lose their Majorana character and their level splitting is comparable to that of the other modes.

Focusing on the energy level splitting of the Majorana modes, the behavior of the disordered Majorana wave function discussed in Sec.2.7.1 ought to dictate the splitting. We saw that three components characterize the wave functions: i) the gap-protected robust envelope, whose localization is determined by the magnitude of the superconducting gap ii) a second decaying envelope due to disorder, whose localization is determined from the underlying Anderson problem (see Eq.2.91) iii) and the sub-envelope random oscillations dictated by the same Anderson problem. The first two determine the average scale of energy splitting of the degenerate zero-energy states in a finite size wire. The crossing of these states is determined by the third aspect; in the next subsection, we study these crossings in detail and their direct connection with fermion parity switches.

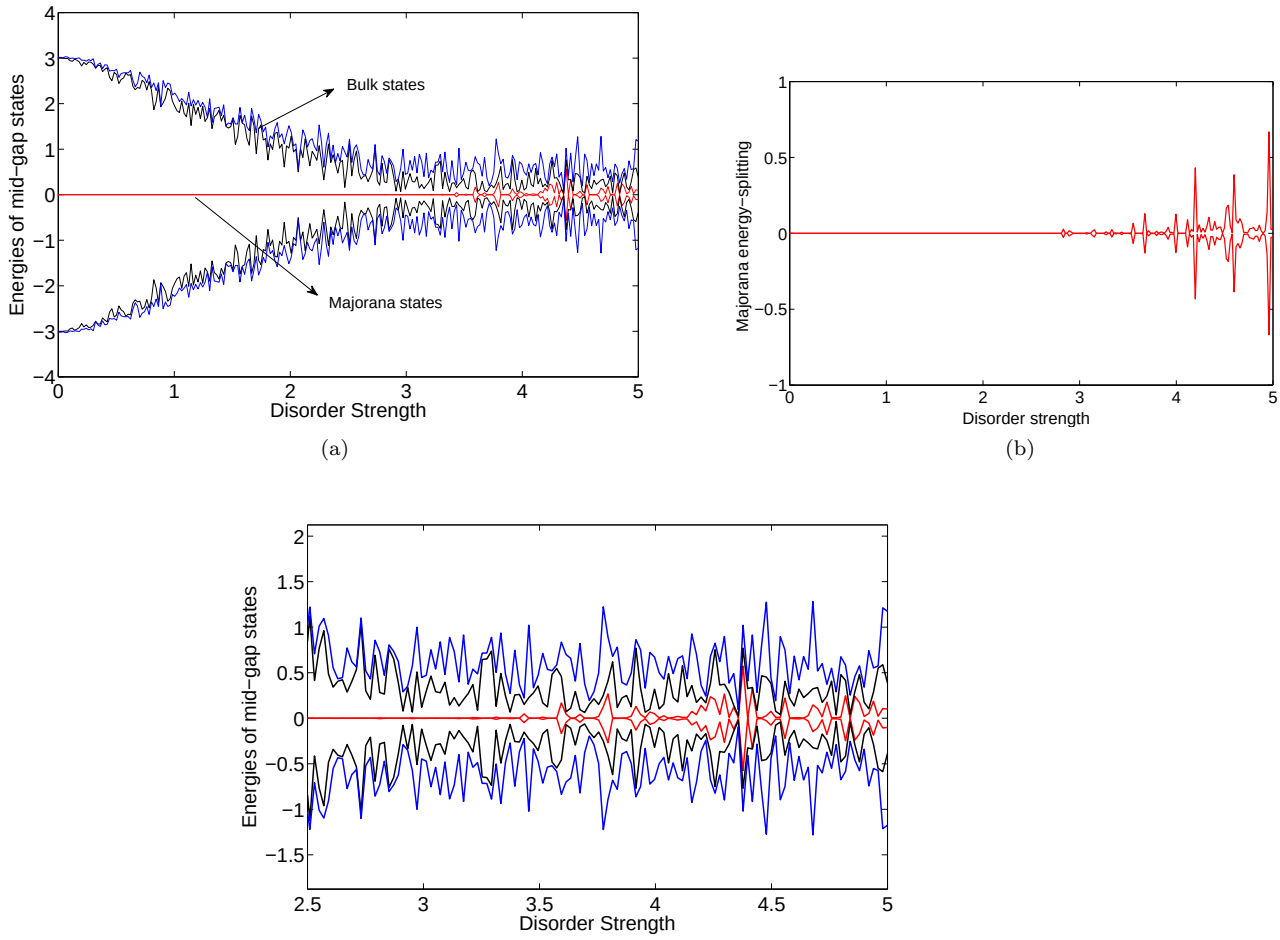

Figure 2.12: (a)Variation of a set of lowest energy levels (first 3 states) of the Kitaev chain as a function of disorder strength for box disorder 2.90 and other parameters fixed to $\Delta = 0.6$, $N = 30$. For small disorder width, the Majorana states are well separated from the bulk by a superconducting gap. As the disorder is increased there is a proliferation of the bulk states into the gap.(b) Zoomed in view of the two Majorana states split due to finite size. Their scale is exponentially suppressed compared to the bulk states. These states cross zero energy as the disorder width is varied, inducing a fermion parity switch in the ground state. (c) Griffiths phase: At strong disorder, there is an accumulation of a large number of bulk states near zero energy. Level crossings between these states are forbidden due to level statistics of Class D (level repulsion). Nearing the critical disorder strength, the magnitude of the energy states due to Majorana splitting become comparable to the bulk states.

Scaling of degeneracy-split states

In Ref. [90], it was shown using a scattering matrix approach that the energy level splitting of coupled Majorana end states in a finite sized wire is exponentially small compared to bulk states in the weak disorder limit. Due to large fluctuations, the energies of these mid-gap states themselves do not follow a simple probability distribution. But as is common with random systems, the logarithm of these energies obeys a normal distribution. A central result of Ref. [90] is that for a continuum model of the p-wave superconducting wire, the average of this quantity has the form

$$\langle \ln(\epsilon_{0,max}/2\Delta)\rangle = -L[1/\xi - 1/(2l)], \tag{2.95}$$

where ϵ_0 is the Majorana end state energy in a finite sized wire,Δ is as usual the magnitude of the superconducting gap, ξ is the superconducting coherence length and l is the mean free path of the corresponding disorder configuration.

These results can be understood in the light of our discussion on Majorana transfer matrices. As described before, the degeneracy-split end modes have energies proportional to the overlap of the Majorana wavefunctions. In a finite sized wire of length L, for two end modes having a decaying envelope of localization length $1/\gamma$, this overlap is proportional to $\epsilon_0 \sim e^{\gamma x}e^{\gamma(L-x)} = e^{\gamma L}$. Here, γ is the Lyapunov exponent and is a negative quantity in the topological phase. As shown in Eq. 2.65, $\gamma L = (\gamma_S + \gamma_N)L$ consists of a superconducting and normal piece. Now, as is commonly invoked in treatments of localization physics and random systems, given the multiplicative nature of transfer matrices, the Lyapunov exponent corresponding to the transfer matrix is in general self-averaging. Thus, we expect $\ln(\epsilon_0)$ to have an average value of $L\gamma$; this result is reminiscent of Eq.2.95 where ξ is the length scale associated with superconductivity and l with normal localization properties.

2.7.3 Parity switches - qualitative discussion and numerical results

In Sec.2.6, we outlined how a pair of zero energy Majorana modes form a Dirac fermion state that can be occupied or unoccupied, corresponding to two states of opposite parity. We then showed the manner in which end Majorana modes hybridize in a finite sized uniform chain, giving rise to an energy splitting and an associated unique ground state parity. We charted out the points in phase space where zero energy crossings take place, corresponding to ground state parity switches, and mapped the regions of odd and even parity in the topological phase diagram. Turning to disordered systems, in the previous section, we gave a detailed description of the behavior of low energy states and discussed the distribution of energies associated

with zero energy splittings. Here, we focus on the vanishing of this splitting and show that this occurrence directly corresponds to a ground state parity switch. We also show the manner in which our study of the uniform system informs the ground state parity distribution map for the disordered case.

Zero-energy crossings and parity switches. — Following the discussion on mid-gap states in the previous section, first off, we see that zero-energy level crossings are infact possible as a function of system parameters, such as chemical potential and disorder strength. The RMT result of Eq.2.95 further corroborates that particle-hole symmetric states can undergo zero-energy crossings but other pairs of adjacent states cannot do so due to level repulsion. This suggests that the only states under-going zero-energy crossing are the ones associated with Majorana physics. In other words, zero-energy crossing are concurrent with fermion parity switches. We now demonstrate this explicitly.

In Sec.2.7.1, we saw that the Majorana wavefunction in the disordered case has a decaying enveloping as well as oscillations that are completely dictated by the underlying normal Anderson tight-binding model. In the previous section, we saw that the decaying envelope is directly related to the scale of the average zero-energy splitting and is always finite for a finite length wire. However, the oscillations directly contribute to the fluctuations and, in particular, to the vanishing of the splitting. In principle, just as the correlation between two decaying envelopes gives the average scale for zero-energy splitting, analytic studies of correlations between the oscillations[107] ought to give precise information on the locations where the splitting vanishes. Here, we resort to the numerical methods that we employed in previous sections. Specifically, we use the normal system transfer matrix condition for the existence of a zero energy state given by Eq.2.81, $\tilde{\mathcal{A}}_{11} = 0$. Here, $\tilde{\mathcal{A}}_{11}$ is the appropriate matrix element of the full transfer matrix, $\tilde{\mathcal{A}}$ and the condition dictates that the amplitude of the associated wave function vanish outside the length of the wire.

In Fig.2.13, we plot the matrix element $\tilde{A}_{11}$ as well as the ground state parity for a finite sized disordered wire as a function of disorder strength. Here, we use the Pfaffian measure of Eq. 2.75 for determining the parity. The points of vanishing $\tilde{\mathcal{A}}_{11}$ correspond to points which host a generic zero-energy state. Note that this state also has a zero energy partner, whose transfer matrix can be derived from the initial transfer matrix by replacing Δ with $-\Delta$. While the magnitude of $\tilde{\mathcal{A}}_{11}$ is unimportant for parity switch physics, its increase with disorder strength reflects the increase of the increase of the average energy splitting. Most prominently, we see that the vanishing of $\tilde{\mathcal{A}}_{11}$ is concurrent with the switching of ground state parity. Thus zero energy crossings correspond to the presence of two decoupled Majorana modes and associated degenerate parity states.

In summary, the underlying normal Anderson model dictates zero-energy crossings in the disordered superconducting wire. These zero-energy crossings are exclusively associated with Majorana mode physics

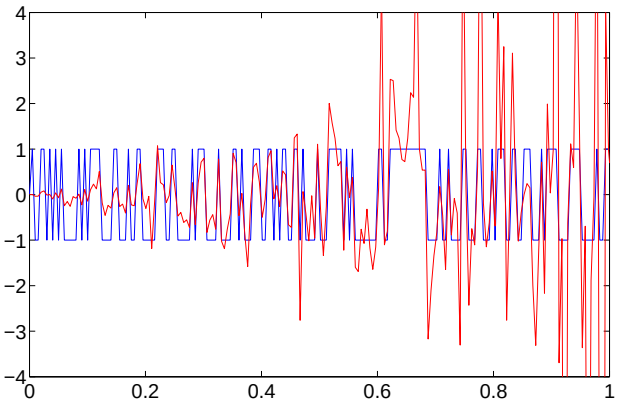

(a)

Figure 2.13: Comparison between the fermion parity in a disordered Kitaev chain and the transfer matrix element $\tilde{\mathcal{A}}_{11}$ as a function of disorder strength(box disorder). The vanishing of the matrix element reflects the existence of a zero-energy Majorana state and can be seen here to coincide with parity switches as with the uniform case of Fig.2.8. Here $N = 40, \Delta = 0.6$

and correspond to the points when the system encounters a parity degeneracy in the process of undergoing a ground state parity switch.

Tracking parity switches in the topological phase diagram. — In obtaining a map of the regions where parity switches occur in the disordered Kitaev chain, we find that our studies from previous sections of the parity distributions in the uniform system serves as a guide. The precise points in parameter space where the switch occurs depend on the particular realization of disorder and are thus random. However, the parity switch phase diagram for the pure case in Fig. 2.7 identifies the broad regimes in which parity switches can or cannot occur. In essence, for a fixed value of the the superconducting gap, anywhere in the uniform chain phase diagram, windows in chemical potential where no parity switch occurs determine the width that the disorder distribution can span in the disordered case before a parity switch occurs. As we explicitly demonstrate, those observations allows us to chart out regimes where parity switches occur or not in the disordered wire.

We first analyze parity switch behavior in chains having an *even* number of lattice sites. Figure 2.14.a shows numerical results for typical parity switching behavior as a function of disorder strength W. In all numerical simulations, the values of μ_n are chosen randomly from a box distribution or a 'window', centered at a mean $< \mu_n >$ value and having a width W. The parity is calculated again using the Pfaffian expression given by Eq. 2.75.

One can see from Fig.2.14.(a) that for the case of an even number of sites no parity switches occur up to a specific disorder window width. Beyond this width, switches start occurring in rapid succession and

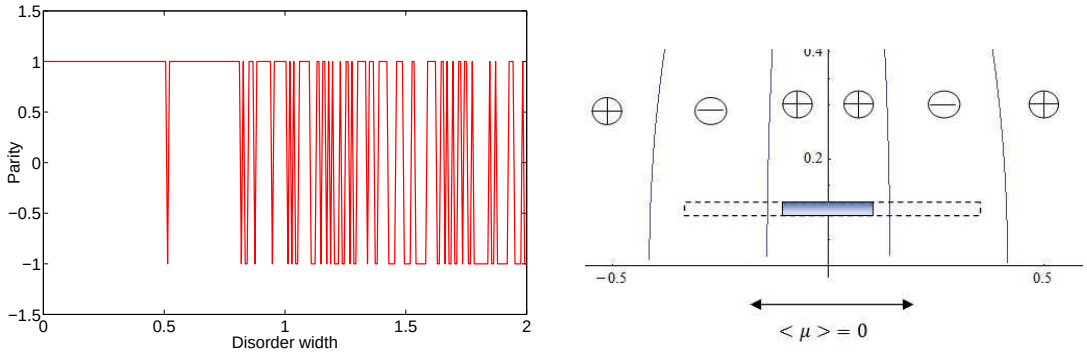

(a) (b)

Figure 2.14: (a) Parity switches in a wire of an even number of lattice sites, $N = 10$, as a function of disorder width for box disorder. Here, $\Delta = 0.6$. Since parity is an even function of chemical potential for even N, the initial disorder window lies within a fixed parity as indicated in the uniform chain phase diagram in (b). As the disorder window is increased beyond a length-dependent value μ^p_{switch} of Eq. 2.96 (dotted line) to include opposite parity sectors, parity switches begin to occur.

follow a random pattern that depends on the specific realization of disorder. As the disorder window width increases and includes opposite parity sectors, number of parity switches increase from being sparse to very dense.

A qualitative picture for the parity switches can be obtained by invoking the properties of the uniform chain phase diagram. As shown in Fig.2.14.(b) and discussed in previous sections, for a fixed wire length, the uniform chain ground state parity changes in a characteristic manner as a function of chemical potential. The chemical potential values at which these parity crossing happen are given by

$$\mu^p_{switch} = 2\sqrt{1-\Delta^2}\cos\left(\frac{\pi p}{N+1}\right), \tag{2.96}$$

where p takes integer values from 1 to $N/2$ for even N. The first crossing occurs for $p = N/2$ and the width of the central parity sector is $2\mu^{N/2}_{switch}$. Thus, any value of chemical potential lying within this window is associated with the same parity. Upon introducing disorder such that the site-dependent chemical potential lies within this width, we would expect no changes in the overall ground state parity. Beyond this width, however, chemical potentials associated with the opposite parity become included in the on-site distribution, allowing for the possibility of a global ground state parity switch. The probability of such a switch increases with increasing disorder window width as it allows a higher chance of on-site chemical potentials being associated with opposite parity. This qualitative picture is consistent with the behavior of parity switches in Fig. 2.14.b. We now show that it accounts for our numerical findings with regards to parity switch behavior as a function of system size, average chemical potential off-set, and odd versus even number of lattice sites.

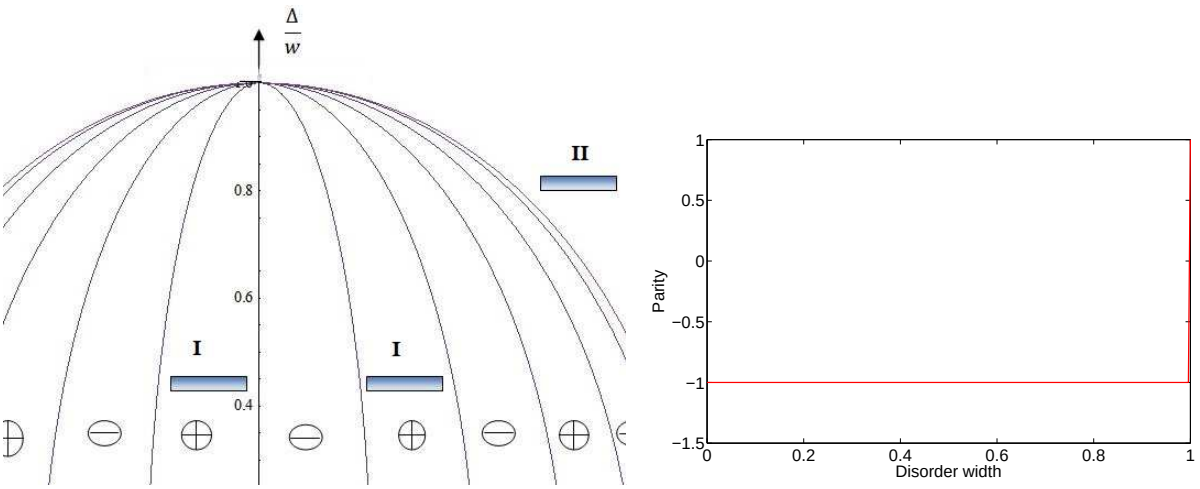

(a) (b)

Figure 2.15: Possibility of no parity switches in the disordered Kitaev chain.(a) Two possible disorder distributions centered around finite chemical potential are shown in which parity switches are not expected - I. Double box disorder in two disjoint sectors of the same parity and II. Box disorder outside the circle of oscillations. (b) In both cases, the plot of parity as a function of disorder strength indeed shows the absence of parity switches.

The occurrence of parity switches highly depends on the system size, N. As can be seen in Eq. 2.96, as N increases, the chemical potential value at which the first parity switch occurs in the uniform case, $\mu_{switch}^{N/2}$, becomes smaller. Thus, in the disordered case, for a wire of longer length, we expect parity switches to commence for smaller disorder window width. We indeed find this to be true.

Chemical potential off-set and absence of parity switches. — As with the case above of disorder centered around zero chemical potential, here we analyze parity switches in the presence of a chemical potential off-set where the mean $< \mu_n > \neq 0$. Once again, the uniform chain parity regimes inform the behavior of the disordered wire. One of the most striking features to emerge is that if the chemical potential off-set and disorder window width are chosen to lie within a region of the uniform chain phase diagram where no parity switches occur, then the disordered wire too shows no ground state parity switch. Specifically, from Eq. 2.96, we see that the chemical potential span of any given parity sector in the uniform wire is given by

$$\Delta\mu_p = 2\sin\left(\frac{\pi(p+1/2)}{N+1}\right)\sin\left(\frac{\pi}{N+1}\right)$$

This sector width shrinks with increasing N. Also for a given size N, this width decreases as one progresses from zero chemical potential to the boundary of the circle of oscillation (COO), i.e. as $p \to 1$. Furthermore, outside the COO, no parity switches occur. These features provide bounds for the values of chemical potential off-set and disorder window width in which no parity crossings occur.

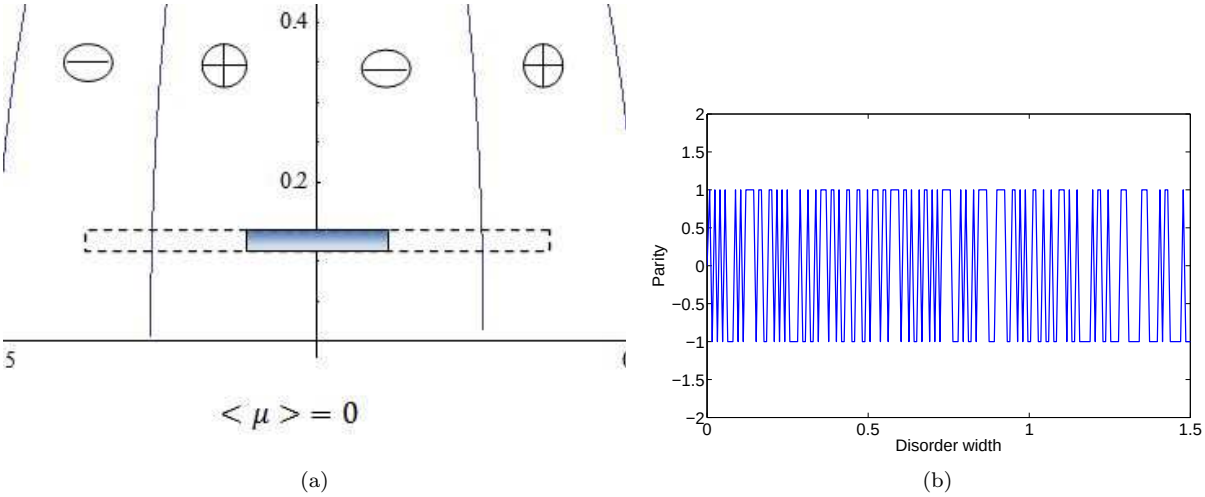

(a) (b)

Figure 2.16: Parity switches in a wire of odd length ($N = 11, \Delta = 0.6$) as a function of disorder strength for box disorder. (a) Given the antisymmetry in parity sectors across $\mu = 0$ for the uniform case, the slightest change in disorder strength is expected to produce a parity switch. This is confirmed in (b), which shows a profusion of random parity switches as a function of disorder strengths starting from the smallest amount of disorder.

In Fig.2.15, we explicitly verify the observations made above. As one example, we consider a double box disorder distribution where two disorder windows are centered around two values of chemical potential such that both windows lie within the same parity sectors in the uniform chain phase diagram. As a second example, we place the disorder window outside the COO, thus expecting no parity switches. Indeed, in both situations parity switches are not observed. While the double box disorder seems unrealistic, the case of taking the window outside the circle might be possible to realize experimentally. One can study the 'Ising-limit' $\Delta = 1$, which is tangential to the circle. In this case taking $< \mu_n >= 0$, the parity switches as a function of width again depends on the number of sites being even or odd. This explicitly shows that there are cases where one need not have any parity switches even in the presence of disorder and when they are present, the behavior completely depends crucially on the features of the parity sectors of the uniform Kitaev chain.

Dependence on even versus odd N. — A noteworthy difference arises in the behavior of parity switches between chains of even and odd number of lattices sites, once again stemming from the structure of the uniform wire ground state parity distribution. The key difference is that the distribution of parity switches is symmetric as a function of chemical potential for the even site case but anti-symmetric for the odd site case. Explicitly, the values of chemical potential for when parity crossing occur are given by Eq. 2.96 for an even number of sites. While the same holds for the odd site case (with values of p ranging from 1 to $(N-1)/2$), a parity switch also occurs at $\mu = 0$. Thus, in the presence of disorder, in contrast to the even site case shown in Fig. 2.14, even the narrowest disorder window centered around zero chemical potential

gives rise to parity switches. This behavior is corroborated in Fig. 2.16.

Thus, we have presented a qualitative study of ground state parity in finite sized disordered Kitaev chains. Salient features are that the uniform Kitaev chain serves to inform parity switches in disordered chains. The transfer matrix, as with the uniform case, tracks zero energy crossings and shows that they are consistent with parity switches, thus attributing all such crossings with Majorana mode physics. For the disordered case, the underlying normal state Anderson problem determines oscillations of the Majorana wavefunctions and associated parity switches. Finite length analyses of the uniform wire have direct bearing on parity switching behavior for the disordered case. Windows in chemical potential that contain fixed parity sectors in the uniform case provide bounds for disorder distribution widths that respect no parity switching. Specifically, this observation results in the characteristic parity switching behavior for even and odd length chains shown in Fig.2.14 and Fig.2.16 as well as regimes in the phase diagram where no parity switching takes place, as shown in Fig.2.15.

2.8 Semiconductor nanowire-superconductor heterostructures

There have been experimental proposals on various platforms and a lot of experimental progress in realizing Majorana modes in condensed matter systems. Extensive reviews have been written on this topic- [5, 6, 113] to mention a few. Latest progress in experiments has been summarised in [1]. One of the key challenges in realizing a model such as the Kitaev chain is in obtaining p-wave superconductivity. Naturally occurring materials that exhibit p-wave pairing superconductivity are very rare. Apart from that getting long-range order in one-dimension is another challenge. Experimental proposals have capitalized on three important ingredients to overcome these challenges: superconducting proximity effects, time-reversal symemtry breaking and spin-orbit coupling [5]. Numerous platforms have been proposed to host the Majorana modes and do operations on them. These include such as semi-conductor nanowire heterostructures[7, 8],topological insulator nanowire [114], Superconductor-Topological insulator (S-TI-S) Josephson junctions [115, 116], Magnetic adatomsNadj-Perge14, quantum dots and cold atoms to name a few. Here the details of the semiconductor nanowire junction platform is presented.

The seminal proposals in [7] and [8] have made use of experimentally accessible ingredients such as one dimensional wires with high spin-orbit coupling, conventional s-wave superconductor and a high magnetic field.

The basic set-up of such a superconductor-semiconductor nanowire heterostructure can be modeled using

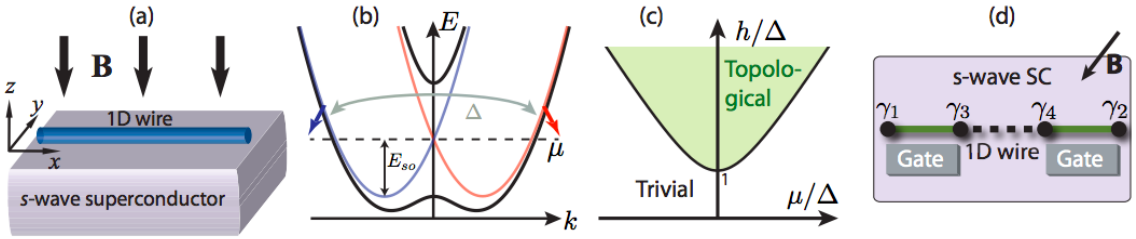

Figure 2.17: (a)Basic set-up for realizing Majorana modes in heterostructure consisting of a semi-conductor nanowire with proximity induced superconductivity and a magnetic field. (b) The colored curves indicate the band structure of the spin-orbit coupled wire. When the magnetic field is applied a gap is opened breaking the time-reversal symmetry. When the chemical potential is set to be within the gap, the induced pairing projected to the lowest band is p-wave. (c) The phase diagram of the model in the plane of h(the magnetic field) and μ(the chemical potential), both scaled with respect to the induced gap Δ. (d) IN the topological phase the Majorana modes are localized at the edges of the wire.

the following Hamiltonian:

$$H = \int dx \psi^\dagger \Big(-\frac{\partial_x^2}{2m} - \mu - i\alpha\sigma^y\partial_x + h\sigma^z \Big)\psi + \int dx \Delta(\psi_\uparrow\psi_\downarrow + h.c) \tag{2.97}$$

Here μ is the chemical potential, α is the strength of the spin-orbit coupling and h is the Zeeman energy from the magnetic field. The superconducting term wuth Δ models the proximity induced superconductivity. Fig.(2.17) shows the schematic of the various ingredients. The spin orbit coupling splits the spin states as indicated by red and blue parabolas in the Fig.(2.17). THe appled magnetic field split the degeneracy in these spin states by lifting the crossing between the parabolas at $k = 0$ as shown in Fig.(2.17 (b)) . When the Fermi level lies withing the field induced gap, the system is effective spinless. Turning on weak superconductivity then effectively gives an effective p-wave pairing. The condition for obtaining a topological phase is then given to be [5] : $h > \sqrt{\Delta^2 + \mu^2}$. The Majorana modes are then trapped at the edges of the wire which form a boundary between the topological phase of the wire and the vacuum.The table in the figure shows the typical experimental values of the parameters.

Zero bias tunneling conductance – Tunneling conductance is one of the measurements in which signatures of Majorana modes can be found. In the absence of a zero mode, the conductance from the resonant tunneling vanishes usually. The presence of a Majorana mode produces a conductance of $2e^2/h$ at zero-bias. Tunneling spectroscopy also provides a method to meaure the local density of states and track it across the topological phase transition. Soon after the theoretical proposals the emergence of zero-bias peak was observed in InAs nanowires [117, 118, 119, 120]. The complication with these measurements were that there were large number of midgap states due to disorder and was challenging to separate the contributions of Majorana mode from

Semiconductors	InAs	InSb
g-factor	8-15	40-50
effective mass m^*	0.023 m_e	0.014 m_e
spin-orbit energy $E_{so} = \frac{m^* \alpha^2}{2\hbar^2}$	0.05 - 1 meV	0.05 - 1 meV
spin-orbit coupling α	0.2 - 0.8 eV· Å	0.2 - 1 eV· Å
spin-orbit length $\lambda_{so} \equiv k_{so}^{-1} = \frac{\hbar^2}{\alpha m^*}$	180 - 40 nm	230 - 50 nm
Superconductors	Al	NbTiN
superconducting gap Δ	0.2 meV	3 meV
critical field B_c	10 mT	10 T
critical temperature T_c	1.2 K	15 K

Figure 2.18: Comparision of the properties of the materials used in the nanowire heterostructure platforms.(Adapted from [1])

those. Later experiments with InSb nanowires have shown lesser midgap states and have been able to isolate the zerobias peak contribution from the Majorana modes[121, 122, 123].

4π-periodic Josephson effect– A electrical supercurrent can flow between two superconductors with a superconducting phase difference and in the absence of an applied voltage. This is related to the Josephson effect.The presence of Majorana modes in the superconductors leaves a signature in the current-phase relationship. The supercurrent is given by $I_J = (2e/\hbar)dE/d\phi$ where E is the energy of the Josephson junction and ϕ is the phase difference between the superconductors. In conventional superconductors, only cooper pairs can tunnel whereas pairs of Majorana modes allow single electrons to tunnel. This leads to doubling of the periodicity of the Josephson energy leading to the relation $E \propto cos(\phi/2)$. If the superconductors enclose a magnetic flux, then the supercurrent I_J has a flux dependence. In the presence of Majorana modes, this flux dependence changes from 2π to 4π periodicity. This is known as the $4\pi-$ periodic Josephson effect and was reported to be measured in [124, 125].

There have been other experimental proposals and measurements using different techniques such as couling to a superconducting island with finite charging energy [126] and Coulomb blockaded islands coupled to leads[127].

2.9 Superconductor-Topological Insulator-Superconductor Josephson junctions

This section presents work done with collaboration with the experiment group of Prof. Dale Van Harlingen at Urbana [128].

As an viable alternative to nanowire systems in which the MBS are physically bound to the end or edges of 1D or 2D structures, here we consider a platform consisting of multiply-connected hybrid superconductor (S)

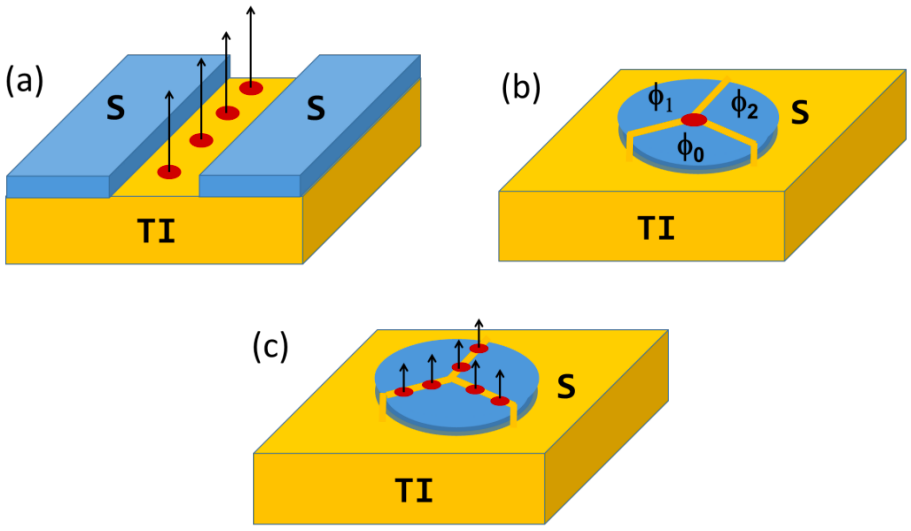

Figure 2.19: Nucleation of Majorana fermion modes in S-TI-S structures: (a) Lateral S-TI-S Josephson junction in a magnetic field with MFs at the location of Josephson vortices, (b) trijunction in zero magnetic field with a single MF in the center induced by appropriate adjustment of the phases on the electrodes, and (c) trijunction in a magnetic field with MFs

- topological insulator (TI) networks for realizing MFs whose locations can be controllably moved, providing additional functionality for braiding and hybridization that perform non-Abelian operations. In fact the earliest experimental proposals for realising MBS involved the S-TI-S Josephson junctions where MBS are trapped in the vortices or phase slips.

S-TI-S Josephson junctions offer an attractive platform for MBS manipulations for the following reasons: (1) MFs in this system are zero-energy Andreev bound states enabled by the spin-momentum locking of topological surface states in the TI and stabilized by the phase of the Josephson coupling; (2) in contrast to other systems such as semiconductor nanowires, nucleation of the MFs does not require a large magnetic field, enabling phase-sensitive measurements; (3) magnetic fields instead play a different role by localizing MFs at Josephson vortex cores, which allows us to move the MFs by moving the vortices, easily done in controlled ways by applying currents, voltages, or phase differences; (4) the MFs can be created in a controlled way in uniform junction regions and are not subject interface issues, unlike with nanowires in which the MFs exist at interface between topological and non-topological regions; and (5) junction networks are easily scalable to create quantum circuits and and surface codes for performing universal quantum computing in networks of Josephson junctions have already been proposed [129, 130, 131].

Here we begin our extensive treatment of the proposed S-TI-S architecture by describing a single extended Josephson junction, nucleation of MBSs and the effects of their coupling.

2.9.1 Effective model of low-energy junction modes

The basic element for the junction geometries studied here is as shown in Fig. 2.19. The full-fledged hybrid structure would comprise of a topological insulator slab having two superconducting islands deposited on its upper surface. We assume here that the slab is much thicker than coherence length of the proximity-induced superconductivity within it. We restrict ourselves to a well-established effective model that focuses on the low-energy states found along the junction interfaces .

Let us consider a S-TI-S system, similar to the one described in Ref.[116] having a line junction of width L along y-axis as shown in the Fig. 2.19 a. The superconducting gap varies as : $\Delta(x) = \Delta e^{i\phi(y)}$ for $x > d/2$ and $\Delta(x) = \Delta e^{-i\phi(y)}$ for $x < -d/2$. A magnetic field pierces through this junction with flux Φ_B. The flux leads to a spatial variation of the superconducting phase difference along the junction to vary as

$$\phi(y) = \pi y/l_B, \tag{2.98}$$

where $l_B = L\Phi_0/\Phi_B$. Here $\Phi_0 = h/(2e)$ is the flux quantum appropriate for paired superconductivity.

It can be shown [116] that under these circumstances, there exists a pair of dispersive Majorana modes, $\gamma_{R/L}$ counter-propagating along the junction. The desired MBSs are particular localized states composed of these modes. Their low-energy effective Hamiltonian has the form

$$H = i\hbar v_M(\gamma_L\partial_y\gamma_L - \gamma_R\partial_y\gamma_R) + i\Delta\cos(\phi(y)/2)\gamma_L\gamma_R. \tag{2.99}$$

Here $v_M = v[\cos(\frac{\mu W}{\hbar v}) + (\frac{\Delta}{\mu})\sin(\frac{\mu W}{\hbar v})]\frac{\Delta^2}{(\mu^2+\Delta^2)}$, where v is the velocity corresponding to the edge state of the TI and μ is the chemical potential . For a S-TI-S junction of $Al - Bi_2Se_3 - Al$ the estimated values are $v = 10^5 ms^{-1}$,$\Delta = 150\mu eV$,$\mu = 10meV$ [115, 116].

The form of Eq. 2.99 respects the Dirac equation for massive particle, where the gap function $\Delta\cos(\phi(y)/2)$ represents a spatially varying mass function. For a linear variation of the flux-dependent $\phi(y)$, the gap function too can be linearized around regions where $\phi(y)$ crosses an odd integer multiple of π. In this case, there exists a zero-energy eigenstate that shows exponential decay away from the crossing point. This eigenstate has the appropriate linear combination of γ_R and γ_L such that they are real functions, making them the desired Majorana bound states (MBSs). As the magnetic field piercing through the junction is increased, the number of zeros of the gap function increases, thus capturing more number of Majorana modes in the junction. A new Majorana mode appears with the incremental change of the net flux by one quantum, thus confining one Majorana bound state per one Josephson vortex.

A few comments are in order here with regards to several simplifying assumptions made in this model. Here we assume the width d to be small. The profile for the phase variation will in general be altered in realistic situations having thicker width. For example, one could consider a extended Josephson junction in which the gap function shows a *tanh*-like spatial variation yielding a Josephson soliton . Here too, respecting the generic change of sign in the gap function, it can be shown that there exists a Majorana bound state[132]. Another issue is that the system requires that the MBSs appear in pairs. In Ref. [116], the full three-dimensional nature of the system is taken into account and it is assumed that the partner of a single MBS is at the bottom surface of the TI. For this to hold, the induced superconducting penetration length within the TI ought to be much greater than its thickness. Here, we consider the opposite limit. We thus expect that for an isolated MBS in the junction, there exists a partner, perhaps extended, along the periphery of the superconducting islands. We now turn to a detailed analysis of the MBS within the context of our model employing numerical simulations.

Here we analyze the situation in which the applied flux is strong enough to generate multiple vortices and MBSs. In particular, we study the case of four MBSs present along the junction; such a situation is the minimum necessary for quantum information protocols. Through numerical simulation of the model presented in the sub-section above, we show the explicit realization of these MBS states, their mid-gap spectral properties, and the manner in which these features can be controlled by altering the local phase profile.

We first consider the instance where the phase variation in Eq. 2.99 varies linearly and increases from $-\pi N/2$ to $\pi N/2$ as the coordinate along the junction, y, spans the junction from $-L/2$ to $L/2$ and N is the number of flux quanta. This situation encompasses four half-flux quanta within the junction, which ought to lead to four MBS. We explicitly ascertain this MBS distribution and related features by numerically diagonalizing the Hamiltonian in Eq. 2.99; Fig. 2.20 shows the numerical results.

For this case of two flux quanta piercing the junction, Figure 2.20 (a) shows the variation of the gap function along the junction. Correspondingly, Fig.2.20(b) shows the energy spectrum. Most energy states lie outside a gap region centered around zero energy. As expected, four states however are mid-gap states effectively at zero energy. Our analyses also show that with increasing flux, the formation of new MBSs occurs through select states lying outside the gap entering the gap region and nucleating towards zero energy. Plotting the eigenstates of the corresponding wavefunctions in Fig. 2.20(c) indeed shows them to be isolated, evenly spaced, bound states localized along the junction at the zeroes of the gap function. Each of the bound states shows exponential decay in isolation. Moreover, the eigenfunction is completely real, making it of the

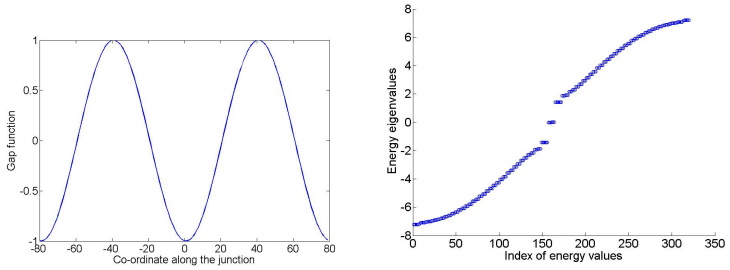

(a) (b)

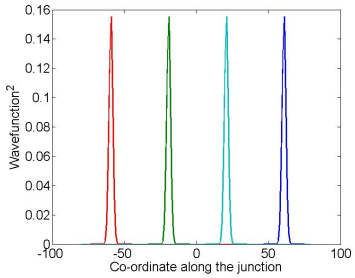

(c)

Figure 2.20: (a) The application of a magnetic field leads to variation of the phase difference along the Josephson junction and the gap function. The gap function, plotted as a function of distance along the junction, goes to zero when the SC phase difference crosses multiples of π. (b) The spectrum of Andreev bound states(in units of $\hbar v$) obtained from the diagonalisation of model Hamiltonian Eq. 2.99 for the given gap function profile. The mid gap state correspond to the Majorana zero modes. (c) shows the wavefunction profile of the Majorana modes localised at the zero crossing of gap.

Majorana form. The MBS wavefunction at a distance δy away from its center respects the form

$$\gamma(y) \approx \xi(x) e^{-|\delta y|/\lambda_M}. \tag{2.100}$$

Here, the decay length is characterized by $\lambda_M = \sqrt{\hbar v_M l_B/\Delta}$.

The MBSs are effectively isolated when their separation is significantly greater than their decay length. However, when brought closer, a pair of MBSs becomes coupled due to the overlap in their wavefunctions [47]. This coupling between the neighboring MBSs, say γ_a and γ_b separated by distance L_{ab}, leads to an effective Hamiltonian of the tunneling form

$$H_{ab} \approx i t_{ab} \gamma_a \gamma_b, \quad t_{ab} \approx e^{-L_{ab}/\lambda_M} \tag{2.101}$$

This is due to the overlap of the wavefunctions of the two Majoranas in the junction across the distance L_{ab} . This coupling results in a tunnel splitting between the degenerate zero energy states associated with the MBS pair.

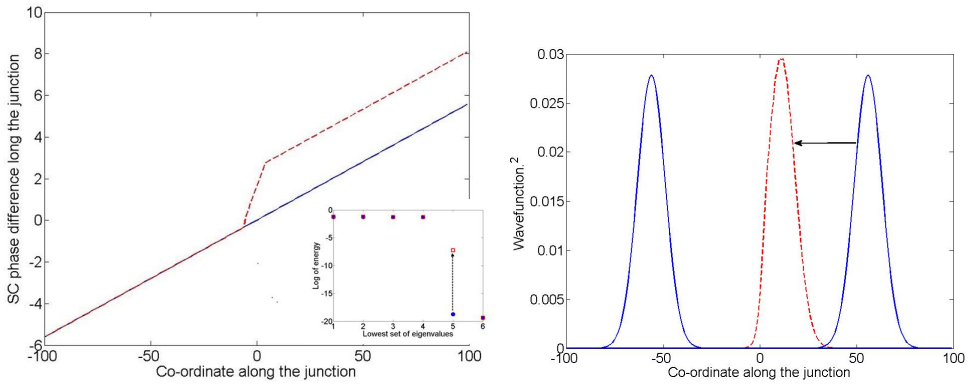

(a) (b)

Figure 2.21: The phase profile with and without change in the local SC phase is shown in (a). The slope of the phase is change in a small region between the Majorana modes. This results in a displacement of one of the Majorana modes as shown in (b). There is a corresponding shift in the energy of MBS as shown in the inset of (a)

The proposed S-TI-S architecture here hinges on the ability to move and couple MBS pairs. Our proposed schemes for such manipulation primarily involve changing the local phase variation. As an example, consider the case of two MBSs initially far apart, as shown in Fig.2.21. Now, changing the local phase more rapidly between the two MBSs, as shown in Fig.2.21.a, decreases their separation, as shown in Fig.2.21.b. The inset in Fig.2.21.a shows that the MBSs have come close enough to result in a numerically discernible tunnel splitting.

Such controlled MBS mobility and tunable coupling are essential ingredients in braiding schemes considered here. These schemes require the four-MBS configuration. Generalizing Eq. 2.101, the tunnel coupled effective Hamiltonian takes the form

$$H = it_{12}\gamma_1\gamma_2 + it_{23}\gamma_2\gamma_3 + it_{34}\gamma_3\gamma_4 \tag{2.102}$$

We will see that this Hamiltonian can be used to demonstrate an effective braiding by tuning one of the couplings. In the case of semi-conductor wire heterostructures, the values of t_{12} ,t_{23},t_{34} range around 0.5-30 μeV [133, 134] . For S-TI-S junctions of order of $1\mu m$ length and MBS separate by $0.1\mu m$, the strength of coupling between them would be of the order of $10^{-1}\mu eV$

The primary building blocks for non-Abelian rotations and braiding within the Josephson junction architecture are contained in Fig. 2.19 . The elements forming the basis of these non-Abelian rotation are the MBSs localized at Josephson vortices. Here we briefly outline the underlying principles, discussing the relevant Hilbert space, operations, and the physical manifestations associated with these rotations.

2.9.2 Braiding through physical motion of the MBSs

The simplest instance of braiding through involves four MBSs, say denoted by γ_1, γ_2, γ_3, γ_4. Any pair of MBSs forms a Dirac (electronic) state that can be occupied or not. As a specific choice, consider $c_A = (\gamma_1 + i\gamma_2)/2$,$c_B = (\gamma_3 + i\gamma_4)/2$. In the absence of coupling between the MBSs, the degenerate ground state manifold is spanned by

$$|N_A, N_B\rangle : |0,0\rangle, |1,1\rangle, |1,0\rangle, |0,1\rangle \tag{2.103}$$

where N_A, N_B denote the occupation of the electronic states. For N pairs of MBSs, the ground state is 2^N fold degenerate. The occupation of all such parity states decides the net fermionic parity of the ground of the system. Thus unlike conventional superconducting ground state, which is always a superposition of states having an even number of electrons in form of Cooper pairs, a topological superconductor can have states with net fermion parity to be either even or odd.

The simplest braiding operation is an exchange in the positions of the two MBSs. How does this exchange in the position space affect the space of ground state? It can be shown that [53] the exchange of two Majoranas γ_i,γ_j is represented in the ground state manifold as a unitary rotation in the space $\{|0,0\rangle, |1,1\rangle, |1,0\rangle, |0,1\rangle\}$ given by

$$U_{ij} = exp(\pm i\pi\gamma_i\gamma_j/4). \tag{2.104}$$

For example, if we start with a state $|0,0\rangle$, then exchanging γ_2, γ_3 results in

$$U_{23}|0,0\rangle = (|0,0\rangle - i|1,1\rangle)/\sqrt{2} \tag{2.105}$$

In principle, one can track such rotations by measuring the fermion occupation i.e the fermion parity of the electronic states in the ground-state manifold. The order of consecutive exchanges matter as the unitary operations do not commute: $U_{12}U_{23} \neq U_{23}U_{12}$. Thus the name non-Abelian rotation.

2.9.3 Effective braiding through tuning MBS coupling

A key feature of the topological qubit formed by the electron parity state is its non-locality. It is shared by to MBS states confined to vortices that can be very far apart. We have seen the manner in which physical exchange results in non-Abelian rotations in the Hilbert space of these parity states. An alternate method for performing non-Abelian rotations without physical exchange involves tuning the coupling between an MBS pair.

As a specific example, consider four MBSs $(\gamma_1, \gamma_{1'}, \gamma_2, \gamma_{2'})$, this time with their vortex cores aligned along

a junction, as in Fig.2.19.a . The effective low energy Hamiltonian of this system, is given by

$$H_{12} = it_1\gamma_1\gamma_{1'} + it_{12}\gamma_{1'}\gamma_2 + it_2\gamma_2\gamma_{2'}. \tag{2.106}$$

Here, MBSs $\gamma_{1,1'}$ are coupled with strength t_1, MBSs $\gamma_{2,2'}$ with strength t_2, and $\gamma_{1'}$ and γ_2 with t_{12}. Now let us denote the non-local electronic states by $\Gamma_1 = (\gamma_1 + i\gamma_{1'})/\sqrt{2}$ and $\Gamma_2 = (\gamma_2 + i\gamma_{2'})/\sqrt{2}$. The occupation of these modes is given by $N_1 = \Gamma_1^\dagger\Gamma_1$ and $N_2 = \Gamma_2^\dagger\Gamma_2$. As with the exchange braiding case, the Hilbert space of the system is given by the occupation of these 2 states $|N_1, N_2\rangle : |0,0\rangle, |1,1\rangle, |1,0\rangle, |0,1\rangle$. The Hamiltonian in this Hilbert space is then block diagonal. We focus only on even parity block corresponding to $|0,0\rangle, |1,1\rangle$; the odd parity block is decoupled and contains analogous physics. In the reduced two-component basis of even parity states, the tunnel coupled Hamiltonian of Eq.2.106 takes the form

$$H_{e12} = \begin{pmatrix} t_1 + t_2 & t_{12} \\ t_{12} & -(t_1 + t_2) \end{pmatrix} \tag{2.107}$$

Treating the two states of the Hilbert space $|0,0\rangle, |1,1\rangle$ as the "spin-up" and "spin-down" eigenstates of Pauli matrix σ_z respectively, we can cast the Hamiltonian in terms of Pauli matrices as:

$$H_{e12} = (t_1 + t_2)\sigma_z + t_{12}\sigma_x \tag{2.108}$$

Preparing the system in an initial state, say "spin up" $|0,0\rangle$ and then changing the t_{12} ("a transverse field") would result in the rotation of the state in the spin basis. Effectively, changing the coupling in two Majorana modes would induce non-local parity correlations. It has been explicitly shown that these rotations are equivalent to braiding operations we discussed in the previous section [133] .

Specific sequences of such effective braiding would involve preparing the system in a prescribed initial state in the degenerate Hilbert space, bringing a pair of MBSs to break the degeneracy via coupling, and time evolving the initial state in a manner prescribed by Eq. 2.106. The time scale for varying the coupling is set by the maximum degeneracy splitting; compared to actual braiding, which involves the robust topological operation of exchange, this time scale dependence poses a limitation. Nevertheless, given enough experimental control and knowledge of tuning parameters, qubit operations can be made viable through this procedure.

2.10 Summary and conclusion

To summarize the analysis of the Majorana wavefunctions and fermion parity switches in the finite-sized Kitaev chain, employing the Majorana transfer matrix and studying its properties enabled us to resolve the effect of any general potential landscape on the Majorana wavefunction. The wavefunctions are characterized by decay and oscillations where we found that the latter stems purely from the underlying normal tight-binding model. In the uniform system, these oscillations correspond to band oscillations which, when analyzed as a function of parameter space, allowed us to identify a circular regime in the topological phase in which Majorana wavefunctions oscillate. In the disordered case, the underlying normal tight-binding model is the Anderson model. Thus the underlying oscillations are random oscillations stemming from the Anderson problem and there are large fluctuations between different disorder realizations. Any further investigation on the oscillations and the resulting parity flips can thus bank on the vast literature on disorder and Anderson localization.

The disordered one-dimensional p-wave superconducting wire has been studied extensively in the past for its rich localization and Majorana physics. In spite of the random nature of the parity switches in the presence of disorder, the parity sectors of the uniform Kitaev chain can still dictate various qualitative features of switches in the disordered case. One of the striking observations is the presence of regimes in which no parity switching takes place for a range of disorder strengths. These features can have strong bearing on realistic protocols for topological quantum computation, where the operations are through ground state parity manipulations.

There are various features to be explored concerning Majorana wavefunction features and parity switches. With regards to disorder, several aspects can potentially be studied by invoking known results from the literature on disordered spin chains. One challenge with characterizing topological features in the presence of disorder, just as with non-topological features, is that certain quantities of interest might show large sample-to-sample fluctuations and appropriate quantities need to be identified for disorder averaging. For example, in the case of Anderson localization, the conductance itself has large fluctuations whereas the logarithmic conductance shows a Gaussian distribution in certain limits. Specifically, seeking a quantity for cleanly characterizing parity switches is in order; related studies in the context of Josephson junctions have been performed using random matrix theory [74, 135].

Having a precise handle of the parity landscape in Majorana wires is one of the key requirements for several topological quantum computational considerations. As an example, as shown in Refs.[136, 137, 138, 134, 133], one method of performing non-Abelian rotations in the degenerate Majorana ground state manifold is through tuning the coupling between Majorana modes. This method has formed the basis of various quantum

computational protocols [139, 134, 129, 77, 136, 137, 140]. Thus the detailed knowledge presented here on the degeneracy points in the topological phase diagram, parity switches in a finite length wire, and their behavior in the presence of disorder are all of relevance in this context.

Chapter 3

Non-equilibrium dynamics and topological phases

3.1 Introduction

This chapter focuses on non-equilibrium quench dynamics of the Kitaev chain and the signature of Majorana modes on the dynamics. Non-equilibrium dynamics in quantum many body systems have certain unique features compared to those in classical systems. These unique features are related to the existence of a ground state, a gap in the spectrum separating the ground state from other states and the unitary evolution of the Hamiltonian. There are seversal systems which do not possess a gap and yet have many interesting properties. While the thermal fluctuations lead to very interesting critical behaviour and phase transitions which change the nature of ground state of the system, considerations of quantum fluctuations at zero temperature lead to quantum phase transitions with accompanying critical behaviour [141]. One can tune a parameter of the Hamiltonian of a quantum many body system at zero temperature, such as chemical potential or a magnetic field, to take the system to a point in the parameter space where quantum fluctuations take over and completely rearrange the ground state configuration. At the quantum critical point, where the phase transition occurs, the energy gap that separate the ground state from excited states goes to zero. Therefore, an associated time scale near the quantum critical point diverges. Now, if we imagine the scenario of dynamically tuning a parameter of the Hamiltonian so that it crosses the critical point, the divergence of time scale does not allow the system to relax and leads to excitations above the ground state. One of the interesting outcomes of this is that the non-equilibrium excitations show universal behavior called 'Kibble-Zurek scaling' [142, 143], which informs us about the equilibrium critical points. Such scaling can be observed across 'classical' thermal phase transitions as well.

Bringing in topological phases into picture, we have seen that the ground states of topological phases have non-trivial features. One such feature is the existence of gapless states at the boundaries such as the Majorana zero modes. In this chapter we will study the signature of these Majorana modes on the non-equilibrium dynamics of the Kitaev chain. The ground state fermion parity plays a crucial role in these studies. For a closed periodic system, there is a lack of adiabaticity in the evolution of the ground state in

moving across a critical point. For an open system, there is a non-trivial lack of adiabaticity emerging even far form a critical point and within a topological phase, which is a signature of the Majorana modes. We have termed this lack of adiabaticity as 'parity blocking [43]' and shall be described in detail below.

In the following, we will first review the key aspects of dynamics across quantum critical points, specifically studying the transverse field Ising chain and derive the Kibble-Zurek scaling. Then we will study the non-equilibrium dynamics of the Kitaev chain focusing on the fermion parity effects and the phenomenon of parity blocking. The sections on parity blocking are based on my original work with collaborators, presented in the paper [43].

3.2 Quantum critical points: transverse field Ising chain

The characteristic features of quantum phase transitions are the critical behaviour of the gap and other correlation functions near the critical point. The critical behaviour entails power law scaling of these quantities and the exponents in the power law are independent of the details and only depend on the symmetries and the dimension of the system. Therefore they are called 'universal critical exponents'. For example, the Ising model has a specific set of critical exponents, but it could be used to model systems as distinct as magnets and polymers. We shall see how these critical exponents are of importance even for non-equilibrium behaviour. As mentioned above, the quantum phase transitions are driven by a non-thermal parameter of the Hamiltonian near zero temperature. The point in the parameter space where the phase transitions occur is called the quantum critical point(QCP), at which the ground state energy of the system is a non-analytic function of the parameter. At the QCP, the gap Δ between the ground state and the first excited state vanishes as a power law function of a parameter g [141, 144]:

$$\Delta \propto |g - g_c|^{\nu z} \tag{3.1}$$

Here ν and z are the critical exponents and g_c is the critical point. In a continuous phase transition, there is a characteristic length scale ξ associated with the exponential decay of the correlations in the ground state. As the critical point is approached, this length diverges with the critical exponent:

$$\xi \propto |g - g_c|^{-\nu} \tag{3.2}$$

One can associate a time scale with the vanishing of the energy gap in the system. This time scale ξ_τ

also diverges near the critical point as

$$\xi_\tau \sim \Delta^{-1} \propto |g - g_c|^{-\nu z} \tag{3.3}$$

Therefore the correlation length scale and the time scale are related by:

$$\xi_\tau \propto \xi^z \tag{3.4}$$

Here z is called the dynamical critical exponent.

Therefore, the space and time behaviour is intricately connected with each other in quantum phase transitions.We shall see that this also leads to interesting consequences for non-equilibrium excitations when the system is driven through the critical point.

The prototypical example of a quantum mechanical model exhibiting quantum phase transitions is the transverse field XY spin chain presented in the previous chapter. We shall deduce some of the critical exponents of this model. The Hamiltonian of this spin chain is given by:

$$H = -\sum_{n=1}^{N-1} [J_x \sigma_n^x \sigma_{n+1}^x + J_y \sigma_n^y \sigma_{n+1}^y] - \sum_{n=1}^{N} h\sigma_n^z \tag{3.5}$$

Here we will assume periodic boundary conditions $\sigma_{N+1} = \sigma_1$. As shown in the previous chapter this can be mapped to the Kitaev chain through a Jordan-Wigner transformation:

$$\begin{aligned} H &= \sum_{n=1}^{N-1} [-(J_x + J_y)(c_n^\dagger c_n + 1 + \text{h.c}) + (J_x - J_y)(c_n^\dagger c_{n+1}^\dagger + \text{h.c})] & (3.6) \\ &- (-1)^{N_f} [-(J_x + J_y)(c_N^\dagger c_1 + \text{h.c}) + (J_x - J_y)(c_1^\dagger c_N^\dagger + \text{h.c})] - \sum_{n=1}^{N} (2c_n^\dagger c_n - 1) & (3.7) \end{aligned}$$

Fourier transforming to k-space: $c_k = \sum_{n=1}^{N} c_n e^{-ikn}/\sqrt{N}$, we obtain the Hamiltonian:

$$H = \sum_{k>0} \begin{pmatrix} c_k^\dagger & c_{-k} \end{pmatrix} H_k \begin{pmatrix} c_k \\ c_{-k}^\dagger \end{pmatrix} \tag{3.8}$$

$$H_k = 2 \begin{pmatrix} -(J_x + J_y)\cos(k) - h & i(J_x - J_y)\sin k \\ -i(J_x - J_y)\sin k & (J_x + J_y)\cos k + h \end{pmatrix} \tag{3.9}$$

Here $k : [0, \pi]$. The Hamiltonian can be diagonalized using the Bogoliubov transformation

$$\begin{pmatrix} d_k^\dagger \\ d_{-k}^\dagger \end{pmatrix} = \begin{pmatrix} \sin\theta_k c_k & i\cos\theta_k c_{-k}^\dagger \\ \sin\theta_k c_{-k} & -i\cos\theta_k c_k^\dagger \end{pmatrix} \tag{3.10}$$

The angle θ_k is defined as $\tan 2\theta_k = -\frac{(J_x - J_y)\sin k}{(J_x + J_y)\cos k + h}$. The Hamiltonian is then diagonal and the spectrum is given:

$$\omega_k = 2[h^2 + J_x^2 + J_y^2 + 2h(J_x + J_y)\cos k + 2J_x J_y \cos(2k)] \tag{3.11}$$

The points at which the spectrum vanishes in the k-space are : $0, \pi, k_0 = \arccos(-j(J_x + J_y)/(4J_x J_y))$. The gap closing points in the parameter space are then:$i) J_x + J_y = -h$,$ii) J_x + J_y = h$, $iii) J_x = J_y$ and $|h/J_x| \leq 2$. At these points the gap vanishes linearly $\omega_k \sim k$. Therefore, the dynamical critical exponent of the transverse field Ising chain is given by $z = 1$. Since $\nu z = 1$, the critical exponent $\nu = 1$. We shall see that these critical exponents appear in the non-equilibrium behaviour.

3.2.1 Dynamics across quantum critical points: Kibble-Zurek mechanism

In a quantum many body system that is driven, the relaxation time scale diverges at the critical point as the gap goes to zero. The driving of the Hamiltonian has its own time scale . If the relaxation time scale is smaller than the time scale of the driving, the evolution is adiabatic and the system remains in the ground state. But near the quantum critical point, the relaxation time start growing as a power law faster than the driving of the system. This leads to breakdown of adiabaticity and there will be non-equilibrium excitations over the ground state. The density of the non-equilibrium defects obey a scaling law know as the Kibble-Zurek scaling, which is derived as follows [145, 146, 144]: Suppose, a parameter of the Hamiltonian g is varied to cross the critical point g_c as $\lambda = g - g_c = t/\tau$. The critical point occurs at $t = 0$. Let $\hat{t}$ be the time at which the adiabaticity breaksdown in the driven system. Then $|\lambda/\dot{\lambda}|_{\hat{t}} = \hat{t} = \xi_\tau|_{\hat{t}}$. The relaxation time diverges as $\xi_\tau \sim |g - g_c|^{-\nu z}$. Therefore,

$$\hat{t} \sim \tau^{\nu z/(\nu z+1)} \tag{3.12}$$

For a slow variation of the Hamiltonian i.e. large τ, one can focus on the low-energy modes as the higher energy modes follow adiabatic evolution. Assuming that the domain of defects are of the size $\xi \sim \xi_\tau^{1/z}$, the

density of defects in d dimensions is given by

$$n \sim \frac{1}{\xi^d} \sim \tau^{-d\nu/(\nu z+1)} \tag{3.13}$$

Thus the density of non-equilibrium defects produced by driving the system across a critical point obeys universal scaling with the exponents given by the equilibrium point . This is called the Kibble-Zurek scaling. This was first proposed in the context continuous symmetry breaking phase transitions in early universe by Kibble [147] and was later extended to condensed matter systems by Zurek [143]. It was also extended to QCPs of quantum phase transitions.

Now we'll proceed to study the non-equilibrium dynamics of the Kitaev chain. The presence of Majorana modes in the topological phase have a non-trivial effect when the system is driven in a linear way even within the topological phase. It shows a breakdown of adiabaticity very different than the Kibble-Zurek mechanism.

3.3 Fermion parity effects in non-equilibrium dynamics

As we saw in the previous chapter, the Kitaev chain is one of the paradigmatic systems exhibiting topological phases and also has quantum critical points as phase boundaries between topologically non-trivial and trivial phases. Within the topological phase, considerations of fermion parity of the ground state give rise to more detailed features in the phase diagram such as the circle of oscillations and the fermion parity sectors for a finite chain. He we will study the dynamical tuning of parameters across the quantum critical point as well as the fermion parity sectors and see how they lead to drastic effect in the dynamics.

3.3.1 Topological blocking

Before studying a open system with Majorana modes at the edges, let us consider a system with closed boundary conditions. The non-trivial effects of ground state fermion parity was shown to lead to something called 'topological blocking' [2]. To understand this recall the factor of $(-1)^{N_f}$ appearing in the fermionized version of the transverse Ising chain in Eq.(3.7). Here N_f is total fermion number in the chain. So the factor $T_z = (-1)^{N_f}$ is the parity of the total fermion number in the chain and it also encodes the boundary conditions in the system. $T_z = -1$ gives the periodic sector and has odd number of fermions and $T_z = +1$ gives the anti-periodic sector and has even number of Fermions. When the system has closed boundary conditions, the degeneracy in the ground state can change the overall fermion parity. In the anti-periodic sector with even number of fermions the allowed momenta are given by $k = \frac{2\pi}{N}(n+1/2)$, $n \in [-N/2, N/2-1]$.

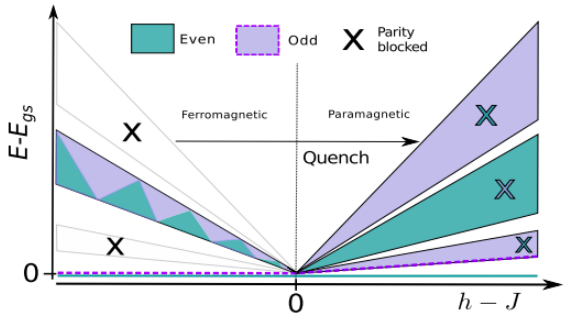

(a)

Figure 3.1: Schematic showing topological blocking across the quantum critical point in a transverse field Ising chain. The ferromagnetic phase has double degeneracy in the ground state. The degenerate states are labeled by the fermion parity(indicated by lines of different colors). In paramagnetic phase,the ground state is unique and always lies in the even parity sector. Therefore, the odd parity sector in the ferromagnetic phase is blocked from evolving into the lowest energy state on crossing the critical point.(Figure adapted from [2])

This does not include the values of $0, \pi$. The ground state is given by

$$|GS\rangle = \prod_{Nk/\pi odd} (\cos\theta_k + i \sin\theta_k c_k^\dagger c_{-k}^\dagger) |0\rangle \tag{3.14}$$

In the periodic sector with odd number of fermions, the allowed momenta are given by $k = \frac{2\pi}{n}$, $n \in [-N/2, N/2 - 1]$. These include the values of momenta $0, \pi$. The ferromagnetic phase $J > h$, $\cos\theta_0 = 0, \sin\theta_0 = 1$ and $\cos\theta_\pi = 1, \sin\theta_\pi = 0$. Thus the $k = 0$ zero mode $c_0^\dagger$ contributes to the fermion number and the parity of the ground state can be even:

$$|GS\rangle_{odd} = c_0^\dagger \prod_{Nk/\pi even} (\cos\theta_k + i \sin\theta_k c_k^\dagger c_{-k}^\dagger) |0\rangle \tag{3.15}$$

For very large N, the the odd and even fermion parity state are degenerate. In the paramagnetic case $h > J$, the odd fermion parity sector has a $k = 0$ state with $\cos\theta_0 = 1, \sin\theta_0 = 0$. The ground state would have these modes unoccupied. Therefore, the odd fermion parity sector is not in the ground state in the paramagnetic phase. The ground state always lies in an even parity sector.Therefore, the the ferromagnetic case has a double degeneracy in the ground state with the degenerate states labelled by even and odd fermion parity. The paramagnetic phase always has ground state in the even parity sector and the odd parity sectors in the excited states. Thus one gets a scenario as shown in Fig.(3.1).

Now considering dynamically varying the parameters of the system across the critical point one gets a scenario as shown in Fig.(3.1). As the Hamiltonian evolution of an initial ground state preserves fermion

parity, if one starts with a odd fermion parity ground state in the ferromagnetic phase and the system is taken across the critical point, it is blocked from being in the ground state as one enters the paramagnetic phase. Thus in the adiabatic limit,only the even sectoral state in the ferromagnetic phase flows into the lowest energy state in the paramagnetic phase. The lack of adiabaticity in the evolution of one of the sectors on crossing the critical point is termed as 'topological blocking'. Though the discussion was on the transverse field Ising chain, the arguments were made in the fermionic basis, which corresponds to the Kitaev chain with appropriate boundary conditions. There instead of ferromagnetic and paramagnetic phases, one has topological trivial phases. Opening the boundary conditions in the Kitaev chain leads to Majorana modes localised at the edges of the chain in the topological phase. This gives rise to non-trivial effects in the dynamical evolution with the topological phase itself.

3.4 Non-equilibrium dynamics in Majorana wires with open boundary conditions and parity blocking.

Now we consider a finite-sized Kitaev chain and study the effect of fermion parity in its non-equilibrium dynamics. We specifically consider a linear variation with time of the chemical potential of the system so as to go across the critical line $\mu = 2w$,

$$\mu(t) = (2 - \mu_i)t/\tau + \mu_i. \tag{3.16}$$

Here μ_i is the initial chemical potential at $t = 0$ and $1/\tau$ is the quench rate. Due to the finite rate of variation of μ, the system cannot remain exactly in its ground state and will exhibit non-equilibrium behavior. Namely, excitations (or defects) will be produced in the ground state; this lead to an excess energy of the system and may also lead to a ground state which is in a different topological sector than the initial ground state. These effects can be characterized by the following quantities.

- Defect density: The number of defects produced in the ground state configuration, which is given by the sum over all the excitations.

- Adiabatic Fidelity $\mathcal{O}(t)$: This is the inner product of the instantaneous ground state $|\psi_{ins}(t)\rangle$ of the time-dependent Hamiltonian with the time evolved initial ground state $|\Psi(t)\rangle$,

$$\mathcal{O}(t) = |\langle \Psi(t) \, | \psi_{ins}(t) \rangle \, |. \tag{3.17}$$

- Residual energy E_{res}: This is the energy in excess of the instantaneous ground state of the system.

We will define this as the dimensionless quantity

$$E_{res} = [\langle\Psi(t)|H(t)|\Psi(t)\rangle - E_G(t)]/|E_G(t)|, \tag{3.18}$$

where E_G is the energy of the ground state at time t.

3.4.1 Real space formalism for studying quenching dynamics for open boundary conditions

In the limit of very large system size or with periodic boundary conditions, one can Fourier transform the Hamiltonian to momentum space. The form of the Hamiltonian is very simple as seen in a previous section. Therefore, doing calculations in k-space one can obtain expressions for the defect density, adiabatic fidelity and residual energy. In the limit of long time t, all these quantities have a universal power law scaling as a function of the quench rate which is related to the post-quench excitations. This is the well studied Kibble-Zurek scaling [148, 149, 144, 147, 142, 143, 150, 151, 152, 153, 154, 146, 155, 156, 157, 158, 159, 160, 161, 162, 163, 164, 165, 166, 167, 168, 169, 170, 171, 172, 173, 174, 175, 57, 176, 177, 178, 179, 180, 181, 182, 183]. Given the quench rate $1/\tau$, the defect density and residual energy scale as $1/\sqrt{\tau}$ and the adiabatic fidelity scales as $\exp(c/\sqrt{\tau})$ in this one-dimensional Majorana wire[2].

For the Majorana wire with open boundary conditions, while it has been found that the single particle bulk states still obey the Kibble-Zurek scaling for the defect density, the quench for an initial state with a Majorana end mode has been found to be non-universal and dependent on the topological features of the system [173]. The end states are not robust with respect to the quench and they delocalize to merge with the bulk states. This leads to a scaling of the defect density as τ^0 (i.e., independent of the quenching rate), which is very different from the Kibble-Zurek scaling.

Here we will study the quenching dynamics in the above mentioned quantities for an open Majorana wire. We will mainly focus on the many-body states rather than the single particle states and the parity switching mechanism, which comes about in the topological phase due to the coupling between the Majorana end modes.

In comparison to the translationally invariant systems with periodic boundary conditions , a challenge encountered in these finite-sized systems with open boundary conditions is that one cannot exploit the momentum basis. In principle, we are faced with the full-fledged 2^N -dimensional Hilbert space associated with fermions on a N-site lattice associated with the Fock space formed by fermion occupancy on each site. Here, a dynamic many-body technique to reduce the problem to a numerically tractable form is developed

using the Heisenberg picture so that the crux of the information on the time evolution is given by the relation between fermionic creation/annihilation operators at different times and using an analog of Wicks theorem for Majorana operators. The computation then reduces to dealing with time-dependent $2N \times 2N$ matrices.

Let us start with a general time-dependent Hamiltonian which is quadratic in Majorana operators a_j $(j = 1, 2, \cdots, 2N)$,

$$H = i \sum_{i,j=1}^{2N} a_i M_{ij}(t) a_j. \tag{3.19}$$

Here $M(t)$ is a real antisymmetric matrix; its elements will be functions of w, Δ and μ for the Majorana wire Hamiltonian

$$H = -\frac{i}{2} \sum_{n=1}^{N-1} \Big[(w - \Delta) a_{2n-1} a_{2n+2} - (w + \Delta) a_{2n} a_{2n+1} \Big] - \frac{i\mu}{2} \sum_{n=1}^{N} a_{2n-1} a_{2n}.$$

This can be converted to the canonical form

$$H = 4 \sum_{j=1}^{N} \lambda_j(t) b_j^\dagger(t) b_j(t), \tag{3.20}$$

up to a constant, by a time-dependent transformation $B(t)$,

$$\bar{b}(t) = B(t) \bar{a}. \tag{3.21}$$

Here $\bar{b}(t)$ is a $(2N)$-component vector $\bar{b} = (b_1, b_2, \cdots, b_N, b_1^\dagger, \cdots, b_N^\dagger)^T$ and so is $\bar{a} = (a_1, a_2, \cdots, a_{2N})^T$. The $(2N)$-dimensional matrix $B(t)$ comprises of the eigenvectors of $H(t)$ and it belongs to the group $U(2N)$ with $det(B) = \pm 1$. The eigenvalues of the Hamiltonian are $\pm\lambda_j$.

Adiabatic fidelity calculation: As defined in a previous section the adiabatic fidelity is given by $\mathcal{O}(t) = |\langle \psi_{ins}(t) | \Psi(t) \rangle|$. The corresponding annihilation operators of these many-body states satisfy the relations $b_j(t) |\psi_{ins}(t)\rangle = 0$ and $\beta_j(t) |\Psi(t)\rangle = 0$, where $|\Psi(t)\rangle = S(t,0)\Psi(0)$ and $\bar{\beta}(t) = B(0)S(t,0)\bar{a}$. Here $S(t,0) = \mathcal{T} exp(-4 \int_0^t M(t')dt')$ is the evolution operator, with $\mathcal{T}$ denoting time ordering. The two sets of annihilation operators are related by

$$\bar{\beta}(t) = B(0)S(t,0)[B(t)]^{-1} \bar{b}(t) = G(t)\bar{b}(t). \tag{3.22}$$

The key idea underlying the calculation in real space is to express the quantities of interest to us in terms of objects which can be calculated numerically in a simple way. Given the form of the initial Hamiltonian $H(0)$ and the time-dependent $H(t)$, we can see that the quantities $B(0)$, $B(t)$, $S(t,0)$ and $G(t)$ can be easily

computed. Given these and the annihilation operators for the ground states, the calculation of the adiabatic fidelity reduces to a computation of the determinant of an antisymmetric matrix A given by

$$\begin{aligned} A_{jk} &= \langle\psi_{ins}(t)|\, \bar{\beta}_j(t)\bar{\beta}_k(t)\, |\psi_{ins}(t)\rangle \quad \text{for} \quad j<k, \\ &= -\langle\psi_{ins}(t)|\, \bar{\beta}_k(t)\bar{\beta}_j(t)\, |\psi_{ins}(t)\rangle \quad \text{for} \quad j>k, \\ &= 0 \quad \text{for} \quad j=k. \end{aligned}$$

We now directly state an important result, deferring the detailed derivation to Appendix A. The adiabatic fidelity defined in Eq. (3.17) is given by

$$\mathcal{O}(t) = |det(A)|^{1/4}. \tag{3.23}$$

Given this relation and the Hamiltonian $H(t)$, we can numerically calculate the adiabatic fidelity as a function of time for a system with open boundary conditions. This can naturally be extended to periodic/antiperiodic boundary conditions as well.

Residual energy calculation: Another quantity of interest, the residual energy, defined in Eq. (3.18), measures the excess energy contained in the time-evolved quench dependent state compared to the instantaneous ground state energy. This quantity can also be calculated with the real space formalism developed in this section. Following the same strategy as for the adiabatic fidelity, the final expression can simply be expressed in terms of the matrix $G(t)$,

$$E_{res} = [4\sum_{j,k}^{N} \lambda_j G^{-1}_{N+j,k}(t) G^{-1}_{j,k+N}(t)]/|E_G(t)|. \tag{3.24}$$

The details of the derivation are given in Appendix .

We now present the results that we obtain for an open Majorana wire with N sites with the Hamiltonian given in Eq. (3.20), where μ varies linearly in time as shown in Eq. (3.16). Given the specific form of $H(t)$ in Eq. (3.20), where μ varies linearly in time as shown in Eq. (3.16), one can numerically calculate all the quantities $B(0)$, $B(t)$ in Eq. (3.21), $S(t,0)$, $G(t)$ in Eq. (3.22) and finally the adiabatic fidelity $\mathcal{O}(t)$ in Eq. (3.23) and the residual energy E_{Res} in Eq. (3.24). For a fixed Δ and N, the parity changes sign as we sweep across the topological phase by varying μ. The initial parity of the system is set by the value of μ_i and the number of sites N. As we will see below, the choice of μ_i can have drastic consequences, especially for an odd number of sites.

3.4.2 Adiabatic fidelity and Parity blocking

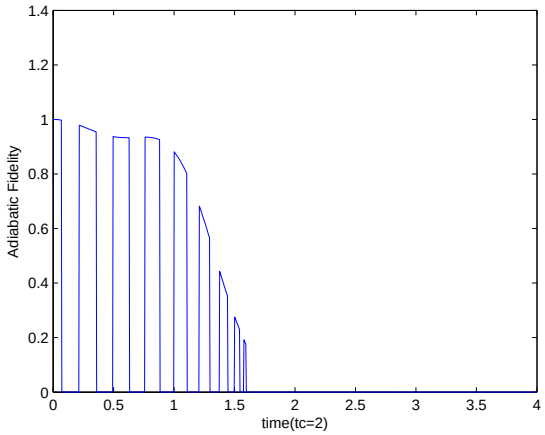

(a) Adiabatic fidelity for $N = 34$.

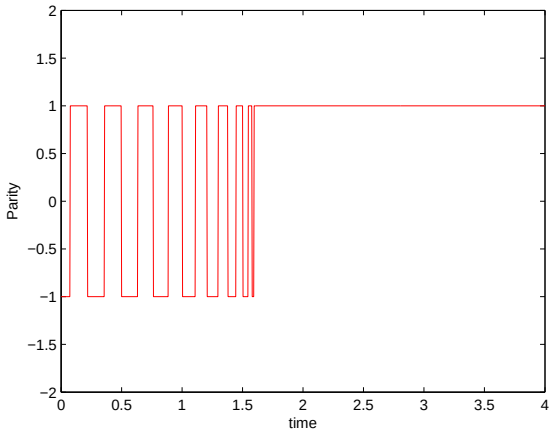

(b) Parity for $N = 34$.

Figure 3.2: (Color online) Numerical results for the (a) adiabatic fidelity $\mathcal{O}(t)$ and (b) parity of the instantaneous ground state for an even number of sites. The times at which the parity switches its sign are exactly the points where parity blocking occurs, resulting in the adiabatic fidelity plummeting down to zero. Depending on the parameters chosen, the parity after crossing the quantum critical point changes from the initial ground state parity thereby leading to parity blocking for the entire topologically trivial region.

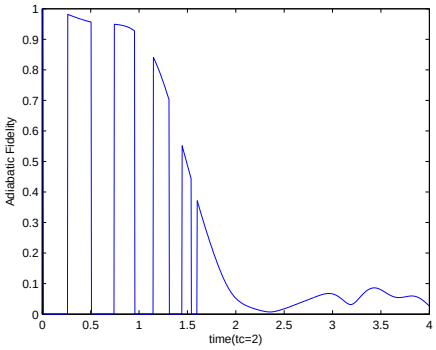

(a) Adiabatic fidelity for $N = 17$ with $\mu_i \neq 0$.

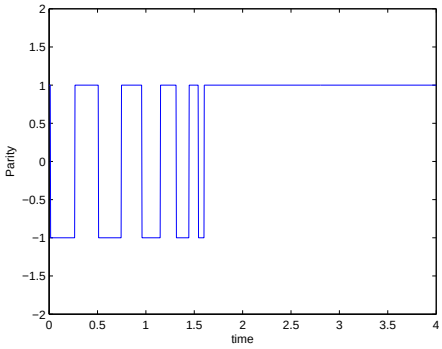

(b) Parity for $N = 17$ with $\mu_i \neq 0$.

Figure 3.3: Numerical results for (a) adiabatic fidelity $\mathcal{O}(t)$ and (b)parity of the instantaneous ground state for an odd number of sites. In this case the system has the same parity as the initial ground state on crossing the quantum critical point (Figure (b)) and therefore has a non-vanishing overlap with it.

Figures 3.2 and 3.3 show the numerical results for the adiabatic fidelity $\mathcal{O}(t)$ along with the parity of the instantaneous ground state for an open chain with an even and odd number of sites, respectively. The case of the initial value $\mu_i = 0$ for an odd number of sites will be discussed later. We can see from Figs. 3.2 and 3.3 that for both even and odd number of sites, the system starts in a particular fermion parity sector, and as it moves within the topological phase the instantaneous ground state switches parity

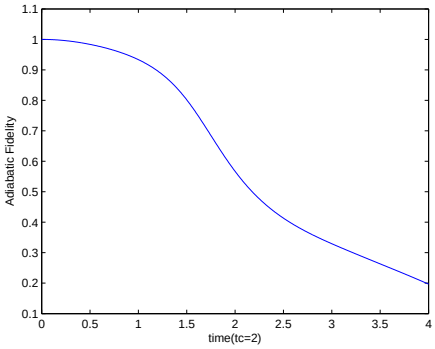

Figure 3.4: Numerical results for quenching with $\mu_i > 2\sqrt{1-\Delta^2}$. i.e outside the domain of oscillations as shown in the phase diagram. Here the nature of Majorana wave functions at the edges are purely decaying and their coupling would not have any oscillations, which would result in the ground state parity not switching as one sweeps through the parameter space.

regularly. On crossing the critical point it can either have opposite parity from the initial state or the same parity, depending on the initial parity sector. On the other hand, as we are dealing with parity conserved systems, the state which is time evolved from the initial ground state continues to have the same fermion parity. Thus the overlap of the time evolved state with the instantaneous ground state plunges to zero at times when the instantaneous parity becomes opposite to the initial parity. We call these parity oscillations, which occur for an open Majorana wire, as the parity blocking effect. The initial ground state is blocked from having any non-zero overlap with the instantaneous ground state for certain values of μ. Finally, on crossing the quantum critical point it becomes zero at all times if the parity is flipped from the initial ground state; this is also a manifestation of parity blocking. Hence, in Fig. 3.2, the case of an even number of sites, the parities of the initial and final ground states are the opposite and the system shows parity blocking for the entire topologically trivial phase, while in Fig. 3.3, the parities are matched and there is some residual overlap in the trivial phase.

Domain with no parity blocking: The parity oscillations do not occur throughout the parameter space corresponding to the topological phase. Namely, there are no oscillations if $\mu^2 > 4(w^2 - \Delta^2)$. This implies that there ought to be no parity blocking in the adiabatic fidelity. We indeed see this in the numerical results shown in Fig. 3.4.

Fermion parity degeneracy for an odd number of sites: For an open chain with an odd number of sites, and for states which belong to the odd fermion sector, the $\mu_i = 0$ point is special in that it has two degenerate ground states. To see this, let us define an operator

$$C \;=\; i^{N(N-1)/2}\; a_1 a_4 a_5 a_8 \cdots\,, \tag{3.25}$$

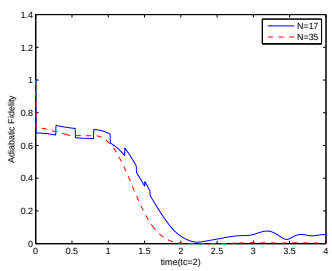

(a) Partial blocking in adiabatic fidelity for different N.

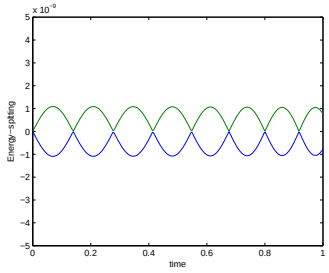

(b) No energy splitting at $t = 0$.

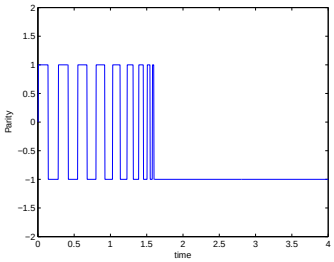

(c) Usual parity switching of the instantaneous ground state.

Figure 3.5: Numerical results for quenching with $\mu_i = 0$ for the odd sector. This is the special case where the initial state is in a superposition of the odd and even parity states.Thus the time evolved states will not be completely 'parity blocked' but the amplitude of adiabatic fidelity will be reduced. As we go to smaller N the splitting is exponentially enhanced and one can clearly see the effect of it in 'skewing' the superposition towards the state which contributes to the ground state.

where the last term on the right hand side is given by a_{2N-1} if N is odd and a_{2N} if N is even. We note that C is both Hermitian and unitary, so that $C^2 = I$. Recalling that $f_n = (1/2)(a_{2n-1} + ia_{2n})$ and $f_n^\dagger = (1/2)(a_{2n-1} - ia_{2n})$, we find that C generates the particle-hole transformation

$$\begin{aligned} Cf_nC &= (-1)^{n+N-1} f_n^\dagger, \\ Cf_n^\dagger C &= (-1)^{n+N-1} f_n. \end{aligned} \tag{3.26}$$

This is a symmetry of the Hamiltonian if $\mu = 0$. We now note that the parity and charge-conjugation operators P and C satisfy $PC = (-1)^N CP$. Thus P and C anticommute if the number of sites N is odd. Since P and C both commute with H if $\mu = 0$, every energy of a system with an odd number of sites will have a two-fold degeneracy with the two eigenstates having opposite fermion parities. (This can be shown as follows. If $|\psi_+>$ is an eigenstate of H and P with eigenvalues E and $+1$ respectively, the relations $PC = -CP$ and $HC = CH$ imply that $|\psi_->= C|\psi_+>$ is an eigenstate of H and P with eigenvalues E and -1 respectively).

Therefore, starting from $\mu_i = 0$ means starting with parity states whose degeneracy is not split. The time evolution of an arbitrarily chosen ground state would therefore be that of a linear combination of both parity states. Even though the parity of the instantaneous ground state would keep switching as one sweeps through the topological phase, the overlap would be finite as the time evolved state will be in a superposition of both parities. But the value of the adiabatic fidelity will be smaller than in the parity blocked case as the amplitude is split between the two superposed states. Figure 3.5 shows the results for this unique case of quenching. We can clearly see in Fig. 3.5 that the splitting is zero at time $t = 0$. This change in the initial

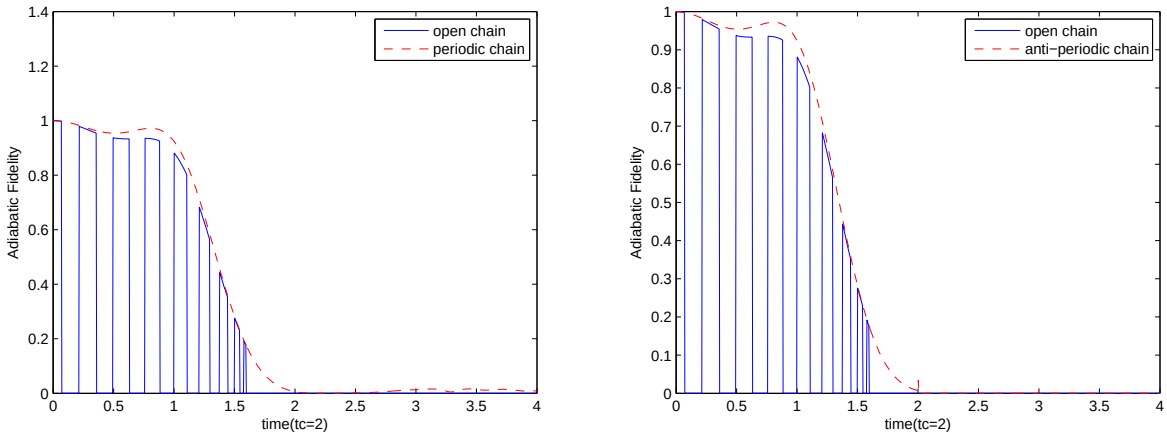

(a) (b)

Figure 3.6: Numerical calculation of $\mathcal{O}(t)$ for a closed chain with 34 sites. The periodic and antiperiodic closed chains represent even and odd fermion sectors respectively. One can see that there is blocking in the second case, whereas a small amount of overlap persists in the first case after crossing the critical point. Also the envelope of the adiabatic fidelities for closed chains is compared with that of the open chain for the same number of sites. Even though there is no 'parity blocking' within the topological phase in the case of closed chain due to absence of the edge modes, the overall the behavior remains qualitatively the same.

condition drastically affects the evolution of the ground state and we do not see complete parity blocking in this case.

Comparison with a closed chain: The case of parity blocking in closed chains with periodic and antiperiodic boundary conditions has been studied in detail [2]. While the previous analysis involved momentum modes, simplifying the problem to a set of two-level Landau-Zener systems, the real space formalism is easily extended here to compute all the quantities for a closed chain. The numerical results are shown in Fig. 3.6. Even though there is parity blocking in the case of an open chain, we may still expect the envelope of the adiabatic fidelity to be comparable with that of the periodic case. In Fig. 3.6, we see a good match between the envelopes in the two cases. For a closed chain, the final parity can flip from the initial state depending on the boundary conditions. As can be seen, the parity does not change for the periodic closed chain and therefore one still has a finite overlap. The match between the envelopes in the open and closed chain cases is very close. This suggests that overall the open chain would also respect the Kibble-Zurek behavior for the defect production and excitation density that was found in the closed chain case. The crucial difference between open and closed chains is the parity blocking and switching due to the coupling of the two Majorana end modes.

3.4.3 Residual Energy

The numerical results for the variation of the residual energy with time using the full many-body formulation in Eq. (3.24) is shown in Fig. 3.7 for both open and closed chains. The two cases have the same average behavior. Both show a rapid increase in the energy of the system above the instantaneous many-body ground state as they approach the critical point. This rapid rise is due to the system falling out of equilibrium upon approaching the critical point and thus losing adiabaticity. Far beyond the critical point, we find that the energy asymptotes to a fixed average value.

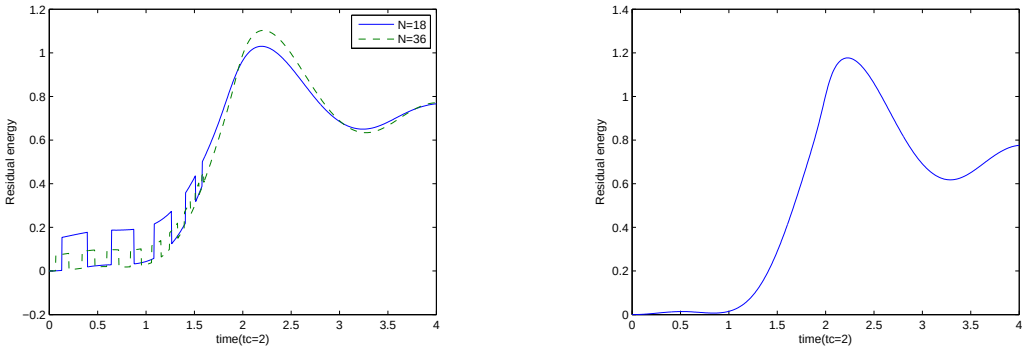

(a) Residual energy for an open chain with $N = 36$ and $N = 18$.

(b) Residual energy for a periodic closed chain with $N = 34$

Figure 3.7: Residual energy plots with the critical point occurring at $t = 2$. One can notice in the case of open chain the oscillations before crossing the critical point, which arise due to the oscillation of mid-gap states.One can see that the steps arising due to the splitting scales inversely with the system size.

Effect of Majorana end modes: The crucial difference between the open and closed chains in Fig. 3.7 is the presence of the abrupt jumps at small times in the case of the open chain. Reflecting the behavior of adiabatic fidelity, these jumps correspond to switching back and forth between the ground state and excited states due to parity blocking. Upon comparing the behavior of the residual energy with the energy splitting and parity switching, we find that there is a complete match between the points at which the jumps in the residual energy take place and the points where the parity switching occurs.

Signatures of Loschmidt echoes: In addition to parity blocking, there is evidence for the Majorana-mode related physics found in previous work on single particle dynamics in quenching [184]. The Loschmidt echo studied in this work calculates the probability for an initial Majorana mode to become a single-particle bulk excitation as a function of time as one sweeps through the critical point. If one varies $\mu(t)$ extremely slowly so as to be close to the adiabatic limit, the gap between the mid-gap end states and bulk states scales as $1/N$ on approaching the critical point since the dynamical critical exponent is equal to 1. The level spacing of the low lying bulk states also scales as $1/N$. Hence the Loschmidt echo turns out to be a periodic

function with period N as one quenches to or across the critical point.

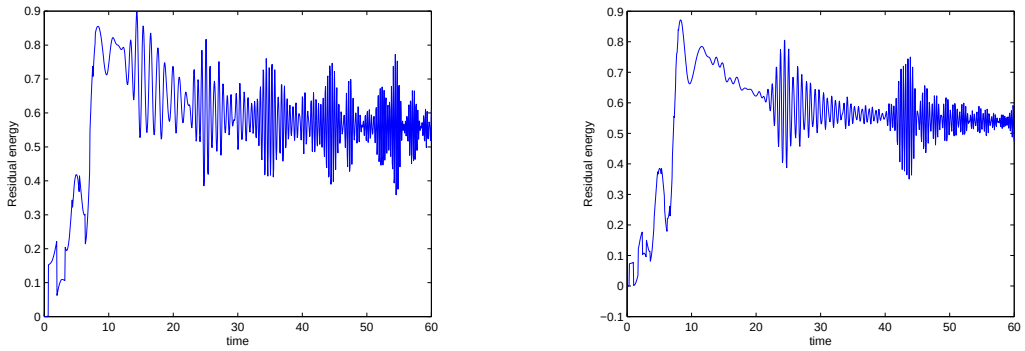

(a) $N = 18$ (b) $N = 36$

Figure 3.8: The residual energy plots for a very small quench rate which is nearly adiabatic. In this case one can see the periodic recurrence of excitations at times after crossing the critical point. The period is doubled if we double the system size.

In the results from the real space many-body formalism, these echoes appears as 'chirps' of excitations whose occurrence has a period of N. These excitations contribute to the overall energy of the state. Note that this is true only if the quench rate is extremely slow. As shown in Fig. 3.8, one can see these oscillations in the numerical results at a low quench rate like $1/\tau = 0.1$. The frequency of occurrence of these chirps in the excitations is indeed halved when the system size is doubled. These chirps also appear in the adiabatic fidelity.

To summarize, open and closed chains broadly show similar average behaviors as expected for quench dynamics, However, both in the adiabatic fidelity and residual energy, distinct non-analytic features arise in the form of jumps only for an open chain, and these can be attributed directly to the presence of end modes and their associated fermion parity.

3.5 Real-space formalism for non-equilibrium dynamics

Here we present the details of the real-space formalism used for calculation of Adiabatic fidelity, ground-state Fermion parity and residual energy.

3.5.1 Calculation of adiabatic fidelity $\mathcal{O}(t)$

Let us start with a general Hamiltonian which is quadratic in Majorana operators a_j,

$$H = i \sum_{i,j=1}^{2N} a_i M_{ij}(t) a_j. \tag{3.27}$$

The antisymmetric Hermitian matrix iM has real eigenvalues which come in pairs $\pm\lambda_j$ with corresponding eigenvectors x_j and x_j^*, which are orthonormal to each other. We define a set of linear combinations of Majorana operators in terms of these eigenvectors as

$$\begin{aligned} b_j^\dagger(t) &= \frac{1}{\sqrt{2}} \sum_{i=1}^{2N} (x_j^T)_i a_i, \\ b_j(t) &= \frac{1}{\sqrt{2}} \sum_{i=1}^{2N} (x_j^\dagger)_i a_i. \end{aligned} \tag{3.28}$$

In terms of a $(2N)$-component vector $\bar{b} = (b_1, b_2, \cdots, b_N, b_1^\dagger, \cdots, b_N^\dagger)^T$, Eq. (A2) can be expressed as a linear transformation

$$\bar{b}(t) = B(t)\bar{a}. \tag{3.29}$$

The rows of the $(2N)$-dimensional matrix B are the eigenvectors x_j^T and $x_j^\dagger$, and B belongs to the unitary group $U(2N)$ with $det(B) = \pm 1$. In terms of b_j, the Hamiltonian (A1) becomes, up to a constant,

$$H = 4 \sum_{j=1}^{N} \lambda_j b_j^\dagger b_j. \tag{3.30}$$

If $|\Psi(0)\rangle$ is the initial ground state of H at $t = 0$, then $b_j(0)|\Psi(0)\rangle = 0$. The instantaneous ground state $|\psi_{ins}(t)\rangle$ of $H(t)$ is annihilated by $b_j(t)$, namely, $b_j(t)\,|\psi_{ins}(t)\rangle = 0$.

We now want to find the adiabatic fidelity $\langle\Psi(t)|\psi_{ins}(t)\rangle$. Let us examine the operators which annihilate the time evolved state $|\Psi(t)\rangle$ and some of their properties. Let us say $\beta_j(t)\,|\Psi(t)\rangle = 0$. We want to put the information of the time evolution with $H(t)$ into $\beta_j(t)$. The time evolution of the Majorana operators a_j is given by their Heisenberg equations of motion:

$$\frac{da_j(t)}{dt} = -i[H(t), a_j(t)] = -4 \sum_{k=1}^{2N} M_{jk}(t) a_k(t). \tag{3.31}$$

In terms of a $(2N)$-component vector $\bar{a}$, the solution of the equation $d\bar{a}(t)/dt = -4M(t)\bar{a}(t)$ is given by the

evolution operator

$$\bar{a}(t) = S(t,0)\bar{a}(0). \tag{3.32}$$

Here $S(t,0) = \mathcal{T}exp(-4\int_0^t M(t')dt')$ which can be calculated numerically for a given $M(t)$. It can now be shown that $\bar{\beta}(t) = B(0)\bar{a}(t) = B(0)S(t,0)\bar{a}(0)$, where $\bar{\beta}(t)$ is the $(2N)$-component vector comprising of $\beta_j(t), \beta_j^\dagger(t)$ similar to $\bar{b}(t)$. Therefore the relation between $\bar{\beta}(t)$ and $\bar{b(t)}$ is given by

$$\bar{\beta}(t) = B(0)S(t,0)[B(t)]^{-1}\bar{b}(t). \tag{3.33}$$

The key idea underlying the calculation in real space is to express all the quantities of interest in terms of those which can be calculated numerically. We can see that given the form of the initial Hamiltonian $H(0)$ and the time-dependent $H(t)$, the quantities $B(0)$, $B(t)$ and $S(t,0)$ can be easily computed. Given these and the annihilation operators of the ground states, we will now derive the final expression for the adiabatic fidelity.

Consider the Fock space of 2^N states $|\phi_a\rangle$, $a = 1, 2, \cdots, 2^N$. Their fermionic occupation numbers are given by $\beta_j^\dagger(t)\beta_j(t) = 0$ or 1. For a $|\Psi(t)\rangle$ belonging to this Fock space, $\beta_j(t)\,|\Psi(t)\rangle = 0$; hence $\beta_j^\dagger(t)\beta_j(t)\,|\Psi(t)\rangle = 0$ for all j. We now define the following operators L_j

$$L_j = \beta_j(t) \text{ for } 1 \le j \le N, \tag{3.34}$$

$$= \beta_{2N+1-j}^\dagger \text{ for } N+1 \le j \le 2N. \tag{3.35}$$

In the Fock space, $|\Psi(t)\rangle$ is the only state which is not annihilated by the product $L_1 L_2 \cdots L_{2N}$. In fact,

$$L_1 L_2 \cdots L_{2N}\,|\Psi(t)\rangle = |\Psi(t)\rangle\,. \tag{3.36}$$

We will make use of this fact to reduce the calculation in the 2^N dimensional Fock space to a matrix computation in $2N$ dimensions as follows. Consider the quantity

$$\begin{aligned}
&\langle\psi_{ins}(t)|\,L_1 L_2 \cdots L_{2N}\,|\psi_{ins}(t)\rangle \\
&= \langle\psi_{ins}(t)|\,L_1 L_2 \cdots L_{2N} \sum_{a=1}^{2^N} |\phi_a\rangle\,\langle\phi_a\,|\psi_{ins}(t)\rangle \\
&= \langle\psi_{ins}(t)|\,L_1 L_2 \cdots L_{2N}\,|\Psi(t)\rangle\,\langle\Psi(t)|\psi_{ins}(t)\rangle \\
&= |\langle\psi_{ins}(t)\,|\Psi(t)\rangle\,|^2.
\end{aligned} \tag{3.37}$$

This can be simplified further using a form of Wick's theorem given in Ref. [189], in terms of a $(2N)$-dimensional antisymmetric matrix A defined as

$$\begin{aligned} A_{jk} &= \langle\psi_{ins}(t)|\, L_j L_k \,|\psi_{ins}(t)\rangle \quad \text{for} \quad j<k, \\ &= -\langle\psi_{ins}(t)|\, L_k L_j \,|\psi_{ins}(t)\rangle \quad \text{for} \quad j>k, \\ &= 0 \quad \text{for} \quad j=k. \end{aligned}$$

This matrix can be calculated using the relation between $\bar{\beta}(t)$ and $\bar{b}(t)$ and the fact that $b_j(t)\,|\psi_{ins}\rangle\,(t)=0$. Finally we get

$$\langle\psi_{ins}(t)|\, L_1 L_2 \cdots L_{2N} \,|\psi_{ins}(t)\rangle = Pf(A) = |\langle\psi_{ins}(t)\,|\Psi(t)\rangle\,|^2.$$

Since the Pfaffian is given by $Pf(A)=\pm\sqrt{det(A)}$, we see that the adiabatic fidelity is

$$|\langle\psi_{ins}(t)\,|\Psi(t)\rangle\,| = |det(A)|^{1/4}. \tag{3.38}$$

Now we need to calculate the matrix elements A_{jk}. Since A is antisymmetric, we need to calculate only the elements for $j<k$. These are given by

$$\begin{aligned} & A_{jk} \\ = \;& \langle\psi_{ins}(t)|\, \beta_j \beta_k \,|\psi_{ins}(t)\rangle \quad \text{for} \quad j\le N, k\le N, \\ = \;& \langle\psi_{ins}(t)|\, \beta_j \beta^\dagger_{2N+1-k} \,|\psi_{ins}(t)\rangle \quad \text{for} \quad j\le N, k>N, \\ = \;& \langle\psi_{ins}(t)|\, \beta^\dagger_{2N+1-j} \beta^\dagger_{2N+1-k} \,|\psi_{ins}(t)\rangle \quad \text{for} \quad j\le N, k>N. \end{aligned}$$

We need to evaluate each of these terms. We introduce $G(t)=B(0)S(t,0)B^{-1}(t)$ so that $\beta(t)=G(t)b(t)$. Consider the first case $j\le N, k\le N$:

$$\begin{aligned} & \langle\psi_{ins}(t)|\, \beta_j \beta_k \,|\psi_{ins}(t)\rangle \\ = \;& \sum_{m,n} \langle\psi_{ins}(t)|\, G_{jm}\bar{b}_m G_{kn}\bar{b}_n \,|\psi_{ins}(t)\rangle \\ = \;& \sum_{m,n} G_{jm} D_{mn} G_{kn}. \end{aligned} \tag{3.39}$$

The matrix D is given by

$$\begin{aligned} D_{jk} &= \langle\psi_{ins}(t)|\, \bar{b}_j \bar{b}_k \,|\psi_{ins}(t)\rangle \\ &= \langle\psi_{ins}(t)|\, b_j b_k \,|\psi_{ins}(t)\rangle = 0 \quad \text{for} \quad j \leq N, k \leq N, \\ &= \langle\psi_{ins}(t)|\, b_j b^{\dagger}_{k-N} \,|\psi_{ins}(t)\rangle = \delta_{j,k-N} \quad \text{for} \quad j \leq N, k > N, \\ &= \langle\psi_{ins}(t)|\, b^{\dagger}_{j-N} b_k \,|\psi_{ins}(t)\rangle = 0 \quad \text{for} \quad j > N, k \leq N, \\ &= \langle\psi_{ins}(t)|\, b^{\dagger}_{j-N} b^{\dagger}_{k-N} \,|\psi_{ins}(t)\rangle = 0 \quad \text{for} \quad j > N, k > N. \end{aligned}$$

Using this fact, we get

$$\begin{aligned} & \langle\psi_{ins}(t)|\, \beta_j \beta_k \,|\psi_{ins}(t)\rangle \\ = & \sum_{m \leq N} G_{jm}(t) G_{k,m+N}(t) \\ = & \text{(first half of j-th row of G)} \times \text{(second half of k-th row of G)}^T. \end{aligned} \tag{3.40}$$

Similarly the other elements of A_{jk} can be found and numerically evaluated as a function of time. Once we have the matrix A, the adiabatic fidelity is simply related to its determinant.

3.5.2 Parity in a two-site problem

For an open chain, the overall parity of the ground state is decided by the fermion parity of the split energy states arising from the overlap of the Majorana end modes. We will consider here the effective Hamiltonian for such a system and illustrate how $det(B)$ determines the parity of the system. The effective Hamiltonian for the coupled Majoranas is given by

$$H_f = i2Ja_1 a_{2N}. \tag{3.41}$$

The eigenvalues are given by $\lambda = \pm J$ and the eigenvectors are x and its conjugate x^*, where

$$x = \frac{1}{\sqrt{2}} \begin{pmatrix} 1 \\ -i \end{pmatrix}. \tag{3.42}$$

Using these eigenvectors we can construct the matrix B which transforms the Hamiltonian into the canonical form.

$$B = \frac{1}{2} \begin{bmatrix} 1 & i \\ 1 & -i \end{bmatrix}$$

Now suppose that J changes sign; then the eigenvalues are flipped and the rows in B are also flipped. The sign of the determinant of a matrix changes when two of its rows are interchanged. The value of J also changes sign, the energy corresponding to the state with a particular fermion parity changes. The sign of $det(B)$ precisely tracks this flip in the parity of the energy level which contributes to the ground state.

One can also see this from the calculation of the Pfaffian of the Hamiltonian for the two-site problem. The Hamiltonian in the Majorana basis is given by:

$$\begin{pmatrix} 0 & -i\mu/2 & 0 & i(-w+\Delta)/2 \\ i\mu/2 & 0 & i(w+\Delta)/2 & 0 \\ 0 & -i(w+\Delta)/2 & 0 & -i\mu/2 \\ -i(-w+\Delta)/2 & 0 & i\mu/2 & 0 \end{pmatrix}$$

The Pfaffian of this Hamiltonian is given by

$$Pf(H) = \frac{\mu^2}{4} - \frac{w^2-\Delta^2}{4} \tag{3.43}$$

From this expression the Pfaffian changes its sign at $\frac{\mu^2}{4} = \frac{w^2-\Delta^2}{4}$. One can see that this is precisely the condition we have in Eq. (2.82) for $N = 2$. As shown in Kitaev's paper [47] we have the condition:

$$P(H) = sgn[Pf(H)] = sgn[det(B)]. \tag{3.44}$$

3.5.3 Calculation of residual energy

The residual energy is defined as

$$E_{res} = [\langle\Psi(t)|H(t)|\Psi(t)\rangle - E_G(t)]/|E_G(t)|, \tag{3.45}$$

where $E_G(t)$ is the instantaneous ground state energy. Let us calculate the first term in the expression, $\langle H(t)\rangle$. The matrix $B(t)$ transforms the time-dependent Hamiltonian to the canonical form

$$\begin{aligned} H(t) &= 4\sum_{j=1}^{N}\lambda_j(t)b_j^\dagger(t)b_j(t) - 2\sum_{j=1}^{N}\lambda_j(t) \\ &= 4\sum_{j=1}^{N}\lambda_j(t)\bar{b}_{N+j}(t)\bar{b}_j(t) - 2\sum_{j=1}^{N}\lambda_j(t). \end{aligned} \tag{3.46}$$

Therefore, $\langle H(t)\rangle = 4\sum_{j=1}^{N}\lambda_j \langle\Psi(t)|\,\bar{b}_{N+j}(t)\bar{b}_j(t)\,|\Psi(t)\rangle - 2\sum_{j=1}^{N}\lambda_j(t)$. From Eq. (A7) and using the definition $G(t) = B(0)S(t,0)B(t)^{-1}$ from the last section, we obtain

$$\bar{b}_i(t) = \sum_j G^{-1}_{ij}(t)\bar{\beta}_j(t). \tag{3.47}$$

As before, let us try to reduce everything to quantities which can be numerically computed.

$$\begin{aligned}
&\langle H(t)\rangle + 2\sum_{j}^{N}\lambda_j(t) \\
=\;& 4\sum_{j}^{N}\lambda_j(t)\,\langle\Psi(t)|\,\bar{b}_{N+j}(t)\bar{b}_j(t)\,|\Psi(t)\rangle \\
=\;& 4\sum_{j,k,l}^{N}\lambda_j(t)\,\langle\Psi(t)|\,G^{-1}_{N+j,k}(t)\bar{\beta}_k(t)G^{-1}_{j,l}(t)\bar{\beta}_l(t)\,|\Psi(t)\rangle \\
=\;& 4\sum_{j,k,l}^{N}\lambda_j(t)G^{-1}_{N+j,k}(t)\,\langle\Psi(t)|\,\bar{\beta}_k(t)\bar{\beta}_l(t)\,|\Psi(t)\rangle\, G^{-1}_{j,l}(t).
\end{aligned}$$

Now using

$$\begin{aligned}
\bar{\beta}_j &= \beta_j \;\text{ for }\; j \le N, \\
\bar{\beta}_j &= \beta^{\dagger}_j \;\text{ for }\; N < j \le 2N,
\end{aligned}$$

we have

$$\begin{aligned}
&\langle\Psi(t)|\,\bar{\beta}_k(t)\bar{\beta}_l(t)\,|\Psi(t)\rangle \\
=\;& \langle\Psi(t)|\,\beta_k(t)\beta_l(t)\,|\Psi\rangle\,(t) = 0 \;\text{ for }\; k \le N, l \le N \\
=\;& \langle\Psi(t)|\,\beta_k(t)\beta^{\dagger}_{l-N}(t)\,|\Psi(t)\rangle = \delta_{k,l-N} \;\text{ for }\; k \le N, l > N, \\
=\;& \langle\Psi(t)|\,\beta^{\dagger}_{k-N}(t)\beta_l(t)\,|\Psi(t)\rangle = 0 \;\text{ for }\; k > N, l \le N, \\
=\;& \langle\Psi(t)|\,\beta^{\dagger}_{k-N}(t)\beta^{\dagger}_{l-N}(t)\,|\Psi(t)\rangle = 0 \;\text{ for }\; k \le N, l \le N.
\end{aligned}$$

Hence the required expression simplifies to

$$\langle H(t)\rangle = 4\sum_{j,k}^{N}\lambda_j(t)G^{-1}_{N+j,k}(t)G^{-1}_{j,k+N}(t) - 2\sum_{j}^{N}\lambda_j(t). \tag{3.48}$$

Finally the expression for the residual energy is given by

$$E_{res} = [4\sum_{j,k}^{N} \lambda_j(t) G^{-1}_{N+j,k}(t) G^{-1}_{j,k+N}(t)]/|E_G(t)|. \tag{3.49}$$

E_G is calculated simply by summing over all the negative eigenvalues of the numerically diagonalized Hamiltonian, namely, $-\sum_{j=1}^{N} \lambda_j(t)$, and the first term is calculated from G, which we already have to calculate numerically to find the adiabatic fidelity.

3.6 Summary and conclusion

The study of non-equilibrium behavior in finite-sized Majorana wires demonstrates that the features of topological phases can dramatically alter quench dynamics. We have seen here that the coupling between Majorana end modes and the associated ground state parity flips as a function of a tuning parameter gives rise to a drastic manifestation of parityblocking due to a succession of switches between topological sectors within a single topological phase. As a result, some common measures studied in the quench dynamics literature, such as wave function overlaps between time-evolved states and instantaneous ground states (the adiabatic fidelity), and residual energies, show a series of non-analytic structures in the form of characteristic jumps which are not observed in standard Kibble-Zurek physics. Although the energy splitting between the Majorana modes goes to zero as we increase the chain length, the number of fermion parity switches increases linearly with the length. This has a dramatic consequence for the adiabatic fidelity under a quench, namely, parity blocking occurs more frequently as we increase the system size. (This is very different from conventional finite size effects which typically vanish in the thermodynamic limit). We therefore see that parity blocking is not merely a finite size effect, but is a relevant manifestation of the physics of Majorana modes and their topological nature in any real system.

This study shows that quench dynamics serves well as a probe of topological phases. While blocking features need not be unique to topological systems in that the invariants in other systems can possibly have similar effects, they are necessary conditions under appropriate circumstances (for instance, open boundary condition in the case studied here). Moreover, unlike in most other systems, such as ferromagnets having local order, we expect this blocking phenomenon to be robust against local perturbations.

In fact, the issue of parity forms the basis of several discussions and proposals for Majorana wires, particularly in light of the potential experimental discovery of isolated Majorana end modes and their implications for topological braiding and quantum computing. Several schemes involve changing the on-site chemical potential at specific locations as a means of manipulating and dynamically moving the isolated

end modes. A popular study regarding the end modes is the fractional Josephson effect (see, for instance, [47, 69, 185, 68, 74, 72]), which involves parity switches between two finite-sized Majorana wires connected to each other at their ends and their effect on Josephson physics (in principle, other zero energy end bound states could mediate such an effect). The study here is highly relevant to these lines of investigation and it provides a dynamic quantum many-body formulation that goes beyond quasi-static approximations.

An experimental setup probing the predictions of parity blocking would be remarkable. In the setting involving spin-orbit coupled wires, where the isolated end modes have potentially been observed, in principle, ground state parity switches can be observed by coupling the wire to another system. For instance, a possible read-out could involve tunnel-coupling to a quantum dot or STM tip (see, for example, [76, 186]). Cold atomic systems [187] are another promising avenue where topological phases could be realised and parity effects could be probed .

Finally, the study of parity blocking in quench dynamics presented here and the associated quantum many-body formulation offer wide scope for further exploration. Several aspects of this initial study require more detailed investigation, for instance, more involved studies of system size, and further connections with Kibble-Zurek scaling and single-particle physics, including anomalous scaling due to boundary effects and appearance of Loschmidt echoes. Oscillations have been found in the derivative of the Renyi entropy with respect to the chemical potential in [188] and it may be interesting to see if there are such effects related to the oscillations in the ground state parity. A host of open issues related to topological blocking in Majorana wires include constraints on thermalization imposed by topological phases, effects of external potentials, such as quasiperiodic potentials and disorder, and higher dimensional analogs, such as the Kitaev honeycomb model.

Chapter 4

Hawking-Unruh effect and quantum Hall effect

Interlude: On structural parallels

The human mind is still ahead of the computer, for the moment and for a long time to come I hope, to detect the structural analogies between theories which look quite different in content, but in which the same kind of phenomena appear. Translation will never be a literal one, and there will always be two texts written in two different languages and there will never be a one to one correspondence between the words of one language and the words of the other. But there will be these strange hints which may well evaporate if you try to rush and write them down too precisely. There are boxes that are very well understood on one side - and not understood at all on the other. Even if it doesnt provides a key to open something, it binds us, it forces us to think from the other side. – Alain Connes

Thus we seem to have partially demonstrated that even in foundations, not substance but invariant form is the carrier of the relevant mathematical information. –F. William Lawvere

The real voyage of discovery consists not in seeking new landscapes, but in having new eyes. – Marcel Proust

4.1 Introduction: Parallel structures

In physics, we see appearance of certain structures, models or concepts in multitudinous settings and at different scales, even though their physical interpretation would be different within each context. A simple harmonic oscillator and the two-level system are such prototypical quantum mechanical models that occur in various contexts from atomic physics to superconducting systems . As Sidney Coleman says "The career of a young theoretical physicist consists of treating the harmonic oscillator in ever-increasing levels of abstraction". It captures certain fundamental manifestations of quantum mechanics such as existence of

vacuum, occurrence of discrete spectrum, transition to classical picture and so on. The Ising model is also such a model at a higher level of sophistication and captures many-body physics. It is one of the prototypical modes for a class of classical and quantum phase transitions, predicting the critical exponents without the requirement of details and only considering the dimension and symmetry of the model. We have various such constructs that are of immense value in understanding phenomena across broad scales, such as the Dirac equation, conformal field theories, Luttinger liquids etc.

There is also the emergence of very simple single particle quantum mechanics in complex many-body systems. Such examples involve phase dynamics in Josephson junctions, quantum optics and quasiparticle dynamics in lowest Landau level. All these examples take the form of 'single-particle' Schrodinger equations in certain interesting potentials such as the Mathieu potential, Poschl-Teller potential for example. There are also themes that historically appeared first in high energy physics, but are now part of mainstream condensed matter physics. Dirac monopoles, Majorana fermions, Skyrmions and anomalies are just a few examples to quote. Bear in mind that these structures are now accepted as the description of these systems rather than as treating them as mere analogies to things that happened to appear first historically. The emergence of certain bare structures of fundamental quantum mechanics at the level of condensed matter systems that form the basis of standard experiments in labs, gives a tremendous opportunity to probe those structures in depth. The concept of symmetry is a good guiding principle in trying to seek similar structures in different phenomena. But once the concept of symmetry is invoked, one must be aware of all the mathematical aspects it brings along because of its articulation in terms of group theory. From quarks to new topological phases, symmetry arguments are extremely powerful.

In this chapter, we will be studying such parallel structures that arise in black hole spacetimes and quantum Hall effect through symmetries, specifically in the context of thermality. On one hand, in the quantum Hall effect one starts with a simple consideration of electrons in a magnetic field in two dimensions. This gives rise to Landau levels, non-commutativity in the lowest Landau levels, quantized Hall conductance, edge localisation, topological band structure, fractionalisation, anyons and many more fascinating phenomena[18]. This problem is one of the simplest instances of introducing gauge fields into quantum mechanics resulting in non-trivial effects such as the Berry's phase. On the other hand, black holes are one of the most intriguing astrophysical objects. They are one of the simplest macroscopic objects in nature in that they are described by their mass, angular momentum and charge[10]. Their 'construction', at least classically, is purely geometrical and yet they exhibit a plethora of features such as the singularities, one-way membrane, quasinormal modes and wormholes[11] . Further, on introducing quantum mechanics, there is the emergence of Hawking radiation[15] followed with the issue of its thermal interpretation and the information paradox.

These phenomena continue to baffle us to this day and is an ongoing field of intense research. A black hole is the key phenomenological entity in nature that forms the ground for interplay between quantum mechanics and gravity. In fact, describing black hole thermality would be a test bed for theories of quantum gravity. In this chapter, we will see that certain bare essential structures that appear in the description of thermality in the presence of black hole horizons, also appear in the context of quantum Hall effect and the common model appearing in both contexts is a simple quantum mechanical Hamiltonian of the inverted Harmonic oscillator. This model is realised through applying a saddle potential to a quantum Hall system. The saddle potential has been studied and well known in the field of quantum Hall effect and used to model systems with point contacts[190, 191]. Quantum point contacts are an integral part of many experimental set ups for conductance measurements. These are very important for studying shot noise and Anyon interferometry. Therefore, the parallels constructed between the black hole phenomena and quantum Hall effect are easily accessible to experiments. While it might be ambitious to expect such experimentally accessible parallels to help in investigations on quantum gravity, the process of investigating these parallels is in itself a very fruitful process. It helps us re-appreciate certain aspects of fundamental quantum mechanics. Casting the well known physics of quantum Hall effect in the light of structures parallel to black hole physics, could lead to better understanding of the quantum Hall phenomena.

This chapter is organised as follows: In the next section, an overview is given about the kind of parallels we will be drawing between the two settings. This will be followed by a section where the basics of black hole physics is reviewed. Black hole/Rindler thermality is derived using both path integrals and mode exapnsion and the derivation of black hole quasinormal modes is presented. Then, the basics of quantum Hall physics and lowest Landau levels is presented. Finally, the exact parallels of black hole thermality and quasinormal modes are shown in lowest Landau level in the presence of an applied potential

4.2 An overview on structural parallels in quantum Hall effect

This section hopes to achieve two things. One is to paint in very simple terms, the heuristics appearing in the emergence of the Hawking radiation or the Unruh effect and identifying parallel ones in the quantum Hall systems. The aim is to try to boil both down to a unifying theme of quantum mechanical scattering theory and its subtelties. This is to provide a simpler and intuitive picture to a reader not familiar with these topics. The second aim is to summarize in succinct and exact terms, the parallels of the mathematical structures and logical steps seen in these two disparate settings. The parallels we will be drawing are in terms of exact mathematical isomorphisms and can be stated in minimal set of sentences. This will be a

bit technical and terse, but serves the purpose of giving the exact crux of the parallels and also to give an expert a quick but a complete glimpse. Both the discussions will not involve details.

Heuristics– A black hole is an astrophysical, macroscopic object emerging from the collapse of a star under its own gravitational field. Inspite of the vast number of constitutional, thermodynamic, hydrodynamic and other macroscopic complications that could arise in the collapsing star, the end product of a black hole is a pure geometric entity. It is determined by a metric of a curved spacetime and can be defined completely though quantities like Killing vectors which characterize the symmetries of the spacetime. A black hole spacetime is defined by the existence of an 'event horizon' or from now just termed as the horizon. This is defined locally as a light-like or a null surface frozen at a particular region in spacetime.To understand in simple terms, consider a light wave front passing by an observer. The observer cannot travel to pass through that light front again as its is forbidden by relativity to travel faster that the speed of light. One can consider the horizon to be a closed, locally static lightfront through which objects can pass through but cannot travel back. Thus the horizon bifurcates the spacetime into two parts- which we shall call 'inside' and 'outside' of the black hole. Geometrically, there is nothing 'singular' happening at the horizon itself. An observer outside the black hole can set up a co-ordinates system to describe the physics happening outside but because of the horizon property of the black hole cannot describe the inside. On the other hand, an observer freely falling into the black hole does not see any thing special at the horizon(at at least classically) and can set up another co-ordinate description of physics. This description would then cover the entire spacetime except at the singularity.

When quantum mechanical degrees of freedom are considered on such a black hole spacetime, Hawking showed that a far away observer sees the black hole radiating thermally and it decays(evaporates) gradually through radiation. One can describe the story of black hole formation and evaporation as a scattering scenario in the following way, paying attention to the spatial and temporal boundary conditions : A far away observer at 'spatial infinity' sees at some 'initial time' an incoming state('in-state') of a matter-energy in some suitable 'vacuum state' collapsing radially to form a black hole. Once the black hole is formed the outside observer does not have access to the physics happening within the event horizon. But at 'later times', the observer at 'spatial infinity' sees the '*decaying out-state*' of the evaporating black hole. Thus, an observer 'restricted' to the outside of a horizon, sees an incoming state decay into a thermal state. Having the boundary conditions mentioned here in mind, we will draw parallels between this thermality in the black hole case and the transmission probability in the context of quantum mechanical scattering off an inverted Harmonic oscillator(IHO).

A scattering problem off an inverted oscillator potential is depicted in Fig. (4.1). In terms of boundary

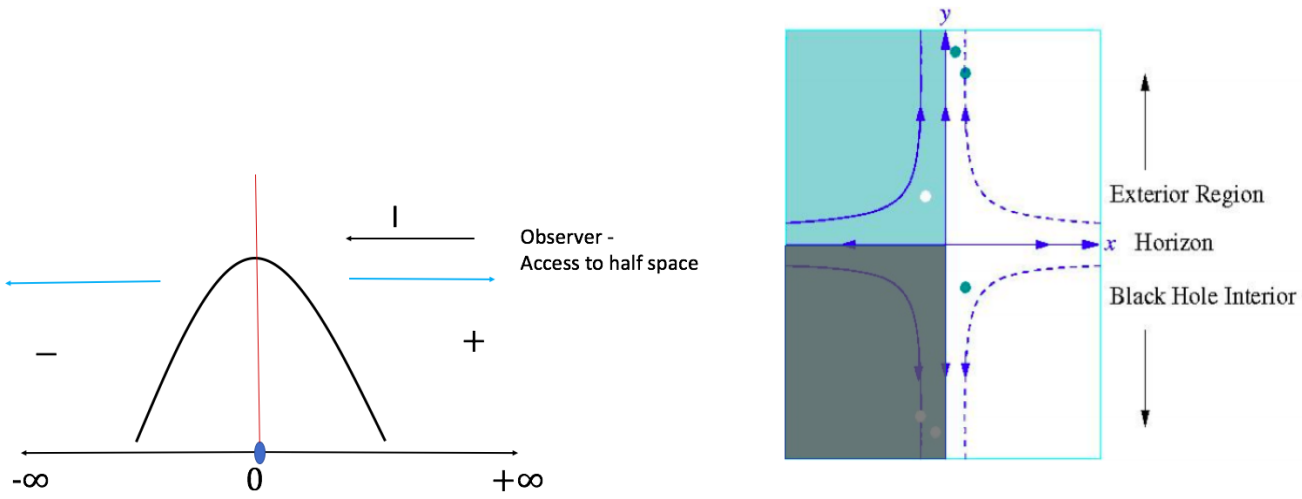

Figure 4.1: Figure on the left shows the scattering barrier of an IHO. The scattering barrier divides the region into half-spaces. There are incoming, reflected and transmitted states that belong to the energy spectrum. Purely incoming and outgoing states have support only on one side, similar to the situation for observer outside the event Horizon of a black hole. On the right is the scattering problem in a quantum Hall system with an applied saddle potential (Figure adapted from [3])

conditions we have a similar situation to that of a black hole. Instead of 'outside' and 'inside', we have the $\pm$ region corresponding to the left and right regions(Caution that we are not making an exact correspondance between the two regions of black hole and those of the inverted oscillator). For an 'an observer' at 'spatial infinity' on the right side, there are 'in-' and 'out- states'. It happens that in the case of IHO, these 'in- and out-' quantum mechanical states have support either only on the right side or the left side of the barrier. The exact energy eigenstates on the other hand have tunneling and reflecting parts on either sides.(Note that the purely incoming or outgoing states need not be real energy eigenstates of the Hamiltonian) . The very setting of the scattering problem allows for a two-fold doubling (right and left) of purely outgoing energy eigen states . But the observer on the right side can only measure one of them. Further, suppose you take a purely ingoing state (that can be seen as a wavepacket of the energy eigenstates) the scattered state would decay in time and would be a purely out-state on the right. This corresponds to the quasinormal or resonant decay seen also in black hole scattering . The calculated tunneling and reflection amplitudes have exactly the thermal form for the inverted oscillator scattering (this is not true for all scattering potentials) . Though this is an illustrative sketch of an argument, we can already see that the time and space boudary conditions play a very important role in the thermality appearing in both the black hole and the IHO scattering problem. In fact, t'Hooft has proposed a scattering matrix (S-matrix) formulation of the black hole evaporation [192] and a recent work [193] derives the black hole S-matrix from the inverted oscillator in some approximation. On a technical side note, it must be mentioned that the S-matrix description is limited to matter-energy

fields on the spacetime that do not have a back reaction and change the background metric.

To relate the scattering scenario to a physical set up, let us actually consider the first work where parallels to Hawking radiation was proposed in the quantum Hall effect. In [3],M. Stone proposed that by applying a saddle potential to a quantum hall system and restricting to the lowest Landau level, one can engineer the semi-classical trajectories of the chiral states at the edge so as to get an analog of Hawking radiation. As shown in Fig.4.1, the trajectories of chiral states branch out at $y = 0$ and have opposite velocities . A transition between them is classically forbidden, thus demarcating $y = 0$ as the 'event horizon'. But one can have quantum mechanical tunneling between the branches and the tunneling probability is of the 'thermal form' $|t|^2 = 1/(1 + e^{\beta\epsilon})$(This will be explicitly calculated later)[250]. The applied saddle potential when restricted to the lowest Landau level is the inverted harmonic oscillator(IHO) . Here one can think of 'integrating out' the states 'inside' the black hole (shaded region in the figure) to obtain a thermal state on the 'outside'. An entanglement perspective is also given in [3] by showing that one can get a thermal density matrix by integrating out the 'inside' of the effective black hole. Further, an effective metric description can be written based on the velocity profile of the chiral state in the presence of the saddle potential.

There have been several other works in the field of 'Analog gravity' in trying to 'mimic' black hole spacetimes in superfluids, metamaterials, polaritons etc [194, 19, 195, 196, 197, 198, 199, 200] . The 'spacetimes' here resemble near-horizon behaviour of actual curved spacetimes but the idea is more of replicating the equation of motion of a field in curved spacetime. These are realised as equations of motion of a field in an engineered inhomogeneous condensed matter medium such as a superfluid or a metamaterial. It is remarkable that quantum fluctuations considered along with such equations of motion give rise to Hawking-type radiation and a thermal distribution like the one above.

Another route which we shall pursue here is to 'go beyond the appearance'. Our goal here is not so much to construct a spacetime lookalike but to capture bare minimum structures necessary for obtaining the Hawking-Unruh effect. The symmetry structures are the central actors and lead us in directions that are unexplored in quantum Hall physics. In the paragraphs above, an intuitive picture was painted about the thermality emerging in a black hole setting, how there are parallels to the scenario of a scattering problem and its realisation in a quantum Hall set up. The intention was to motivate the discussion on the parallels between two disparate physical phenomena of black holes and quantum Hall effect.

Exact statements of the parallels– In the following we will be more precise and state succinctly what are the structures of interest in black hole physics and their parallels in the quantum Hall effect . All the concepts will be explained in detail in the following sections. The intention here is to show how elegantly the black hole thermality is captured by very minimal set of concepts such as spacetime structure, symmetry

and their interplay with quantum mechanical states. It is exactly these structures we tap into when drawing parallels with quantum Hall effect.

- *Spacetime structure and horizons:* A black hole spacetime have event horizons that are locally one-way membranes that restrict certain set of observers from accessing information beyond the horizon. One has a similar situation in a simpler setting of uniformly accelerating observers in Minkowksi spacetime. They are restricted to a part of the Minkowski spacetime called the 'Right Rindler wedge'(Rindler spacetime) bound by the lightcone/ 'Rindler horizon' (4.2). In fact, the description of a general spacetime with a horizon reduces to Rindler wedge near the horizon and contains most of the relevant structure for the emergence of thermality.This forms a simpler stage for understanding thermality in the presence of horizons.

- *Spacetime symmetries*–The lightcone structure of the Minkowski spacetime is preserved by the transformations belonging to the Poincare group.The Lorentz boost is one of such transformations.

- *Quantum fields*– One has a quantum field defined over the Minkowski spacetime with a ground state and operators acting on them.

- *Hawking Unurh effect*– Given all this, the statement of Unruh effect is - " The vacuum in a Minkowski spacetime restricted to the right Rindler wedge is a thermal state".

- One of the crucial facts related to all this is - "The time translation τ in the right Rindler wedge is a boost with rapidity τ with respect to the Minkowski spacetime." i.e "Rindler Hamiltonian(generator of time translation) is a boost with rapidity τ".

We will explain in detail all the technical terms mentioned above.It would be a grave omission to not mention that these statements are actually the basic ingredients of the 'Bisognano-Wichmann theorem' [201] which was adapted by Sewell [202] as a formal proof of the Hawking-Unruh effect. Our discussion in this chapter will not be explicitly involving this theorem. But for completeness its salient aspects are mentioned here without going to technical details. It starts by considering a Hilbert space, a vacuum state and some bounded operators acting on them (satisfying conditions of locality, hermiticity and covariance). These are defined on a Minkowki spacetime whose symmetries form the Poincare group. There is a unique PCT(Parity, Charge conjugation and Time reversal symmetry) operation defined on these fields. Now the theorem states that considering a set of operators localised within the Right Rindler wedge, the vacuum is a thermal state with respect to the time-translations generated by the Lorentz boost[1] . The theorem identifies

[1]More technically, the 'modular evolution' of the vaccum vector and the Rindler wedge is given by a unitary representation

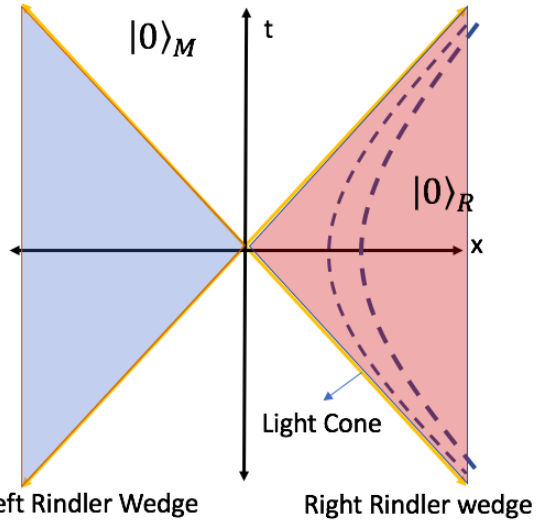

Figure 4.2: Minkowski spacetime (t, x) with the lightcone structure. The right quadrant forms the 'Right Rindler wedge'. A family of uniformly accelerating observers indicated by hyperbolae, are confined to the this region. The statement of Hawking Unurh effect is that the Minkwoski vacuum restricted to the right Rindler wedge is a thermal state with respect to the time translationsin the right wedge.

the operators within the right Rindler wedge with their counterparts which are complex conjugates but are localised within the left Rindler wedge, thus implementing in an abstract way the Bogoliubov particle-hole mixing and the Hawking-Unurh effect. This ends the quick discussion on the theorem noting that it brings together in a fundamental manner certain key elements of spacetime structure, quantum field theory and quantum statistical mechanics. There have been works that have made use of the theorem in the context of condensed matter physics [203, 204] , black holes and information paradox [205] and has been of importance in relating entanglement aspects of quantum field theories to gravity and geometry [206, 207, 208, 209]. [2] [3]. There are other approaches to the phenomena of Hawking-Unurh effect, such as tunneling [212, 213] and anomalies [214].

Let us give an idea of what thermality entails in this context in familiar terms, one can imagine an

of the Lorentz boosts, which maps the Rindler wedge onto itself. On restriction to right Rindler wedge the operators acting on the vacuum follow the KMS condition(after Kubo-Martin-Schwinger) $\langle A(\tau)B\rangle = \langle BA(\tau + i\hbar\beta)\rangle$, where β is the inverse temperature. The KMS condition is the technical way of stating equilibrium thermality.

[2]To give a broader perspective of things. The mathematical machinary associated with the Bisognano-Wichmann theorem is called the Tomita-Takesaki theory. This branch of mathematical physics, dealing with operator algebras, has been used to give a formal foundation for quantum field theory[210] and quantum statistical mechanics[211]. It has become even more important with recent developments in quantum field theory and entanglement [206]. Its relevance for the enigma of black hole thermality[205, 208] makes it all the more crucial. The parallels to quantum Hall effect stated in this thesis are but the first few steps in trying to see the relevance of these fundamental structures in condensed matter systems.

[3]On a personal note, during the initial days of working on this project, coming across these fundamental aspects was the most exciting and happiest moments of my grad school life, only matching the excitement of learning general relativity and quantum mechanics for the first time as an undergraduate. The possibility of getting to learn these topics and see if they manifest in phenomena of different settings such as black holes and condensed matter has made the pursuit of physics in general exciting than ever.

observer in uniform accelerated motion in Minkowski spacetime. The statement that Minkowski vaccum looks thermal to that observer is usually written as the observer measuring the particle content of the Minkowski vacuum and finds it to be a thermal distribution:

$$\langle n \rangle = \frac{1}{e^{\beta E} - 1}, \tag{4.1}$$

where β is the inverse temperature.

The question now is whether some or all of these mathematical structures, such as the symmetry group, a Rindler-like partition and the evolution given by a Rindler Hamiltonian, be captured in a non-spacetime like condensed matter setting. The lowest Landau level of the quantum Hall effect provides such a platform. In fact the Lowest Landau level(LLL) physics is not restricted to quantum Hall but emerges in other systems such as rotating Bose-Einstein condensates, skyrmionic systems, topological phases etc. One of the characteristic feature of LLL is the non-commutativity of the so called guiding center co-ordinates

$$[X, Y] = i \tag{4.2}$$

This commutation relation constrains the kind of Hamiltonians that can be written within the LLL. These Hamiltonians are directly related to the kind of potentials we apply on a realistic quantum Hall set-up. This constraint can be physically understood as follows- Restriction to the lowest Landau level means that we need to preserve the applied magnetic field or the flux through the system. Therefore, any potential applied on the quantum Hall system must preserve the area or the flux through the system. The set of symmetry operations which achieves that are part of the $\mathfrak{sl}(2, \mathbb{R})$ Lie-algebra, which have a specific set of commutations relations between set the generators of the symmetry. Now we present the exact statement of our parallels between the Hawking-Unruh effect and saddle potential in a quantum Hall system.

- The lowest Landau level is characterised by the commutation relation between the guiding center co-ordinates $[X, Y] = i$.
- The set of potentials in the Lowest Landau level are a set of area preserving transformations in two dimensions. The generator of such operations form the Lie-algebra $\mathfrak{sl}(2, \mathbb{R})$.
- The generators of $\mathfrak{sl}(2, \mathbb{R})$ are the Hamiltonians acting on the single particle states in Lowest Landau level. There are two hyperbolic transformations and one rotation.
- There is an isomorphism between the symmetry generators of the Lorentz group in 2+1 dimensions and the symmetry generators of $\mathfrak{sl}(2, \mathbb{R})$. This is the isomorphism $\mathfrak{sl}(2, \mathbb{R}) \sim \mathfrak{so}(2, 1)$. The Lorentz

Lie algebra consists of two boosts and a rotation. Thus one can identify the as parallels of Lorentz kinematics in the lowest Landau level. [4]

- The Hamiltonian in the LLL corresponding to one of the boosts is the inverted Harmonic oscillator Hamiltonian(IHO).
- The IHO acts as a parallel to the Rindler Hamiltonian and generates Unruh-like effect in the quantum Hall systems.
- The quasinormal modes are identified with the resonances of the IHO.
- The parallels can be generalized to phase space dynamics because of the isomorphism to the symplectic Lie algebra: $\mathfrak{sl}(2,\mathbb{R}) \sim \mathfrak{so}(2,1) \sim \mathfrak{sp}(2,\mathbb{R})$

Each of the technical terms and the statements made here will be will be fleshed out in detail in the section on quantum Hall effect and the section on parallels. The key message here is that the parallels of structures drawn in the quantum Hall system are tapping directly into the bare structures responsible for the Hawking-Unurh effect through exact isomorphisms. These bare structures are in terms of general concepts of spacetime symmetries, which carries much more baggage than just being specific to the phenomena at hand. The added advantage of this is that it does more than the intended task of getting an analogue of Hawking-Unurh effect. It gives us 'new eyes' to see the quantum Hall phenomena in terms of Lorentz kinematics. Further, it gives a unified picture for both facilitating exchange of insights between the disparate setting of black holes and quantum Hall effect. Nevertheless, if these are too abstract, one can always revert back to the more intuitive picture of scattering off an inverted oscillator, which by itself has more insights to offer. The last chapter of this thesis is dedicated to the study of various features of the IHO.

This concludes an overview of the parallels and now we shall proceed to lay out the basics of both the worlds of black hole physics and the quantum Hall effect before demonstrating the parallels. I

4.3 Spacetime physics, gravity and black holes

We shall start with a very quick review of the fundamental aspects of special and general relativity, stressing on the aspects of symmetry generators, rapidity of boosts, Killing vectors which will help in understanding

[4]The idea of considering isomorphisms of Lie algebras was inspired by some of old works by Dirac[215] and Kim and Wigner[216]. Dirac in his "Forms of relativistic dynamics" gives a prescription for constructing a Hamiltonian dynamics that obeys the principle of relativity. His idea is to identify the generators and the algebra of the canonical transformations in the phase space to the generators of the Poincare algebra of relativity. He then proceeds to argue that there are different ways of realising this using constraints. We are not following Dirac's methods in this work though the idea of identifying the Lorentz algebra with $\mathfrak{sl}(2,\mathbb{R})$ was inspired by that. The approach followed here is much closer to the work of Wigner and Kim, where they build parallels of Lorentz Kinematics in quantum optics using the isomorphism $\mathfrak{so}(2,1) \sim \mathfrak{su}(1,1)$.

the defining properties of black holes and the Hawking-Unurh effect.

The special and general theories of relativity form one of the foundations of physics as they provide the framework and structure for the laws of physics. Let us first consider the special theory of relativity. In contrast to the typical approach of focusing more on 'things being relative', length's contracting, time dilating etc, the precise content of special relativity lies more in what remains invariant and how physical quantities transform relative to different frames of description. The postulates of special theory of relativity are :

1) Covariance: The physical description of nature are covariant with respect to inertial frames of reference. 2) Universality of speed of light: Light always propagates in empty space with a definite velocity c which is independent of the velocity of the observer in uniform motion.

Most laws of physics are stated in terms of mathematical relations between certain 'physical quantities'. Some of these physical quantities are directly measurable. The value of the physical quantities can change as the state of its observer changes. But if the laws of physics, which are precise relations between these quantities, change in an indefinite manner, a consistent description of nature would be difficult. The statement of covariance is that the *the form* of these relations that are the laws of nature must remain the same with respect to frames of reference that move with constant velocity with respect to another. This is called 'Lorentz covariance'. Given this exact form, one could then deduce how quantities transform relative to different frames. The startling revelation of special relativity is that space and time themselves change with respect to different frames much in contrast with everyday experience. This follows from the other postulate of relativity that the velocity of light is constant irrespective of the state of motion of the observer. This necessitates that space and time comprise a bigger manifold called the 'space-time', where space and time can change but leaves a particular structure of that manifold *invariant*.

This is where geometry enters into the picture and gives a structure to what Lorentz-covariance should look like. It dictates that the spacetime structure is a *geometric* one. The spacetime relevant for the description of physics with respect to inertial observers is given by a manifold with a metric $\eta_{\mu\nu}$. The interval or the line element is then given by -

$$ds^2 = c^2dt^2 - dx^2 - dy^2 - dz^2 = \eta_{\mu\nu}dx^\mu dx^\nu \tag{4.3}$$

where 'c' is the speed of light and $\eta_{\mu\nu}$ is the Minkowski metric $\eta_{\mu\nu} = \text{diag}(1, -1, -1, -1)$ (We will usually take c=1 unless otherwise specified.). Suppose one makes a transformation of co-ordinates $x'^\mu = \Lambda^\mu_\nu x^\mu$ then , the interval ds^2 in the x'^μ co-ordinates must remain the same. For that to be so, the spacelike distances

and time-like intervals must change correspondingly. This results in the famous length contraction and time dilation. The quantities defined over such a spacetime, be it a velocity vector, a gauge field or the electromagnetic field tensor must transform in a 'covariant' manner such that the laws of physics remain the same in different frames, though the physical manifestations will differ. Consider the example of Maxwell's equations for electromagnetism $\partial_\alpha F^{\alpha\beta} = J^\beta$, where $F^{\alpha\beta}$ is the Field strength tensor whose components are electric and magnetic fields and J^β is the4- current. If one makes a transformation $x'^\mu = \Lambda^\mu_\nu x^\mu$, the quantities in the equation must 'transform as Lorentz tensors' such that the form of Maxwell's equations does not change: $\partial'_\alpha F'^{\alpha'\beta'} = J'^{\beta'}$. The physical manifestation of this is that the field strength tensor manifests as an electric field for a static observer and would manifest with a component of magnetic field for a moving observer.But in each of these frames Maxwell's equations are satisfied. In this sense we want the laws of physics to be Lorentz covariant.

Lorentz group and Lorentz Lie Algebra:

There are very specific set of transformations that can keep the metric of the Minkowski form invariant- i) Spatial rotations about 3-axis (with 3 parameters) ii) Lorentz transformations in 3 directions(3 parameters) ii) Translations in all 4 directions(4 parameters). The group of these transformations form the 10-parameter Poincare group in 3+1-dimensions. The subgroup of this that excludes the translations is called the 'Lorentz group'. This group structure dictates the kind of quantities that can be written and the form of relations between them, if one wants a relativistic theory in terms of those quantities. The Lorentz group is important as it is the symmetry group of Maxwell's electromagnetism, Dirac's equation and the Standard model. The Lorentz group is represented as $SO(d,1)$ to indicate that it belongs to a group of special orthogonal rotations on a space with a Lorentzian signature of one time-like component and d space-like components. One can think of these as rotations of 4-vectors of the form (A^0, A^1, A^2, A^3) preserving the length $A^\alpha A_\alpha = A^0A_0 - A^1A_1 - A^2A_2 - A^2A_2$.

The 2+1- dimensional Lorentz group $SO(2,1)$and its Lie algebra $\mathfrak{so}(2,1)$ will be quite important for our further discussions and that will be our point of contant in drawing parallels to black hole phenomena in quantum Hall physics. The arguments that we give would also be valid for the $SO(3,1)$, the Lorentz group of the spacetime of the so called 'real world'. The $SO(2,1)$ group is a collection of 3 transformations - Two boosts and a rotation. A familiar form of representation of these transformations acting on (t, x_1, x_2) is

given by [216]:

$$B(0,\beta) = \exp -i\beta K_1 = \begin{pmatrix} \cosh\beta & 0 & \sinh\beta \\ 0 & 1 & 0 \\ \sinh\beta & 0 & \cosh\beta \end{pmatrix} \tag{4.4}$$

$$B(\theta = \pi/2, \eta) = \exp -i\eta K_2 = \begin{pmatrix} 1 & 0 & 0 \\ 0 & \cosh\eta & \sinh\eta \\ 0 & \sinh\eta & \cosh\eta \end{pmatrix} \tag{4.5}$$

$$R(\theta) = \exp -i\theta L_3 = \begin{pmatrix} \cos\theta & -\sin\theta & 0 \\ \sin\theta & \cos\theta & 0 \\ 0 & 0 & 1 \end{pmatrix} \tag{4.6}$$

The first two are the boosts along x_1 and x_2 directions and the last one is a rotation in the (x_1, x_2) plane. The entities of interest to us are the generators of these transformations (K_1, K_2, L_3). These generators form a Lie-algebra defined through the relations [216]:

$$[K_1, K_2] = -iL_3, \quad [K_3, L_3] = iL_1, \quad [L_3, K_1] = iK_2 \tag{4.7}$$

Given this algebra and a representation for the generators, one can generate transformations on the space-time manifold as well as the functions defined on them. This structure is extremely important in understanding the Hawking-Unruh effect and making parallels to it in the quantum Hall effect. We will see that the boost generator is crucial in generating thermality and a potential acting on the Lowest Landau level acts as a boost generator.

Causal structure of the spacetime- The metric gives a very specific causal structure for the spacetime. Based on the sign of the metric, the separation between two space-time points are classified as i) Space-like if $ds^2 < 0$. Such points are called 'Space-like' separated and are causally disconnected. ii) Time-like if $ds^2 > 0$. Such points are time-like separated and are causally connected through exchange of matter and energy. iii) Null-like if $ds^2 = 0$. Such points are connected though light rays. All other four-vectors are similarly classified as space-like, time-like and null-like. The Lorentz group generators mentioned above preserve this structure under transformations. Its important to note that special relativity puts a constraint on the regions of spacetime we can access. The inaccessibility of the full region of the spacetime leads to bifurcaton into half-space and becomes quite important in our discussion on black hole physics and thermality.

Boost as an imaginary rotation– Boost is one of the transformations in Lorentz group that takes the observer from one frame to another and it can be view as a hyperbolic rotation in space-time. This way of writing the boost will be extremely useful in understanding the Unruh effect. Transforming from a fame with co-ordinates (x, t) to frame (x', t') moving velocity v is written as

$$t' = t\cosh(\beta) + x\sinh(\beta) \tag{4.8}$$

$$x' = x\sinh(\beta) + t\cosh(\beta) \tag{4.9}$$

Here β is called the *'Rapidity'* parameter, given in terms of the usual Lorentz factor by $\cosh\beta = \frac{1}{\sqrt{1-v^2}}$. In this way of writing the transformation, it can be easily seen by taking $t \to it$, a boost with rapidity β is a rotation of angle β in Euclidean spacetime (x, it). Also, the rapidities add with successive boosts unlike velocities. If $\Lambda(\beta)$ is the Lorentz transformation, then $\Lambda(\beta_1)\Lambda(\beta_2) = \Lambda(\beta_1 + \beta_2)$. This provides an easier way of understanding relativistic phenomena such as Wigner rotation. Note that We will make use of the picture of boost as imaginary rotation in spacetime to derive the thermality in the Unruh effect.

General relativity: The key message of special relativity is that space and time are to be taken together as a flat Minkowski spacetime geometry and the laws of physics for inertial observers are written on that space-time manifold. The general theory of relativity is an extension to curved spacetimes. It makes an explicit statement that a theory of gravity and its interaction with matter is a theory of geometry on curved spacetime. Therefore, the line element ds^2 now contains a metric which is a function of the space-time.

$$ds^2 = g_{\mu\nu}(x^\mu)dx^\mu dx^\nu \tag{4.10}$$

The metric tensor $g_{\mu\nu}$ is the main physical quantity in the theory that describes the space-time. The curvature of the spacetime is directly related to the stress-energy tensor of the matter considered. The metric tensor is calculated as a solution to Einstein's equations

$$R_{\mu\nu} = \frac{1}{2}Rg_{\mu\nu} = \frac{8\pi G}{c^2}T_{\mu\nu} \tag{4.11}$$

Here $R_{\mu\nu}$ and R are the Ricci tensor adn Ricci scalar which determine the curvature of the spacetime. $T_{\mu\nu}$ is the stress-energy tensor that characterizes the matter causing the spacetime curvature and G is the universal gravitational constant. The Einstein's equations form 10 linearly independent non-linear differential equations and one must solve them to obtain the metric of the spacetime. Put in very simple terms, the central message here is that the matter-energy tells spacetime how to curve and the spacetime curvature

tells matter-energy how to move.

Once the metric is determined, various physical features of the spacetime and the behaviour of matter on the spacetime can be calculated. The geodesic equation for the matter particles is obtained to be:

$$\frac{d^2x^\mu}{ds^2} + \Gamma^\mu_{\alpha\beta}\frac{dx^\alpha}{ds}\frac{d^2x^\beta}{ds} = 0, \tag{4.12}$$

where 's' is a scalar parameter and $\Gamma^\mu_{\alpha\beta}$ is the Christoffel connection, which captures how the local bases change on parallel transporting a vector along the trajectory.The particle trajectories obtained from these would be curved trajectories. Therefore, what was thought of as motion of a particle under the influence of a gravitational force of another massive object is nothing but a geodesic on the curved spacetime created by the presence of a massive object in accordance with Einstein equations. The reader is referred to the vast literature[11] on the theory of gravitation to experience it in its full grandeur. Here only the minimal basics necessary for understanding the Unruh-Hawking effect is presented. Most of the relevant details are presented by making use of the elegant Killing vector formalism.

Proper time in relativity: As we will using the concept of proper time quite often in the following discussions, lets understand that here. Time is usual choice for parametrization of dynamics and trajectories. But in relativistic cases, time transforms as one of the components of a four vector in the spacetime. A suitable quantity that transforms as a scalar under Lorentz transformation is required and 'proper time' is such a quantity. For a trajectory with time-like vector defined at every point, the proper time is defined as the time measured by a comoving observer. For a co-moving observer, $ds^2 > 0$ because of the time-like condition and $dx = 0$ as the observer is at rest in the co-moving frame. Then the proper time is given by

$$\Delta d\tau = \int ds = \int \sqrt{g_{\mu\nu}dx^\mu dx^\nu} \tag{4.13}$$

4.3.1 Symmetries and Killing vectors

Symmetries play a crucial role in the theory of space, time and gravitation. A given set of symmetries dictate the nature of solutions of Einstein's equation and thus the resulting spacetimes. For example, there are uniqueness theorems for spacetimes with spherical symmetry and asymptotic flatness. Any solution of Einstein's equations with those conditions will be related to Schwarzschild spacetime. One can make use of these symmetries and obtain a lot of information about the spacetime without having to use specific co-ordinates. Killing vectors provide one such way.

Consider a spacetime with the metric $g_{\alpha\beta}$ and vector field ξ^α defined on it. Moving along the vector field,

the metric changes as a function of spacetime $g^{\alpha\beta}(x^\alpha + \xi^\alpha)$ and to compare the change one must transform the metric with the local basis change along the vector field. This difference is called the Lie derivative along the vector field ξ^α [11, 10]:

$$\mathcal{L}_\xi g^{\alpha\beta} = g^{\alpha\beta}(x^\alpha + \xi^\alpha) - g^{\alpha'\beta'}(x^{\alpha'}) \tag{4.14}$$

This is equal to zero if the vector field ξ^α happens to be in the direction of symmetry .i.e the metric does not change along the vector field. Then ξ^α is called a Killing vector field. The equation $\mathcal{L}_\xi g^{\alpha\beta} = 0$ can be solved to obtain the Killing vector field. We will make use of such Killing vectors to define features of a black hole.

4.3.2 Black holes

The presentation of black holes physics in this section is highly influenced by Prof. C. V. Vishveshwara. Parts of this section follows the unpublished draft of an undergraduate textbook on black hole physics I wrote with him before coming to graduate school.[5]

"Black Holes of nature are the most perfect macroscopic objects there are in the universe: the only elements in their construction are out concepts of space and time. And since the general theory of relativity provides only a single unique family of solutions for their descriptions, they are the simplest objects as well - S.Chandrasekhar in 'Prologue to "The Mathematical Theory of Black Holes" [10]

Black holes are one of the most intriguing predictions of Einstein's general relativity. As mentioned in the introduction, black holes are formed by the gravitational collapse of a massive star, but inspite of all the complications in the details of the matter-energy content of the collapsing star, black holes are obtained as pure geometrical objects in the general theory of relativity. They are obtained as solutions to Einstein's equation of gravitation. They are characterised by the existence of an 'event horizon', a surface of no-return, which we shall define precisely below. Black holes also have a spacetime singularity at their 'center' where geometrical quantities such as the curvature tensor diverge. The form of the black hole solutions to Einstein's equations is completely determined by the symmetry of the spacetime and the boundary conditions. The typical boundary conditions for astrophysical black holes is 'asymptotic flatness' i.e at spatial infinity of the spacetime it should approach the limit of a flat Minkowski spacetime. Birkhoff's theorem[11] states that Any spherically symmetric vacuum solution of Einsteins equation which is asymptotically flat must be a static solution like Schwarzschild. . To illustrate the nature of the features appearing in black holes, consider the

[5] I had the privilege of learning about black holes from Prof. C. V. Visveshwara. He introduced me to the beautiful world of Killing vectors and symmetries. He pioneered the use of Killing vectors to define the properties of black holes before the name 'black hole' was coined. In his paper [217], he elegantly demonstrates the properties of null surface, static limit and infinite redshift in black holes using the Killing vectors. Some of his other works employ Killing vectors to study various other aspects of general relativity - [218, 219, 220].

Schwarzschild spacetime written in the Schwarzschild co-ordinates -

$$ds^2 = \left(1 - \frac{2M}{r}\right)dt^2 - \frac{dr^2}{\left(1 - \frac{2M}{r}\right)} - r^2(d\theta^2 + d\phi^2 \sin^2\theta) \tag{4.15}$$

The ranges of the co-ordinates are given by

$$-\infty < t < \infty, \quad 0 < r < \infty, \quad 0 \leq \theta \leq \pi, \quad 0 \leq \theta \leq 2\pi \tag{4.16}$$

Here M is the Mass of the black hole One can see that there is a singularity at $r = 2M$, but this can be removed by making an appropriate co-ordinate transformations. The actual singularity at $r = 0$ is the curvature singularity and cannot be removed. The Schwarzschild co-ordinates are valid only outside the $r = 2M$ surface and do not give a complete description of the spacetime. As we shall see the $r = 2M$ surface is the 'event horizon' and this is the object of our interest.The defining properties of the horizon are described below. Before jumping into that let us note that there is a conjecture called 'No-hair conjecture' which states that a steady-state black hole is parametrised by only three independent parameters- mass, charge and angular momentum. The Schwarzschild black hole is characterised only by its mass. The solutions to Einstein's equations that describe rotating and charged black holes are called Kerr and Reissner-Nordstrom solutions respectively. We shall not delve into those aspects here.

Defining properties of a Black Hole– .

Lets first consider stationary spacetimes with time translation symmetry. A given spacetime could have other symmetries in the space-like co-ordinates. Exploiting these symmetries will simplifies the calculation and give insights to various phenomena without having to deal with co-ordinates [217].

We shall do so by defining a Killing vector $\xi^\alpha = (1, 0, 0, 0)$, which is along the direction of the time translation symmetry. These vectors can be used in the description of various physical phenomena in a very simple manner. The projection of certain quantities, say momentum, along the Killing vector direction, will be conserved along a geodesic. This would simplify the equation of motion. Most importantly, the killing vectors are directly related to the geometry of spacetime. So, expressing phenomena in terms of these will give a direct geometric and co-ordinate invariant description.

1. Static limit– Consider the scalar formed by the time-like Killing vector ξ^α is

$$\xi^2 = \xi^\alpha \xi_\alpha = g_{\alpha\beta} \quad \xi^\alpha \xi^\beta = g_{00} \tag{4.17}$$

As the scalar remains invariant under transformations, we can use it for a co-ordinate independent description

to classify the vectors.

$$\xi^2 > 0 \quad Timelike \tag{4.18}$$

$$\xi^2 < 0 \quad Spacelike \tag{4.19}$$

$$\xi^2 = 0 \quad Null \tag{4.20}$$

Four velocity of a static observer is given by $U_\alpha = (dx^\alpha/ds) = 1/\sqrt{g_{00}}(1,0,0,0)$ Expressed in terms of Killing Vectors

$$U^\alpha = \xi^\alpha/\sqrt{\xi^\alpha \xi_\alpha} \tag{4.21}$$

We see that U^α becomes imaginary at $\xi^2 < 0$ and we cannot define the four-velocity in that region. Thus, the surface $\xi^2 = 0$ or g_{00} is a static limit beyond which one cannot have static observers in the spacetime.

2. Infinite redshift surface–

The energy measured by an observer with four velocity U_α is

$$E = P^\alpha U_\alpha \tag{4.22}$$

For example in flat spacetime $P^\alpha = \frac{m}{\sqrt{1-v^2}}(1,\vec{v})$ For an observer at rest $U^\alpha = (1,0,0,0)$

$$P^\alpha U_\alpha = \frac{m}{\sqrt{1-v^2}} \tag{4.23}$$

Since this is locally true it should be true in general relativity in arbitrary metric also. Therefore energy measured by a static observer in a gravitational field :

$$P^\alpha U_\alpha = (P^\alpha \xi_\alpha)/\sqrt{\xi^\alpha \xi_\alpha} \tag{4.24}$$

Suppose P^α is the four-momentum of a geodesic and if ξ^α is a killing vector of a symmetry, then $P^\alpha \xi_\alpha$ is conserved along the geodesic. One can see from Noether's theorem that the conjugate momentum is conserved. Therefore for a static observer, the energy

$$E = (P^\alpha \xi_\alpha)/\sqrt{\xi^\alpha \xi_\alpha}) \tag{4.25}$$

Now let us derive the formula for gravitational red shift in a very simple way using the above concepts. Suppose there are two static observers at two different points in a gravitational field and one of them sends

a photon to another. The ratio of the energies measured at the two points is

$$\frac{E_1}{E_2} = \frac{p^\alpha \xi_\alpha}{\sqrt{(\xi^\alpha \xi_\alpha)_1}} \frac{\sqrt{(\xi^\alpha \xi_\alpha)_2}}{P^\alpha \xi_\alpha} \tag{4.26}$$

$P^\alpha \xi_\alpha$ is constant along a geodesic and since $\sqrt{(\xi^\alpha \xi_\alpha)_1} = (\sqrt{g_{00}})_1$ we have

$$E_1/E_2 = (\sqrt{g_{00}})_2/\sqrt{g_{00}})_1 \tag{4.27}$$

(4.9) Taking the energies to be quantized $E = h\nu$,we have

$$\nu_1/\nu_2 = (\sqrt{g_{00}})_2/\sqrt{g_{00}})_1 \tag{4.28}$$

Thus, the frequency of a photon changes its frequency when exchanged between two static observers. But now the points on which $g_{00} = 0$ is the horizon. Therefore, far away observer sees a photon infinitely redshifted as it approaches the horizon.

3. One-way membrane – Consider an equation for a surface $\phi(x^\alpha) = constant$, which has a normal

$$n_\alpha = \frac{\partial \phi(x^\alpha)}{\partial x^\alpha} \tag{4.29}$$

On the surface , $n_\alpha dx^\alpha = d\phi = 0$n.Therefore, $n_\alpha \perp dx^\alpha$.

$$n^2 = n^\alpha n_\alpha = g^{\alpha\beta} \phi_{,\alpha} \phi_{,\beta} \tag{4.30}$$

As usual $n^2 > 0$ implies a time-like surface , $n^2 < 0$ a spacelike surface and $n^2 = 0$ a null-surface.

Let us consider few examples in flat space . a) Consider the surface $t = constant$. Its normal $n_\alpha = (1, 0, 0, 0)$ and $n^2 = 1 > 0$. Therefore it is time-like. All directions in the surface are outside the null cone. We have only space like vectors here. All time-like curves can cross this surface only once, which is the consequence of the fact that we cannot go back in time unless we travel faster than the speed of light.

b) Consider the surface $y = constant$, $n_\alpha = (0, 0, 1, 0)$,$n^2 = -1 < 0$. Therefore it is a space-like surface. Space-like, time-like and null vectors can exist in this surface. It can also be crossed both the ways .

c) Now consider a surface $t - y = constant$. $n_\alpha = (1, 0, -1, 0)$ and $n^2 = 0$, making it a null-surface. The normal to the surface is orthogonal to the tangent to the surface which itself is null. Therefore this surface is self orthogonal. Time like curves can cross it in one direction but cannot cross it again. Unlike the case of time-like surface, the null surface does not define a particular moment of time which cannot be recaptured.

The best example is that of a light wave front. Once a wave front passes, you cannot overtake to cross it again making it a one-way membrane. Now lets consider a curved spacetime with a metric $g_{\alpha\beta}$ and examine the condition $g^{00} = 0$ at which there is a horizon:

$$g'^{\alpha\beta}\frac{\partial x^0}{\partial x'^{\alpha}}\frac{\partial x^0}{\partial x'^{\beta}} = g^{00} = 0 \tag{4.31}$$

This is an equation for a hypersurface: $x^0 = \phi(x'^{\alpha}) = constant$. Anormal to this surface is given by

$$\bar{\xi}_{\alpha} = \phi_{,\alpha} = \frac{\partial x^0}{\partial x'^{\alpha}} \tag{4.32}$$

Due to the null surface condition, we have

$$g'^{\alpha\beta}\bar{\xi}_{\alpha}\bar{\xi}_{\beta} = 0 \tag{4.33}$$

This shows the known fact that the normal $\bar{\xi}_{\alpha}$ is a null vector. If dx'^{α} is a tangent to the hypersurface $\phi = 0$, then we have

$$d\phi = \phi_{,\alpha}dx'^{\alpha} = \bar{\xi}_{\alpha}dx'^{\alpha} = 0 \tag{4.34}$$

The contravariant component of the normal vector is $\bar{\xi}^{\alpha}$.The differential dx'^{α} is in the direction of $\bar{\xi}^{\alpha}$,orthogonal to the null vector. Therefore we can see that the hypersurface contains a tangent null vector at every point. Through every point of x'^{α} we can draw a cone of vectors dx'^{α}. Therefore we have a local light cone at every point of the hypersurface. Since the a light cone acts as a one-way membrane the hypersurface also has the one-way membrane property at each point. The null hypersurface marks the points beyond which information cannot be accessed by an outside observer making it an event horizon.

One can see that for a Schwarzschild black hole, at $r = 2M$ surface is the static limit, infinite redshift surface and the one-way membrane coincide. This is not the case for a Kerr black hole.

4.3.3 Myths about black holes

Here let us consider some commonly stated misconceptions about black holes and clarify them stressing on the importance of the notion of a horizon. These myths were first stressed by C. V. Vishveshwara[221]. The gravitational pull of a black hole is so strong that nothing, not even light, can escape it It is true that the gravitational effects near the black hole are extremely strong. The very fact that black hole is purely a general relativistic notion suggests that. But it is certainly not that the strength of the gravitational pull which is the sole reason for light not being able to escape the black hole. It is the property of the one

way membrane which does not allow anything to come out of the black hole. Let us demonstrate this more clearly. The spacetime curvature is the exact indicator of the strength of a gravitational field. From principle of equivalence a free falling frame is locally equivalent to an inertial frame. But over longer time and length scales there exist tidal forces, which lead to deviations from inertial frame like behaviour. These tidal forces are directly related to the curvature. Now the curvature of the Schwarzschild spacetime and the tidal forces are proportional to the mass divided by the cube of the radial distance $R \sim M/R^3$. Consider a neutron star of one solar mass with a radius of ten kilometers. One can show that the tidal force at the surface of this neutron star is larger than the tidal force one could encounter at the event horizon of the black hole of over five solar masses and radius of fifteen kilometers. Counter intuitively higher the mass of the black hole the smaller the tidal force at its horizon. If you consider a white dwarf of one solar mass and with size of earth, the force at its surface would be greater than that at the event horizon of a black hole of about hundred thousand masses and above. It is only that the thrust required for sustaining a static observer at the event horizon would be infinitely large. This is the notion of static limit. Therefore to say that nothing escapes a black hole because of its strong gravitational field is an imprecise statement.

Let us consider another myth : A Black hole is so dense that it does not allow light or anything to escape. As we have seen, a black hole is defined by a surface or a membrane. A surface in space is devoid of any material content and the space it contains is empty except for the matter that has collapsed to the center. There for the density of a black hole is not a well defined concept. If we could divide the mass of the black hole by the volume of the sphere of Schwarzschild radius, we end up with a huge number for a solar mass black hole. But if one calculates it for a super massive black hole it will be extremely small. Sir Oliver Ridge calculated that for a black hole made up of million billion suns the density would be around million-billionth of the density of the water. Therefore one cannot exactly define such a density. But we stress again that the reason for objects not being able to escape the black hole is due to the one way membrane property.

These myths show us the one-way membrane or the horizon feature of the black hole is fundamental to many properties associated with it. As we shall see it is also the horizon property that leads to Hawking-Unurh effect. The horizon being a null-surface or a one-way membrane restricts an observer outside to the information within the horizon. This leads to the black hole thermality. Now that we have reviewed the basics of black hole physics, let us focus on the description of physics near the horizon, where the features of Rindler spacetime can be used.

4.4 Horizon physics: Rindler spacetime, horizon and Rindler Hamiltonian

Before trying to understand the Hawking radiation and black hole thermality, it is useful to understand a simpler version of it that occurs in accelerating frames called as the Unruh effect [222]. For an accelerating observer, the vacuum in the Minkowski spacetime is a thermal state. This simpler scenario is shown to completely capture the essential structures that give rise to Black hole thermality. The principle of equivalence is at the heart of this relation between the two - An accelerating frame has effects of similar nature as those present in the curved spacetime of gravitation. In fact Unruh was motivated along these lines[222]. Additionally, a spacetime associated with an accelerating observer called the 'Rindler spacetime' will be important in its own right for studying this effect. Here we will present the key aspects of relativity concerning the the Rindler spacetime and then consider the quantum mechanics on top of that leading towards different derivations and perspective on the Unruh effect. Throughout the discussion, the bare essential structures necessary for the Unruh effect are highlighted and will be shown how they emerge in the quantum Hall effect in a later section.

4.4.1 Accelerating observers and Rindler spacetime

Uniformly accelerating observers – The metric of a Minkowski spacetime in 1+1- dimensional spacetime is given by

$$ds^2 = dt^2 - dx^2 = \eta_{\mu\nu} dx^\mu dx^\nu \tag{4.35}$$

We want to calculate the trajectory $(x(\tau), t(\tau))$ of the uniformly accelerating observers with acceleration a. The relativistic velocity parametrised by proper time τ along the observer's trajectory is $u^\mu(\tau) = \frac{dx^\mu}{d\tau} = (\gamma c, \gamma \vec{v})$, where γ is the lorentz factor $1/\sqrt{1-v^2}$ and $\vec{v}$ is the usual velocity. Using the condition $\eta_{\mu\nu} u^\mu u^\nu = 1$ and the acceleration defined as $a^\mu(\tau) = \dot{u}^\mu(\tau)$ is orthogonal to the velocity $\eta_{\mu\nu} a^\mu u^\nu = 0$. This leads to a convariant condition for constant acceleration [223]

$$\eta_{\mu\nu} a^\mu a^\nu = -a^2 \tag{4.36}$$

. From this one obtains the equation $\frac{d}{dt}(v/\sqrt{1-v^2}) = a$. From this the trajectory of a uniformly accelerating observer is given by a branch of the hyperbola $x^2 - t^2 = a^{-2}$.

Now, to get the trajectories $(x(\tau), t(\tau))$, remember that the proper time τ is related to the Minkowski

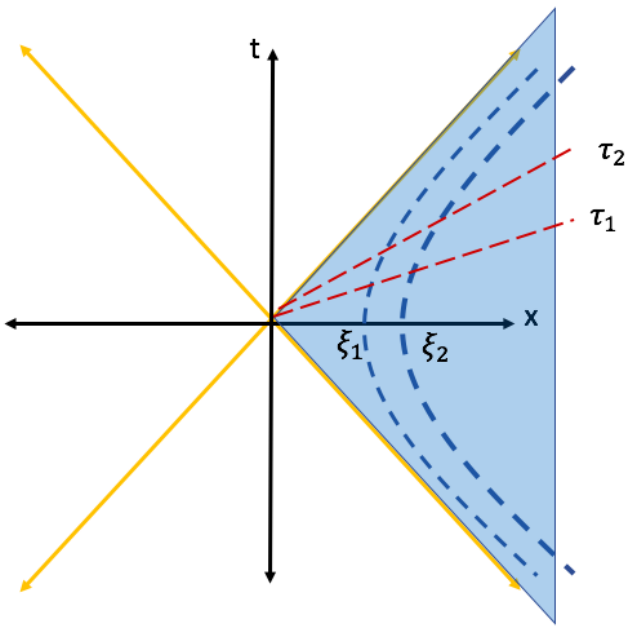

Figure 4.3: Spacetime diagram for Minkowski spacetime and the right Rindler wedge. The lightcone structure in the Minkowski spacetime bifurcates the spacetime into spacelike and time like regions. A family of observers with constant acceleration are indicated by hyperbolic trajectories. These observers are confined to the spacelike region shaded in blue. This region is known as the 'right Rindler wedge', which can be described in terms of co-ordinates (τ, ξ). The constant time slices are shown by slanted lines. The trannlsation can be seen to be a hyperbolic rotation in the Minkowski space.

time t by : $\tau = \int_0^t dt' \sqrt{1 - v(t')^2}$. From this the trajectories are obtained:

$$t(\tau) = \frac{1}{a}\sinh(a\tau) \quad x(\tau) = \frac{1}{a}\cosh(a\tau) \tag{4.37}$$

Rindler Spacetime and Rindler horizon: The trajectories derived for a uniformly accelerating observer by themselves form geodesics of a spacetime called the 'Rindler spacetime'. Rather than considering trajectories of observers in Minkowski spacetime, we can study the Rindler spacetime and its causal structure. They are solutions of the Einstein's equations. This spacetime plays a very important prototype for understanding the black hole thermal physics.

The trajectories Eq.(4.37) with positive acceleration are restricted to the 'right wedge' of the Minkowski spacetime: $x > 0$ and $|t| < x$. The lightcone $t - x = 0$ acts as a 'horizon' for these set of observers: The observers in that part of the spacetime cannot access any information on $t > x$. Similarly, the accelerating observers with negative a are restricted to the 'left wedge' and have a horizon. We are primarily interested in such horizons in spacetimes, which when considered along with quantum mechanics give interesting results. An observer at rest in the Minkowski spacetime$(T(t), X(t) = (t, x))$ can recieve information from the region

$t > x$ and do not percieve such a Horizon. Therefore, this notion of horizon is an observer dependent concept with a dependence on the family of causal curves we consider.

A broad class of spacetimes including curved spacetimes of gravity, with a metric that is 'conformally' equivalent to the Minkowski metric are relevant for studying the horizon physics. Such a metric has the form:

$$ds^2 = \Omega(\xi^0, \xi^1)((d\xi^0)^2 - (d\xi^1)^2), \tag{4.38}$$

where the Conformal factor $\Omega(\xi^0, \xi^1)$ is a non-zero function. The trajectories of the light rays form the 'light-cone'. If one has a family of curves such as Eq.(4.37) then $t - x$ act as a horizon. For a co-moving observer with proper time τ, $(\xi^0(\tau), \xi^1(\tau)) = (\tau, 0)$ on such a trajectory. The change of co-ordinates from the Minkowski spacetime to a conformally equivalent spacetime is then determined from that condition to be-

$$\xi^0(\tau) = \frac{e^{\kappa\xi^1}}{\kappa}\sinh(\kappa\xi^0) \quad \xi^1(\tau) = \frac{e^{\kappa\xi^1}}{\kappa}\cosh(\kappa\xi^0) \tag{4.39}$$

Here the acceleration of the observers is replaced by the parameter κ of the Rindler spacetime and we shall stick to this use. The metric now reads:

$$ds^2 = e^{2\kappa\xi^1}((d\xi^0)^2 - (d\xi^1)^2). \tag{4.40}$$

These co-ordinates have a range: $-\infty < \xi^0 <= \infty$, $-\infty < \xi^1 < +\infty$. This covers only the quarter of the Minkowski spacetime i.e the 'right Rindler wedge'. The family of $\xi^0 = \text{constant}, \xi^1 = \text{constant}$ curves are shown in Fig.4.3. The family of accelerated observers also cannot perceive distances larger than κ^-1 in the direction opposite to the acceleration [224]. An observer at a space-like co-ordinate $\xi^1 = 0, \xi^0 = 0$ (an observer with acceleration κ in Minkowski basically) measures an infinite range of co-ordinates $-\infty < \xi^1 < 0$, measure the distance:

$$d = \int_{-\infty}^{0} \exp\kappa\xi^1 d\xi^1 = \frac{1}{\kappa} \tag{4.41}$$

This is restating that an accelerating observer cannot measure the entire Minkowski spacetime and is bound by the horizon. One can change to a different space co-ordinate $(1 - \kappa\bar{\xi}^1) = e^{\kappa\xi^1}$ to write the metric as

$$ds^2 = (1 + \kappa\bar{\xi}^1)(d\xi^0)^2 - d(\bar{\xi}^1)^2 \tag{4.42}$$

Finally, making a transformation $(1+\kappa\xi^1) = \sqrt{2\kappa\ell}$ and $\tau = \xi^0$ we get,

$$ds^2 = (2\kappa\ell)d\tau^2 - \frac{d\ell^2}{2\kappa\ell} \tag{4.43}$$

This form of the metric is quite important especially for focusing on the physics near a horizon. The horizon in this case is located at $\ell = 0$. The advantage of this metric is that it can be exteneded to negative values of ℓ to cover all four quadrants of the spacetime [225].

As will be shown below the Rindler metric is extremely important for the following reasons:

- Other curved spacetimes with horizons can be approximated to the Rindler spacetime of the above form near their horizon.
- This set of co-ordinates are also useful in making an 'extension' to cover the full Minkowski spacetime. This is technically known as the 'Maximal extension' and is used in extending the Schwarzschild co-ordinate that covers spacetime outside the black hole to Kruskal-Szekeres co-ordinate that covers the entire spacetime except the singularity.
- A non-trivial transformation between how the clocks tick (time translation) in the Rindler space and the completed space is the key feature in giving rise to thermality near horizons and black holes.

4.4.2 Rindler approximation to black hole horizons

Now we shall show that a general curved static spacetime with a horizon can be approximated near its Horizon can be to Rindler spacetime. This discussion will closely follow the elegant line of reasoning similar to [225]. We saw that the Schwarzschild metric is of the form:

$$ds^2 = f(r)dt^2 - \frac{dr^2}{f(r)} + r^2 d\Omega^2, \quad f(r) = \left(1 - \frac{2M}{r}\right) \tag{4.44}$$

The horizon in this case was located at $r = 2M$. One can in fact consider metrics of the above form with an arbitrary function $f(r)$, that has a simple zero at $r = r_H$, which is the event horizon. The near the horizon, the metric can be written as (focusing only on the time-like and space-like part of the metric) :

$$ds^2 \approx f'(r_H)(r - r_H)dt^2 - \frac{dr^2}{f'(r_H)(r - r_H)} \tag{4.45}$$

Introducing $\kappa = f'(r_H)/2$ and $\ell = (r - r_H)$, the metric reads as

$$ds^2 \approx 2\kappa\ell dt^2 - \frac{d\ell^2}{2\kappa\ell} \tag{4.46}$$

This is exactly the form of the Rindler metric we derived in the previous sections. This derivation is made rigorous for a general spacetime in the following. This illustration that any black hole horizon spacetime approximates to Rindler spacetime near the horizon is extremely important especially for the Hawking-Unruh effect as the aspects of Rindler spacetime directly feed into its derivation.

Consider a spacetime $ds^2 = g_{\mu\nu}dx^\mu dx^\nu$with the following conditions:

1. Static in that given co-ordinate representation of the metric $g_{0\nu} = 0, g_{ab}(t, x) = g_{ab}(x)$
2. $g_{00}(x) = N^2(x)$ that vanishes on a 2-hypersurface $\mathcal{H}$. The hypersurface is defined by the equation $N^2 = 0$.
3. $\partial_\mu N$ is finite and non-zero on $\mathcal{H}$
4. All other metric components remain finite and regular on $\mathcal{H}$

The metric is then written as:

$$ds^2 = N^2(x^a)dt^2 - \gamma_{ab}(x^a)dx^a dx^b \tag{4.47}$$

Now, a family of observers can be constructed similar to the accelerating observers in Minkowski spacetime. These observers are characterized by $\vec{x} = constant$, four-velocity $u_\mu = N\delta^0_\mu$ and four acceleration $a^\mu = u^\mu\partial_\mu u^\mu = (0, -a)$. The spatial components of this are given by $a_a = (\partial_a N)/N$. The unit normal to the hypersurface $N = constant$ is $n_a = \partial_\mu N(g^{\mu\nu}\partial_\mu N\partial_\nu N)^{1/2} = a_a(a_b a^b)^{-1/2}$. The normal component of the four-acceleration is related to the surface gravity κ.

We can go to a co-ordinate where N is treated as one of the spatial co-ordinates and other spatial co-ordinates x^A are along the transverse directions to the N=constant surface. Such a co-ordinate change is valid atleast locally. The components of the acceleration along N is given by $a^N = a^\mu\partial_\mu N = Na^2$. The metric components in this set of co-ordinates are

$$g^{NN} = \gamma^{ab}\partial_\mu N\partial_\nu N = N^2a^2, \quad g^{NA} = Na^A \tag{4.48}$$

The metric line element now reads:

$$ds^2 = N^2dt^2 - \frac{dN^2}{(Na)^2} - d\Omega^2_\perp \tag{4.49}$$

where $d\Sigma^2$ is the line element on the transverse surface.

The unit vector normal to the constant N surface as we calculated is given by n_a and the component of the acceleration along this vector becomes the surface gravity of the horizon κ at the N=0 surface i.e in the the limit $N \to 0$,$Na \to \kappa$. Therefore, in the limit of going towards the horizon $N \to 0$, the metric reads:

$$ds^2 = N^2 dt^2 - \frac{dN^2}{\kappa^2} - d\Omega_\perp^2 \tag{4.50}$$

Finally to switch to Rindler-like metric the transformation is $d\ell = dN/a$, $\ell \approx N^2/(2\kappa)$:

$$ds^2 = 2\kappa\ell dt^2 - \frac{d\ell^2}{2\kappa\ell} + d\Omega_\perp^2 \tag{4.51}$$

We have shown that a general static spacetime with a horizon can be approximated to the Rindler spacetime in the limit of going towards horizon. This could be extended to stationary spacetime like the Kerr too but with much more complicated analysis.

4.4.3 Boost as Rindler time-translation

"The time translation τ in the right Rindler wedge is a boost with rapidity τ with respect to the Minkowski spacetime."

This is one of the key facts that forms the crux of Unruh effect. The generator of time translation of in the right Rindler wedge being identified with a boost, a symmetry generator of the Minkowski spacetime that preserves the Rindler wedge, has non-trivial consequence and lead to thermality. One of the simplest ways to see this in the Rindler spacetime is to go to lightcone co-ordinates. Typically the boost along x-direction is given by : $t \to t\cosh\beta + x\sinh\beta$, $x \to t\sinh\beta + x\cosh\beta$, where β is the *rapidity*. If we switch to lightcone co-ordinates $u = t - x, v = t + x$, the boost looks much simpler : $u \to ue^{\beta}$, $v \to ve^{-\beta}$. Now relating the lightcone co-ordinates to the Rindler co-ordinates :

$$u = e^{\xi+\tau} \quad v = e^{\xi-\tau} \tag{4.52}$$

One can immediately see from the above that a time translation τ would look like a boost in the lightcone co-ordinates.

A much general discussion of this fact involves showing that the time-like Killing vector in the Rindler wedge is the Boost Killing vector in the Minkowski. This result holds for other general metrics we saw to be approximated to Rindler wedge spacetimes.

Another useful approach is to view boost as a complex rotation with parameter $i\beta$, as the hyperbolic functions become trigonometric. Now, using this fact one can see that:

Time translation τ in the Rindler wedge is a rotation in the Euclidean time $\tau_E = i\tau$ This fact becomes important in the path- integral derivation of the Unruh effect.

4.5 Unruh effect and Hawking radiation

Now that the ingredients on the side of classical system of relativistic spacetimes are described, we can derive the Hawking-Unruh effect by considering quantum mechanical degrees of freedom on the spacetimes with horizons. Three different approaches for the description of Hawking-Unruh effect are presented. The path integral approach is very strong in terms of capturing the bare essence of the phenomena purely in terms of symmetry structures and properties of the quantum mechanical degrees of freedom.

Before getting into the derivations, it must be confessed that the discussion here does not cover the crucial entanglement aspects of the Hawking-Unruh effect in much detail. But we note that entanglement is at the heart of this phenomena and the reader is referred to the literature on it [226, 206].

4.5.1 Path integral approach

As presented in the previous section, the trajectories of the accelerating observers are restricted to the right Rindler wedge in the full Minkowski spacetime. We also saw that in general static spacetimes with horizons can be approximated to Rindler spacetime near the horizon. Therefore, we shall restrict to using the Rindler spacetime in the below. Now, everything is set to bring quantum mechanics into the scene and derive the Hawking-Unurh effect. The statement of Hawking-Unruh effect is this: Consider the vacuum of quantum mechanical degrees of freedom on the Mikowski spacetime. On restriction to the right Rindler wedge, the density matrix of the quantum mechanical state is a thermal one, given by :

$$\rho = e^{-2\pi H_R/(\hbar\kappa)} = e^{-\beta H_R}, \tag{4.53}$$

where H_R being the Rindler Hamiltonian/ boost generator and $\beta = 2\pi/(\hbar\kappa)$ is the inverse temperature of the thermal state .

To show this, we just need the vacuum state of a quantum field theory defined on the Minkowski spacetime and the Rindler Hamiltonian. We shall follow the path integral approach to derive the density matrix in the Rindler wedge [225, 206, 227]. In the path integral approach, it is convenient and illustrative to work in

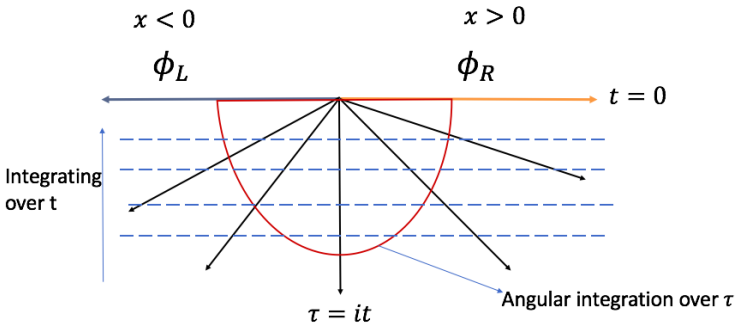

Figure 4.4: Time evolution in the lower half plane for the vacuum wave functional is covered in two different ways for Minkowksi and Rindler co-ordinates . The Minkwoski time slices are dashed horizontal lines whereas the euclidean time is along the angular direction. The initial state is given on the $t = 0$ surface which includes the full range $-\infty < x < \infty$. For Rindler time slice τ, only the half-space is covered. The Rindler time evolution in Euclidean time is a complex rotation in (t, x) space and is generated by the boost of rapidity τ.

Euclidean time $\tau = it$. Making use of the Euclidean time evolution, we can get the ground state as :

$$|0\rangle = \lim_{\tau\to\infty} e^{-H\tau} |\chi\rangle \tag{4.54}$$

Here $|\chi\rangle$ is any other state with $\langle\chi| 0 >\neq 0$. Then one can see that taking $E = 0$ to be the vacuum state

$$\lim_{\tau\to\infty} e^{-H\tau} |\chi\rangle = \lim_{\tau\to\infty} \sum_E e^{-E\tau} |E\rangle \langle E| \chi >= |0\rangle \langle 0| \chi > \tag{4.55}$$

The vacuum wave functional can then be written as a Feynman path integral over different field configurations

$$\Psi_0[\phi] = \lim_{t\to\infty} \langle\phi| e^{-tH} \chi = \int_{\phi(t\to-\infty)=\chi}^{\phi(t=0)=\phi} \mathcal{D}\phi e^{-S/\hbar} \tag{4.56}$$

Here S is the Euclidean action corresponding to the Hamiltonian H. The initial state is given on a $t = 0$ hypersurface on the whole range of $-\infty < x < \infty$. This separates into two regions belonging to left and right Rindler wedges. The field configurations in those regions is indicated by $(|\phi_R\rangle, x > 0), (|\phi_L x < 0\rangle$. The metric for the right Rindler wedge in Euclidean time is given by

$$ds^2 = \kappa\ell^2 d\tau^2 + d\ell^2 \tag{4.57}$$

Here τ can be used as an angular co-ordinate with periodicity $2\pi/\kappa$. The time evolution in Minkowski time $t = -\infty$ to $t = 0$ is therefore mapped to evolution along the angular co-ordinate from $t = \pi \to 0$ as shown in Fig.(4.4). The lower half-plane in the time evolution in the path integral is covered in two

different way for the Minkowski and Rindler co-ordinates. One can slice the path integral into integration over field configurations at constant time slices. At each time slice the range of $-\infty < x < \infty$ is covered in the Minkowski spacetime. On the other hand, for each constant τ, the range of $\infty > x > 0$ is covered in the Rindler co-ordinates. This allows us to write the path integral as

$$\Psi_0[\phi] = \int_{\phi(\tau\to\pi/\kappa)=\phi_L}^{\phi(\tau=0)=\phi_R} \mathcal{D}\phi e^{-S/\hbar} \tag{4.58}$$

Now the generator of complex rotation is a boost operator or the Rindler Hamiltonian. Due to the partition from the Rindler wedge the state $\langle\phi|$ is now a tensor product of $\langle\phi_L| \otimes \langle\phi_R|$. Considering these, the path integral takes the form

$$\Psi_0[\phi_L, \phi_R] = \langle\phi_R| e^{-\pi H_R/\kappa} J |\phi_L\rangle \tag{4.59}$$

The final state ϕ_L is written as $J|\phi_L\rangle$, where J is the PCT(parity, charge conjugation and time-reversal) conjugation operator which comes along with the Lorentz symmetry. Now integrating over the fields ϕ,

$$|0\rangle = \int \mathcal{D}\phi_L \mathcal{D}\phi_R |\phi_L\rangle |\phi_R\rangle \langle\phi_R| e^{-\pi H_R/\kappa} J |\phi_L\rangle = \int \mathcal{D}\phi_L |\phi_L\rangle e^{-\pi H_R} J |\phi_L\rangle \tag{4.60}$$

Finally, we can obtain the density matrix with suitable normalisation

$$\rho = \mathrm{Tr}_L |0\rangle \langle 0| = e^{-2\pi H_R/\kappa} \tag{4.61}$$

The above discussion clearly shows that the quantum mechanical degrees of freedom on the right and left Rindler wedge are entangled in the vacuum state and restricting to one of the wedge 'integrates' over the other to give a thermal density matrix. This derivation illustrates the fundamental nature of this effect. The key ingredients in the entire discussion involved the Lorentz symmetry of the spacetime and the path integral formalism of the quantum mechanics. This also links back to the discussion about the Bisognano-Wichmann theorem in the overview section.

4.5.2 Wave-equation, mode expansion and particles

Now we move on to deriving and interpreting the Hawking-Unruh effect using wave equation of fields and mode expansion in terms of particle states [224]. This derivation is along the lines of derivation in Hawking and Unurh's original papers [15, 228, 222]. This gives a more intuitive derivation in terms of known concepts of particles but that is also its drawback. One runs into issues about the interpretation of the particle content corresponding to the thermality of the Hawking-Unurh effect [229].

There is a way to define the particles and compare the particle content in the Minkowski and Rindler frames. Then one arrives at the result that the Minkowski vaccum is a thermal bath of particles for the Rindler observer. "Particles" are defined as positive frequency modes of a given field. But the positive frequency is defined with rest to the proper time of the observer. As we saw the time co-ordinate in the Minkowski (t) and the accelerating frame (ξ^0) are related in a non-trivial way. The Rindler time translation is a Lorentz boost. As a result, comparing the positive frequency modes results in a Bogoliubov transformation operators associated with the hyperbolic transformation of the boosts. Thus the notion of "particle" changes when we switch frames and leads to the Hawking-Unruh effect.

To show this consider a massless scalar field in $1+1$-dimensional spacetime,

$$S[\phi] = \frac{1}{2}\int g^{\alpha\beta}\phi_{,\alpha}\phi_{,\beta}\sqrt{-g}d^2x \tag{4.62}$$

This action is conformally invariant and therefore the actions in Minkowski and Rindler co-ordinates look the same.

$$S = \frac{1}{2}\int[(\partial_t\phi)^2 - (\partial_x\phi)^2]dtdx = \frac{1}{2}\int[(\partial_{\xi^0}\phi)^2 - (\partial_{\xi^1}\phi)^2]d\xi^0 d\xi^1 \tag{4.63}$$

In lightcone co-ordinates, the field equations become

$$\partial_u\partial_v\phi = 0 \quad \partial_{\tilde{u}}\partial_{\tilde{v}} = 0 \tag{4.64}$$

The right-moving positive frequency solutions in the Minkowski space are given by

$$\phi \propto e^{-i\omega u} = e^{-i\omega(t-x)} \tag{4.65}$$

The rightmoving positive frequency solutions in the Rindler space is given by

$$\phi \propto e^{-i\Omega\tilde{u}} = e^{-i\Omega(\xi^0-\xi^1)} \tag{4.66}$$

Now we shall do a mode-expansion for the fields in the two spacetimes.The Minkowski vacuum $|0_m\rangle$ is annihilated by the operator

$$\hat{a_\omega}\,|0_M\rangle = 0 \tag{4.67}$$

Similarly the Rindler vacuum $|0_R\rangle$ is annihilated by

$$\hat{b_\Omega}\,|0_R\rangle = 0 \tag{4.68}$$

Given these the mode-expansion is given by

$$\hat{\phi} = \int_0^\infty \frac{d\omega}{\sqrt{4\pi\omega}}[e^{-i\omega u}\hat{a}_\omega + e^{i\omega u}\hat{a}_\omega^\dagger] + (leftmoving) \tag{4.69}$$

$$\hat{\phi} = \int_0^\infty \frac{d\Omega}{\sqrt{4\pi\Omega}}[e^{-i\Omega\tilde{u}}\hat{b}_\Omega + e^{i\Omega\tilde{u}}\hat{b}_\Omega^\dagger] + (leftmoving) \tag{4.70}$$

These operators obey the commutation relations

$$[\hat{a}_\omega, \hat{a}_{\omega'}^\dagger] = \delta(\omega - \omega') \tag{4.71}$$

$$[\hat{b}_\Omega, \hat{b}_{\Omega'}^\dagger] = \delta(\Omega - \Omega') \tag{4.72}$$

The two operators are related by Bogoliubov transformations

$$\hat{b}_\Omega = \int_0^\infty d\omega[\alpha_{\Omega\omega}\hat{a}_\omega - \beta_{\Omega\omega}\hat{a}_\omega^\dagger] \tag{4.73}$$

The co-efficients $\alpha_{\Omega\omega}$ and $\beta_{\Omega\omega}$ are given by

$$\alpha_{\Omega\omega}, \beta_{\Omega\omega} = \pm\frac{1}{2\pi a}\sqrt{\frac{\Omega}{\omega}}e^{\pm\frac{\pi\Omega}{2a}}exp\left(\frac{i\Omega}{a}ln\frac{\omega}{a}\right)\Gamma(-i\Omega/a) \tag{4.74}$$

Now that we have all the ingredients in place, we can compute the expectation value of the number of particles $\hat{N}_\Omega = \hat{b}_\Omega^\dagger\hat{b}_\Omega$ in the Minkowski vacuum

$$\langle\hat{N}_\Omega\rangle = \langle 0_M|\,\hat{b}_\Omega^\dagger\hat{b}_\Omega\,|0_M\rangle = \int d\omega|\beta_{\omega\Omega}|^2 \tag{4.75}$$

From this, the average density of the number of particles is given by

$$n_\Omega = \frac{\langle\hat{N}_\Omega\rangle}{V} = \frac{1}{exp(2\pi\Omega/a) - 1} \tag{4.76}$$

Thus, for an accelerating observer, the Minkowski vacuum looks like a thermal distribution of particles with temperature given in terms of the acceleration

$$T = \frac{a}{2\pi} \tag{4.77}$$

One can

Schwarzschild black hole and Hawking radiation— Recall that the metric in the Schwarschild co-ordinates is given by

$$ds^2 = \left(1 - \frac{2M}{r}\right)dt^2 - \frac{dr^2}{\left(1 - \frac{2M}{r}\right)} - r^2(d\theta^2 + d\phi^2 \sin^2\theta) \tag{4.78}$$

Introducing the Torotise co-ordinate,

$$dr_* = \frac{dr}{1 - 2M/r} \tag{4.79}$$

the metric (considering only the radial and time part)becomes

$$ds^2 = (1 - \frac{2M}{r(r_*)})[dt^2 - dr_*^2] \tag{4.80}$$

The tortoise co-ordinates is called so as it makes r change slower on approaching the horizon and takes the horizon to $r^* \to -\infty$. Now introducing the tortoise lightcone co-ordinates $\tilde{u} = t - r_*$ and $\tilde{v} = t + r_*$, the metric simplifies to

$$ds^2 = \left(1 - \frac{2M}{r(\tilde{u}, \tilde{v})}\right)d\tilde{u}d\tilde{v} \tag{4.81}$$

Schwarzschild and tortoise co-ordinates cover only the region outside the black hole and becomes singular at the horizon.. Kruskal-Szekeres co-ordinates are used to extend the description of spacetime to the interior. The transformation to kruskal-Szekeres co-ordinates are given by

$$u = -4Mexp(-\tilde{u}/4M) \quad , v = 4Mexp(\tilde{v}/4M) \tag{4.82}$$

The metric is now written as

$$ds^2 = \frac{2M}{r(u,v)}exp\left(1 - \frac{r(u,v)}{2M}\right)dudv \tag{4.83}$$

Now we make the analogy to the derivation of Unruh effect in Minkowski space. Since the tortoise co-ordinate covers only the exterior of the black hole, its similar to the Rindler spacetime. The KS co-ordinate system which covers the entire spacetime except the singularity at the center, is similar to the Minkowski spacetime. In fact the KS and the tortoise co-ordinates are related formally in exactly similar way as the Minkowski and Rindler co-ordinates. The acceleration is replaced here by surface gravity $\kappa = 1/4M$. Thus the derivation of thermal distribution of particles in Kruskal vacuum follows similarly and the temperature of the Hawking radiation is given by

$$T_H = \frac{\kappa}{2\pi} = \frac{1}{8\pi M} \tag{4.84}$$

Thus, using both the path integral and the mode expansion approaches, we have seen the derivation of the Hawking-Unruh effect. The key essence is that observer outside the horizon do not have access ot the information inside the horizon. Therefore, when one considers a vacuum of a quantum field on the full spacetime, observers outside the black hole or within the Rindler wedge perceive the vacuum as a thermal state. The key concept central to both derivations is that the Rindler time translation is generated by the boost. The boost being a complex rotation in euclidean time, acts on the quantum mechanical states leading to thermality.

4.6 Black hole perturbations and quasinormal modes

Quasinormal modes are another manifestly characteristic phenomena associated with black holes. They were pioneered in the context of black hole stability by C. V. Vishveshwara in [13] and has been studied extensively since then [230, 231, 232]. It was shown that the late time decay behaviour of black holes are completely determined by the black hole parameters such as mass, charge and angular momentum alone. Here we collectively refer to the resonances in the scattering problem arising from a wave equation in curved spacetimes as quasi-normal modes. The Hawking-Unruh effect was a purely quantum mechanical effect. The quasinormal modes on the other hand can arise in the scattering of classical or quantum mechanical field. Scattering resonances or the quasinormal modes are not extraneous or exotic as one might consider. On contrary they are immediate consequences of having open boundary conditions in a scattering system. We shall see more on the subtleties and surprises regarding boundary conditions and scattering theory in the section on the IHO and scattering physics. Here we will show the basic set-up for studying a wave-equation in a black hole spacetime and how a scattering problem arises in this context. We will show the appearance of IHO in the limit of WKB approximation. Wave equations appear as equations of motion for fields that can correspond matter or energy in the background of a metric. These could arise from perturbations of scalar or higher spin fields without any back reactions on the metric. Or from the perturbation of the metric itself, in which case the waves obtained are the gravitational waves.

The equation of motion for a masless scalar field is given by the Laplacian written for a curved metric [231]

$$\Box\phi = \frac{1}{\sqrt{-g}}\frac{\partial}{\partial x^\nu}\left(g^{\mu\nu}\sqrt{-g}\partial_\mu\phi\right) \tag{4.85}$$

If it is a Maxwell field (spin-1 gauge field), then Maxwell's equation with no source reads

$$\frac{1}{\sqrt{-g}}\frac{\partial}{\partial x^\nu}\left(g^{\rho\mu}g^{\sigma\nu}\sqrt{-g}F_{\rho\sigma}\right) = 0 \tag{4.86}$$

If we are considering the perturbation of a metric $g_{\mu\nu} = g^0_{\mu\nu} + \delta g_{\mu\nu}$, then the linearised Einstein's equation is

$$\delta R_{\mu\nu} = \kappa\delta(T_{\mu\nu} - 1/(D-2)Tg_{\mu\nu}) + \frac{2\Lambda}{D-2}\delta g_{\mu\nu} \tag{4.87}$$

In stationary spacetimes, one can always do a decomposition of the field into a 'radial part' and an 'angular' part. The angular part is given by simple/ vector/ tensor spherical Harmonics. For example, for a scalar field:

$$\phi(t, r, \theta, \phi) = e^{-i\omega t}Y_l(\theta, \phi)\psi(r)/r \tag{4.88}$$

Here r is the radial co-ordinate for example in the Schwarzsschild spacetime. On such substitution the wave equation reduces to the following form:

$$\frac{\partial}{\partial r_*^2}\psi + V(r, \omega)\psi = \omega^2\psi \tag{4.89}$$

This resembles a quantum mechanical problem of scattering off a potential barrier $V(r)$. The potential V(r) for a Schwarzschild spacetime is given by

$$V(r) = \left(1 - \frac{2M}{r}\right)\left(\frac{l(l+1)}{r^2} + \frac{2M(1-s^2)}{r^3}\right) \tag{4.90}$$

For scalar field the spin $s = 0$, for Maxwell gauge fields $s = 1$ and for gravitational perturbation of axial type $s = 2$

Suppose, r_1, r_2 are the turning points of the potential V, the WKB wavefunctions outside the turning points are given by [233]

$$\psi_i(r) \approx V^{-1/4} exp\left(\pm i \int_r^{r_i} [V(r')]^{1/2} dr'\right) \tag{4.91}$$

Within the region between the turning points, the potential can be approximated by a parabola. Thus

$$V(r) = V_0 + 1/2V_0''(r)(r - r_0)^2 + O((r - r)^3) \tag{4.92}$$

Then the scattering equation becomes

$$\frac{d^2\psi}{dx^2} + (\nu + \frac{1}{2} - \frac{1}{4}x^2)\psi = 0 \tag{4.93}$$

where $x = (2V_0'')^{1/4}e^{i\pi/4}(r - r_0)$, $\nu + 1/2 = -iV_0/(2V_0'')^{1/2}$. This is known as Weber's equation, which is also the Schrodinger equation in the quantum mechanical problem of scattering against an IHO potential. This

derivation shows an equivalence between the classical scattering in a gravitational spacetime and a quantum mechanical scattering problem. .

The general solution of the Weber equation/ IHO Schrodinger equation is given by

$$\psi = AD_{\nu}(x) + BD_{-\nu-1}(ix) \tag{4.94}$$

The asymptotic forms at large $x \to \infty$ is given by [233]

$$\begin{aligned} \psi &\sim Be^{-3i\pi(\nu+1)/4}(4k)^{-(\nu+1)/4}(x-x_0)^{-(\nu+1)}e^{i\sqrt{k}(x-x_0)^2/2} && (4.95) \\ &+ [A + B\sqrt{2\pi}e^{-i\nu\pi/2}/\Gamma(\nu+1)]e^{i\pi\nu/4}(4k)^{\nu/4}(x-x_0)^{\nu}e^{-i\sqrt{k}(x-x_0)^2/2} && (4.96) \end{aligned}$$

Here $k = 1/2Q_0''$ and $\gamma(\nu)$ is the Gamma function. To obtain purely outgoing wave, set the co-efficient of the incoming wave to zero. This involved finding ν such that $\Gamma(-\nu) = \infty$. This leads to a condition that ν can take only integer values

$$Q_0/\sqrt{2Q_0''} = i(n+1/2) \quad n = 0, 1, 2 \tag{4.97}$$

Thus one can interpret this as the Schrodinger equation having imaginary and discrete eigenvalues and the corresponding eigenfunctions as outgoing modes. We shall get back to the detailed study of quasinormal modes as resonances with an eye for the sensitivity to boundary conditions and wave function normalisibility, in the next chapter on the IHO.

QNMs are as fundamental characteristics of physical systems as its normal modes or the bound states. In the context of black holes, the existence of a horizon explicitly makes it a dissipative phenomena, in the sense that it absorbs all the energy fall into it and decays by emission of thermal radiation. In a general open system, the boundary conditions necessitates the existence of QNMs to allow for purely incoming or outgoing boundary conditions. The QNMs depend purely on the parameters of the black hole such as the mass, charge and angular momentum and not any other details. This makes them the direct probes to detect black holes. In fact, the first LIGO measurements achieved precisely that. For a Schwarzschild black hole of one solar mass, the calculated decay time is 0.35ms [234]. The decay time in the remarkable first measurement by LIGO from binary black hole merger was 4 milliseconds [235]. The QNMs hav ealso become extremely important in the context of holography. They correspond to the poles of the retarded green function of the boundary theory that is dual to a bulk geometrical spacetime.

Now that we have described the Unruh effect associated with spacetime horizons and the quasinormal modes we can proceed to study their parallels in the quantum Hall effect. In the next section the basics

of the quantum Hall effect and lowest Landau levels are presented to prepare for identifying the Lorentz algebra structures appearing as the applied potentials.

4.7 Quantum Hall effect and the Lowest Landau level

Here we will review the basics of integer quantum Hall effect, existence of Landau levels, degeneracy in the lowest Landau level and edge localisation are reviewed. Throughout the discussion, the points key for drawing the parallels to black hole phenomena are highlighted

The quantum Hall effect is one of the most non-trivial macroscopic manifestations of quantum mechanics. Historically, it was discovered through a dramatic experimental observation of von Klitzing and group [16] that the fine structure constant could be determined with high precision through resistance measurements in Hall systems. It was found that the Hall resistance is expressed only in terms of the fundamental constants h(the Planck's constant) and the elementary charge e, and does not depend on the properties of the material under consideration. This was the discovery of the integer quantum Hall effect that the Hall conductance is quantized in the integer multiples of (e^2/h) [18]. The discovery of fractional quantum Hall effect was even more intriguing as the conductance quantization was in fractions of (e^2/h) . Investigations to understand these phenomena have led to exploration of a rich variety concepts such as Berry's phase, topological quantum numbers, Anderson localisation, Chern-Simons theory and so on [9, 18]. This has given rise to the field of topological phases which continues to be a topic of active investigation to this day.

Here we will show that the intriguing structures appearing in the context of relativistic spacetimes such as black holes can be found in the quantum Hall systems by applying external potentials. The physical set up of the integer quantum Hall effect consists of a two dimensional electron gas formed in a semiconductor heterostructure such as a thin layer of GaAs sandwiched in between AlAs semiconductors. The electrons are trapped in the layer of GaAs. This heterostructure is subject to strong magnetic fields of the order of few Teslas and low temperatures($< 4K$). The measured transverse resistivity ρ_{xy} is found to be quantized and occurs as plateaus as a function of the magnetic field. The longitudinal resistivity is zero whenever the transverse one is on a plateau. The values of the resistivity on the plateaus are given by:

$$\rho_{xy} = \frac{2\pi\hbar}{e^2}\frac{1}{\nu}, \quad \nu = 1, 2, 3.... \tag{4.98}$$

The integer ν is measured to be precise upto 1 part in a billion. Such robust 'quantization' cannot be captured through classical physics and is purely a manifestation of quantum mechanics.

We shall start with the quantum mechanical Hamiltonian of a single particle in the presence of a magnetic

fields we are not considering interactions here

$$H_0 = \frac{1}{2m}\left(\vec{p} - e\vec{A}\right)^2 \tag{4.99}$$

Here $\vec{A}$ is the vector potential related to the magnetic field $\nabla \times \vec{A} = B\hat{z}$. The canonical momentum operator (termed as the Kinetic momentum)is given by

$$\pi_i = p_i - eA_i \tag{4.100}$$

The commutation relations between the kinetic momenta and the co-ordinates are then given by

$$[x_i, \pi_i] = i\delta_{ij}, [\pi_i, \pi_j] = i\frac{\epsilon_{ij}}{\ell_b^2}, \tag{4.101}$$

where the magnetic length is given by $\ell_B = \sqrt{1/eB}$. The generator of translations in this case is not the kinetic momentum but is given by a pseudo-momentum operator that commutes with the Hamiltonian [45]:

$$\vec{K} = \vec{p} - \vec{A} + e\vec{B} \times \vec{r}, \tag{4.102}$$

where $\vec{r}$ is the regular position operator and $[K, H_0] = 0$. Then the operator for a translation of $\vec{\delta}$ is given by $T(\vec{\delta}) = e^{-i\vec{\delta}.\vec{K}}$. The components of pseudo-momenta do not commute with each other:

$$[K_x, K_y] = -ieB \tag{4.103}$$

This results in the non-commutativity of the translation operators :

$$T(\vec{a})T(\vec{b}) = T(\vec{b})T(\vec{a}) \exp\left(-i\frac{[\vec{a} \times \vec{b}]_z}{\ell_B^2}\right) \tag{4.104}$$

This non-commutativity is a direct manifestation of the emergence of Aharonov-Bohm phase in the presence of gauge fields in quantum mechanics. The theme of non-commutativity runs throughout our discussion and is one of the key structures in the emergence of the Hawking-Unruh effect in the quantum Hall systems. As already mentioned, we are focusing on the electron system in absence of electron-electron interactions. So, transition to many particle physics can be done through product of single particle states.

Now, we would like to determine the form of single-particle energy eigenfunctions. To proceed, let us choose the Landau gauge $\vec{A} = xB\hat{y}$. Note that on making a gauge transformation the wavefunctions gain a

phase factor and probability densities are not affected. The Hamiltonian in this gauge is given by

$$H_0 = \frac{1}{2m}(p_x^2 + (p_y + eBx)^2) \tag{4.105}$$

As p_y commutes with the Hamiltonian, the energy eigenstates can be written as

$$\psi_k(x, y) = e^{iky} f_k(x), \tag{4.106}$$

where k is the momentum along y. Therefore, for each k one can write the Hamiltonian as that of a Harmonic oscillator displaced from the origin

$$H_k = \frac{1}{2m}p_x^2 + \frac{m\omega_c^2}{2}(x + k\ell^2) \tag{4.107}$$

Here $\omega_c = B/m$ is the cyclotron frequency. Therefore, for each k the the spectrum is that of a harmonic oscillator

$$E_n = \hbar\omega_c(n + \frac{1}{2}) \tag{4.108}$$

The energy levels E_n are called the *Landau levels*.

Degeneracy in the Landau levels– Using the Landau gauge helps us see the degeneracy in each Landau level. Let us considered a system on a confined rectangular region $L_x \times L_y$. This quantizes the plane wave states along y-direction in the increments of $k_y = \frac{2\pi}{L_y}$. The harmonic oscillator eigenfunctions along the x-direction are localised around points $x_0 = -k\ell^2$ in the range $0 \leq x_0 \leq L_x$. This also imposes a constraint on the allowed values of k: $-L_x/\ell^2 \leq k \leq 0$. Then one can calculate the number of states per each energy level:

$$N = \frac{L_y}{2\pi}\int_{-L_x/\ell^2}^{0} dk = \frac{eB(L_xL_y)}{2\pi\hbar} = \frac{\Phi}{\Phi_0} \tag{4.109}$$

where $\Phi_0 = 2\pi\hbar/e$ is the flux quantum and $\Phi = B(L_xL_y)$ is the total flux through the system. This indicates that the number of states in the Landau level is given by the flux quanta through the system. Such a finite sized system has edges and there are states that are localised near these edges. These *edge states* play an important role in quantum hall physics.

Confining potential and edge-localisation: The edge of the system can be taken into consideration by introducing a confining potential $V(x)$ to the system along x direction. The assumptions about the potential are that it varies slowly in the scale of ℓ and that it is smooth and differentiable. Taylor expanding the

potential around the x_0 points and considering it in the Hamiltonian, we get

$$H_k = \frac{p_x^2}{2m} + \frac{1}{2}m\omega_c^2(k\ell^2 + x)^2 + V_0 + x\frac{\partial V}{\partial x}\bigg|_{x_0} \tag{4.110}$$

Since the additional terms are constants, completing the squares, the Hamiltonian can be modified into (upto a constant)

$$H_k = \frac{p_x^2}{2m} + \frac{1}{2m\omega_c^2}\left(k\ell^2 + \frac{\partial V}{\partial x}\frac{1}{m\omega_c^2} + x\right)^2 - \frac{1}{2m\omega_c^2}(\frac{\partial V}{\partial x})^2 - k\ell^2\frac{\partial V}{\partial x} \tag{4.111}$$

The energy eigenvalues are now modifed as

$$E_n(k) = \hbar\omega_c(n + \frac{1}{2}) - \frac{1}{2m\omega_c^2}(\frac{\partial V}{\partial x})^2 - k\ell^2\frac{\partial V}{\partial x} \tag{4.112}$$

From the above expression one can calculate the group velocity of the wavepackets composed of different momenta

$$v_y = \frac{\partial E}{\partial k} = -\frac{1}{eB}\frac{\partial V}{\partial x}. \tag{4.113}$$

From this one can deduce that the group velocity at the two edges will be opposite to each other. Therefore, the left and right moving states are confined to different edges of the system. Thus the time reversal symmetry is explicitly broken in the system. Let us note at this point that one way of creating black hole horizon behaviour in the quantum Hall system is by explicitly engineering the spatial profile of this group velocity [3].

Now one can explicitly compute the conductance in the system by calculating the current when a chemical potential difference of $\Delta\mu$ is applied across the ends of the system

$$I_y = -\frac{e}{L_y}\int dk\frac{L_y}{2\pi}v_y(k) = \frac{e}{2\pi\ell^2}\int dx\frac{1}{eB}\frac{\partial V}{\partial x} = \frac{e}{2\pi\hbar}\Delta\mu \tag{4.114}$$

By noting that $V_H = \Delta\mu/e$,

$$\sigma_{xy} = \frac{I_y}{V_H} = \frac{e^2}{2\pi\hbar} \tag{4.115}$$

In the presence of high magnetic fields, the system will be constrained to be in the lowest level state of the ground states of the system. This state is called the lowest Landau level(LLL). We will be focused mostly on the physics in the lowest Landau level.

Lowest Landau level– The symmetric gauge $\vec{A} = 1/2\vec{B}\times\vec{r}$ will be particularly convenient for studying

the LLL. Also introduce two types of momenta π, π' defined as $\pi = p + \vec{eA}, \pi' = \vec{p} - e\vec{A}$. The two momenta commute with each other $[\pi_i, \pi_i'] = 0$ and also obey $[\pi_x', \pi_y'] = ie\hbar B$. Now introduce the ladder operators $a = (\pi_x - i\pi_y)/\sqrt{2e\hbar B}$ and $a' = (\pi_x' + i\pi_y')/\sqrt{2e\hbar B}$. The Hamiltonian is now given by

$$H_0 = \frac{\hbar\omega_c}{2}\left(a^\dagger a + \frac{1}{2}\right) \tag{4.116}$$

The second set of operators a' generate the degeneracy within the Landau level. The general state in the Hilbert space is given by $|n, m\rangle = \frac{(a^\dagger)^n (b^\dagger)^m}{\sqrt{n!m!}} |0, 0\rangle$. For $n = 0$ (i.e the LLL), the wavefunctions take a simple and illustrative form if they are expressed in complex co-ordinates $z = x - iy, \bar{z} = x + iy$. Then the operator a takes the form:

$$a = -i\sqrt{2}\left(\ell\bar{\partial} + \frac{z}{4\ell}\right) \tag{4.117}$$

The state that is annihilated by this operator gives the LLL wavefunction:

$$\psi_{LLL}(z, \bar{z}) = f(z)e^{-|z|^2/4\ell^2} \tag{4.118}$$

The states within the degenerate space can be generated using the operators $b = -i\sqrt{2}(\ell\partial + \bar{z}/4\ell)$. The basis of LLL wavefunctions is then given by acting with $b^\dagger$ and one obtains a space of holomorphic functions (called the Bargmann space):

$$\psi_{LLL,m} \sim \left(\frac{z}{\ell}\right)^m e^{-|z|^2/4\ell^2} \tag{4.119}$$

This representation is illustrative as there is a natural interpretation of the states in terms of angular momentum. If one defines an angular momentum operator $J = \hbar(z\partial - \bar{z}\bar{\partial})$. Then the LLL states are eigenstates of the angular momentum operator

$$J\psi_{LLL,m} = \hbar m \psi_{LLL,m} \tag{4.120}$$

As we will see later, the applied potentials on the quantum Hall system when projected to LLL act as Hamiltonians on the space of functions $f(z)$. One then obtains a simpler form of Schrodinger equations in the LLL.

This covers some of the basics of the vast subject of quantum Hall effect. One can find detailed exposition in this vast subject in many textbooks and review articles [18, 45, 9]. Now we will turn our attention to the potentials applied on the quantum Hall system that will lead to parallels with Lorentz Kinematics and Hawking-Unruh effect. First we will study the application of saddle potential on the quantum hall system

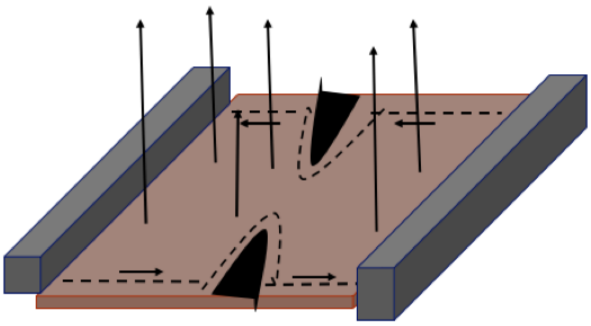

Figure 4.5: A quantum Hall system comprises of a two dimensional electron gas in the presence of a strong magnetic field. The states at the edges have a chiral nature and are unidirectional. Point contacts are applied as probes for conductance measurements and are modeled with a saddle potential $V(x, y) = \lambda(x^2 - y^2)$.

without restricting it to the LLL and then look into the types of restricted potentials in the LLL.

4.8 Saddle potential and emergence of inverted harmonic oscillator

Quantum mechanical tunneling in the saddle potential has been of interest in the condensed matter setting since 1950's [190, 191] because of its relevance to the semiclassical motion of electrons in metals with complicated Fermi surfaces and also in the presence of high magnetic fields. Since the discovery of quantum Hall effect, it has become even more important especially because of its relevance to systems involving point contacts. Point contacts are key tools in conductance experiments and are used as probes for anyon interferometry and shot noise. It was shown by Fertig and Halperin [190] that the Hamiltonian for electrons in two dimensions in the presence of a high magnetic field and a saddle potential, splits into two commuting parts. One corresponding to a harmonic oscillator and the other to an inverted harmonic oscillator. The tunneling between the semi-classical orbits is completely determined by the tunneling across the inverted Harmonic potential. We will see that the inverted Harmonic oscillator will turn out to be the parallel of the Rindler Hamiltonian in the quantum Hall system. Here will provide a gauge invariant derivation of Fertig and Halperin's result.

The Hamiltonian for the quantum Hall system in a saddle potential is given by

$$H = \frac{1}{2m}\left(\frac{1}{i}\nabla + \vec{A}\right)^2 + \lambda(x^2 - y^2) \tag{4.121}$$

Let us introduce the operators (assuming no specific gauge) $b = \frac{1}{\sqrt{B}}(\pi_x + i\pi_y), [b, b^\dagger] = 1$. (From this point

we shall work in the units of $\hbar = c = e = 1$).Now define the 'guiding center co-ordinates'

$$R_i = x_i + \frac{1}{B}\epsilon_{ij}\pi_j \tag{4.122}$$

These will be of crucial importance in the LLL physics and they form a non-commutative plane.

$$[R_i, R_j] = -i\frac{1}{B}\epsilon^{ij} \tag{4.123}$$

They commute with the kinetic momenta: $[R_i, \pi_j] = 0$. One can construct ladder operators from these guiding center co-ordinates $a = -i\sqrt{B/2}(R_x - iR_y)$:

$$[a, a^\dagger] = 1 \quad [a, b] = [a^\dagger, b] = 0 \tag{4.124}$$

In the terms of these operators, the Hamiltonian reads

$$H = \frac{\omega_c}{2}b^\dagger b + \frac{\lambda}{B}(a^2 + (a^\dagger)^2 + b^2 + {b^\dagger}^2 - a^\dagger b - b^\dagger a) \tag{4.125}$$

One can see that the a and b operators are coupled in the above form and it is suitable to decouple them. Making a rotation of basis that preserves the commutation rule

$$\begin{pmatrix} a \\ b \end{pmatrix} = \begin{pmatrix} e^{i\phi/2}\cos(\theta) & \sin(\theta) \\ -\sin(\theta) & e^{-i\phi/2}\cos(\theta) \end{pmatrix} \begin{pmatrix} c_1 \\ c_2 \end{pmatrix} \tag{4.126}$$

The choice of $\phi = 0$ and $\tan(2\theta) = -4\lambda/(B\omega_c)$ removes the cross terms of the type $c_1^\dagger c_2$,$c_1 c_2$., the Hamiltonian is then simplified to:

$$H = \Omega c_1^\dagger c_1 + \frac{\lambda}{B}(c_1^2 + {c_1^\dagger}^2) - \left|\Omega - \frac{\omega_c}{2}\right| c_2^\dagger c_2 + \frac{\lambda}{B}(c_2^2 + {c_2^\dagger}^2) \tag{4.127}$$

Here,

$$\Omega = \frac{\tan\theta}{\tan^2\theta - 1} \quad \Omega - \frac{\omega_c}{2} = \frac{1}{\tan^2\theta - 1} \tag{4.128}$$

The parameter Ω is always positive for a given value of θ. A Bogoliubov transformation can be made to diagonalize a part of the Hamiltonian with the choice of $\tanh(2\theta_1) = \Omega B/\lambda$ and $\tanh(2\theta_2) = -\lambda/(B|\Omega -$

$\omega_c/2|$).

$$\begin{pmatrix} c_i \\ c_i^\dagger \end{pmatrix} = \begin{pmatrix} \cosh\theta_i & \sinh(\theta_i) \\ \sinh(\theta_i) & \cosh(\theta_i) \end{pmatrix} \begin{pmatrix} \gamma_i \\ \gamma_i^\dagger \end{pmatrix} \tag{4.129}$$

The Hamiltonian reduces to the form $H = H_1 + H_2$, where

$$H_1 = E_1(\gamma_1^2 + {\gamma_1^\dagger}^2) \tag{4.130}$$

$$H_2 = E_2(\gamma_2^\dagger\gamma_2 + 1/2) + constant \tag{4.131}$$

We see that H_1 corresponds to a squeezing operator whereas H_2 corresponds to the harmonic oscillator. Making another transformation $X = (\gamma_1^\dagger - \gamma_1)/(\sqrt{2}i)$, $P = (\gamma_1 + \gamma_1^\dagger)/\sqrt{2}$ and $x = (\gamma_2^\dagger + \gamma_2)/\sqrt{2}$, $p = (\gamma_2 - \gamma_2^\dagger)/(\sqrt{2}i)$, we get

$$H = E_1(P^2 - X^2) + E_2/2(p^2 + x^2) \tag{4.132}$$

Thus the Hamiltonian for the quantum Hall system in a saddle potential is a sum of an inverted oscillator and a harmonic oscillator, a result similar to that obtained in [190], but in a gauge invariant way. In the limit $B \to \infty$, the system is restricted to one of the Harmonic oscillator levels and is equivalent to a Landau level. Expressed explicitly in terms of guiding center co-ordinates, the Hamiltonian in the lowest Landau level is the inverted oscillator. The transmission co-efficient is one of the key quantities derived in this set-up as it relates directly to the conductance. The transmission co-efficient is given by: $|t|^2 = 1/(1 + e^{2\pi E})$ and is completely determined by the physics of the inverted harmonic oscillator [190] In the following we will examine the algebraic structure of the class of such potentials that can be written within the lowest Landau level.

4.9 Lowest Landau level physics, applied potentials and strain generators

On imposing the condition of preserving the flux through the quantum Hall system, the kind of potentials that can be applied on the system is constrained. The external electrostatic potentials applied on the system are important for conductance measurements. With recent advances in the understanding of response of the quantum Hall system to geometric deformations, the generators of strain in the system that preserve the flux are also important. Here we will consider both of them, study their algebraic structure and their

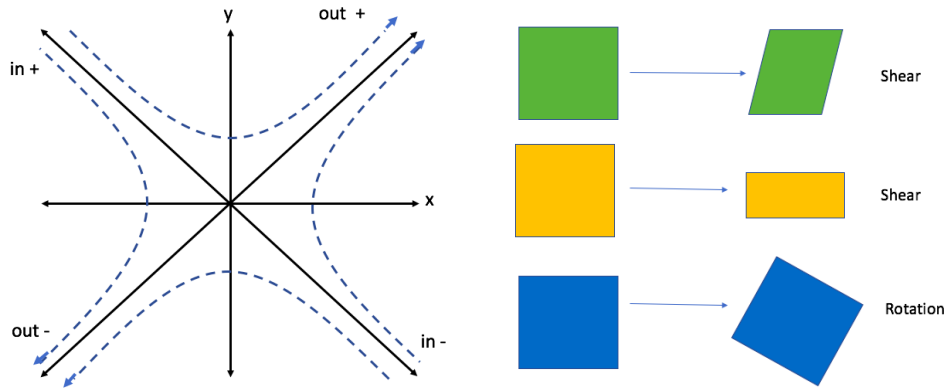

Figure 4.6: Figure on the left shows the semiclassical trajectories for single particle states in a saddle potential and scattering across the branches. Figure on the left shows the 3 different area preserving transformations applied to the quantum Hall system in the lowest Landau level.

projection to the lowest Landau level.

Strain generators– To study the geometrical deformation on a quantum Hall system consider unifrom area preserving deformations of a two dimensional system in a magnetic field. [6]. Consider the transformations on (x_i, π_i) generated by generators J_{ij}: $S = e^{-i\lambda_{ij}J_{ij}}$, $\Lambda = e^{\lambda}$ and expect that $Sx_iS^{-1} = \lambda_{ji}x_j, S\pi_iS^{-1} = \Lambda^{-1}_{ij}\pi_j$ This gives us the algebraic relations:

$$i[J_{ij}, \pi_k] = \delta_{ik}\pi_j \tag{4.133}$$

$$i[J_{ij}, x_k] = -\delta_{jk}x_i \tag{4.134}$$

$$i[J_{ij}, J_{kl}] = \delta_{il}J_{kj} - \delta_{jk}J_{il} \tag{4.135}$$

The last condition defines the algebra of these generators which is the $\mathfrak{sl}(2, \mathbb{R})$ lie algebra (we shall study that soon). The strain generators can be written in terms of the (x_i, π_i) from the above conditions [236]:

$$J_{ij} = -\frac{1}{2}\{x_i, \pi_j\} + \frac{1}{4}\{x_i, \pi_j\}\delta_{ij} + \frac{B}{2}\epsilon_{ik}x_jx_k \tag{4.136}$$

The first two terms generate shear in the absence of magnetic field. This can be easily seen from the fact that π_i are the generator of 'kinetic translations'. The last term appears in the presence of a magnetic field as gauge transformations and also compensates for the non-commutativity of kinetic momenta.

[6] Thanks to Barry Bradlyn for the notes on strain generators in lowest Landau level

Three independent generators are given. The rotation generator is given by:

$$L = -\frac{1}{2}\epsilon^{ij}J_{ij} = -\frac{1}{4}\left(B|\vec{R}|^2 + \frac{1}{B}|\vec{\pi}|^2\right) \tag{4.137}$$

Two shear generators are then given by

$$J_a = \frac{1}{2}\sigma^z_{ij}J_{ij} = \frac{1}{4B}\{\pi_x, \pi_y\} + \frac{B}{4}\{R_x, R_y\} \tag{4.138}$$

$$J_b = \frac{1}{2}\sigma^x_{ij}J_{ij} = \frac{B}{4}(R_y^2 - R_x^2) + \frac{1}{4B}(\pi_y^2 - \pi_x^2) \tag{4.139}$$

Quadratic potentials– Now, in the same spirit one can write down the allowed quadratic electrostatic potentials

$$V_1 = \lambda_1(x^2 + y^2), \quad V_2 = \lambda_2(xy), \quad V_3 = \lambda_3(x^2 - y^2) \tag{4.140}$$

Expressing in terms of guiding center and kinetic co-ordinates

$$V_1 = \lambda\left[R_x^2 + R_y^2 + \frac{1}{B^2}(\pi_x^2 + \pi_y^2) + \frac{2}{B}(R_y\pi_x - R_x\pi_y)\right] \tag{4.141}$$

$$V_2 = \lambda\left[\frac{1}{2}\{R_x, R_y\} - \frac{1}{2B^2}\{\pi_x, \pi_y\} + \frac{1}{B}(R_x\pi_y + R_y\pi_x)\right] \tag{4.142}$$

$$V_3 = \lambda\left[R_x^2 - R_y^2 + \frac{1}{B^2}(\pi_y^2 - \pi_y^2) - \frac{2}{B}(R_y\pi_x + R_x\pi_y)\right] \tag{4.143}$$

Projection to the lowest Landau level – One can restrict to the LLL to study the electron dyamics in the presence of high magnetic fields. We will see that the above mentioned potential take a simpler form of Schrodinger equations when projected to LLL. Consider the Hamiltonian of the following form:

$$H = H_0 + V = \frac{1}{2m}\pi_i^2 + V = \omega_c\left(b^\dagger b + \frac{1}{2}\right) + V \tag{4.144}$$

The potentials V can be one of the electrostatic potentials V_i . The Hamiltonians in the presence of strain generators are:

$$H_a = H_0 + \frac{4\lambda}{B}J_a, \quad H_a = H_0 + \frac{4\lambda}{B}J_b, \quad H_L = H_0 + \frac{4\lambda}{B}L \tag{4.145}$$

Let us introduce the lowest Landau level projection operator P_{LLL} that satisy the following relations with Landau level lowering/raising operators and the angular momentum operators:$[b, P_{LLL}] = -P_{LLL}b, \quad [a, P_{LLL}] =$

0 For a normal ordered function ofa, b operators, $f(b, b^\dagger, a, a^\dagger) = \sum_{n,m} g_{nm}(a, a^\dagger)(b^\dagger)^n b^m$, the LLL projection is then given by $P_{LLL} f(b, b^\dagger, a, a^\dagger) = g_{00}(a, a^\dagger)$ The a operators are given only in terms of the guiding center co-ordinates : $a = -i\sqrt{B/2}(R_x - iR_y)$ and the b operators are similarly given in terms of the kinetic momenta π_i. The projection to LLL leaves us with expression only involving R_x, R_y. Also using the relation for the strain generators $P_{LLL} J_{ij} P_{LLL} = \frac{B}{4}\epsilon^{jk}\{R_i, R_k\} + \mathcal{O}(1)$, one can see that LLL projections are given by

$$P_{LLL} V_1 P_{LLL} == P_{LLL} H_L P_{LLL} = |\vec{R}|^2 + \mathcal{O}(1) \tag{4.146}$$

$$P_{LLL} V_2 P_{LLL} = P_{LLL} J_a P_{LLL} = \frac{1}{2}\{R_x, R_y\} + \mathcal{O}(1) \tag{4.147}$$

$$P_{LLL} V_3 P_{LLL} = P_{LLL} J_b P_{LLL} = (R_x^2 - R_y^2) + \mathcal{O}(1) \tag{4.148}$$

Thus, we see that the strain generators and the electrostatic potentials lead to the identical forms of Hamiltonian when projected to the LLL. This is grounded in the fact that both the potentials are generators of the $\mathfrak{sl}(2, \mathbb{R})$. From the above we can see that on projection to the LLL, the kinetic terms drop out and the potentials V_i act as the Hamiltonians acting on the LLL states [237]. We see that what we have are 3 simple quadratic potentials. These generate the Hamiltonian dynamics in the LLL. Now connecting back to Hawking-Unurh effect, recall that the Hamiltonian is the time translation generator and the boost playing the role of Hamiltonian gave rise to the thermality. In the next section, we shall see that one of the above potentials in the LLL are parallels to the Lorentz transformations and rotation in the Minkwoski case.

4.10 Lorentz Kinematics in the lowest Landau level

	Hawking Unruh	Lowest Landau Level
Platform	Spacetime (x, t)	Non-commutative plane $[R_x, R_y] = -i\ell_B^2$ in LLL
Invariant structure	Spacetime metric $ds^2 = dt^2 - d\vec{x}^2$	Commutation relation $[R_i, R_j] = -i\ell_B^2\epsilon_{ij}$
Symmetry transformations	Metric preserving Lorentz transformations $\mathfrak{so}(2,1)$: Boost (K_1, K_2) and rotations K_0	Area preserving potentials $\mathfrak{sl}(2, \mathbb{R})$: Shears/Saddle (K_1, K_2) and rotation/Harmonic K_0
Rindler Hamiltonian	Boost	Inverted Harmonic oscillator
Algebra of transformations $[K_1, K_2] = -iK_0$, $[K_0, K_1] = iK_2$, $[K_2, K_0] = iK_1$		
$\mathfrak{so}(2,1) \approx \mathfrak{sl}(2, \mathbb{R})$		

Table 4.1: Table highlighting the parallels between the symmetry structures and platforms in the Hawking-Unruh effect and the lowest Landau level

Let us rewrite the forms of the LLL potentials identifying $P = R_x/\sqrt{\ell_B}$, $X = R_y/\sqrt{\ell_B}$ and renaming

V_1, V_2, V_3 as K_0, K_1, K_3 respectively. Then we have the Hamiltonian in the LLL generated by applied potential to be of the form

$$K_0 = (P^2 + X^2), \quad K_1 = (PX + XP), \quad K_2 = (P^2 - X^2) \tag{4.149}$$

In the basis of LLL wavefunctions (Bargmann space), these can be written as differential operators [237]

$$K_0 = \frac{1}{4}\Big(- \frac{\partial^2}{\partial z^2} + z^2\Big), \quad K_1 = \frac{i}{2}(z\frac{\partial}{\partial z} + \frac{1}{2}), \quad K_2 = \frac{1}{4}\Big(- \frac{\partial^2}{\partial z^2} - z^2\Big) \tag{4.150}$$

These are exactly the generators of $\mathfrak{sl}(2,\mathbb{R})$ (in a given representation). The group $SL(2,R)$ consists to 2 dimensional matrices of unit determinant. One could think of these are area preserving deformations in two dimensions and there are three generators of such a deformation. To get some intuition, one could think of a square(4.6): it can be rotated within its plane and the area does not change- this is done by the rotation generator K_0. One can stretch it sideways increasing the length and decreasing the width preserving the area or one could deform it to a parallelogram. These two are the shear transformations. The non-trivial part is that the order of successive transformations do not commute, but the non-commuting part will always be related to the third generators. This is expressed as the $\mathfrak{sl}(2,\mathbb{R})$ 'Lie-Algebra':

$$[K_1, K_2] = -iK_0, \quad [K_0, K_1] = iK_2, \quad [K_2, K_0] = iK_1 \tag{4.151}$$

These generators are now the Hamiltonians acting on the LLL states. One can also think of them as the generators of canonical transformations that preserve the commutation relation $[R_x, R_y] = -i\ell_B^2$. Such an algebra that is present in the context of the symmetries of the Minkowski spacetime is the $\mathfrak{so}(2,1)$ which was reviewed in one of the previous sections. In that context, the generators lead to transformation of the spacetime $(t, \vec{x})$ such that the metric $ds^2 = dt^2 - d\vec{x}^2$ is preserved. The generators were those of one rotation and two boosts. The exact mathematical relation between two Lie algebras is a Lie algebra isomorphism.

$$\mathfrak{sl}(2,\mathbb{R}) \sim \mathfrak{so}(2,1) \tag{4.152}$$

Roughly speaking, one can map from one set to the other such that the algebraic relation in Eq.(4.151) is always preserved. *In this sense*, the shear generators or the saddle- electrostatic potentials are equivalent to the boosts and the rotation generators in LLL to rotation generators in spacetime. One must be cautioned that this parallel atleast at the level of Lie algebra isomorphism should not be taken too literally, in the sense

of treating the two dimensional quantum Hall system as a spacetime. We are particularly interested in the action of the generator on the quantum mechanical states. In the quantum Hall system, these generators are the Hamiltonians in the LLL and generate the time evolution of states. A summary of the parallels in the structures between the two setting is given in the table 4.1.

This connection is extremely powerful as one can now think of generating quantum mechanical behaviour that is generated by relativistic transformations, particularly Lorentz Kinematics. In the following, we shall explore only a facet of this which manifests in the quantum hall effect as an equivalent to the Unruh effect.

4.10.1 Rindler Hamiltonian and the Hawking-Unruh effect in the LLL

We have seen that in the relativistic case, the boost acts as a generator of time translation or more precisely angular time translation in euclidean time $\tau = it$. In the specific case of a Rindler spacetime, the generator of time translation was in fact the boost and was called the 'Rindler Hamiltonian'. The immediate consequence of the Rindler Hamiltonian/boost acting the quantum mechanical states was the Unruh effect. Therefore, let us examine the shear generator/ saddle potential K_3 that is *parallel* to the boost in the sense as discussed above.

$$K_2 = \frac{1}{4}(P^2 - X^2). \tag{4.153}$$

The above operator nothing but a quantum mechanical Hamiltonian for an inverted Harmonic oscillator(IHO)() . This is also equivalent to the generator K_1 through a canonical transformation:

$$K_1 = i\frac{1}{2}(XP + PX) \tag{4.154}$$

This is called the dilatation generator and is an extremely important object in conformal field theory and generates scaling transformations. We will make use of both the representations in out study of the IHO.

This identification of the inverted oscillator with the Rindler hamiltonian and the ensuing thermality has been explored in the context of string theory in the name of $c = 1$ Matrix model. But more recently following ideas of t'Hooft [192] of treating black hole collapse and decay as a scattering problem (as discussed in the overview section.), Betzios et al [193] have shown that to an approximation the S-matrix of the black hole can be exactly obtained from an inverted Harmonic oscillator. They have made use of the method of projective light-cone construction to show the equivalence between the boost and the dilatation operator and finally recognizing it as the IHO. In this context let us note even though we have considered the Lorentz lie-algebra in 2+1- dimensions, the identification of the boost generator with the IHO is valid in 3+1-dimensions as well [193].

Now, let us consider the problem of quantum mechanical scattering off an inverted Harmonic oscillator and show the appearance of a thermal-like tunneling probability. We start with the form of the Hamiltonian:

$$H = \frac{1}{2}(\frac{p^2}{2m} - x^2) \tag{4.155}$$

The left and right sides of the barrier are denoted by $\pm$ and we take the mass $m = 1/2$ for convenience. The scattering matrix relates the incoming states from left and right directions to the outgoing states on the left and right, at energy E. The energy spectrum is a continuum in $E : (-\infty, \infty)$.

The S-matrix relates the out and in states as follows

$$\begin{pmatrix} |E,+\rangle_{out} \\ |E,-\rangle_{out} \end{pmatrix} = \hat{\mathcal{S}} \begin{pmatrix} |E,+\rangle_{in} \\ |E,-\rangle_{in} \end{pmatrix} \tag{4.156}$$

$$\hat{\mathcal{S}} = \frac{1}{\sqrt{2\pi}}\Gamma\left(\frac{1}{2} + iE\right) \begin{pmatrix} e^{i\pi/4}e^{-\pi E/2} & e^{-i\pi/4}e^{-\pi E/2} \\ e^{i\pi/4}e^{-\pi E/2} & e^{-i\pi/4}e^{\pi E/2} \end{pmatrix} \tag{4.157}$$

The derivation of the scattering properties and analysis of the IHO is given in detail in the next chapter as it deserves a detailed treatment. Here we just state the results. From this the tunneling probability can be immediately calculated

$$|t|^2 = \frac{1}{1 + e^{2\pi E}} \tag{4.158}$$

The form of the tunnleing probability resembles a thermal distribution of degrees of freedom with energy E similar to the one we encountered in the Hawking-Unruh effect.

One can obtain the thermal density matrix interpretation to this result by expressing an in-coming state to the outgoing state [3]:

$$|0, in\rangle = N\exp\left[i\int_{-\infty}^{+\infty} e^{-E\pi}(\hat{b}_E^{out,+}\hat{b}_E^{out,-} + \hat{b}_{-E}^{out,-}\hat{b}_{-E}^{out,+})\frac{dE}{2\pi}\right]|0, out\rangle \tag{4.159}$$

The above $\hat{a}_E, \hat{b}_E$ operators act on the vacua $|0, in\rangle, |0, out\rangle$ respectively. A thermal density matrix can be obtained by tracing out states on the $-$side:

$$\hat{\rho} = \Sigma_i e^{-2\pi E_i}|E_i,+\rangle \otimes \langle E_i,+| \tag{4.160}$$

For completeness, let us also write down an effective metric in the quantum Hall system following[3] and relating to the discussion on Rindler spacetime in the previous section. The effective velocity of the

electron in the quantum Hall system under the application of the potential $V(x,y) = \lambda(x^2 - y^2)$ is given $v_{eff} = \frac{\lambda}{eB}\partial V/\partial y = -(\lambda e/B)y$. This vanishes at $y = 0$ and that point can be interpreted as the event horizon. The effective space-time metric with an 'event horizon' is then given by

$$ds^2 = -dt^2 + \frac{1}{v_{eff}(y)^2}dy^2 \tag{4.161}$$

Using the $v_eff = -\kappa y$ with $\kappa = \lambda/eB$, we can write the metric in Euclidean time $\tau = it$ as

$$ds^2 = \Omega^2(y)(dy^2 + \kappa^2 y^2 d\tau^2) \tag{4.162}$$

where $\Omega(y) = 1/(\kappa^2 y^2)$ is a conformal factor. This is equivalent to the Rindler metric we had studied in the previous section.

Thus, we have shown that the Rindler Hamiltonian, the crucial element in the the phenomenon of Unruh effect can be captured as an exact mathematical isomorphism in the context of quantum Hall effect. The thermality arises in the tunneling probability of scattering off an inverted oscillator potential. One can also obtain a thermal density matrix and an effective Rindler space description in the quantum Hall system. This concludes the demostration of the parallels of Hawking-Unurh effect in the quantum Hall effect with a saddle potential.

4.11 Wavepacket scattering and quasinormal modes

QNM decay was originally predicted in the context of the stability of Schwarzschild black holes by C. V. Vishveshwara in Ref. [13], as damped outgoing oscillations in response to incoming Gaussian wave packets.. Here, our map of black hole scattering to the quantum IHO problem [238, 233] and the resultant S-matrix Eq. (4.157) enable us to explicitly characterize these damped oscillations, even if to the simplest approximation. The map also connects the black hole QNMs to previously unexplored dynamics of quantum Hall systems in a saddle potential.

The S-matrix of Eq. (4.157) directly accesses the QNMs in its pole structure when analytically extended to the complex energy plane[239]. Specifically, the residues of the poles are resonant (quasi-stationary, or Gamow) states[240, 241]. These states explicitly decay in time and thus lie outside the standard Hilbert space [242, 243]. The S-matrix for the IHO in Eq. (4.157) has poles at $E_n = -i(n + \frac{1}{2}); n = 0, 1, 2..$, coming from the Gamma function (see Fig. (4.7)). In order to probe these poles, as in both quantum scattering[239] and black hole perturbations[231, 244], we employ a *dynamic* scattering process of impinging wavepackets

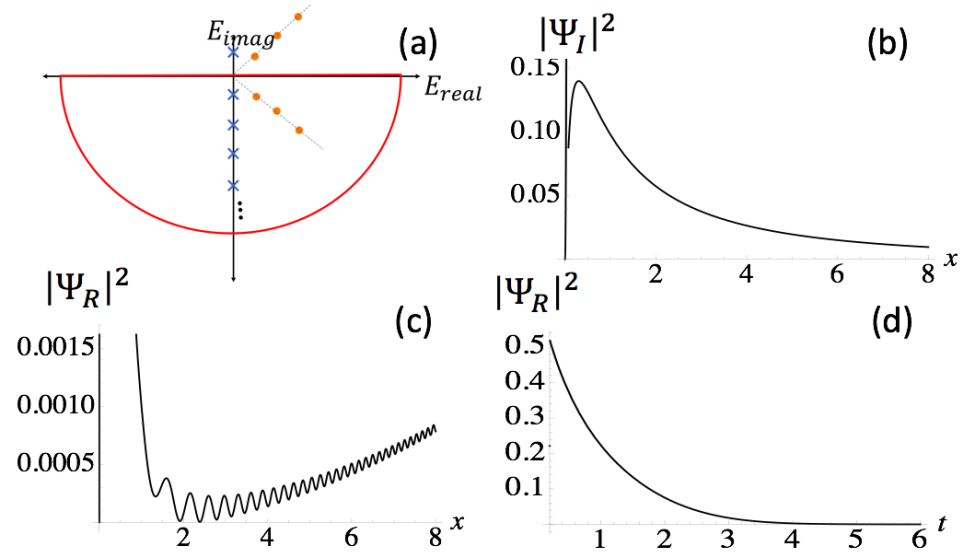

Figure 4.7: Plots of wave-packet scattering off the IHO showing quasinormal mode behavior, as obtained form analytical calculations.(a) Pole structure of the S-matrix of the IHO in the complex energy plane. The blue crosses indicate the resonant poles of the IHO, and the purple boxes indicate generic resonance poles for some arbitrary potential barrier. Closing the contour in the lower half plane is determined by the fact that we have picked outgoing boundary conditions (b) A wave-packet composed of scattering energy eigenstates, impinging on the barrier from the right. (c) The scattered wavepacket shows the "quasinormal ringdown"; the form takes into account only a single pole for illustrative purposes. The scattered state escapes to infinity as seen in its finite amplitude at large x, but as shown in (d), it exhibits an exponential time decay for a given point x after $t > \log|x|$

onto the potential, rather than energy eigenfunctions.

The wave packets for probing the scattering potentials comprise of a collection of scattering states that are also eigen states. The asymptotic form of the scattering energy eigenfunctions of the IHO are given by [26] (We shall derive them in the chapter on IHO):

$$\chi_E(x \to -\infty) \sim i\sqrt{\frac{2}{|x|}}(1+e^{-2\pi E})^{1/2} exp\{-i(\frac{x^2}{4} + E\log|x| + \phi/2 + \pi/4)\} \quad \text{incident} \tag{4.163}$$

$$- \; e^{-\pi E} exp\{i(\frac{x^2}{4} + E\log|x| + \phi/2 + \pi/4)\} \quad \text{reflected} \tag{4.164}$$

$$\chi_E(x \to +\infty) \sim \sqrt{\frac{2}{|x|}} exp\{i(\frac{x^2}{4} + E\log|x| + \phi/2 + \pi/4)\} \quad \text{Transmitted} \tag{4.165}$$

Here

$$e^{i\phi(E)} = e^{\pi E/2}\frac{(1+e^{-2\pi E})^{1/2}}{\sqrt{2\pi}}\Gamma(\frac{1}{2} - iE) \tag{4.166}$$

In a textbook scattering problem in quantum mechanics, we have potentials such as square barrier, which have a finite range. In such a case, we consider the plane waves of the form e^{ikx} to be the solution of the Schrodinger equation asymptotically away from the barrier. The scattering problem is to calculate the reflection and transmission amplitudes when these plane wave are incident on the barrier. In the IHO problem, the scattering potential is no bounded, but the eigen-solution can be solved exactly and the asymptotic form of incident, transmitted and reflected parts are given above. The modes e^{ikx^2} can be considered as the 'plane waves' of this problem.

To capture the effect of resonances which are specific poles of the scattering matrix, we need to consider an incident wavepacket composed of scattering states of different eigen-energies following the notation in [26]:

$$\Psi_i = i\sqrt{\frac{1}{|x|}}\int dE\tilde{f}(E)exp\{-i(\frac{x^2}{4} + E\log|x| + \phi/2 + \pi/4)\}e^{-iEt} \tag{4.167}$$

The envelope function $\tilde{f}(E)$ is peaked near E_0 and is normalised as $2\pi\int dE|\tilde{f}(E)|^2 = 1$. Lets rewrite

$$\Psi_i = i\sqrt{\frac{1}{|x|}}e^{-iE_0 - i\Phi_0}\int dE[\tilde{f}(E)exp(-i(\phi-\phi_0)/2)]exp(-i(E-E_0)(t+log|x|)) \tag{4.168}$$

Here $\Phi_0 = E_0 log|x| + x^2 + \phi_0/2 + \pi/4$ and $f_i(E) = \tilde{f}(E)exp(-i(\phi-\phi_0)/2)$ We choose the wave-packet to be Gaussian:

$$\int_{-\infty}^{+\infty} dEf_i(E)e^{-i(E-E_0)t} = \int_{-\infty}^{+\infty} dE(\frac{1}{2\pi^{3/2})^{1/2}\Delta}e^{\frac{(E-E_0)^2}{2\Delta^2}}e^{-i(E-E_0)t} = (\frac{\Delta}{\pi^{1/2}})^{1/2}e^{-t^2\Delta^2/2} \tag{4.169}$$

$$\Psi_i = iexp(-iE_0t - i\Phi_0)\sqrt{\frac{1}{|x|}}(\frac{\Delta}{\pi(1/2)})^{1/2}exp(-\Delta^2(t+log|x|)^2/2) \tag{4.170}$$

The reflected wave-packet is then given by

$$\Psi_R = -i\frac{e^{-\pi E_0}}{(1+e^{-2\pi E_0})^{1/2}}e^{-iE_0t+i\Phi_0}\sqrt{\frac{1}{|x|}}\int dEf_r(E)exp(-i(E-E_0)(t-log|x|)) \tag{4.171}$$

$$f_r(E) = \frac{1}{\sqrt{2\pi^{3/2}\Delta}}e^{\frac{-(E-E_0)^2}{2\Delta^2}}\left[\frac{1-e^{-2\pi E_0}}{1+e^{-2\pi E}}\right]^{1/2}\frac{e^{-\pi E}}{e^{\pi E_0}}e^{i(\phi-\phi_0)} \tag{4.172}$$

Substituting

$$e^{i\phi} = e^{\pi E/2}\frac{(1+e^{-2\pi E})^{1/2}}{(2\pi)^{1/2}}\Gamma(\frac{1}{2} - iE), \tag{4.173}$$

$$\mathcal{F}_r = \int dE f_r e^{-i(E-E_0)(t-log|x|)} = \int dE \frac{e^{-(E-E_0)^2}/(2\Delta^2)}{\sqrt{2\pi^{3/2}\Delta}} e^{-\pi(E-E_0)/2} \frac{\Gamma(\frac{1}{2}-iE)}{\Gamma(\frac{1}{2}-iE_0)} e^{-i(E-E_0)(t-log|x|)} \tag{4.174}$$

Now, using standard methods of scattering theory we can extend the above integral into complex plane. We see from above that the Gamma function within the integral has a pole in the lower half energy plane. To access the lower half plane, we consider the times $t > log|x|$. The poles of the Gamma function $\Gamma(x)$ are at $x = -n; n = 0, 1, 2$. There for the poles of $\Gamma(1/2 - iE)$ are given by:

$$E_n = -i(n + \frac{1}{2}) \tag{4.175}$$

The corresponding residue of the integral for reflection amplitude is then given by:

$$\text{Res}[\mathcal{F}_r; E = -i(n+1/2)] = \frac{e^{-(-i(n+\frac{1}{2})-E_0)^2}/(2\Delta^2)}{\sqrt{2\pi^{3/2}\Delta}} e^{-\pi(-i(n+\frac{1}{2})-E_0)/2} \frac{(-1)^n}{\Gamma(\frac{1}{2}-iE_0)n!} e^{-i(-i(n+\frac{1}{2})-E_0)(t-log|x|)} \tag{4.176}$$

Lets pay close attention to the dependence on time and space in the above expression:

$$\Psi_r \sim e^{-t/2} e^{log|\sqrt{2}x|} \tag{4.177}$$

This indicates that the reflected wave decays exponentially in time and has finite amplitude at large x. This is shown in Fig. 4.7. A Gaussian wavepacket is incident on the barrier in (b) and the reflected packet is seen to escape to infinity in (c). At a later time the amplitude can be seen to be exponential suppressed (as seen in (c))and has finite amplitude at large distances form the center. These are characteristic of the quasinormal modes occurring in the context of black holes. While we study resonances here as arising from the poles of the S-matrix a wave-packet scattering, they can be equivalently cast as states in a Rigged Hilbert space having complex eigen-energies [242, 243, 240, 241, 245] arising in an open system with purely outgoing boundary conditions. It is these boundary conditions that allow for seemingly nonunitary decay. Such QNM decay arises in any system having a potential landscape characterized by a local maxima, such as in Gamow's theory of radioactivity[28]. Thus, this analysis predicts the existence of black hole-type QNMs in our quantum Hall setting.

4.12 Experimental signatures

The existence of the quasinormal decay has not be explored in the context of the quantum Hall systems. A direct measure of QNM decay would require a time-resolved non-equilibrium setting. In the black hole situation, the LIGO breakthrough recorded ringdown signals in cataclysmic black hole mergers, ushering in the era of multi-messenger astronomy. For a Schwarzschild black hole of one solar mass, the calculated decay time is 0.35ms [234]; the decay time in the remarkable first measurement by LIGO from binary black hole merger was 4 milliseconds [235].

We now propose a setup in the quantum Hall situation for observing QNMs and derive analogous estimates. A pinched point contact geometry creates a saddle potential in the bulk of the quantum Hall system. Sources of bulk or edge state quasiholes undergo saddle potential scattering and tunneling as described in the previous section. An indirect measure of QNM poles in the scattering matrix would be a Lorentzian form for the associated tunneling conductance, known as the Breit-Wigner distribution:

$$G(E) = \frac{(1/\tau)^2}{(E - E_0)^2 + (1/\tau)^2} \tag{4.178}$$

, where τ is the QNM decay rate and E_0 is the real part of the resonant pole due to a confining potential. Observing such features would allows to detect QNM behaviour. This has been done in certain point contact experiments[246].

A direct measure would require a dilute beam of incoming quasiholes [247] that could enable time resolving QNMs in the out-going beam. Considering a point contact of width d, for applied voltage V and a background magnetic field B, we have that $\tau = d^2B/2V$, and $\lambda = eV/d^2$. Putting in typical numbers for a split-gate graphene junction [248], we find that $\tau \sim 400ps$, while $\hbar_{eff}\lambda \sim 125mK \ll \hbar\omega_c$, and $\ell_B \sim 5nm$. We anticipate then that the ringdown associated with quasihole wavepackets should be observable at a distance of order $100nm$ from the point contact at times on the order of nanoseconds. Finally, we note that realistic scattering potentials would have finite range, unlike the unbounded IHO; the Pöschl-Teller potential yields a tractable candidate for such analyses [249, 191]. We suggest that the actual recorded temporal decay in a given measurement would serve to recreate the underlying potential.

4.13 Summary and outlook

In this chapter, we have considered two fundamental phenomena of physics- black holes on the astronomical scale and quantum Hall effect on the mesoscopic scale. We have seen that the black hole thermality and

quasinormal decay can be captured in terms of their essential structures in the quantum Hall effect. Black holes are characterised by existence of an event horizon and bifurcates the spacetime based on the accessibility of information. This leads to non-trivial effects when quantum mechanical degrees of freedom are considered in the full spacetime. The region outside the black hole does not have access to the region inside the event horizon. This 'restriction' of the quantum mechanical states to outside the horizon leads to the vaccum in the full spacetime emerging as a thermal state for the region outside. This phenomena can be captured in a much simpler setting of the Unruh effect where one starts with a Minkowski flat spacetime. The Minkowski vacuum restricted to a Rindler wedge is then the thermal state. This can be derived from minimal considerations of the spacetime-structure, symmetry transfromations on the spacetime and the action of these symmetry generators on the quantum mechanical states. The key element in the derivation is that the generator of RIndler time translation/ the Rindler Hamiltonian is the boost. The Euclidean time evolution then results in a thermal density matrix.

One can capture these essential structures in the context of a quantum Hall system with an applied saddle potential. Restricting to the lowest Landau level, the allowed Hamiltonians are restricted to the generators of $\mathfrak{sl}(2,\mathbb{R})$ algebra. Making use of the isomorphism with the Lorentz group $\mathfrak{sl}(2,\mathbb{R}) \sim \mathfrak{so}(2,1)$, one can identify the action of shear generator or the saddle potential on the LLL states to be similar to the the action of boosts. The shear generator/ saddle potential when restricted to the LLL takes the form of the inverted harmonic oscillator. The IHO is a prototypical scattering problem and provides a more physically intuitive analogy with the black hole situation. The setting of the IHO scattering problem allows for purely incoming and outgoing states on both sides of the barrier thus leading to a doubling in the quantum mechanical states. Accessing the tunneling or reflected state on only side can be thought of as integrating the states on the other side. This gives a natural interpretation of the thermal form of the tunneling probability. In the quantum Hall system, the tunneling probability manifests directly in terms of conductance and can be directly measured. The symmetry parallels between quantum Hall potentials and the relativistic generators also allows one to explore Lorentz Kinematics in the LLL.

One of the immediate manifestations of open boundary conditions in a scattering problem is the existence of quasinormal decay. These are the purely outgoing or incoming states with a characteristic and quantised decay times. These are similar to the quasinormal modes one gets from the effective potential scattering in the context of black holes. The time decaying behaviour and finite amplitude at spatial infinity are characteristics of these states. These states can be obtained as eigenfunctions with the imaginary eigenvlalues of the Hamiltonian. The states no longer belong to the regular Hilbert space but to a Rigged Hilbert space. These are not to be seen as exotic and unusual characteristics of the system. The resonant states are as

fundamental as the usual real energy eigenstates. They are a consequence of opening up the boundary conditions in a scattering problem and this leads to emergence of features that are usually not explored in the bound or closed quantum systems. The quasinormal decay manifests in the quantum Hall systems as Breit-Wigner distribution in the conductance. One can also directly access them through time-resolved measurements. The existence of these resonant modes have close connects to quantum chaos and thermality in open quantum systems.

The formal aspects of the derivation of the Hawking-Unruh effect in the relativistic setting involve the Bisognano-Wichmann theorem, which is further based on Tomita-Takesaki theory of operator algebras. These formalisms are of fundamental importance in quantum field theory [201], quantum statistical mechanics[211] and more recently in quantum gravity[206, 207, 209]. Our derivation of Hawking-Unruh type effect in the quantum Hall system has tried to access some elements in those frameworks. It would be very useful to transfer more insights from those to quantum Hall physics and could lead to a better understanding of quantum Hall physics and thermality in general. The parallels we have drawn in the context of LLL have much broader scope. The LLL structure is manifest not only in quantum Hall effect but in various other settings such as skyrmionic systems, rotating BECs and metamaterials. Further, broadly much of what we have said is applicable to the framework of phase space quantum dynamics that involves canonical transformations, coherent states and Wigner functions. It would certainly be interesting to explore the concepts of quasinormal decay and thermality in that setting.

One of the key problems both in the context of Hawking-Unruh and quantum Hall is the interpretation of thermality. The current paradigm seeks description of thermality in terms a statistical mechanics of some discrete quantum mechanical degrees of freedom. One of the key requirements is the extensive scaling of the thermodynamic quantitites with the bulk of the system assuming that the statistical degrees of freedom lie with in the bulk. The entire frame work of Hawking-Unruh effect and the thermality appearing in that context seem strange from that point of view. One of the key challenges would be to understand this issue. But given that the parallels in quantum Hall effect are much easier to access experimentally, it would hopefully provide some window to breakdown these issues into problems tractable through measurements.

Chapter 5

A primer on inverted harmonic oscillator and scattering theory

The IHO model exhibits potential scattering features that have made the model invaluable in a broad variety of contexts since the birth of quantum mechanics [25, 250, 26, 27]. From its infancy, phenomena such as particle decay [28] and metastability [29] have been analyzed using the IHO. In developments across the decades, the IHO has played key roles in the context of chaos theory[30, 31, 32], decoherence [33, 34, 35] and quantum optics [36] . In modern high energy physics and cosmology, it has provided a basis for understanding 2D string theory, tachyon decay[37, 38, 39, 40] and even inflation in the early universe[41]. There have been many works that have studied in depth, the physics of inverted Harmonic oscillator[242, 243, 26, 27]. Here we will present the salient aspects of the model such as the PCT symmetries, the energy spectrum, existence of time decay states, importance of boundary conditions etc, highlighting the features that are usually overlooked in the bound-state quantum mechanics presented in the textbooks.

5.1 Canonical transformations and different representations

The Hamiltonian for the inverted Harmonic oscillator in the position basis is given :

$$H = \frac{1}{2}(P^2 - X^2) \tag{5.1}$$

Here P and X are the usual momentum and position operators. In the position space basis, one gets a Schrodinger equation

$$H = \frac{1}{2}\Big(- \frac{\partial^2}{\partial x^2} - x^2 \Big) \tag{5.2}$$

This is a Schrodinger equation for scattering off a parabolic potential barrier. Much like the harmonic oscillator being the prototype for the bound state quantum mechanics, the IHO is a prototype for scattering off smooth potentials.

One can make a canonical transformation from the position basis to the''light-cone' basis $u^{\pm}$:

$$u^{\pm} = \frac{p \pm x}{\sqrt{2}} \tag{5.3}$$

The canonical commutation relation is still preserved in this basis: $[\hat{u}^{+}, \hat{u}^{-}] = i$. In this basis the Hamiltonian is written as

$$H = \frac{1}{2}(u^{+}u^{-} + u^{-}u^{+}) = - \pm i\left(u^{\pm}\partial_{u^{\pm}} + \frac{1}{2}\right) \tag{5.4}$$

The states in this basis correspond to the incoming and outgoing states on the two sides of the barrier denoted by $\pm$. The Hamiltonian in this form is also called the 'dilatation generator' which generates scaling on the functions it acts on. Expansion in its eigenbasis is called the Mellin transform, as we will see in a following section. This form is also known as the 'Berry-Keating' Hamiltonian studied in relation to quantum chaos.

Another representation of the IHO is in the form of 'Squeezing operator' which is well studied in quantum optics. This representation is in terms of the operators $a, a^{\dagger}$ $u^{+} = (a + a^{\dagger})/\sqrt{2}$ and $u^{-} = (a - a^{\dagger})/\sqrt{2}$. The Hamiltonian is then given by

$$H = \frac{1}{2i}((a^{\dagger})^2 - a^2) \tag{5.5}$$

5.2 Properties of the Hamiltonian

Self-adjoint in the Hilbert space – The self-adjoint property of the Hamiltonian is a necessary condition for the unitary evolution in quantum mechanics. Typically in finite dimensional cases, self-adjoint property ensures Hermitian or symmetric property on operators. One needs to be careful in infinite dimensional cases and for unbounded operators. The momentum operator in the position representation is the simplest example where one is not guaranteed Hermitian property from the self-adjoint property. Here we will prove the self-adjoint property of the IHO. In most of the following discussions, we will be using the 'light-cone' basis : $H = i(u\partial_u + \frac{1}{2})$, dropping the $\pm$ label for now. Let us define the operator:

$$U = e^{-iHt} = e^{t/2}e^{tx\partial_x} \tag{5.6}$$

U acts on functions belonging to the Hilbert space $\psi \in L^2(\mathbb{R})$:

$$U\psi(x) = e^{t/2}\psi(e^t x) \tag{5.7}$$

One can show that for $\psi, \phi \in L^(\mathbb{R})$:

$$\langle U\psi| \, |U\phi\rangle = \int_{-\infty}^{\infty} U\bar{\psi}(x)U\phi(x) = \int_{-\infty}^{\infty} e^t\psi(\bar{e^t}x)\phi(e^t x) = \int_{-\infty}^{\infty} \psi(\bar{y})\phi(y)dy = \langle\psi| \, \phi\rangle \tag{5.8}$$

This ensures unitarity of H and by Stone-von Neumann theorem, H is self-adjoint in $L^2(R)$

PCT symmetries: Defining the parity operator as : $PxP^{-1} = -x$ and $PpP^{-1} = -p$, one can see that the Hamiltonian is P-symmetric.

$$PHP^{-1} = H \tag{5.9}$$

The IHO has interesting time-reversal properties for a simple quantum mechanical Hamiltonian. As shown by Wigner, the T operator can be realised either as a Unitary or an anti-unitary operator. In the case of bound Hamiltonian, one chooses T to be anti-unitary, to exclude negative energy eigenvalues. IHO is an unbounded operator and with a unitary T satisfies the relation

$$TH + HT = 0 \tag{5.10}$$

Therefore,

$$H\,|\psi_E\rangle = E\,|\psi_E\rangle\,, \quad HT\psi_E = -ET\psi_E \tag{5.11}$$

Therefore, IHO has a both negative and positive energy spectrum. Time reversal operation also acts as the Fourier transformation in this system $T\phi(x,t) = F[\phi](x,t)$:

$$F[\phi](x,t) = \frac{1}{\sqrt{2\pi}} \int e^{ikx}\phi(k,t)dk \tag{5.12}$$

PCT invariance– We have a simple complex conjugation operator C defined in the simple quantum mechanical setting: $c\psi = \bar{\psi}$. The IHO Hamiltonian is both CT and PCT invariant [242]:

$$[H, CT] = [H, PCT] = 0 \tag{5.13}$$

There fore if $H\psi_E = E\psi_E$, then $HF[\bar{\psi_E}] = EF[\psi_E]$

5.3 Energy Spectrum

The PCT properties of the IHO allow for some interesting properties in the spectrum of the Hamiltonian. As the Hamiltonian is unbounded, the spectrum of real energy eigen values is continuous and ranges from

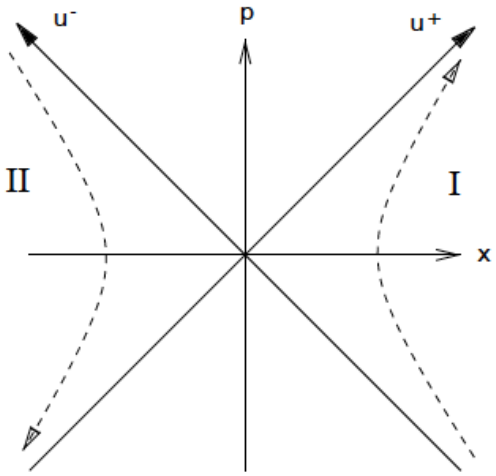

Figure 5.1: Phase space showing different co-ordinates and semi-classical trajectories of the IHO. $u^{\pm}$ indicate the 'light-cone' basis obtained through a canonical transformation from the (X, P) basis. The state in the $u^{\pm}$ basis are purely incoming and outgoing states. I and II represent the two sides of the IHO. The dotted curves are the hyperbolic trajectories of constant energy.

$-\infty$ to ∞. The parity invariance leads to a doubly degenerate spectrum. This is associated with the states on the two sides of the barrier.

We shall reintroduce the labels $u^{\pm}$.The u^{+} basis describe the ingoing states and u^{-} the outgoing states and these two basis are related by[193, 38]:

$$\langle u^{+}|\, u^{-}\rangle = \frac{1}{\sqrt{2\pi}} e^{iu^{+}u^{-}} \tag{5.14}$$

In this basis the Hamiltonian can be written as

$$H = \frac{1}{2}(u^{+}u^{-} + u^{-}u^{+}) = - \pm i\left(u^{\pm}\partial_{u^{\pm}} + \frac{1}{2}\right) \tag{5.15}$$

The time-dependent Schrodinger equation are of the form

$$i\partial_t \psi_{\pm}(u^{\pm}, t) = \mp i(u^{\pm}\partial_{u^{pm}} + 1/2)\psi_{\pm}(u^{\pm}, t) \tag{5.16}$$

As shown in the Fig. 5.1, there are two sets of energy eigenstates corresponding to regions I and II. The state $|E, \pm\rangle$ correspond to the states in the two regions respectively. These are written in the in-going and

out-going bases. In terms of in-going bases,

$$\langle u^+|\, E,+\rangle_{in} = \frac{1}{\sqrt{2\pi}}(u^+)^{iE-1/2}\Theta(u^+) \tag{5.17}$$

$$\langle u^+|\, E,-\rangle_{in} = \frac{1}{\sqrt{2\pi}}(-u^+)^{iE-1/2}\Theta(-u^+) \tag{5.18}$$

where $\Theta(u^+)$ is the Theta-step function. Writing in terms of outgoing bases:

$$\langle u^-|\, E,+\rangle_{out} = \frac{1}{\sqrt{2\pi}}(u^-)^{-iE-1/2}\Theta(u^-) \tag{5.19}$$

$$\langle u^-|\, E,+\rangle_{out} = \frac{1}{\sqrt{2\pi}}(-u^-)^{-iE-1/2}\Theta(-u^-) \tag{5.20}$$

These states correspond to the 'steady state' scattering states. The IHO also allows for complex eigenvalues and these are related to the resonant / quasinormal decay states, which we shall study soon.

5.4 S-matrix of IHO : Mellin Transform

Now that we have the eigensolutions, we can calculated the scattering matrix for the IHO. In a typical text book quantum mechanics scattering problem, one considers plane waves to scatter against a barrier. These plane waves are eigenmodes of the momentum operator. The spatial bounded natures of the scattering potential allows one to consider plane wave states at infinity. Any other state is expanded in the basis of plane waves resulting in a Fourier transfrom. Mellin transform, which is a multiplicative version of Fourier transform becomes important when dealing with dilatation operator form of IHO which generates scaling. Lets define Mellin transform as

$$\tilde{F}(\epsilon) = \int_0^\infty f(u)u^{i\epsilon-1}du \tag{5.21}$$

and the inverse is given by:

$$f(u) = \frac{1}{2\pi}\int_{-\infty}^{\infty} |u|^{i\epsilon}\tilde{F}(\epsilon)d\epsilon \tag{5.22}$$

From the above it can be seen that Mellin transform is an expansion in the basis of eigenfunctions of the IHO. Now we shall make use of this in the derivation of the S-matrix for the IHO . Mellin transform has been shown to useful in the context of AdS-CFT too [251, 252, 253] and in general scattering theory.

The mode expansion for a superposition of incoming states is given by

$$\hat{\psi}_{in}(u^+) = \frac{1}{\sqrt{2\pi}} \int_{-\infty}^{\infty} dE[(u^+)^{iE-1/2} \hat{a}_E^{in,+} + (-u^+)^{iE-1/2} \hat{a}_E^{in,-}] \tag{5.23}$$

The mode expansion for the outgoing state is given by

$$\hat{\psi}_{out}(u^-) = \frac{1}{\sqrt{2\pi}} \int_{-\infty}^{\infty} dE[(u^-)^{-iE-1/2} \hat{b}_E^{out,+} + (-u^-)^{-iE-1/2} \hat{b}_E^{out,-}] \tag{5.24}$$

The above $\hat{a}_E, \hat{b}_E$ operators act on the vacua $|0, in\rangle, |0, out\rangle$ respectively.

The S-matrix relates the out and in states as follows

$$\begin{pmatrix} |E,+\rangle_{out} \\ |E,-\rangle_{out} \end{pmatrix} = \hat{\mathcal{S}} \begin{pmatrix} |E,+\rangle_{in} \\ |E,-\rangle_{in} \end{pmatrix} \tag{5.25}$$

For the above-defined in and out states are then related by

$$\hat{\psi}_{out}(u^-) = [\hat{\mathcal{S}}](u^-) = \int_{-\infty}^{+\infty} \frac{du^+}{\sqrt{2\pi}} e^{-iu^+u^-} \hat{\psi}_{in}(u^+) \tag{5.26}$$

For simplifying the above we shall make use of the Mellin transforms

$$\int_{-\infty}^{\infty} du^+ e^{iu^+u^-} |u^+|^{-iE-1/2} = e^{i\pi/4} e^{E\pi/2} |u^-|^{iE-1/2} \Gamma(\frac{1}{2} - iE) \tag{5.27}$$

$$\int_{-\infty}^{\infty} du^+ e^{-iu^+u^-} |u^+|^{-iE-1/2} = e^{-i\pi/4} e^{-E\pi/2} |u^-|^{iE-1/2} \Gamma(\frac{1}{2} - iE) \tag{5.28}$$

The S-matrix is given by

$$\begin{pmatrix} \hat{b}_E^{out,+} \\ \hat{b}_E^{out,-} \end{pmatrix} = \hat{\mathcal{S}} \begin{pmatrix} \hat{a}_E^{in,+} \\ \hat{a}_E^{in,-} \end{pmatrix} \tag{5.29}$$

$$\hat{\mathcal{S}} = \frac{1}{\sqrt{2\pi}} \Gamma\left(\frac{1}{2} + iE\right) \begin{pmatrix} e^{i\pi/4} e^{-\pi E/2} & e^{-i\pi/4} e^{-\pi E/2} \\ e^{i\pi/4} e^{-\pi E/2} & e^{-i\pi/4} e^{\pi E/2} \end{pmatrix} \tag{5.30}$$

5.5 Scattering states in x-basis: Parabolic cylinder functions

The solutions of IHO Hamiltonian in x- basis are known to be parabolic cylinder functions. We can obtain them easily from the solutions in $u^{\pm}$ basis.

$$\langle x\,|E,+\rangle = \int du^{+} \langle x\,|u^{+}\rangle\,\langle u^{+}\,|E,+\rangle \tag{5.31}$$

The canonical transformation from $\{X,P\}$ to $\{u^{+},u^{-}\}$ operators has a corresponding representation given by [38, 242, 243]

$$\langle x\,|u+\rangle = \exp[i(\frac{x^2}{2} - 2u^{+}x + u^{+^2})] \tag{5.32}$$

Therefore, there transformation now reads

$$\langle x\,|E,+\rangle = \int_0^{\infty} du^{+}\exp[i(\frac{x^2}{2} - 2u^{+}x + u^{+^2})]u^{+^{iE-1/2}} \tag{5.33}$$

Using the integral representation of the parabolic cylinder function,

$$D_{-iE-1/2}(x) = \frac{e^{\frac{-x^2}{4}}}{\Gamma(\frac{1}{2}+iE)}\int_0^{\infty} dt|t|^{iE-\frac{1}{2}}\exp(\frac{-t^2}{2} - xt) \tag{5.34}$$

$$\langle x\,|E,+\rangle = N_0 e^{\pi\frac{E}{4}}\Gamma(\frac{1}{2}+iE)D_{-iE-\frac{1}{2}}(x) \tag{5.35}$$

5.6 Analytic S matrix: Gamma function

From the above derivations one can see that the IHO S-matrix and the energy eigenstates $\langle x\,|E,+\rangle$ have the Gamma functions $\Gamma(iE+\frac{1}{2})$. The analytic properties of the Gamma function in the complex energy plane determine the analytic properties of the S-matrix and the wavefunctions. one cannot extract all the crucial properties of the Hamitlonian especially in scattering theory from the real energy eigen states alone. The resonant modes that determine the quasinomal decay are also fundamental characteristics of the system and these are uncovered by the analytic properties in the complex energy plane.

The gamma function $\Gamma(z)$ has simple poles at $z=-n$, where $n=0,1,2....$ Therefore the poles of the IHO scattering problem lie at the imaginary values of :

$$\tilde{E}_n = i\left(n+\frac{1}{2}\right) \tag{5.36}$$

These are the resonant poles of the problem and can be interpreted as complex energy eigenvalues. But the states corresponding to the complex energy eigenvalues do not belong to the Hilbert space $L^2(\mathbb{R})$. These states also decay in time are known as quasinormal modes.

5.7 Resonant modes and quasinormal decay : Operator method

To obtain the wavefunctions and the time behaviour of the resonant modes of IHO, lets introduce ladder operators in the 'lightcone basis' [254]

$$b^{\pm} = (x \pm p)/\sqrt{2} = \frac{1}{\sqrt{2}}\left(x \mp i\frac{d}{dx}\right) \tag{5.37}$$

These operators obey the commutation relations $[b^+, b^-] = -i, [b\pm, b^{\pm}] = 0$. Defining $N = \{b^+, b^-\}/2 = (b^+b^- + n^-b^+)/2$, the Hamiltonian is given by $H = -N$. This leads to relation between ladder operators and the Hamiltonian, similar to that in the Harmonic oscillator:

$$[H, b^{\pm}] = \mp i b^{\mp} \tag{5.38}$$

Now, with this machinery one can construct the resonant states of the IHO. Lets assume that there are set of states satisfying the condition:

$$b^{\mp}u_0^{\pm} = \left(\frac{d}{dx} \mp ix\right)u_0^{\pm} = 0 \tag{5.39}$$

The solutions of this equation are given by

$$u_0^{\pm} = B_0^{\pm}e^{\pm ix^2/2} \tag{5.40}$$

These solutions do not belong to the regular Hilbert space and belong to the 'Rigged Hilbert space'. Now one can verify that

$$Hu_0^{\pm} = \mp\frac{i}{2}u_0^{\pm} \tag{5.41}$$

Therefore, thes states can be interpreted as the complex energy eigenstates with eigenvalues $\mp i/2$. One can construct a series of states starting form this with the ladder operators: $(b^{\pm})^n u_0^{\pm}$. The nth states obey the relation:

$$Hu_n^{\pm} = E_n^{\pm}u_n^{\pm} \tag{5.42}$$

Observing that

$$\left[\frac{1}{\sqrt{2}}\left(\mp i\frac{d}{dx}+x\right)\right]^n u_0^{\pm}(x) = B_0^{\pm}\left(\frac{\pm i}{\sqrt{2}}\right)^n e^{\pm ix/2} e^{\mp ix^2}\frac{d^n}{dx^n}e^{\pm ix^2} \tag{5.43}$$

Thus one obtains:

$$u_n^{\pm}(x) = B_n^{\pm} e^{\pm ix^2/2} H_n \pm (x) \tag{5.44}$$

where $H_n^{\pm}(x) = (\mp)^n e^{\mp ix^2}\frac{d^n}{dx^n}e^{\pm ix^2}$.

5.8 Outgoing/Incoming states: Time-decay and probability current flux

Now we can study the behaviour of these resonant states which are starkly different than the stationary states with real eigenvalues. The wavefunction of these states are now given by

$$\psi_n^{\pm}(t,x) = A_n^{\pm} B_n^{\pm} e^{\mp(n+1/2)t} e^{\pm ix^2} H_n^{\pm}(x) \tag{5.45}$$

The immediate observation is that these states decay in time. To understand the full picture of this behaviour we calculate the probability densities and the currents. The probability densities are given by

$$\rho_n^{\pm}(t,x) = |A_n^{\pm}|^2 |B_n^{\pm}|^2 e^{\mp(2n+1)t} H_n^{\mp}(x) H_n^{\pm}(x) \tag{5.46}$$

and the currents are given by

$$j_n^{\pm}(t,x) = \pm|A_n^{\pm}|^2|B_n^{\pm}|^2 e^{\mp(2n+1)t}(xH_n^{\mp}(x)H_n^{\pm}(x) \pm 2n\mathrm{Im}[H_n^{\mp}(x)H_(n-1)^{\pm}(x)]) \tag{5.47}$$

These satisfy the continuity equation:

$$\frac{\partial}{\partial t}\rho_n^{\pm}(t,x) + \frac{\partial}{\partial x} j_n^{\pm}(t,x) = 0 \tag{5.48}$$

Finally the asymptotic behaviour of the currents is given by

$$j_n^{\pm}(t,x) \approx \pm e^{\mp(2n+1)t} x^{2n+1} \tag{5.49}$$

Thus from the above we see that the probability density decays in time and but the current conservation ensures that this decay manifests as a finite current that goes out to infinity(thus the finite value at infinity).

Therefore, the resonant modes correspond to purely incoming states or purely outgoing states in one direction(left or right). Therefore, they need to have finite amplitude at infinity thus not belonging to the regular Hilbert space. One needs to enlarge the Hilbert space to so called 'Rigged Hilbert space' [241]. The purely outgoing behaviour is intricately related to the time decay of the wavefunctions and probabilities. Thus, with the model as simple as the IHO one can see that in a scattering problem, opening up the boundary conditions lead to time decay behaviour . Such behaviour is captured in the resonant pole structure of the problem and can be interpreted as the complex energy eigen values. From the above expression one can also see that the 'decay rates' of the wavefunctions are quantized as $(n+1/2)$, much like the bound state energies of the simple Harmonic oscillator. This minimum value of decay rate is the 'zero-point' factor of $1/2$ which is coming purely from quantum fluctuations associated with the commutation relation $[X, P] = i$.

5.9 Lessons from scattering

Studying the IHO problem or a scattering problem in general, makes one get exposed to many aspects of quantum mechanics typically overlooked or seen as unconventional from the perspective of restricting to studying quantum mechanics of bound or closed systems. But scattering problems are as ubiquitous and as important as the bound state problems. In fact most of our important measurement schemes in experiments heavily use scattering , be it crystallography, tunneling spectroscopy or conductance measurements. To get a bigger picture, a comparison is given in the table 5.1 between the features of harmonic oscillator and inverted harmonic oscillator. One can see that every fundamental aspect of quantum mechanics such as the state, evolution and boundary conditions, manifest in a unique way in the two prototypical problems and give rise to the fundamental quantum mechanical characteristics such as the existence of a vacuum state in the case of a harmonic oscillator or a bound on the decay rate in the IHO[1].

[1]It is humbling and a satisfying thing to conclude my PhD thesis on something as basic as the tenets of quantum mechanics and something as simple as the inverted harmonic oscillator.

Prototype	Harmonic oscillator $H = \frac{P^2}{2m} + \frac{m\omega^2}{2}X^2$	Inverted oscillator $H = \frac{P^2}{2m} - \frac{m\omega^2}{2}X^2$
	Bound state QM(Closed system).	Scattering QM (Open system).
State $\|\psi\rangle$	Belongs to Hilbert space of $L^2(\mathbb{R})$ normalizable functions.	Requires rigged Hilbert space.
Boundary conditions	Wavefunctions vanish at spatial infinities.	Wavefunctions can have finite probability current at spatial infinity.
Behaviour of states in time	Eternal and stationary states.	Also allows states decaying in time.
Time evolution	Unitary evolution e^{iHt} on the Hilbert space	Unitary on the Hilbert space but also gives irreversible(semi-group) evolution on distributions(Rigged Hilbert space)
Spectrum	Discrete and real eigenvalues .	Has a continuous spectrum of real eigenvalues and a discrete spectrum of imaginary eigenvalues(Scattering resonances).
Non-commutativity of phase space$[X, P] = i\hbar$	Gives rise to zero-point/ vacuum energy $E_0 = \frac{\hbar\omega}{2}$.	Bound on the decay rate $\frac{1}{\tau} = \frac{\omega}{2}$.

Table 5.1: A comparision between the features of a simple harmonic oscillator and an inverted harmonic oscillator, highlighting how the basic tenets of quantum mechanics manifest differently in the two protypical models

References

[1] R. M. Lutchyn, E. P. A. M. Bakkers, L. P. Kouwenhoven, P. Krogstrup, C. M. Marcus, and Y. Oreg. Majorana zero modes in superconductor-semiconductor heterostructures. *Nature Reviews Materials*, 3(5):52–68, May 2018.

[2] G Kells, D Sen, J K Slingerland, and S Vishveshwara. *Phys. Rev. B*, 89:235130, 2014.

[3] M. Stone. An analogue of Hawking radiation in the quantum Hall effect. *Classical and Quantum Gravity*, 30(8), April 2013.

[4] P. W. Anderson. More is different. *Science*, 177(4047):393–396, 1972.

[5] Jason Alicea. New directions in the pursuit of majorana fermions in solid state systems. *Reports on Progress in Physics*, 75(7):076501, 2012.

[6] M. Franz. Majorana's wires. *Nature Nanotechnology*, 8(3):149–152, 2013.

[7] Roman M. Lutchyn, Jay D. Sau, and S. Das Sarma. Majorana fermions and a topological phase transition in semiconductor-superconductor heterostructures. *Phys. Rev. Lett.*, 105:077001, Aug 2010.

[8] Yuval Oreg, Gil Refael, and Felix von Oppen. Helical liquids and majorana bound states in quantum wires. *Phys. Rev. Lett.*, 105:177002, 2010.

[9] C. Nayak, S.H. Simon, A. Stern, M. Freedman, and S. Das Sarma. Non-abelian anyons and topological quantum computation. *Reviews of Modern Physics*, 80(3):1083, 2008.

[10] S. Chandrasekhar. Clarendon Press/Oxford University Press (International Series of Monographs on Physics. Volume 69), 1983.

[11] Charles W. Misner, Kip S. Thorne, and John A. Wheeler. *Gravitation*. New York : W.H. Freeman and Company, 1973.

[12] A. Einstein. Die Feldgleichungen der Gravitation. *Sitzungsberichte der Königlich Preußischen Akademie der Wissenschaften (Berlin), Seite 844-847.*, 1915.

[13] C. V. Vishveshwara. Scattering of gravitational radiation by a schwarzschild black-hole. *Nature*, 227:936 EP, 1970.

[14] William H. Press. Long Wave Trains of Gravitational Waves from a Vibrating Black Hole. *Astrophys. J.*, 170:L105–L108, 1971.

[15] S. W. Hawking. Black hole explosions? *Nature*, 248:30 EP, 1974.

[16] K. von Klitzing, G. Dorda, and M. Pepper. *Phys. Rev. Lett.*, 45:494, 1980.

[17] D. C. Tsui, H. L. Stormer, and A. C. Gossard. *Phys. Rev. Lett.*, 48:1559, 1982.

[18] R.E. Prange and S.M. Girvin. *The Quantum Hall Effect*. Springer, 1987.

[19] C. Barceló, S. Liberati, and M. Visser. Analogue gravity. *Living Reviews in Relativity*, 8:12, December 2005.

[20] S. A. Hartnoll, A. Lucas, and S Sachdev. *Holographic quantum matter*. MIT press, 2018.

[21] F. D. M. Haldane. Geometrical description of the fractional quantum hall effect. *Phys. Rev. Lett.*, 107:116801, Sep 2011.

[22] Zhao Liu, Andrey Gromov, and Zlatko Papić. Geometric quench and nonequilibrium dynamics of fractional quantum hall states. *Phys. Rev. B*, 98:155140, Oct 2018.

[23] Matthew F. Lapa, Andrey Gromov, and Taylor L. Hughes. Geometric quench in the fractional quantum hall effect: exact solution in quantum hall matrix models and comparison with bimetric theory. 2018.

[24] Andrey Gromov and Dam Thanh Son. Bimetric theory of fractional quantum hall states. *Phys. Rev. X*, 7:041032, Nov 2017.

[25] Edwin Crawford Kemble. *The Fundamental Principles of Quantum Mechanics*. McGraw-Hill, 1937.

[26] G. Barton. Quantum mechanics of the inverted oscillator potential. *Annals of Physics*, 166(2):322, 1986.

[27] C Yuce, A Kilic, and A Coruh. Inverted oscillator. *Physica Scripta*, 74(1):114, 2006.

[28] G Gamow. Zur quantentheorie des atomkernes. *Zeitshrift fur Physik*, 51:204, 1928.

[29] Daniel Boyanovsky, Richard Holman, Da-Shin Lee, Joao P. Silva, and Anupam Singh. A Note on thermal activation. *Nucl. Phys.*, B441:595–608, 1995.

[30] M. V. Berry and J. P. Keating. *H=xp and the Riemann Zeros*. Springer US, Boston, MA, 1999.

[31] Germán Sierra and Paul K. Townsend. Landau levels and riemann zeros. *Phys. Rev. Lett.*, 101:110201, Sep 2008.

[32] R. K. Bhaduri, Avinash Khare, and J. Law. Phase of the riemann ζ function and the inverted harmonic oscillator. *Phys. Rev. E*, 52:486–491, Jul 1995.

[33] Paul A. Miller and Sarben Sarkar. Fingerprints of classical instability in open quantum dynamics. *Phys. Rev. E*, 58:4217–4225, Oct 1998.

[34] F. M. Cucchietti, D. A. R. Dalvit, J. P. Paz, and W. H. Zurek. Decoherence and the loschmidt echo. *Phys. Rev. Lett.*, 91:210403, Nov 2003.

[35] S Baskoutas and A Jannussis. Quantum tunnelling effect for the inverted caldirola-kanai hamiltonian. *Journal of Physics A: Mathematical and General*, 25(23):L1299, 1992.

[36] Silvia Gentilini, Maria Chiara Braidotti, Giulia Marcucci, Eugenio DelRe, and Claudio Conti. Physical realization of the glauber quantum oscillator. *Scientific Reports*, 5:15816, 2015.

[37] J. J. Friess and H. Verlinde. Hawking Effect in 2-D String Theory. *ArXiv High Energy Physics - Theory e-prints*, November 2004.

[38] Juan Martin Maldacena and Nathan Seiberg. Flux-vacua in two dimensional string theory. *JHEP*, 09:077, 2005.

[39] Sera Cremonini. Tachyon backgrounds in 2d string theory. *Journal of High Energy Physics*, 2005(10):014, 2005.

[40] Kareljan Schoutens, Herman Verlinde, and Erik Verlinde. Quantum black hole evaporation. *Phys. Rev. D*, 48:2670–2685, Sep 1993.

[41] Alan H. Guth and So-Young Pi. Quantum mechanics of the scalar field in the new inflationary universe. *Phys. Rev. D*, 32:1899–1920, Oct 1985.

[42] Suraj S. Hegde and Smitha Vishveshwara. Majorana wave-function oscillations, fermion parity switches, and disorder in kitaev chains. *Phys. Rev. B*, 94:115166, Sep 2016.

[43] Suraj Hegde, Vasudha Shivamoggi, Smitha Vishveshwara, and Diptiman Sen. Quench dynamics and parity blocking in majorana wires. *New Journal of Physics*, 17(5):053036, 2015.

[44] Suraj S. Hegde, Varsha Subramanyan, Barry Bradlyn, and Smitha Vishveshwara. Quasinormal Modes and Hawking-Unruh effect in Quantum Hall Systems: Lessons from Black Hole Phenomena. *arXiv e-prints*, page arXiv:1812.08803, Dec 2018.

[45] Eduardo Fradkin. *Field Theories of Condensed Matter Physics*. Cambridge University Press, 2 edition, 2013.

[46] Andreas W W Ludwig. Topological phases: classification of topological insulators and superconductors of non-interacting fermions, and beyond. *Physica Scripta*, T168:014001, dec 2015.

[47] A.Y. Kitaev. Unpaired majorana fermions in quantum wires. *Phys. Usp.*, 44:131, 2001.

[48] Paul Adrien Maurice Dirac and Ralph Howard Fowler. A theory of electrons and protons. *Proceedings of the Royal Society of London. Series A, Containing Papers of a Mathematical and Physical Character*, 126(801):360–365, 1930.

[49] B.A. Bernevig and T.L. Hughes. *Topological insulators and topological superconductors*. Princeton university Press, 2013.

[50] Shun-Qing Shen, Wen-Yu Shan, and Hai-Zhou Lu. Topological insulator and the Dirac equation. *arXiv e-prints*, page arXiv:1009.5502, Sep 2010.

[51] Oskar Vafek and Ashvin Vishwanath. Dirac Fermions in Solids: From High-T_c Cuprates and Graphene to Topological Insulators and Weyl Semimetals. *Annual Review of Condensed Matter Physics*, 5:83–112, Mar 2014.

[52] Ettore Majorana. Teoria simmetrica dellelettrone e del positrone. *Nuovo Cim.*, 14:171–184, 1937.

[53] D. A. Ivanov. Non-abelian statistics of half-quantum vortices in p-wave superconductors. *Phys. Rev. Lett.*, 86:268, 2001.

[54] E. Lieb, T. Schultz, and D. Mattis. Two soluble models of an antiferromagnetic chain. *Annals of Physics*, 16(3):407, 1961.

[55] P. Pfeuty. The one-dimensional ising model with a transverse field. *Annals of Physics*, 57(1):79, 1970.

[56] N. Read and D. Green. Paired states of fermions in two dimensions with breaking of parity and time-reversal symmetries and the fractional quantum hall effect. *Phys. Rev. B*, 61(15):10267, 2000.

[57] W. DeGottardi, D. Sen, and S. Vishveshwara. Topological phases, majorana modes and quench dynamics in a spin ladder system. *New J. Phys.*, 13:065028, 2011.

[58] W DeGottardi, M Thakurathi, S Vishveshwara, and D Sen. *Phys. Rev. B*, 88:165111, 2013.

[59] Olexei Motrunich, Kedar Damle, and David A. Huse. Griffiths effects and quantum critical points in dirty superconductors without spin-rotation invariance: One-dimensional examples. *Phys. Rev. B*, 63:224204, May 2001.

[60] Maria-Theresa Rieder, Piet W. Brouwer, and Inanc Adagideli. Reentrant topological phase transitions in a disordered spinless superconducting wire. *Phys. Rev. B*, 88:060509, Aug 2013.

[61] Y. Niu, S.B. Chung, C.-H. Hsu, I. Mandal, S. Raghu, and S. Chakravarty. Majorana zero modes in a quantum ising chain with longer-ranged interactions. *Phys. Rev. B*, 85(3):035110, 2012.

[62] Eytan Barouch and Barry McCoy. Statistical mechanics of the xy model. ii. spin-correlation functions. *Phys. Rev. A*, 3:786, Feb 1971.

[63] Josef Kurmann, Harry Thomas, and Gerhard Mller. Antiferromagnetic long-range order in the anisotropic quantum spin chain. *Physica A: Statistical Mechanics and its Applications*, 112(12):235 – 255, 1982.

[64] Salvatore M. Giampaolo, Gerardo Adesso, and Fabrizio Illuminati. Separability and ground-state factorization in quantum spin systems. *Phys. Rev. B*, 79:224434, Jun 2009.

[65] Tzu-Chieh Wei, Smitha Vishveshwara, and Paul M. Goldbart. Global geometric entanglement in transverse-field xy spin chains: Finite and infinite systems. *Quantum Info. Comput.*, 11(3):326, March 2011.

[66] L. Amico, F. Baroni, A. Fubini, D. Patanè, V. Tognetti, and Paola Verrucchi. Divergence of the entanglement range in low-dimensional quantum systems. *Phys. Rev. A*, 74:022322, Aug 2006.

[67] S. M. Giampaolo, S. Montangero, F. Dell'Anno, S. De Siena, and F. Illuminati. Universal aspects in the behavior of the entanglement spectrum in one dimension: Scaling transition at the factorization point and ordered entangled structures. *Phys. Rev. B*, 88:125142, Sep 2013.

[68] H.-J. Kwon, K. Sengupta, and V.M. Yakovenko. Fractional ac josephson effect in p- and d-wave superconductors. *The European Physical Journal B - Condensed Matter and Complex Systems*, 37(3):349–361, 2004.

[69] Liang Fu and C. L. Kane. Josephson current and noise at a superconductor/quantum-spin-hall-insulator/superconductor junction. *Phys. Rev. B*, 79:161408, Apr 2009.

[70] Gilad Ben-Shach, Arbel Haim, Ian Appelbaum, Yuval Oreg, Amir Yacoby, and Bertrand I. Halperin. Detecting majorana modes in one-dimensional wires by charge sensing. *Phys. Rev. B*, 91:045403, Jan 2015.

[71] M Thakurathi, O Deb, and D Sen. Majorana modes and transport across junctions of superconductors and normal metals. *Journal of Physics Condensed Matter*, 27:275702, 2015.

[72] Francois Crépin and Björn Trauzettel. Parity measurement in topological josephson junctions. *Phys. Rev. Lett.*, 112:077002, Feb 2014.

[73] Jay Sau and Eugene Demler. Bound states at impurities as a probe of topological superconductivity in nanowires. *Phys. Rev. B*, 88:205402, Nov 2013.

[74] C. Beenakker, J. Edge, J. Dahlhaus, D. Pikulin, Shuo Mi, and M. Wimmer. Wigner-poisson statistics of topological transitions in a josephson junction. *Phys. Rev. Lett.*, 111:037001, Jul 2013.

[75] Alex Zazunov, Pasquale Sodano, and Reinhold Egger. Evenodd parity effects in majorana junctions. *New J. Phys.*, 15(3):035033, 2013.

[76] Martin Leijnse and Karsten Flensberg. Parity qubits and poor man's majorana bound states in double quantum dots. *Phys. Rev. B*, 86:134528, Oct 2012.

[77] F Hassler, A R Akhmerov, and C W J Beenakker. The top-transmon: a hybrid superconducting qubit for parity-protected quantum computation. *New J. Phys.*, 13(9):095004, 2011.

[78] Parsa Bonderson and Roman M. Lutchyn. Topological quantum buses: Coherent quantum information transfer between topological and conventional qubits. *Phys. Rev. Lett.*, 106:130505, Mar 2011.

[79] E. Ginossar and E. Grosfeld. Microwave transitions as a signature of coherent parity mixing effects in the Majorana-transmon qubit. *Nature Communications*, 5:4772, September 2014.

[80] J. I. Väyrynen, G. Rastelli, W. Belzig, and L. I. Glazman. Microwave signatures of Majorana states in a topological Josephson junction. *ArXiv e-prints*, April 2015.

[81] Yasuhiro Hatsugai. Chern number and edge states in the integer quantum hall effect. *Phys. Rev. Lett.*, 71, 1993.

[82] P. Markos and C.M. Soukoulis. *Wave Propagation*. Princeton University Press, 2008.

[83] Lukasz Fidkowski. Entanglement spectrum of topological insulators and superconductors. *Phys. Rev. Lett.*, 104:130502, 2010.

[84] P. W. Brouwer, A. Furusaki, I. A. Gruzberg, and C. Mudry. Localization and delocalization in dirty superconducting wires. *Phys. Rev. Lett.*, 85:1064, 2000.

[85] P. W. Brouwer, A. Furusaki, and C. Mudry. Universality of delocalization in unconventional dirty superconducting wires with broken spin-rotation symmetry. *Phys. Rev. B*, 67:014530, Jan 2003.

[86] Ilya A. Gruzberg, N. Read, and Smitha Vishveshwara. Localization in disordered superconducting wires with broken spin-rotation symmetry. *Phys. Rev. B*, 71:245124, 2005.

[87] Maria-Theresa Rieder and Piet W. Brouwer. Density of states at disorder-induced phase transitions in a multichannel majorana wire. *Phys. Rev. B*, 90:205404, Nov 2014.

[88] M.-T. Rieder, G. Kells, M. Duckheim, D. Meidan, and P. W. Brouwer. Endstates in multichannel spinless p-wave superconducting wires. *Phys. Rev. B*, 86:125423, Sep 2012.

[89] Falko Pientka, Graham Kells, Alessandro Romito, Piet W. Brouwer, and Felix von Oppen. Enhanced zero-bias majorana peak in the differential tunneling conductance of disordered multisubband quantum-wire/superconductor junctions. *Phys. Rev. Lett.*, 109:227006, Nov 2012.

[90] Piet W. Brouwer, Mathias Duckheim, Alessandro Romito, and Felix von Oppen. Probability distribution of majorana end-state energies in disordered wires. *Phys. Rev. Lett.*, 107:196804, Nov 2011.

[91] P. Neven, D. Bagrets, and A. Altland. Quasiclassical theory of disordered multi-channel Majorana quantum wires. *New Journal of Physics*, 15(5), May 2013.

[92] Dmitry Bagrets and Alexander Altland. Class d spectral peak in majorana quantum wires. *Phys. Rev. Lett.*, 109:227005, 2012.

[93] Hoi-Yin Hui, Jay D. Sau, and S. Das Sarma. Generalized eilenberger theory for majorana zero-mode-carrying disordered p-wave superconductors. *Phys. Rev. B*, 90:064516, 2014.

[94] Alejandro M. Lobos, Roman M. Lutchyn, and S. Das Sarma. Interplay of disorder and interaction in majorana quantum wires. *Phys. Rev. Lett.*, 109:146403, 2012.

[95] Benjamin M. Fregoso, Alejandro M. Lobos, and S. Das Sarma. Electrical detection of topological quantum phase transitions in disordered majorana nanowires. *Phys. Rev. B*, 88:180507, 2013.

[96] Tudor D. Stanescu, Sumanta Tewari, Jay D. Sau, and S. Das Sarma. To close or not to close: The fate of the superconducting gap across the topological quantum phase transition in majorana-carrying semiconductor nanowires. *Phys. Rev. Lett.*, 109:266402, 2012.

[97] Jay D. Sau and S. Das Sarma. Density of states of disordered topological superconductor-semiconductor hybrid nanowires. *Phys. Rev. B*, 88:064506, 2013.

[98] C. W. J. Beenakker. Random-matrix theory of majorana fermions and topological superconductors. *Rev. Mod. Phys.*, 87:1037, 2015.

[99] D. I. Pikulin, J. P. Dahlhaus, M. Wimmer, H. Schomerus, and C. W. J. Beenakker. A zero-voltage conductance peak from weak antilocalization in a Majorana nanowire. *New Journal of Physics*, 14(12), December 2012.

[100] I. C. Fulga, F. Hassler, A. R. Akhmerov, and C. W. J. Beenakker. Scattering formula for the topological quantum number of a disordered multimode wire. *Phys. Rev. B*, 83:155429, 2011.

[101] A. R. Akhmerov, J. P. Dahlhaus, F. Hassler, M. Wimmer, and C. W. J. Beenakker. Quantized conductance at the majorana phase transition in a disordered superconducting wire. *Phys. Rev. Lett.*, 106:057001, 2011.

[102] Wade DeGottardi, Diptiman Sen, and Smitha Vishveshwara. Majorana fermions in superconducting 1d systems having periodic, quasiperiodic, and disordered potentials. *Phys. Rev. Lett.*, 110:146404, 2013.

[103] Alexander Altland, Dmitry Bagrets, Lars Fritz, Alex Kamenev, and Hanno Schmiedt. Quantum criticality of quasi-one-dimensional topological anderson insulators. *Phys. Rev. Lett.*, 112, May 2014.

[104] E. Abrahams, P. W. Anderson, D. C. Licciardello, and T. V. Ramakrishnan. Scaling theory of localization: Absence of quantum diffusion in two dimensions. *Phys. Rev. Lett.*, 42:673–676, Mar 1979.

[105] D J Thouless. A relation between the density of states and range of localization for one dimensional random systems. *Journal of Physics C: Solid State Physics*, 5(1):77, 1972.

[106] Alexander D. Mirlin. Statistics of energy levels and eigenfunctions in disordered systems. *Physics Reports*, 326(56):259, 2000.

[107] D. A. Ivanov, M. A. Skvortsov, P. M. Ostrovsky, and Ya. V. Fominov. Hybridization of wave functions in one-dimensional localization. *Phys. Rev. B*, 85:035109, Jan 2012.

[108] Daniel S. Fisher. Critical behavior of random transverse-field ising spin chains. *Phys. Rev. B*, 51:6411–6461, Mar 1995.

[109] Leon Balents and Matthew P. A. Fisher. Delocalization transition via supersymmetry in one dimension. *Phys. Rev. B*, 56:12970–12991, Nov 1997.

[110] J. E. Bunder and Ross H. McKenzie. Effect of disorder on quantum phase transitions in anisotropic $\boldsymbol{XY}$ spin chains in a transverse field. *Phys. Rev. B*, 60:344, 1999.

[111] D J Thouless. Localization distance and mean free path in one-dimensional disordered systems. *Journal of Physics C: Solid State Physics*, 6(3):L49, 1973.

[112] Alexander Altland and Martin R. Zirnbauer. Nonstandard symmetry classes in mesoscopic normal-superconducting hybrid structures. *Phys. Rev. B*, 55:1142–1161, Jan 1997.

[113] Martin Leijnse and Karsten Flensberg. Introduction to topological superconductivity and majorana fermions. *Semiconductor Science and Technology*, 27(12):124003, 2012.

[114] A. Cook and M. Franz. Majorana fermions in a topological-insulator nanowire proximity-coupled to an s-wave superconductor. *Phys. Rev. B*, 84:201105, Nov 2011.

[115] Liang Fu and C. L. Kane. Superconducting proximity effect and majorana fermions at the surface of a topological insulator. *Phys. Rev. Lett.*, 100:096407, 2008.

[116] Andrew C. Potter and Liang Fu. Anomalous supercurrent from Majorana states in topological insulator Josephson junctions. *Physical Review B*, 88(12):121109, Sep 2013.

[117] V. Mourik, K. Zuo, S.M. Frolov, S.R. Plissard, E.P.A.M. Bakkers, and L.P. Kouwenhoven. Signatures of majorana fermions in hybrid superconductor-semiconductor nanowire devices. *Science*, 336(6084):1003, 2012.

[118] A. Das, Y. Ronen, Y. Most, Y. Oreg, M. Heiblum, and H. Shtrikman. Zero-bias peaks and splitting in an al-inas nanowire topological superconductor as a signature of majorana fermions. *Nature Physics*, 8(12):887, 2012.

[119] M.T. Deng, C.L. Yu, G.Y. Huang, M. Larsson, P. Caroff, and H.Q. Xu. Anomalous zero-bias conductance peak in a nb-insb nanowire-nb hybrid device. *Nano Letters*, 12(12):6414, 2012.

[120] A.D.K. Finck, D.J. Van Harlingen, P.K. Mohseni, K. Jung, and X. Li. Anomalous modulation of a zero-bias peak in a hybrid nanowire- superconductor device. *Physical Review Letters*, 110(12):126406, 2013.

[121] Önder Gül, Hao Zhang, Jouri D. S. Bommer, Michiel W. A. de Moor, Diana Car, Sébastien R. Plissard, Erik P. A. M. Bakkers, Attila Geresdi, Kenji Watanabe, Takashi Taniguchi, and Leo P. Kouwenhoven. Ballistic Majorana nanowire devices. *arXiv e-prints*, page arXiv:1603.04069, Mar 2016.

[122] Jun Chen, Peng Yu, John Stenger, Moïra Hocevar, Diana Car, Sébastien R. Plissard, Erik P. A. M. Bakkers, Tudor D. Stanescu, and Sergey M. Frolov. Experimental Phase Diagram of a One-Dimensional Topological Superconductor. *arXiv e-prints*, page arXiv:1610.04555, Oct 2016.

[123] Fabrizio Nichele, Asbjørn C. C. Drachmann, Alexander M. Whiticar, Eoin C. T. O'Farrell, Henri J. Suominen, Antonio Fornieri, Tian Wang, Geoffrey C. Gardner, Candice Thomas, Anthony T. Hatke, Peter Krogstrup, Michael J. Manfra, Karsten Flensberg, and Charles M. Marcus. Scaling of majorana zero-bias conductance peaks. *Phys. Rev. Lett.*, 119:136803, Sep 2017.

[124] L.P. Rokhinson, X. Liu, and J.K. Furdyna. The fractional a.c. josephson effect in a semiconductor-superconductor nanowire as a signature of majorana particles. *Nature Physics*, 8(11):795, 2012.

[125] Dominique Laroche, Daniël Bouman, David J. van Woerkom, Alex Proutski, Chaitanya Murthy, Dmitry I. Pikulin, Chetan Nayak, Ruben J. J. van Gulik, Jesper Nygård, Peter Krogstrup, Leo P. Kouwenhoven, and Attila Geresdi. Observation of the 4π-periodic Josephson effect in InAs nanowires. *arXiv e-prints*, page arXiv:1712.08459, Dec 2017.

[126] Liang Fu. Electron teleportation via majorana bound states in a mesoscopic superconductor. *Phys. Rev. Lett.*, 104:056402, Feb 2010.

[127] S. M. Albrecht, A. P. Higginbotham, M. Madsen, F. Kuemmeth, T. S. Jespersen, J. Nygård, P. Krogstrup, and C. M. Marcus. Exponential protection of zero modes in Majorana islands. *Nature*, 531(7593):206–209, Mar 2016.

[128] Suraj Hegde, Yuxuan Wang, Erik Huemiller, Guang Yue, D. J. Van Harlingen, and Smitha Vishveshwara. Topological josephson junction platform for realizing majorana modes andnon-abelian rotations. *In preparation.*

[129] B van Heck, A R Akhmerov, F Hassler, M Burrello, and C W J Beenakker. Coulomb-assisted braiding of majorana fermions in a josephson junction array. *New Journal of Physics*, 14(3):035019, 2012.

[130] G. de Lange, B. van Heck, A. Bruno, D. J. van Woerkom, A. Geresdi, S. R. Plissard, E. P. A. M. Bakkers, A. R. Akhmerov, and L. DiCarlo. Realization of microwave quantum circuits using hybrid superconducting-semiconducting nanowire josephson elements. *Phys. Rev. Lett.*, 115:127002, 2015.

[131] Sagar Vijay, Timothy H. Hsieh, and Liang Fu. Majorana fermion surface code for universal quantum computation. *Phys. Rev. X*, 5:041038, Dec 2015.

[132] Eytan Grosfeld and Ady Stern. Observing majorana bound states of josephson vortices in topological superconductors. 108(29):11810, 2011.

[133] F. J. Burnell. Correlated parity measurements as a probe of non-abelian statistics in one-dimensional superconducting wires. *Phys. Rev. B*, 89:224510, Jun 2014.

[134] Jay D. Sau, David J. Clarke, and Sumanta Tewari. Controlling non-abelian statistics of majorana fermions in semiconductor nanowires. *Phys. Rev. B*, 84:094505, 2011.

[135] C. W. J. Beenakker, D. I. Pikulin, T. Hyart, H. Schomerus, and J. P. Dahlhaus. Fermion-parity anomaly of the critical supercurrent in the quantum spin-hall effect. *Phys. Rev. Lett.*, 110:017003, 2013.

[136] Parsa Bonderson, Michael Freedman, and Chetan Nayak. Measurement-only topological quantum computation. *Phys. Rev. Lett.*, 101:010501, 2008.

[137] Parsa Bonderson. Measurement-only topological quantum computation via tunable interactions. *Phys. Rev. B*, 87:035113, 2013.

[138] M. Burrello, B. van Heck, and A. R. Akhmerov. Braiding of non-abelian anyons using pairwise interactions. *Phys. Rev. A*, 87:022343, 2013.

[139] J. Alicea, Y. Oreg, G. Refael, F. Von Oppen, and M.P.A. Fisher. Non-abelian statistics and topological quantum information processing in 1d wire networks. *Nature Physics*, 7(5):412, 2011.

[140] C. Knapp, M. Zaletel, D. E. Liu, M. Cheng, P. Bonderson, and C. Nayak. How quickly can anyons be braided? Or: How I learned to stop worrying about diabatic errors and love the anyon. *ArXiv e-prints*, 2016.

[141] S. Sachdev. *Quantum Phase Transitions*, 1999.

[142] T.W.B. Kibble. *Phys. Rep.*, 67:183, 1980.

[143] W.H. Zurek. Cosmological experiments in superfluid helium? *Nature*, 317(6037):505, 1985.

[144] A. Dutta, U. Divakaran, D. Sen, B.K. Chakrabarti, T.F. Rosenbaum, and G. Aeppli. *Quantum phase transitions in transverse field spin models: from statistical physics to quantum information*. Cambridge University Press, 2015.

[145] W.H. Zurek, U. Dorner, and P. Zoller. Dynamics of a quantum phase transition. *Physical Review Letters*, 95(10):105701, 2005.

[146] A. Polkovnikov and V. Gritsev. Breakdown of the adiabatic limit in low-dimensional gapless systems. *Nature Physics*, 4(6):477, 2008.

[147] T.W.B. Kibble. Topology of cosmic domains and strings. *Journal of Physics A: General Physics*, 9(8):1387, 1976.

[148] J. Dziarmaga. Dynamics of a quantum phase transition and relaxation to a steady state. *Advances in Physics*, 59(6):1063, 2010.

[149] A. Polkovnikov, K. Sengupta, A. Silva, and M. Vengalattore. Colloquium: Nonequilibrium dynamics of closed interacting quantum systems. *Reviews of Modern Physics*, 83(3):863, 2011.

[150] W.H. Zurek. Cosmological experiments in condensed matter systems. *Physics Report*, 276(4):177, 1996.

[151] J Dziarmaga. *Phys. Rev. Lett.*, 95:245701, 2005.

[152] B Damski. *Phys. Rev. Lett.*, 95:035701, 2005.

[153] B Damski and W H Zurek. *Phys. Rev. A*, 73:063405, 2006.

[154] A Polkovnikov. *Phys. Rev. B*, 72:161201(R), 2005.

[155] P. Calabrese and J. Cardy. Evolution of entanglement entropy in one-dimensional systems. *J. Stat. Mech.*, 0504(4):P04010, 2005.

[156] P. Calabrese and J. Cardy. *Phys. Rev. Lett.*, 96(13):136801, 2006.

[157] R W Cherng and L S Levitov. *Phys. Rev. A*, 73:043614, 2006.

[158] V Mukherjee, U Divakaran, A Dutta, and D Sen. *Phys. Rev. B*, 76:174303, 2007.

[159] U Divakaran, A Dutta, and D Sen. *Phys. Rev. B*, 78:144301, 2008.

[160] S. Deng, G. Ortiz, and L. Viola. Dynamical non-ergodic scaling in continuous finite-order quantum phase transitions. *EPL (Europhysics Letters)*, 84(6):67008, 2008.

[161] U. Divakaran, V. Mukherjee, A. Dutta, and D. Sen. *J. Stat. Mech.*, 2009:P02007, 0000.

[162] V Mukherjee and A Dutta. *EPL*, 92:37004, 2010.

[163] K. Sengupta, D. Sen, and S. Mondal. Exact results for quench dynamics and defect production in a two-dimensional model. *Physical Review Letters*, 100(7):077204, 2008.

[164] S. Mondal, D. Sen, and K. Sengupta. *Phys. Rev.*, 78:045101, 2008.

[165] D. Sen, K. Sengupta, and S. Mondal. *Phys. Rev. Lett.*, 101:016806, 2008.

[166] S. Mondal, K. Sengupta, and D. Sen. *Phys. Rev.*, 79(4):045128, 2009.

[167] C. De Grandi, R.A. Barankov, and A. Polkovnikov. *Phys. Rev. Lett.*, 101(23):230402, 2008.

[168] R. Barankov and A. Polkovnikov. *Phys. Rev. Lett.*, 101:076801, 2008.

[169] C. De Grandi, V. Gritsev, and A. Polkovnikov. Quench dynamics near a quantum critical point. *Phys. Rev. B*, 81(1):012303, 2010.

[170] D. Patane, A. Silva, L. Amico, F. Rosario, and G.E. Santoro. *Phys. Rev. Lett.*, 101:175701, 2008.

[171] D. Patane, A. Silva, L. Amico, F. Rosario, and G.E. Santoro. *Phys. Rev. B*, 80:024302, 2009.

[172] A. Bermudez, D. Patane, L. Amico, and M.A. Martin-Delgado. *Phys. Rev. Lett.*, 102(13):135702, 2009.

[173] A. Bermudez, L. Amico, and M.A. Martin-Delgado. *New J. Phys.*, 12:055014, 2010.

[174] J.H.H. Perk and H. Au-Yang. New results for the correlation functions of the ising model and the transverse ising chain. *Journal of Statistical Physics*, 135(4):599, 2009.

[175] D. Sen and S. Vishveshwara. *EPL*, 91:66009, 2010.

[176] F. Pollmann, S. Mukerjee, A.G. Green, and J.E. Moore. *Phys. Rev. E*, 81:020101(R), 2010.

[177] A. Dutta, R.R.P. Singh, and U. Divakaran. *Europhys. Lett.*, 89:67001, 2010.

[178] T. Hikichi, S. Suzuki, and K. Sengupta. Slow quench dynamics of the kitaev model: Anisotropic critical point and effect of disorder. *Phys. Rev. B*, 82(17):174305, 2010.

[179] A. Chandran, A. Erez, S.S. Gubser, and S.L. Sondhi. Kibble-zurek problem: Universality and the scaling limit. *Phys. Rev. B*, 86(6):064304, 2012.

[180] A. Chandran, F.J. Burnell, V. Khemani, and S.L. Sondhi. Kibble-zurek scaling and string-net coarsening in topologically ordered systems. *J. Phys.: Condens. Matter*, 25(40):404214, 2013.

[181] A.A. Patel, S. Sharma, and A. Dutta. Quench dynamics of edge states in 2-d topological insulator ribbons. *European Physical Journal B*, 86(9):367, 2013.

[182] S. Mostame, C. Castelnovo, R. Moessner, and S.L. Sondhi. Tunable nonequilibrium dynamics of field quenches in spin ice. *Proceedings of the National Academy of Sciences of the United States of America*, 111(2):640, 2014.

[183] M.S. Foster, V. Gurarie, M. Dzero, and E.A. Yuzbashyan. *Phys. Rev. Lett.*, 113:076403, 2014.

[184] A Rajak and A Dutta. *Phys. Rev. E*, 89:042125, 2014.

[185] K. T. Law and Patrick A. Lee. Robustness of majorana fermion induced fractional josephson effect in multichannel superconducting wires. *Phys. Rev. B*, 84:081304, Aug 2011.

[186] E.J.H. Lee, X. Jiang, M. Houzet, R. Aguado, C.M. Lieber, and S. De Franceschi. Spin-resolved andreev levels and parity crossings in hybrid superconductor-semiconductor nanostructures. *Nature Nanotechnology*, 9(1):79, 2014.

[187] Leonardo Mazza, Alejandro Bermudez, Nathan Goldman, Matteo Rizzi, Miguel Angel Martin-Delgado, and Maciej Lewenstein. An optical-lattice-based quantum simulator for relativistic field theories and topological insulators. *New Journal of Physics*, 14(1):015007, 2012.

[188] L. Dai and M.-C. Chung. Breakdown of local convertibility through Majorana modes in a quantum quench. *ArXiv e-prints*, April 2015.

[189] S Bravyi and R Koenig. *Comm. Math. Phys.*, 316:641, 2012.

[190] H. A. Fertig and B. I. Halperin. Transmission coefficient of an electron through a saddle-point potential in a magnetic field. *Phys. Rev. B*, 36:7969, 1987.

[191] M. Büttiker. Quantized transmission of a saddle-point constriction. *Phys. Rev. B*, 41:7906–7909, 1990.

[192] G. 't Hooft. The Scattering Matrix Approach for the Quantum Black Hole:. AN Overview. *International Journal of Modern Physics A*, 11:4623, 1996.

[193] P. Betzios, N. Gaddam, and O. Papadoulaki. The black hole S-Matrix from quantum mechanics. *Journal of High Energy Physics*, 11:131, November 2016.

[194] W. G. Unruh. Experimental black-hole evaporation? *Phys. Rev. Lett.*, 46:1351–1353, May 1981.

[195] GE Volovik. Vierbein walls in condensed matter. *Journal of Experimental and Theoretical Physics Letters*, 70(11):711–716, 1999.

[196] Uwe R. Fischer and Ralf Schützhold. Quantum simulation of cosmic inflation in two-component bose-einstein condensates. *Phys. Rev. A*, 70:063615, Dec 2004.

[197] Ralf Schützhold and William G. Unruh. Hawking radiation in an electromagnetic waveguide? *Phys. Rev. Lett.*, 95:031301, Jul 2005.

[198] A. Roldán-Molina, Alvaro S. Nunez, and R. A. Duine. Magnonic black holes. *Phys. Rev. Lett.*, 118:061301, Feb 2017.

[199] H. S. Nguyen, D. Gerace, I. Carusotto, D. Sanvitto, E. Galopin, A. Lemaître, I. Sagnes, J. Bloch, and A. Amo. Acoustic black hole in a stationary hydrodynamic flow of microcavity polaritons. *Phys. Rev. Lett.*, 114:036402, Jan 2015.

[200] U. Leonhardt and P. Piwnicki. Relativistic effects of light in moving media with extremely low group velocity. *Phys. Rev. Lett.*, 84:822–825, Jan 2000.

[201] Joseph J. Bisognano and Eyvind H. Wichmann. On the duality condition for quantum fields. *Journal of Mathematical Physics*, 17(3):303–321, 1976.

[202] Geoffrey L Sewell. Quantum fields on manifolds: Pct and gravitationally induced thermal states. *Annals of Physics*, 141(2):201 – 224, 1982.

[203] Brian Swingle and T. Senthil. Geometric proof of the equality between entanglement and edge spectra. *Phys. Rev. B*, 86:045117, Jul 2012.

[204] G. Giudici, T. Mendes-Santos, P. Calabrese, and M. Dalmonte. Entanglement Hamiltonians of lattice models via the Bisognano-Wichmann theorem. *Physical Review B*, 98(13):134403, Oct 2018.

[205] Kyriakos Papadodimas and Suvrat Raju. State-dependent bulk-boundary maps and black hole complementarity. *Phys. Rev. D*, 89(8):086010, Apr 2014.

[206] Edward Witten. Notes on Some Entanglement Properties of Quantum Field Theory. *arXiv e-prints*, page arXiv:1803.04993, Mar 2018.

[207] Srivatsan Balakrishnan, Thomas Faulkner, Zuhair U. Khand ker, and Huajia Wang. A General Proof of the Quantum Null Energy Condition. *arXiv e-prints*, page arXiv:1706.09432, Jun 2017.

[208] Ro Jefferson. Comments on black hole interiors and modular inclusions. *arXiv e-prints*, page arXiv:1811.08900, Nov 2018.

[209] Nima Lashkari. Constraining quantum fields using modular theory. *Journal of High Energy Physics*, 2019(1):59, Jan 2019.

[210] Rudolf Haag. *Local quantum physics*. Springer-Verlag Berlin Heidelberg, 1996.

[211] Ola Bratteli and Derek W Robinson. *Operator Algebras and Quantum Statistical Mechanics- 2 Volumes*. Springer-Verlag Berlin Heidelberg, 1987.

[212] Maulik K. Parikh and Frank Wilczek. Hawking radiation as tunneling. *Phys. Rev. Lett.*, 85:5042–5045, Dec 2000.

[213] L. Vanzo, G. Acquaviva, and R. Di Criscienzo. Tunnelling methods and Hawking's radiation: achievements and prospects. *Classical and Quantum Gravity*, 28(18):183001, September 2011.

[214] Sean P. Robinson and Frank Wilczek. Relationship between hawking radiation and gravitational anomalies. *Phys. Rev. Lett.*, 95:011303, Jun 2005.

[215] P. A. M. Dirac. Forms of relativistic dynamics. *Rev. Mod. Phys.*, 21:392–399, Jul 1949.

[216] Y. S. Kim and E. P. Wigner. Canonical transformation in quantum mechanics. *American Journal of Physics*, 58(5):439–448, 1990.

[217] C. V. Vishveshwara. Generalization of the "schwarzschild surface" to arbitrary static and stationary metrics. *Journal of Mathematical Physics*, 9(8):1319–1322, 1968.

[218] Eli Honig, Engelbert L. Schucking, and C. V. Vishveshwara. Motion of charged particles in homogeneous electromagnetic fields. *Journal of Mathematical Physics*, 15(6):774–781, 1974.

[219] B R Iyer and C V Vishveshwara. The frenet-serret formalism and black holes in higher dimensions. *Classical and Quantum Gravity*, 5(7):961–970, jul 1988.

[220] B. R. Iyer and C. V. Vishveshwara. Frenet-serret description of gyroscopic precession. *Phys. Rev. D*, 48:5706–5720, Dec 1993.

[221] C. V. Vishveshwara. *Einstein's Enigma or Black Holes in My Bubble Bath*. CSpringer-Verlag Berlin Heidelberg, 2006.

[222] W. G. Unruh. Notes on black-hole evaporation. *Phys. Rev. D*, 14:870–892, Aug 1976.

[223] L. D Landau and E. M Lifshitz. *Classical theory of fields: Course on theoretical physics vol.2*. Elsevier Butterworth-Heinemann.

[224] V.F Mukhanov and S Winitzki. *Quantum effects in gravity*. Cambridge university press, 2007.

[225] T. Padmanabhan. Gravity and the thermodynamics of horizons. *Phys. Rept.*, 406(2):49–125, Jan 2005.

[226] Luís C. B. Crispino, Atsushi Higuchi, and George E. A. Matsas. The unruh effect and its applications. *Rev. Mod. Phys.*, 80:787–838, 2008.

[227] Ted Jacobson. *Black Holes and Hawking Radiation in Spacetime and Its Analogues*, volume 870, page 1. 2013.

[228] S. W. Hawking. Particle creation by black holes. *Communications in Mathematical Physics*, 43(3):199–220, Aug 1975.

[229] J. Earman. The Unruh effect for philosophers. *Studies in the History and Philosophy of Modern Physics*, 42:81–97, 2011.

[230] Kostas D. Kokkotas and Bernd G. Schmidt. Quasi-normal modes of stars and black holes. *Living Reviews in Relativity*, 2(1):2, Sep 1999.

[231] R. A. Konoplya and Alexander Zhidenko. Quasinormal modes of black holes: From astrophysics to string theory. *Rev. Mod. Phys.*, 83:793–836, 2011.

[232] Emanuele Berti, Vitor Cardoso, and Andrei O Starinets. Quasinormal modes of black holes and black branes. *Classical and Quantum Gravity*, 26(16):163001, 2009.

[233] B. F. Schutz and C. M. Will. Black hole normal modes - a semianalytic approach. *apjl*, 291:L33, 1985.

[234] Cecilia Chirenti. Black hole quasinormal modes in the era of ligo. *Brazilian Journal of Physics*, 48(1):102–109, Feb 2018.

[235] B. P Abbott et al. Gw170817: Observation of gravitational waves from a binary neutron star inspiral. *Phys. Rev. Lett.*, 119:161101, Oct 2017.

[236] N. Read and E. H. Rezayi. Hall viscosity, orbital spin, and geometry: Paired superfluids and quantum hall systems. *Phys. Rev. B*, 84:085316, 2011.

[237] S. M. Girvin and Terrence Jach. Formalism for the quantum hall effect: Hilbert space of analytic functions. *Phys. Rev. B*, 29:5617–5625, May 1984.

[238] Hongya Liu and Bahram Mashhoon. On the spectrum of oscillations of a schwarzschild black hole. *Classical and Quantum Gravity*, 13(2):233, 1996.

[239] Askold M Perelomov and Yakov B Zeldovich. *Quantum Mechanics*. WORLD SCIENTIFIC, 1998.

[240] Guido Parravicini, Vittorio Gorini, and E. C. G. Sudarshan. Resonances, scattering theory, and rigged hilbert spaces. *Journal of Mathematical Physics*, 21(8):2208–2226, 1980.

[241] A. Bohm and M Gadella. *Dirac Kets, Gamow Vectors and Gelfand Triplets*. Springer-Verlag Berlin Heidelberg, 1989.

[242] D. Chruscinski. Quantum mechanics of damped systems. *Journal of Mathematical Physics*, 44(9):3718–3733, 2003.

[243] D. Chruscinski. Quantum mechanics of damped systems. II. Damping and parabolic potential barrier. *Journal of Mathematical Physics*, 45:841, 2004.

[244] N. Andersson and B.P. Jensen. *Scattering by black holes*. Academic Press, 2001.

[245] T. Shimbori and T. Kobayashi. Complex eigenvalues of the parabolic potential barrier and Gel'fand triplet. *Nuovo Cimento B Serie*, 115:325, 2000.

[246] P.L. McEuen, B.W. Alphenaar, R.G. Wheeler, and R.N. Sacks. Resonant transport effects due to an impurity in a narrow constriction. *Surface Science*, 229(1):312 – 315, 1990.

[247] E. Comforti, Y. C. Chung, M. Heiblum, V. Umansky, and D. Mahalu. Bunching of fractionally charged quasiparticles tunnelling through high-potential barriers. *Nature*, page 515, 2002.

[248] Martina Floser, Serge Florens, and Thierry Champel. Transmission coefficient through a saddle-point electrostatic potential for graphene in the quantum hall regime. *Phys. Rev. B*, 82:161408, 2010.

[249] J.M. Aguirregabiria and C.V. Vishveshwara. Scattering by black holes: a simulated potential approach. *Physics Letters A*, 210(4):251 – 254, 1996.

[250] L. D Landau and E. M Lifshitz. *Quantum Mechanics(Non-relativistic theory): Course on theoretical physics vol.3*. Elsevier Butterworth-Heinemann.

[251] David A. Lowe. Mellin transforming the minimal model CFTs: AdS/CFT at strong curvature. *Physics Letters B*, 760:494–497, Sep 2016.

[252] Dhritiman Nandan, Anastasia Volovich, and Congkao Wen. On Feynman rules for Mellin amplitudes in AdS/CFT. *Journal of High Energy Physics*, 2012:129, May 2012.

[253] A. Liam Fitzpatrick, Jared Kaplan, Joao Penedones, Suvrat Raju, and Balt C. van Rees. A natural language for ads/cft correlators. *Journal of High Energy Physics*, 2011(11):95, Nov 2011.

[254] T. Shimbori and T. Kobayashi. Supersymmetric quantum mechanics of scattering. *Physics Letters B*, 501:245–248, March 2001.